9 May 2008 | $10

Science

AAAS

COVER

Lake Boku at the Ounianga oasis in remote northeastern Chad, one of the few remaining bodies of water in the almost rainless Sahara. Still sustained by fossil groundwater dating from the humid past, it is doomed because of encroaching dunes. See page 765.

Photo: S. Krüpelin

DEPARTMENTS

711 *Science* Online
713 This Week in *Science*
718 Editors' Choice
722 Contact *Science*
725 Random Samples
727 Newsmakers
815 New Products
816 *Science* Careers

EDITORIAL

717 AIDS and the Next 25 Years
by Alan Bernstein

NEWS OF THE WEEK

Going From *RAGS* to Riches Is Proving to Be Very Difficult 728
Ancient Algae Suggest Sea Route for First Americans 729
>> *Report p. 784*
Genome Speaks to Transitional Nature of Monotremes 730
States Push Academic Freedom Bills 731
SCIENCESCOPE 731
Chinese Province Crafts Pioneering Law to Thwart Biopiracy 732

NEWS FOCUS

The Roots of Morality 734
>> *Science Express Report by M. Hsu et al.*
To Touch the Water of Mars and Search for Life's Abode 738
Talk Nerdy to Me 740
Into the Wild: Reintroduced Animals Face Daunting Odds 742

734

LETTERS

Lost in Transliteration *L. Wang* 745
Evolution and Faith: Empathy Is Misplaced
C. W. Stevens
Evolution and Faith: Empathy Is Crucial *A. Whipple*
Data Discrepancies in Solar-Climate Link
R. T. Pierrehumbert
Living Up to Ancient Civilizations *G. P. Glasby*
CORRECTIONS AND CLARIFICATIONS 746

BOOKS *ET AL.*

Disrupting Science Social Movements, American Scientists, and the Politics of the Military, 1945–1975 747
K. Moore, reviewed by A. J. Wolfe
Architect and Engineer A Study in Sibling Rivalry 748
A. Saint, reviewed by T. P. Hughes

748

POLICY FORUM

Reassessing HIV Prevention 749
M. Potts et al.

PERSPECTIVES

Designer Atomic Nuclei 751
B. M. Sherrill
How the Sahara Became Dry 752
J. A. Holmes
>> *Research Article p. 765*
A STEP into Darkness or Light? 753
J. P. Moore, P. J. Klasse, M. J. Dolan, S. K. Ahuja
Tinkering with Acellular Division 755
J. Lutkenhaus
>> *Reports pp. 789 and 792*
High-Frequency Chip Connections 756
T. J. Spencer, T. Osborn, P. A. Kohl
News About Nitrogen 757
M. C. Hamer-Devine and A. C. Martiny

CONTENTS continued >>

Science

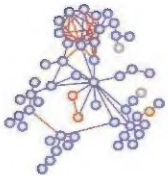

SCIENCE EXPRESS

www.sciencexpress.org

PSYCHOLOGY
The Right and the Good: Distributive Justice and Neural Encoding of Equity and Efficiency
M. Hsu, C. Anen, S. R. Quartz
A brain region linked to emotion-processing systems is activated as humans weigh fairness to an individual against benefit for a group.
>> News story p. 734
10.1126/science.1153651

MICROBIOLOGY
Anticipatory Behavior Within Microbial Genetic Networks
I. Tagkopoulos, Y.-C. Liu, S. Tavazoie
Predictable sequences of environmental signals can be exploited by bacteria so that they learn to anticipate future metabolic needs and thereby gain a competitive edge.
10.1126/science.1154456

CELL BIOLOGY
An in Vivo Map of the Yeast Protein Interactome
K. Tarassov et al.
A method that identifies pairs of proteins that are 8 nanometers apart produces a map of interacting proteins in living yeast, finding known and previously unknown networks.
10.1126/science.1153878

MOLECULAR BIOLOGY
PERSPECTIVE: Slicing and Dicing for Small RNAs
J. A. Birchler and H. H. Kavi
10.1126/science.1159018

TECHNICAL COMMENT ABSTRACTS

ATMOSPHERIC SCIENCE
Comment on "Absence of Cooling in New Zealand and the Adjacent Ocean During the Younger Dryas Chronozone" 746
P. J. Applegate, T. V. Lowell, R. B. Alley
full text at www.sciencemag.org/cgi/content/full/320/5877/746c

Response to Comment on "Absence of Cooling in New Zealand and the Adjacent Ocean During the Younger Dryas Chronozone"
T. T. Barrows, S. J. Lehman, L. K. Fifield, P. De Deckker
full text at www.sciencemag.org/cgi/content/full/320/5877/746e

REVIEW

MEDICINE
Toward an AIDS Vaccine 760
B. D. Walker and D. R. Burton

RESEARCH ARTICLE

ECOLOGY
Climate-Driven Ecosystem Succession in the Sahara: The Past 6000 Years 765
S. Kröpelin et al.
A climate record from lake sediments in Chad shows that the Sahara changed gradually from a tropical ecosystem to a desert, not abruptly as implied by Atlantic dust layers. *>> Perspective p. 752*

REPORTS

APPLIED PHYSICS
Controlled Phase Shifts with a Single Quantum Dot 769
I. Fushman et al.
A single quantum dot coupled to a photonic crystal can be used to shift the phase of light by up to π radians at the single photon level, as needed for quantum logic operations.

APPLIED PHYSICS
Conditional Dynamics of Interacting Quantum Dots 772
L. Robledo et al.
Controlled coherent manipulation is realized in a pair of self-assembled quantum dots: The optical response of one depends on the state of the other.

APPLIED PHYSICS
Subnanometer Motion of Cargoes Driven by Thermal Gradients Along Carbon Nanotubes 775
A. Barreiro et al.
A segment of the outer shell of a multiwall carbon nanotube can move back and forth in response to a thermal gradient created by electrical current passing through the nanotube.

CLIMATE CHANGE
Fracture Propagation to the Base of the Greenland Ice Sheet During Supraglacial Lake Drainage 778
S. B. Das et al.
A large lake on the surface of the Greenland Ice Sheet drained out through and along the base of the Ice Sheet within 2 hours, revealing an efficient basal hydrological system.

CLIMATE CHANGE
Seasonal Speedup Along the Western Flank of the Greenland Ice Sheet 781
I. Joughin et al.
Measurements of ice motion from Greenland show that summer meltwater accelerates ice sheet flow by 50 to 100% overall but has less effect in the faster outlet glaciers.

CONTENTS continued >>

REPORTS *CONTINUED...*

ARCHAEOLOGY

Monte Verde: Seaweed, Food, Medicine, and the Peopling of South America 784
T. D. Dillehay et al.
Carbon-14 dates on seaweed brought to Monte Verde, Chile, show that the site was used 14,000 years ago and that the earliest New World people consumed marine resources. >> *News story p. 729*

ANTHROPOLOGY

DNA from Pre-Clovis Human Coprolites in Oregon, North America 786
M. T. P. Gilbert et al.
Fossil human feces from an Oregon cave predate the Clovis culture by about 1000 years, and DNA from the feces marks the presence of Native Americans in North America.

BIOCHEMISTRY

Spatial Regulators for Bacterial Cell Division Self-Organize into Surface Waves in Vitro 789
M. Loose et al.
Two proteins that define the plane of cell division self-organize into waves and spirals on a flat membrane, suggesting that these patterns underlie their function in vivo. >> *Perspective p. 755*

BIOCHEMISTRY

Reconstitution of Contractile FtsZ Rings in Liposomes 792
M. Osawa, D. E. Anderson, H. P. Erickson
A tubulin homolog from prokaryotes can, without other proteins, assemble into rings around liposomes and constrict, suggesting a primordial cell division mechanism. >> *Perspective p. 755*

BIOCHEMISTRY

Architecture of a Charge-Transfer State Regulating Light Harvesting in a Plant Antenna Protein 794
T. K. Ahn et al.
To protect itself from oxidative damage in bright light, photosystem II operates a tunable shunt that directs excess energy to a yellow accessory pigment that is abundant in corn.

VIROLOGY

Phosphorylation of Retinoblastoma Protein by Viral Protein with Cyclin-Dependent Kinase Function 797
A. J. Hume et al.
A human cytomegalovirus protein takes control of the host cell cycle by mimicking a cell cycle kinase that phosphorylates and inactivates a tumor suppressor.

ECOLOGY

Adaptive Phenotypic Plasticity in Response to Climate Change in a Wild Bird Population 800
A. Charmantier et al.
A 47-year study of great tits in Britain shows that the ability of individual birds to shift their breeding date has enabled the species to thrive as climate has changed.

NEUROSCIENCE

Temperature Sensing by an Olfactory Neuron in a Circuit Controlling Behavior of *C. elegans* 803
A. Kuhara et al.
An olfactory neuron in *Caenorhabditis elegans* also senses the ambient temperature and is necessary for worms' propensity to seek out the temperature at which they were raised.

CELL BIOLOGY

Discovery of a Cytokine and Its Receptor by Functional Screening of the Extracellular Proteome 807
H. Lin et al.
A systematic, functional screen of extracellular proteins in yeast identified a previously unknown receptor-ligand pair: the cytokine interleukin-34 and its receptor.

CELL BIOLOGY

Regulation of the Cellular Heat Shock Response in *Caenorhabditis elegans* by Thermosensory Neurons 811
V. Prahlad, T. Cornelius, R. I. Morimoto
Activation of a heat-sensitive sensory neuron in the worm *Caenorhabditis elegans* unexpectedly triggers a heat-shock response throughout the animal.

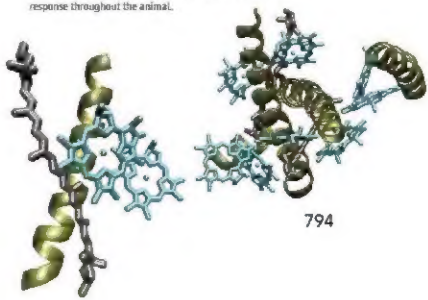

794

AAAS
ADVANCING SCIENCE, SERVING SOCIETY

SCIENCE (ISSN 0036-8075) is published weekly on Friday, except the last week in December, by the American Association for the Advancement of Science, 1200 New York Avenue, NW, Washington, DC 20005. Periodicals Mail postage (publication No. 484460) paid at Washington, DC, and additional mailing offices. Copyright © 2008 by the American Association for the Advancement of Science. The title SCIENCE is a registered trademark of the AAAS. Domestic individual membership and subscription (51 issues): $144 ($74 allocated to subscription). Domestic institutional subscription (51 issues): $770; Foreign postage extra: Mexico, Caribbean (surface mail) $55; other countries (air assist delivery) $85. First class, airmail, student, and emeritus rates on request. Canadian rates with GST available upon request, GST #1254 88122. Publications Mail Agreement Number 1069624. **Printed in the U.S.A.**

Change of address: Allow 4 weeks, giving old and new addresses and 8-digit account number. **Postmaster:** Send change of address to AAAS, P.O. Box 96178, Washington, DC 20090–6178. **Single-copy sales:** $10.00 current issue, $15.00 back issue prepaid includes surface postage; bulk rates on request. **Authorization to photocopy** material for internal or personal use under circumstances not falling within the fair use provisions of the Copyright Act is granted by AAAS to libraries and other users registered with the Copyright Clearance Center (CCC) Transactional Reporting Service, provided that $20.00 per article is paid directly to CCC, 222 Rosewood Drive, Danvers, MA 01923. The identification code for Science is 0036-8075. *Science* is indexed in the *Reader's Guide to Periodical Literature* and in several specialized indexes.

CONTENTS continued >>

Seeing is believing.

SCIENCENOW

www.sciencenow.org

HIGHLIGHTS FROM OUR DAILY NEWS COVERAGE

Seeing Love in a Different Light
Jumping spider mating displays flash a wavelength that researchers thought no animal could detect.

Extra Pounds a Boon?
Fat transplants in mice suggest potential benefit.

Fungus Could Be a Fix for Uranium Pollution
Common soil organisms holds the metal in place, keeping it from spreading.

T cell receptor clustering.

SCIENCE SIGNALING

www.sciencesignaling.org

THE SIGNAL TRANSDUCTION KNOWLEDGE ENVIRONMENT

PERSPECTIVE: TCR Triggering by the pMHC Complex—Valency, Affinity, and Dynamics
R. Varma
Multiple models compete to explain T cell receptor activation.

REVIEW: Is Zinc a Neuromodulator?
A. R. Kay and K. Tóth
Experiments with metal chelators provide the best evidence for zinc as a regulator of synaptic activity.

FORUM: Open Forum on Cell Signaling
N. R. Gough and J. F. Foley
Read highlights from the Experimental Biology 2008 meeting.

An accurate source of career information?

SCIENCE CAREERS

www.sciencecareers.org/career_development

FREE CAREER RESOURCES FOR SCIENTISTS

Opportunities: Research Inc.
P. Fiske
It is useful to think of your research career as a business.

Rumors Fly Online When Jobs Are at Stake
L. Laursen
Can job-rumor Web sites damage your prospects?

Alternative Careers in Chemistry
L. Balbes
Many opportunities in chemistry exist away from the bench.

***Science* Careers Blog**
J. Austin
Read the latest news and information on the scientific workforce.

SCIENCEPODCAST

Download the 9 May *Science* Podcast to hear about the neurobiology of morality, climate change in the Sahara, HIV prevention priorities, and more.
www.sciencemag.org/about/podcast.dtl

CREDITS: (SCIENCE NOW) DARIN LUTHER MARSHALL, UNIVERSITY OF SINGAPORE; (SCIENCE CAREERS) JASON PRATT/CREATIVE COMMONS; (SCIENCE SIGNALING) C. BIESSEL

Separate individual or institutional subscriptions to these products may be required for full-text access.

CREDIT: (TOP TO BOTTOM) SARAH M. DAS, BANDIERA ET AL.

<< Water and Ice

The water at the base of glacial ice sheets lubricates the ice-earth interface, allowing the ice sheet to slide more quickly and easily over the ground below, but its role in how glaciers lose mass is unclear. How will ice-sheet mass loss be affected by climate warming? **Das *et al.*** (p. 778, published online 17 April) describe the disappearance of a large supraglacial lake in Greenland, which occurred with startling speed in the summer of 2006, when a torrent of water emptied into the kilometer-thick ice sheet below it at an average rate of flow greater than that of Niagara Falls. Taking a wider perspective, **Joughin *et al.*** (p.781, published online 17 April) synthesize a wide array of data on ice motion from across Greenland to show how the ice sheet responds to surface melting and suggest that surface melting will probably cause a clear, but not catastrophic, increase in mass loss from the Greenland Ice Sheet in the foreseeable future.

A Not-So-Happy Anniversary

This year marks a quarter-century since the discovery of the human immunodeficiency virus (HIV) as the cause of AIDS. Over this time, enormous effort has been expended in developing a vaccine that will help tackle this global epidemic, but success has not been forthcoming: Last year saw the failure of what many viewed as the most promising vaccine trial to date, coordinated by the National Institutes of Health and Merck. **Walker and Burton** (p. 760) review the principles that have guided HIV vaccine research to date, and discuss the major hurdles that now face the scientific community in generating effective protective immunity to the virus.

The Making of the Sahara

Analysis of mid- and late Holocene environmental and climate change in northern Africa has been hampered by the extreme aridity of the Sahara during recent millennia, which has eradicated most sites that might have provided a depositional record. In an attempt to fill this gap, several expeditions have been undertaken to exploit the paleoclimatic potential of the largest Saharan lakes at Ounianga in Northeast Chad. **Kröpelin *et al.*** (p. 765; see the Perspective by **Holmes**; cover) provide a continuous and well-dated record of climate and ecosystem change over the past 6000 years from one of these lakes, Lake Yoa. The analysis suggests that the present desert became established about 2700 years ago and, contrary to expectations, the pattern of terrestrial ecosystem change from humid to dry was gradual rather than abrupt.

Nanoscale Thermal Motors

Powering very small devices—nanoelectromechanical systems—will require compact ways of converting electrical energy into directed motion. **Barreiro *et al.*** (p. 775, published online 10 April) describe a linear motor in which a multiwall carbon nanotube (MWNT), attached to electrodes at each end, serves as a track. A small section of the MWNT was decorated with a metal plate, and upon application of a large current, the remaining outer walls were ablated to leave a mobile sleeve. Passage of a smaller current through this assembly caused it to move toward one electrode, driven by the creation of a thermal gradient. The motion consisted of translation and rotational steps, and its overall direction was independent of the bias of the applied current.

Quantum Dot Optoelectronics

There is great interest in developing architectures that allow the quantum state of one part of a system to be controlled by the quantum state of another part. The ability to manipulate and control the optical properties and/or the charge and spin states of a single quantum dot have marked them as ideal candidates for further development. **Robledo *et al.*** (p. 772) demonstrate controlled interaction between a pair of self-assembled quantum dots, whereby the optical response of one of the dots is conditioned on the state of its neighbor. In a separate study, **Fushman *et al.*** (p. 769) show that a single quantum dot coupled to a photonic crystal cavity can be used to induce optical phase shift up to $\pi/4$ radians down at the single photon level. The ability to control and manipulate the optoelectronic properties of quantum dots is an essential ingredient for quantum logic applications.

Pre-Clovis South…

Monte Verde, in Chile, provides some of the best evidence for the early inhabitation of the Americas prior to the widespread Paleo-Indian Clovis culture. **Dillehay *et al.*** (p. 784) now provide some direct radiocarbon dates on the antiquity of the site and show that the early inhabitants used a wide variety of marine resources. A variety of different seaweeds were recovered from the site, which was about 15 km from the nearest bay 14,000 years ago. Early tools containing seaweed flakes were also found. This evidence helps confirm the importance of Monte Verde and supports the idea that early settlers relied on marine resources to move rapidly down the coast.

…and Pre-Clovis North

Evidence for a human presence in North America significantly before the appearance of the widespread Clovis complex about 13,000 years ago has been enigmatic. **Gilbert *et al.*** (p. 786, pub-

Continued on page 715

Continued from page 713

lished online 3 April) now report the recovery and genetic typing of human coprolites from a cave deposit in Oregon that predate the Clovis culture by about 1000 years. The coprolites were confirmed as human by several techniques and directly dated and yielded mitochondrial DNA fragments consistent with haplogroups of Native Americans that are thought to have arisen about 18,000 years ago.

Divide and Conquer

During division, the bacterial cell division machinery selects the center of the rod-shaped cell as the division site and uses a protein array to physically separate daughter cells (see the Perspective by **Lutkenhaus**). Several protein components, including MinE and MinD, are known to play a role in selecting the division site. **Loose *et al.*** (p. 789) describe the emergence of self-organized behavior and dynamic pattern formation in a reconstituted system, which includes only the bacterial Min proteins MinE and MinD, a supported lipid bilayer, and energy in the form of ATP. The proteins formed dynamic patterns by a reaction-diffusion mechanism in vitro, which could account for the behavior of these same proteins in selecting the bacterial cell division site. FtsZ, a tubulin homolog, is the primary cell division protein in most bacterial and archaeal species. It is tethered to the membrane by FtsA, and, together with a dozen other proteins, it assembles into the Z ring which constricts to divide the cell.

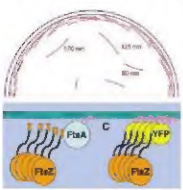

Whether constriction requires proteins other than FtsZ has been unclear. Now **Osawa *et al.*** (p. 792, published online 17 April 2008), in a system that may recapitulate the primordial division machine, have reconstituted Z rings comprised only of a membrane-targeted FtsZ in liposomes and shown that the rings generate a constriction force.

Birds of a Feather Adapt Together

Recent studies of biological responses to climate change have mostly focused on changes in abundance and distribution of species and adaptive evolutionary change. **Charmantier *et al.*** (p. 800) use data from almost five decades of continuous study of a wild bird species—great tits in a UK woodland—to show that phenotypic plasticity can be another effective means for populations to respond to rapidly changing climates. Linking information about individual variation, population-level responses, natural selection, climate, and the timing of the food supply, they show that close tracking of the environment is adaptive, and that the UK great tit population has tracked the changing environment almost perfectly over a very wide range of conditions.

Home Is Where the Hearth Is

The nematode *Caenorhabditis elegans* can "remember" the temperature at which it was grown and will seek out that temperature if later exposed to a gradient of temperatures. In an effort to define the neuronal circuitry that allows this behavior, **Kuhara *et al.*** (p. 803, published online 10 April) found that a neuron known as AWC has an important role in sensing temperature. This came as a surprise because the AWC cell is also known to function as an olfactory neuron. The cell could respond independently to odorants and temperature, even though when sensing temperature the neuron used a similar G protein–mediated intracellular signaling system to that used in olfactory responses.

Identifying Receptor-Ligand Pairs

Secreted proteins that interact with receptors on the cell surface control all sorts of biological processes and provide targets for therapeutic intervention. **Lin *et al.*** (p. 807) used a systematic approach to search for previously unknown ligand-receptor pairs. They produced recombinant proteins from genes that appeared to encode secreted proteins and then tested the proteins individually for effects in a range of in vitro assays. Having identified a new cytokine, interleukin 34 (IL-34), the authors then looked for binding to recombinant extracellular domains of about 1600 transmembrane proteins, which led to the detection of IL-34 binding to the colony-stimulating factor 1 (CSF-1) receptor. Biological effects of IL-34 mediated through the CSF-1 receptor were confirmed in further studies. Thus, the authors' approach can identify important regulatory proteins and their receptors.

CREDIT: OSAWA ET AL.

Alan Bernstein is executive director of the Global HIV Vaccine Enterprise, New York, New York.

AIDS and the Next 25 Years

Later this month, researchers will gather at the Institut Pasteur in Paris to mark the quarter century since human immunodeficiency virus (HIV) was discovered as the cause of acquired immunodeficiency syndrome (AIDS). Since then, over 60 million people have been infected with the virus and over 25 million people have died. These numbers make the results of two "proof of concept" vaccine efficacy trials—the STEP and Phambili trials—extremely disappointing. Indeed, these results have raised questions about whether investments in HIV vaccine research are misplaced and whether a vaccine is even achievable. Those views are misguided. The failure of candidate vaccines or drugs is to be expected. More than ever, investigations in humans are essential to explore concepts, test hypotheses, and delineate the human immune response to HIV immunogens.

The STEP and Phambili trials, cosponsored by the pharmaceutical company Merck & Co. and the U.S. National Institutes of Health, were designed to test the efficacy of a recombinant adenovirus vector cocktail expressing three HIV genes. The vaccine candidate failed to limit viral replication in people who became infected with HIV and failed to prevent the acquisition of HIV. Most disconcertingly, a subset of volunteers appeared to show an increased probability of acquiring HIV (see the Perspective by Moore *et al.*, p. 753). These results reflect our still-limited knowledge of HIV, its interactions with the human immune system, and the formidable, unprecedented challenges that it poses.

Why has developing an HIV vaccine been so difficult? One reason is that HIV has evolved highly sophisticated ways to evade the immune system. Its extraordinarily high degree of sequence diversity, caused by mutation and recombination, makes it especially challenging to design neutralizing antibodies that recognize the broad range of epitopes needed for effective immune protection. Moreover, HIV wipes out some of the very cells needed to mount an effective immune response. Despite progress in characterizing cellular and humoral immune responses to the virus, we still don't know enough about the magnitude, breadth, or types of immune responses necessary for effective vaccine protection, in part because of the lack of a robust animal model that recapitulates critical features of both HIV and the human immune system.

Indeed, these are major challenges, but evidence of immunological protection in certain experimental models of HIV in nonhuman primates, and the intriguing observation that a small proportion of HIV-infected individuals ("elite controllers") can completely suppress the virus for years, suggest that a vaccine may be achievable (see the Review by Walker and Burton, p. 760). Furthermore, new technologies in structural and computational biology are providing novel approaches for designing immunogens that might elicit broadly reactive neutralizing antibodies, and new insights into innate and mucosal immunity are expanding vaccine design strategies.

At meetings over the past few months, including an international workshop convened last week by the Global HIV Vaccine Enterprise, there was broad agreement on many points, particularly that more, not less, basic and early-stage clinical research is needed. Understanding the human immune response to HIV remains a priority. We need to understand the role of both the innate and adaptive immune responses during HIV infection. Better assays are needed that reflect the functional biology of cellular immune responses and incorporate a systems biology approach—that is, encompass the integrative functioning of gene, protein, and biochemical networks—to monitor the immune system. We need to make it much more attractive for young researchers, including those from other fields, to enter the HIV vaccine field. And the continued engagement of industry is essential if we are ever to have a vaccine.

Laboratory research has led to effective drugs against HIV that have prolonged the lives of infected individuals, and epidemiological studies have shown that interventions such as circumcision (see the Policy Forum by Potts *et al.*, page 749) can reduce viral acquisition. However, we know from experience with other pathogens that a vaccine is the best way to stop a virus. The only end for a journey that began 25 years ago should be the development of a safe and effective HIV vaccine.

– Alan Bernstein

10.1126/science.1159797

CLIMATE SCIENCE

Ringing in the Old Years

The annual rings of the bristlecone pine trees in eastern California, extending back in live trees about 8000 years, are a lynchpin for calibrating radiocarbon dates. They have also provided important local climate records, as ring width is thought to reflect temperature and moisture; the length of the record is particularly useful in applying the data toward long reconstructions of global climate. Berkelhammer and Stott have now obtained an annual resolved record, extending back to the year 1700, of the oxygen isotope composition of cellulose from the rings of two California bristlecone pines. Interpreting the record is somewhat complicated, as isotopes are fractionated within the tree and by transpiration from the leaves as relative humidity varies, but large changes in values probably reflect variation in the main sources of storms in the region. The record shows small oscillations every 20 years or so that probably reflect Pacific climate variations. More dramatic is a steep change in the mid-1800s that indicates a change from southern-derived moisture during the time of the Little Ice Age to more northern winter storms since. The effect of such changes on the overall growth of the trees, and thus the ring width used in longer reconstructions, need further study. — BH

Geochem. Geophys. Geosys. **9**, 10.1029/2007GC001803 (2008).

CELL BIOLOGY

Inflammation Activates Neurons

Cell fusion is common in some tissues such as skeletal muscle. Studies using transplanted bone marrow–derived cells (BMDCs) have been complicated by observations that cell fusions between BMDCs and resident cell types can occur. Injury may increase the number of fusion events; however, it is not known whether fusogenic cells are functional.

Johansson *et al.* transplanted single hematopoietic stem cells (HSCs) into lethally irradiated mice and found that Purkinje neurons fused with the HSCs. An alternate method for detecting such fusions entailed joining mice surgically, so that the parabiotic mice (one of which expressed green fluorescent protein) shared a circulatory system; 5 to 6 months after parabiosis, the cerebellums of both mice contained fluorescent Purkinje neurons. When chronic inflammation was present, cerebellar heterokaryon formation was enhanced, and differential gene expression analysis showed that the heterokaryons repressed hematopoietic genes and activated Purkinje neuron genes. — BAP

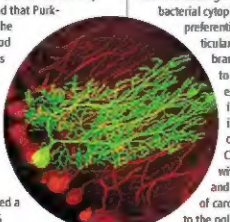

A Purkinje neuron-HSC fusion.

Nat. Cell Biol. **10**, 10.1038/ncb1720 (2008).

BIOPHYSICS

Polar Preferences

In rod-shaped bacteria, proteins that mediate chemotaxis, cell division, and development are observed to localize to the poles. Recent evidence of heterogeneity in the composition of the bacterial cytoplasmic membrane and of the preferential binding of proteins to particular lipids suggests that membrane architecture may contribute to protein localization. For example, cardiolipin is involved in the polar and septal targeting of the *Escherichia coli* osmosensory transporter ProP. Cardiolipin is a phospholipid with high intrinsic curvature, and one proposal is that clusters of cardiolipin localize spontaneously to the poles, where the membrane is constrained by the curved cell wall.

Mukhopadhyay *et al.* have extended their quantitative biophysical model to include the elastic energy of the membrane (which penalizes a deformation of the membrane away from the cell wall–imposed geometry), the interaction energy between lipids, and entropy. They show that variations in osmotic pressure, the force that pins the membrane to the cell wall, can regulate localization. The model predicts the minimum membrane fraction of cardiolipin required for domain formation and a polar localization that are consistent with the experimentally observed critical concentration of cardiolipin required for polar localization of ProP. — VV

Biophys. J. **94**, 10.1529/biophysj.107.126920 (2008).

PHYSICS

Guiding Gamma Rays

Early exposure in high-school science labs to geometrical optics with lenses and mirrors fosters wide familiarity with how to focus and manipulate light in the visible spectrum. A very broad range of convenient focal parameters is available at these wavelengths. As the energy of the photons increases and their wavelengths shrink into the x-ray and gamma-ray regimes, however, conventional lenses and mirrors no longer work. Instead, such high-energy photons must be guided along their path by shallow-angle reflection from specially designed mirrors. Because of the small angles required to avoid absorption losses, the typical focal distances involved are on

CREDITS: (TOP TO BOTTOM) BROOKS MAHON/ISCIENCE; JOHANSSON ET AL., NAT. CELL BIOL. 10.1038/NCB1720/2008

the order of 10 m or so. Though manageable for the likes of large, Earth-based observation stations, these focal parameters are rather unwieldy for medical imaging, space-based observatories, or mobile radioactive material detectors. Tournear *et al.* show that multilayered stacks of gold-palladium and polymer films deposited on a curved silicon substrate can be used to effectively guide gamma rays with a much smaller focal length. Demonstrating the technique for gamma rays of 122 keV, they claim that the focal lengths can be shrunk down to 1 m or less for radiation in the ~100-keV to low-MeV range. — ISO

Appl. Phys. Lett. **92**, 153502 (2008).

CHEMISTRY

Can SWNTs Swim Apart?

Single-walled carbon nanotubes (SWNTs) form as bundles, and to facilitate their processing, they are usually solubilized by some sort of surface treatment, such as coating with surfactants or protonation with superacids. However, unadorned SWNT bundles, when sonicated in dilute *N*-methyl-pyrrolidone (NMP) suspensions, have been observed to disperse and even exfoliate. Bergin *et al.* now show that this process represents true thermodynamic solubility; in other words, the free energy of mixing is negative. This situation is unusual for SWNTs in that the entropy term of mixing for such large molecules is very small, so the enthalpy of mixing must be near zero or even negative. The authors found that as the degree of dilution of SWNT samples in NMP increased, an analysis of bundle sizes (via atomic force microscopy of droplets evaporated on substrates) showed a decrease in bundle diameter, indicating that the samples were approaching equilibrium in solution through spontaneous desorption of SWNTs from the bundles. Light-scattering studies afforded a measurement of the Flory-Huggins parameter, whose sign indicated that the enthalpy of mixing was negative. The authors note that the surface energy of NMP is similar to that of the graphitic surface of the nanotubes; scanning tunneling microscopy (STM) images of the SWNTs after sonication in NMP showed evidence of NMP molecules adsorbed on the SWNTs migrating from inside the bundles to the silicon deposition surface. The authors argue that strong physisorption of NMP onto the SWNT surfaces drives solubilization and that this observation will be key in developing better solvents. — PDS

Adv. Mater. **20**, 10.1002/adma.200702451 (2008).

NEUROSCIENCE

Are You a Morning Person?

Some neurotransmitters, such as dopamine, have been implicated in adjusting a person's mood. The circadian clock mechanisms, meanwhile, keep the organism's physiology tuned for appropriate responses to day or night. Hampp *et al.* have demonstrated how the molecular signaling pathways for circadian rhythms might intersect with the brain's establishment of general mood. They found that the promoter of the gene encoding monoamine oxidase A, which stabilizes some aspects of mood and breaks down dopamine and serotonin, contains binding sites for several clock proteins and showed that circadian oscillation was driven by the *Maoa* promoter in neuroblastoma cells. Mice lacking *Per2*, a gene that stabilizes circadian rhythms, showed damped expression from the *Maoa* promoter. Observations of the *Per2* mutant mice in response to an unavoidable problematic situation—taken as a proxy for despair in humans—showed correlations with disorders of mood. — PJH

Curr. Biol. **18**, 10.1016/j.cub.2008.04.012 (2008).

PSYCHOLOGY

Seen in a Positive Light

A frequently observed and seemingly antisocial behavior is that a morally dubious action taken by oneself will be regarded as less sinful than the same act committed by someone else. Within the currently popular framework of a dual-process model for rendering moral judgments, this asymmetry might arise either at the automatic/intuitive stage of assessment or at the conscious/deliberative stage. Valdesolo and DeSteno describe a study that reveals that the bias in favor of the self grows out of cognitive processes. Diverting some of these cognitive resources by imposing an onerous numerical task while actions were being rated for fairness eliminated the moral bonus awarded to one's own acts, suggesting that the rapid intuitive ranking of behaviors according to norms of fairness operates in an evenhanded and disinterested fashion. In contrast, the higher-level thinking so characteristic of us may, in fact, overrule baser animal instincts for all-too-human motivations, such as the drive toward a positive self-image. — GJC

J. Exp. Soc. Psychol. **44**, 10.1016/j.jesp.2008.03.010 (2008).

DORIAN BERGIN ET AL., ADV. MATER. 10.1002/ADMA.200702451 (2008)

www.sciencemag.org

Science

1200 New York Avenue, NW
Washington, DC 20005
Editorial: 202-326-6550, FAX 202-289-7562
News: 202-326-6581, FAX 202-371-9227

Bateman House, 82-88 Hills Road
Cambridge, UK CB2 1LQ
+44 (0) 1223 326500, FAX +44 (0) 1223 326501

Subscription Services For change of address, missing issues, new orders and renewals, and payment questions: 866-434-AAAS (2227) or 202-326-6417, FAX 202-842-1065. Mailing addresses: AAAS, P.O. Box 96178, Washington, DC 20090-6178 or AAAS Member Services, 1200 New York Avenue, NW, Washington, DC 20005

Institutional Site Licenses please call 202-326-6755 for any questions or information

Reprints: Author Inquiries 800-635-7181
Commercial Inquiries 803-359-4578

Permissions 202-326-7074, FAX 202-682-0816

Member Benefits AAAS/Barnes&Noble.com bookstore www.aaas.org/bn; AAAS Online Store http://www.apisource.com/aaas/ code MKB6; AAAS Travels: Betchart Expeditions 800-252-4910; Apple Store www.apple/eppstore/aaas; Bank of America MasterCard 1-800-833-6262 priority code FAA3YU; Cold Spring Harbor Laboratory Press Publications www.cshlpress.com/affiliates/aaas.htm; GEICO Auto Insurance www.geico.com/landingpage/go51.htm?logo=17624; Hertz 800-654-2200 CDP#343457; Office Depot https://bsd.officedepot.com/portalLogin.do; Seabury & Smith Life Insurance 800-424-9883; Subaru VIP Program 202-326-6417; VIP Moving Services http://www.vipmayflower.com/domestic/index.html; Other Benefits: AAAS Member Services 202-326-6417 or www.aaasmember.org.

science_editors@aaas.org	(for general editorial queries)
science_letters@aaas.org	(for queries about letters)
science_reviews@aaas.org	(for returning manuscript reviews)
science_bookrevs@aaas.org	(for book review queries)

Published by the American Association for the Advancement of Science (AAAS), *Science* serves its readers as a forum for the presentation and discussion of important issues related to the advancement of science, including the presentation of minority or conflicting points of view, rather than by publishing only material on which a consensus has been reached. Accordingly, all articles published in *Science*—including editorials, news and comment, and book reviews—are signed and reflect the individual views of the authors and not official points of view adopted by AAAS or the institutions with which the authors are affiliated.

AAAS was founded in 1848 and incorporated in 1874. Its mission is to advance science and innovation throughout the world for the benefit of all people. The goals of the association are to: foster communication among scientists, engineers and the public; enhance international cooperation in science and its applications; promote the responsible conduct and use of science and technology; foster education in science and technology for everyone; enhance the science and technology workforce and infrastructure; increase public understanding and appreciation of science and technology; and strengthen support for the science and technology enterprise.

Information for Authors

See pages 634 and 635 of the 1 February 2008 issue or access www.sciencemag.org/about/authors

Editor-in-Chief **Bruce Alberts**
Executive Editor **Monica M. Bradford**
Deputy Editors **R. Brooks Hanson, Barbara R. Jasny, Katrina L. Kelner**
News Editor **Colin Norman**

Editorial supervisory senior editor Phillip D. Szuromi; senior editor/perspectives Lisa D. Chong; senior editors Gilbert J. Chin, Pamela J. Hines, Paula A. Kiberstis (Boston), Marc S. Lavine (Toronto), Beverly A. Purnell, L. Bryan Ray, Guy Riddihough, H. Jesse Smith, Valda Vinson; associate editors Jake S. Yeston, Laura M. Zahn; online editor Stewart Wills; associate online editors Robert Frederick, Tara S. Marathe; web content developer Martyn Green; book review editor Sherman J. Suter; associate letters editor Jennifer Sills; editorial manager Cara Tate; senior copy editors Jeffrey E. Cook, Cynthia Howe, Harry Jach, Barbara P. Ordway, Trista Wagoner; copy editors Chris Filiatreau, Lauren Kmec, Peter Mooreside; editorial coordinators Carolyn Kyle, Beverly Shields; publications assistants Ramatoulaye Diop, Joi S. Granger, Jeffrey Hearn, Lisa Johnson, Scott Miller, Jerry Richardson, Jennifer A. Seibert, Brian White, Anita Wynn; editorial assistants Carlos L. Durham, Emily Guise, Patricia M. Moore; executive assistant Sylvia S. Kihara; administrative support Maryrose Madrid

News deputy news editors Robert Coontz, Eliot Marshall, Jeffrey Mervis, Leslie Roberts; contributing editors Elizabeth Culotta, Polly Shulman; news writers Yudhijit Bhattacharjee, Adrian Cho, Jennifer Couzin, David Grimm, Constance Holden, Jocelyn Kaiser, Richard A. Kerr, Eli Kintisch, Andrew Lawler (New England), Greg Miller, Elizabeth Pennisi, Robert F. Service (Pacific NW), Erik Stokstad; intern Elsa Youngsteadt; contributing correspondents Jon Cohen (San Diego, CA), Daniel Ferber, Ann Gibbons, Mitch Leslie, Charles C. Mann, Virginia Morell, Evelyn Strauss, Gary Taubes; copy editors Rachel Curran, Linda B. Felaco, Melvin Gatling; administrative support Scherraine Mack, Fannie Groom; bureaus New England: 207-549-7755, San Diego, CA: 760-942-3252, FAX 760-942-4979, Pacific Northwest: 503-963-1940

Production director James Landry; senior manager Wendy K. Shank; assistant manager Rebecca Doshi; senior specialists Chris Redwood; specialist Steve Forrester; **Preflight** director David M. Tompkins; manager Marcus Spiegler; specialist Jessie Mudjitaba

Art director Kelly Buckheit Krause; associate art director Aaron Morales; illustrators Chris Bickel, Katharine Sutliff; senior art associates Holly Bishop, Laura Creveling, Preston Huey, Nayomi Kevitiyagala; associate Jessica Newfield; photo editor Leslie Blizard

Science International

Europe (science@science-int.co.uk) editorial: international managing editor Andrew M. Sugden; senior editor/perspectives Julia Fahrenkamp-Uppenbrink; senior editors Caroline Ash, Stella M. Hurtley, Ian S. Osborne, Stephen J. Simpson, Peter Stern; editorial support Deborah Dennison, Rachel Roberts, Alice Whaley; administrative support John Cannell, Janet Clements, Louise Smith; news: europe news editor John Travis; deputy news editor Daniel Clery; contributing correspondents Michael Balter (Paris), John Bohannon (Vienna), Martin Enserink (Amsterdam and Paris), Gretchen Vogel (Berlin); intern Laura Cahoon

Asia Japan Office: Asca Corporation, Eiko Ishioka, Fusako Tamura, 1-8-13, Hirano-cho, Chuo-ku, Osaka-shi, Osaka, 541-0046 Japan; +81 (0) 6 6202 6272, FAX +81 (0) 6 6202 6271, asca@os.gulf.or.jp; asia news editor Richard Stone (Beijing: rstone@aaas.org); contributing correspondents Dennis Normile (Japan: +81 (0) 3 3391 0630, FAX 81 (0) 3 5936 3531; dnormile@gol.com); Hao Xin (China: + 86 (0) 10 6307 4439 or 6307 3676, FAX +86 (0) 10 6307 4358; cindyhao@gmail.com); Pallava Bagla (South Asia: +91 (0) 11 2271 2896; pbagla@vsnl.com)

Africa Robert Koenig (contributing correspondent, rob.koenig@gmail.com)

Executive Publisher **Alan I. Leshner**
Publisher **Beth Rosner**

Fulfillment Systems and Operations (membership@aaas.org); director Waylon Butler; customer service supervisor Pat Butler; specialists Laurie Baker, Latoya Casteel, LaVonda Crawford, Vicki Linton; data entry supervisor Cynthia Johnson; specialist Tarrika Hill

Business Operations and Administration director Deborah Rivera-Wienhold; assistant director, business operations Randy Yi; senior financial analysts Michael LoBue, Jessica Tierney; financial analysts Benjamin Aronin, Priti Pamnani; rights and permissions: administrator Emilie David; associate Elizabeth Sandler; marketing director John Meyers; marketing managers Allison Pritchard, Darryl Walter; marketing associates Aimee Aponte, Alison Chandler, Mary Ellen Crowley, Marcia Leach, Julianne Wielga, Wendy Wise; international marketing manager Wendy Sturley; marketing executive Jennifer Reeves; marketing/member services executive Linda Rusk; site license sales director Tom Ryan; sales manager Russ Edra; sales and customer service Iquo Edim, Kiki Forsythe, Catherine Holland, Phillip Smith, Philip Tsolakidis; electronic media: manager Lizabeth Harman; project manager Trista Snyder; assistant manager Lisa Stanford; senior production specialists Christopher Coleman, Walter Jones; production specialists Nichele Johnston, Kimberly Oster

Advertising director worldwide ad sales Bill Moran

Product (science_advertising@aaas.org); midwest Rick Bongiovanni: 330-405-7080, FAX 330-405-7081; west coast/w. canada Teola Young: 650-964-2266; east coast/e. canada Christopher Breslin: 443-512-0330, FAX 443-512-0331; uk/europe/asia Michelle Field: +44 (0) 1223 326524, FAX +44 (0) 1223 326532; japan Mashy Yoshikawa: +81 (0) 33235 5961, FAX +81 (0) 33235 5852; senior traffic associate Dejandra Simms

Commercial Editor Sean Sanders: 202-326-6430

Classified (advertise@sciencecareers.org); u.s.: recruitment sales manager Ian King: 202-326-6528, FAX 202-289-6742; inside sales manager: midwest/canada Daryl Anderson: 202-326-6543; inside sales representative Karen Foote: 202-326-6740; key account manager Joribah Able; northeast Alexis Fleming: 202-326-6578; southeast Tina Burks: 202-326-6577; west Nicholas Hintibidze: 202-326-6533; sales coordinators Erika Foard, Rohan Edmonson, Shirley Young; international: sales manager Tracy Holmes: +44 (0) 1223 326525, FAX +44 (0) 1223 326532; sales Marium Hudda, Alex Palmer, Alessandra Sorgente; sales assistant Louise Moore; japan Mashy Yoshikawa: +81 (0)3 3235 5961, FAX +81 (0)3 3235 5852; advertising production operations manager Deborah Tompkins; senior production specialists Robert Buck, Amy Hardcastle; senior traffic associate Christine Hall; publications assistant Mary Lagnaoui

AAAS Board of Directors retiring president, chair David Baltimore; president James J. McCarthy; president-elect Peter C. Agre; treasurer David E. Shaw; chief executive officer Alan I. Leshner; board Lynn W. Enquist, Susan M. Fitzpatrick, Alice Gast, Linda P. B. Katehi, Nancy Knowlton, Cherry A. Murray, Thomas D. Pollard, Thomas A. Woolsey

AAAS
ADVANCING SCIENCE, SERVING SOCIETY

Place Your Bats

Bats can help reforest the tropics, researchers in Germany say. Artificial bat roosts attract fruit-eating bats, whose droppings help spread seeds beyond the forest edge.

Detlev Kelm of the Leibniz Institute for Zoo and Wildlife Research in Berlin and his colleagues installed simple towers made of sawdust and concrete near a Costa Rica nature reserve ravaged by agriculture and logging. The researchers wanted to lure bats out of their normal forest habitat and into the disturbed regions, which no longer had large, hollow tree trunks in which bats like to hang out during the day.

Bats of 10 different species readily flocked to the roosts, the scientists reported online 25 April in *Conservation Biology*, significantly increasing the number and types of seeds in the neighborhood. "We kick-start the forest succession," says Kelm, who adds that most of the seeds are of "pioneer" species such as nightshade, which grows well in open areas. Although artificial roosts are used for bat conservation, says Thomas Kunz, director of Boston University's Center for Ecology and Conservation Biology, the Costa Rican project is "a very novel idea" that should spur others to harness bats' ability to help restore lost habitat.

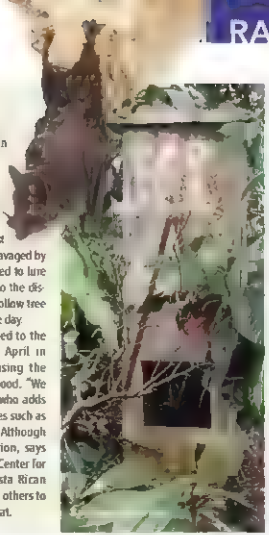

Time 2 Wtr Ur Cottn

Even field crops have caught the text-message craze. A new wireless monitoring system sends leaf temperature data to a computer, which posts the numbers to the Internet and can even text a farmer's cell phone to say it's time to water the crops.

Growers currently under- or overwater many crops, according to plant physiologist James Mahan of the U.S. Department of Agriculture Agricultural Research Service in Lubbock, Texas. Based on 20 years of studying plant temperature stress, Mahan says he's come up with a simple and accurate way to ask a crop whether it's thirsty. Mahan found that, like animals, different plants have different ideal temperatures, around 25°C, depending on the species. In drought, cells warm up and go into heat stress. His new SmartCrop, developed with AccentEngineering company in Lubbock, uses infrared sensors staked among the plants to measure leaf temperature and records other data such as humidity.

Northern Texas farmer Glenn Schur has used a pilot version of SmartCrop in cotton fields for 6 years and says it's saved him about 500 cubic meters of water per hectare, or more than 10% of his annual usage. The basic system was put on the market this spring for $1200; for $500 more, a modem will send the data to a computer that will crunch the numbers and send phone messages.

Handfuls of Satellites

Last week, the Indian space agency shot a record 10 satellites into orbit with one rocket from its space port at Sriharikota, Andhra Pradesh.

Hoisted into orbit by India's Polar Satellite Launch Vehicle were two Indian satellites: the 700-kilogram Cartosat 2A Earth-mapping satellite and a 76-kg remote-sensing satellite that will share images with universities in poor countries. The payload also included eight "nanosatellites" from other countries, weighing between 3 and 16 kilograms each and designed to test money-saving off-the-shelf components.

The feat is a tricky one, says G. Madhavan Nair, chair of the Indian Space Research Organisation in Bangalore. The satellites were released at 20-second intervals by small explosive devices as the rocket coasted at 7.5 kilometers per second 636 kilometers above Earth. If the timing is off the satellites can collide, and if an explosion is too strong it can damage the electronics.

The previous record for a multiple-satellite launch was set by the Russians, who sent up eight in April 2007, 9 months after losing a cargo of 15 satellites when the rocket engine shut down prematurely.

TALK SHOW

Linguists on a half-dozen anthropology and linguistic Web sites are singing the praises of the new World Atlas of Language Structures (WALS) online. WALS, an "awesome resource" as one fan calls it, was launched in April by the Max Planck Digital Library and the Max Planck Institute for Evolutionary Anthropology to give both scientists and non-linguists free access to the data, maps, and analytical texts from the 2005 book and CD-ROM, *The World Atlas of Language Structures*. The book broke new ground by showing scientists the geographical distribution of important patterns of sounds, word structure, and sentence structure in 400 languages. The database expands the number to 2500 and makes the atlas interactive, including 141 maps linked to 6500 references.

A tour of WALS shows the geographic origin of each language as well as the distribution of a vast range of structural properties, including phonological, grammatical, and lexical features. See, for example, the map (left) showing the distribution of "para-linguistic uses of clicks." Or look under "English" and learn that it has a complex syllable structure but no politeness distribution in pronouns.

>> wals.info

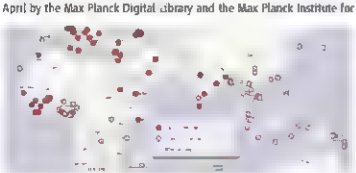

CREDITS: (TOP TO BOTTOM) FRANK GREENAWAY/DORLING KINDERSLEY/DK IMAGES; D. KELM, IZW; D. OLIVIA FORUNE, GOOGLE MAPS

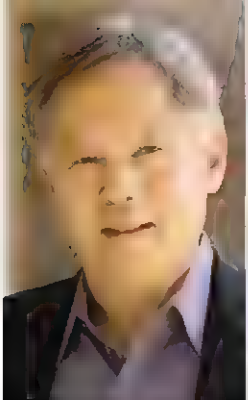

Three Q's >>

David Asai, a cell biologist at Harvey Mudd College in Claremont, California, and longtime grantee of the Howard Hughes Medical Institute, has been named director of HHMI's undergraduate science education program, which gives out $45 million in grants every year. Asai, 54, replaces Stephen Barkanic, who left last August.

Q. How would you characterize the state of U.S. undergraduate science education?

Science education over the last 50 years has been a remarkable engine for creativity and discovery, but science discovery [has] become more multidisciplinary. It's important to tap the very best and brightest, no matter what they look like and where they come from.

Q: Why is diversity so important?

The complexity of some of the problems in life sciences today is impossible to measure. It really helps to have people who come from different [racial, cultural, and disciplinary] backgrounds to think about the same problems.

Q. What will be your biggest challenge?

Working at HHMI, the opportunities for having an impact on students are immense. But I won't be in the classroom anymore. It's not better, it's not worse, but it's going to take some adjustment.

CREDITS: (TOP TO BOTTOM) MARK HARMEL/FOR HHMI; SOURCE; JAY LEONO ZAMBRANO; REUTERS/SIGOU BUCHER/LANDOV

Got a tip for this page? E-mail people@aaas.org

IN PRINT

HOT TYPE. An upcoming paper in *IEEE Transactions on Power Delivery* describes how global warming could shorten the working lives of electrical power transformers. But don't look for "global warming" in the title. The authors replaced it with the watered-down "ambient temperature rise" after an anonymous reviewer asserted that predictions of increasing temperatures were scientifically unfounded.

The self-censorship was done "in the interest of getting the thing published as quickly as possible," says Gerald Heydt, an electrical engineer at Arizona State University in Tempe. Heydt says the reviewer cited 400 scientists who are skeptical that humans are changing Earth's climate. The paper reports that transformers are likely to fail more often if temperatures rise by an average of 4°C over the next century, as predicted by some models.

The journal's editor, Reza Iravani, says Heydt didn't need to change the title and that the reviewer strongly supported publishing the paper. The comments, Iravani says, simply noted that "this range of temperature change has not been established."

IN BRIEF

Michael Kluse has been named director of the Department of Energy's Pacific Northwest National Laboratory in Richland, Washington, which is managed by Battelle. Kluse, who has a master's degree in industrial and systems engineering, has served as interim director of the $760 million facility since August 2007.

The **National Academy of Sciences** last week named 72 new members and 18 new foreign associates. The list is at www.nas.edu.

NONPROFIT WORLD

IN THIS TOGETHER. Freddy Nguyen had such a hard time learning about M.D./Ph.D. programs that he vowed to help other applicants avoid a similar fate. Last month, the organization that grew out of his frustration, the American Physician Scientists Association (APSA), hosted its fourth annual meeting in Chicago. The group is doing well enough for the 26-year-old Nguyen, an M.D./Ph.D. candidate at the University of Illinois, Urbana-Champaign, to step down as president and hand the reins to the next generation.

APSA (www.physicianscientists.org) has more than 1000 student members from about 120 medical schools. It organizes national and regional conferences each year where this rare breed—who face a 10-to-14-year slog—can meet fellow students, present their research, and learn from senior investigators who have traveled the same path. "It's really about connecting people across organizations," says Nguyen.

"Freddy has a remarkable passion for this," says Joseph Bast, director of the M.D./Ph.D. program at the University of Kansas Medical Center, who calls the group "a very worthwhile organization." The new president is James Pauff, who attends Ohio State University in Columbus.

Deaths

JUST CURIOUS. Albert Hofmann, the Swiss chemist whose discovery of LSD (lysergic acid diethylamide) fueled an era of psychedelic art and music, died of a heart attack on 29 April in Basel, Switzerland. He was 102.

Hofmann was working at Sandoz Pharmaceuticals, researching the medicinal properties of plants, when he synthesized LSD in 1938. But only 5 years later did he stumble upon its hallucinogenic effects after accidentally absorbing it through his fingertips. The resulting "fantastic pictures of extraordinary plasticity and intensive color" convinced him that the drug could help treat psychiatric illnesses, and he often used himself as a test subject.

"[Hofmann] managed to keep his almost childlike curiosity for the wonders of nature and creation," said Dieter Hagenbach and Lucius Werthmüller in a written statement from the Gaia Media Foundation, where Hofmann served as a board member.

The platypus decoded 730

Biopiracy protections 732

Middle school students in Ohio learn about aerodynamic principles from NASA scientists as part of a HENAAC program.

U.S. SCIENCE POLICY

Going From *RAGS* to Riches Is Proving to Be Very Difficult

Ray Mellado welcomes contributions to the nonprofit organization he founded 2 decades ago to encourage U.S. Hispanics and other students of color to pursue careers in science and engineering. But the retired Xerox sales executive is wary of an offer from Chinese investors to nearly double the $4 million budget of the Los Angeles–based organization (called HENAAC). They want it to expand its program to rural China in hopes of encouraging students there to pursue technical careers. The offer is a reminder about how much the rest of the world values science, Mellado told an overflow crowd of 450 educators, lobbyists, government officials, and industrial leaders assembled last week in Washington, D.C. "I think we'll see more of that," he said.

Mellado's prediction capped a day of handwringing about the state of the U.S. scientific enterprise. The meeting was held to assess the country's response to a 2005 report by the U.S. National Academies titled *Rising Above the Gathering Storm. Energizing and Employing America for a Brighter Economic Future* (*RAGS*).

A parade of speakers gave the federal government failing grades for not heeding the recommendations in *RAGS* for bigger research budgets, more undergraduate scholarships and graduate fellowships, changes in immigration policy, and an improved environment for innovation (*Science*, 21 October 2005, p. 423). "We have attract[ed] substantial bipartisan support for the notion of investing in research," notes Robert Berdahl, president of the 60-member Association of American Universities in Washington, D.C., citing passage last summer of the America COMPETES Act, a nonbinding promise to fund many of the recommendations in the report (*Science*, 10 August 2007, p. 736). "But we've made no progress in making it a reality. It's a failure of leadership by both the White House and Congress, and it's very disappointing."

Much of that disappointment stems from the last-minute collapse in December of plans to give several science agencies double-digit increases in 2008 (*Science*, 4 January, p. 18). So meeting organizers tried to rally support for adding up to $900 million to the current budgets of the U.S. National Science Foundation, the Department of Energy's Office of Science, and the National Institute of Standards and Technology. President George W. Bush opposes the idea—now pending in Congress as part of a supplemental spending bill to fund the wars in Iraq and Afghanistan—even though he asked for the entire amount more than a year ago as part of his American Competitiveness Initiative (ACI). And three Cabinet secretaries delivered the Administration's message that the Democratic-led Congress is to blame for failing to fully fund ACI. Still, the bipartisan appeal of innovation was evident as seven legislators, representing both parties, described their faith in the country's ultimate ability to compete in a global economy.

The exception to that gloomy report card may be efforts to improve precollege science and math education, with an emphasis on improving the skills of middle and high school teachers. Much of the progress is due to private funding substituting for the proposed government increases. "We couldn't afford to wait for the federal government to act," says Tom Luce, a retired Dallas lawyer and former Department of Education official who is chief executive officer of the National Math and Science Initiative. NMSI, a $140 million effort funded principally by the ExxonMobil Foundation, underwrote last week's meeting.

Last fall, NMSI gave grants to 12 university-based programs to replicate an approach developed at the University of Texas, Austin, called UTeach that draws math and science majors into teaching careers (*Science*, 1 June 2007, p. 1270). Some 52 institutions applied for the 5-year, $2.4 million awards, which Luce sees as resounding support for the idea of scaling up something that has been shown to work. But Luce says that federal dollars—the COMPETES legislation authorizes $150 million a year for the UTeach effort—are needed to take the program nationwide and begin to reverse the huge problem of sending science and math teachers into classrooms with inadequate preparation in those fields.

The higher education community seemed especially disappointed that the report's warning of a "gathering storm" hasn't stirred public interest in strengthening U.S. science, as the Soviet Union's launch of Sputnik did a little more than 50 years ago. Even the popular idea of a national project to achieve clean energy independence, as Senator Lamar Alexander (R-TN) proposed at the meeting, hasn't resonated with the public, notes C. D. "Dan"

CREDIT: HENAAC K-12 EDUCATION PROGRAMS

The moral brain 734
Science news & views 740

Mote, president of the University of Maryland, College Park, and a member of the panel that produced the *Gathering Storm* report.

"The country responds to a crisis, preferably one involving national security," says Mote. "But the country doesn't see a crisis. Congress doesn't see a crisis. People complain about $4-a-gallon gasoline, but nobody sees the connection to not developing enough alternative energy technologies. They blame it on not drilling in ANWR [the Arctic National Wildlife Refuge] or on gasoline taxes." Mote says that the cost of the recently passed economic stimulus package—$168 billion in checks of up to $600 to taxpayers—"could pay for *RAGS* for a decade. As it is, the money doesn't do a damn thing about the underlying problem."

That shortsightedness also bothered veteran CBS reporter Bob Schieffer, who moderated an opening panel. "Is our way of life so good that we have forgotten how we got here?" he wondered. Craig Barrett, former CEO of Intel and another co-author of the *Gathering Storm* report, replied with a stinging indictment of the current political system. "There will be winners and losers," he replied, "and the losers are the ones who insist on looking backwards." Mellado believes that he has met the people who are looking ahead, and it worries him.

–JEFFREY MERVIS

ARCHAEOLOGY

Ancient Algae Suggest Sea Route for First Americans

Evidence is rapidly accumulating that the first Americans came from Asia and spread throughout the New World by at least 14,000 years ago (*Science*, 4 April, p. 37). But did they come by land or by sea? A paper on page 784 of this issue provides some support for the hypothesis that they took the coastal route rather than traveling inland. At the least, the report provides strong evidence that the earliest Americans used algae and other marine resources for food and medicine, and it seems to clinch early dates for one of archaeology's most controversial sites.

The paper "provides a nice seaweed garnish" for the coastal hypothesis, says archaeologist Jon Erlandson of the University of Oregon, Eugene, one of its leading proponents. Geoarchaeologist Michael Waters of Texas A&M University in College Station agrees, adding that the coastal route allowed "for the very rapid movement of people from North to South America."

For the past 30 years, archaeologist Tom Dillehay of Vanderbilt University in Nashville, Tennessee, and his Chilean and American co-workers have been excavating at the southern Chilean site of Monte Verde. The site is replete with evidence of long-term occupation such as huts, tents, and hearths and was previously radiocarbon-dated to 14,200 to 14,600 years ago. Thus, the site has been pivotal to claims that humans arrived in the Americas before the 13,000-year-old Clovis culture, although some researchers challenged the ancient dates.

At the water's edge. This sandy Pacific coastline was one source of seaweed which was found in what may have been an ancient medicinal hut (excavated foundation, inset) at Monte Verde, Chile.

CREDIT: IMAGE COURTESY OF T. D. DILLEHAY

Most recently, while sifting through previously excavated sediments from hearths and floors, the team recovered the remains of nine species of marine algae plus three stone tools. One tool had seaweed remains on its working edge. Direct radiocarbon dates on two of the seaweed samples both clocked in at about 14,000 years.

The new dates "remove any lingering doubts about the antiquity of human presence at that site," says archaeologist Daniel Sandweiss of the University of Maine, Orono, who had earlier counted himself among Monte Verde's skeptics (*Science*, 22 October 1999, p. 657).

Back 14,000 years ago, Monte Verde was located about 90 kilometers east of the sandy Pacific coast and 15 kilometers north of a rocky-shored inland marine bay. Algae from both environments were recovered, including inedible species that are today used as medicines in Chile and elsewhere. Moreover, the algal species found are known to flourish at different times of the year, suggesting to Dillehay's team that the Monte Verdeans were intimately familiar with coastal resources, possibly because they had originally arrived in the region via that route. Erlandson agrees: "The variety of seaweeds implies a pretty deep knowledge of coastal ecosystems and a long history of exploiting them."

Yet the people of Monte Verde also consumed a wide variety of inland plants, including wild potatoes. "There is logic on the side of a coastal route," says Sandweiss, but "it's impossible to say as yet" whether these ancient people might have arrived overland and discovered the bounties of the sea later. Dillehay concedes that this issue is unresolved. "Monte Verde just raises more questions and issues," he says. "We need more data."

–MICHAEL BALTER

GENOMICS

Genome Speaks to Transitional Nature of Monotremes

Zoologists have always thought that the platypus was a missing link in the chain between reptiles and mammals. The furry beaverlike mammal lays small, round, leathery eggs from a reptilelike cloaca, and the hatchlings slurp milk from modified sweat glands off the mother's stomach. Now an analysis of the genome reveals how platypus DNA is also an amalgam of mammalian and reptilian features. Wes Warren of the Genome Sequencing Center at Washington University in St. Louis, Missouri, and 100 authors describe these features in the 8 May issue of *Nature*.

Mammals divide into three groups. Most—from whales to shrews—are eutherians with highly developed placentas. Some are marsupials, which, like kangaroos and opossums, give birth to and then provide milk for immature young outside the womb. The platypus and its cousins, the echidnas, are all that remains of the monotremes, which branched from the marsupials and eutherians some 166 million years ago. "If there is something between reptiles and mammals, it's monotremes," says Stephen O'Brien of the U.S. National Cancer Institute in Frederick, Maryland.

The new genome sequence confirms the ancient split between monotremes and other mammals. "It's a missing part of the big evolutionary genetics puzzle," O'Brien adds.

The clearest traces of the journey from reptile to mammal come from tracking the yolk and milk genes. Chickens have three vitellogenin egg yolk genes; the platypus has just one left. But the casein milk protein genes that mammals have but reptiles don't are all there. And just as in other mammals, in platypus, they are clustered next to the tooth enamel genes from which they are thought to have evolved, the researchers report.

The story of the platypus' march away from the reptilian world is also told in the sex chromosomes. According to Jenny Graves of the Australian National University in Canberra, sex chromosome-wise, "they do it like a chicken." Typically, male mammals have X and Y sex chromosomes, with the Y chromosome carrying a male sex-determining gene called *SRY*. Male birds have two Z chromosomes, which carry a gene called *DMRT1* that is involved in male gender determination in fruit flies, humans (although it's not on the Y chromosome), and, most likely, birds. At first, cytologists thought the platypus was like the mammal. It had X and Y chromosomes, albeit five pairs of them, and it was thought that they were essentially humanlike. Then in 2004, Graves's lab discovered that one of these "X" chromosomes carried *DMRT1*. The genome sequence now shows that one of the platypus X chromosomes (*X5*) has more than just that one bird gene. It's almost entirely equivalent to the chicken Z chromosome. "We suspect *DMRT1* is involved in the platypus sex determination," says Frank Grützner, Graves's former postdoc, who now heads a lab at the University of Adelaide in Australia.

Gene regulation also seems to be more primitive, as platypus genes do not show parental imprinting. In marsupials and eutherians, imprinted genes are dialed to different settings and sometimes shut down altogether, depending on whether they originated from the male's sperm or the female's egg. According to Andrew Pask and Marilyn Renfree of the University of Melbourne, the distribution of repetitive DNA elements in this monotreme may explain the difference. As in other mammals, about 50% of the platypus genome is comprised of repetitive DNA. But although these repeats pepper imprinted genes in marsupials and man, they are largely absent from the equivalent genes in platypus. "Repetitive elements may have been useful for establishing imprinting in the other mammals," Pask suggests.

Another feature the platypus shares with reptiles is that it makes venom, which it delivers from a hind leg spur. The genome analysis indicates that, like snake and lizard venom, platypus venom appears to have evolved from antimicrobial genes known as defensins. However, according to Kathy Belov of the University of Sydney, the platypus genes evolved independently.

A big surprise is the platypus's large endowment of a particular class of vomeronasal receptor genes—about 1000 of them—based on the analysis by Doron Lancet and Tsviya Olender of the Weizmann Institute in Rehovot, Israel. "A typical mammal has a couple of hundred of them," says Lancet. Unlike olfactory receptors, which detect only airborne compounds, these receptors are more like nasal taste buds, able to detect nonvolatile compounds. For instance, dogs taste pheromones in urine by touching their tongue to the vomeronasal organ in their upper palate. Because the platypus spends 90% of its time in water, Lancet speculates that the platypus uses these receptors for detecting water-soluble odorants.

"Looking at the venom, egg, and milk genes is really interesting, but as with comparisons between opossum, mouse, and human genomes, the protein-coding sequences don't explain the interesting developmental transitions," notes John Mattick of the University of Queensland in Brisbane, Australia. Differences in gene regulation, most likely, provide the answer. And in this respect, the platypus researchers still have their work cut out for them, he adds. "[Gene regulation] information is there but is not yet understood."

–ELIZABETH FINKEL

Elizabeth Finkel is a writer in Melbourne, Australia.

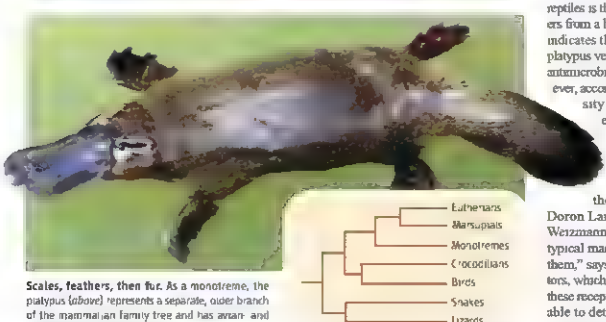

Scales, feathers, then fur. As a monotreme, the platypus (*above*) represents a separate, older branch of the mammalian family tree and has avian- and reptilianlike genetic features.

CREDIT: D. PARKS & E. PARKS COOKE/AUSCAPE

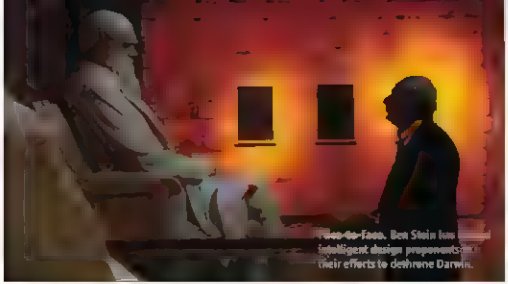

Face-to-Face. Ben Stein has [illegible] intelligent design proponents in their efforts to dethrone Darwin.

EVOLUTION IN THE SCHOOLS

States Push Academic Freedom Bills

If creationism is a mutating virus, as many educators believe, then its latest guise is legislation to protect "academic freedom."

Politicians in five U.S. states are pushing bills to enable educators to teach alternatives to evolution by protecting them "right" to discuss with students the idea of intelligent design (ID). Last week, scientists in Florida heaved a sigh of relief when the state legislature adjourned without reconciling differing versions of a bill seen as promoting ID. Similar legislation appears to have a good chance of passing in Louisiana, however, and is gathering steam in Missouri. Bills have also been introduced in Alabama and Michigan.

The language in the bills is modeled on a statute drafted by the Discovery Institute in Seattle, Washington, a prominent ID think tank. "They provide a permission slip for teachers to teach creationism—as long as it's called 'science,' " says Eugenie Scott of the National Center for Science Education in Oakland, California. "If any one of them passes, it is going to be very encouraging to creationists in other states." Backers are hoping for a lift from a current movie with actor Ben Stein, called *Expelled*, that accuses scientists of silencing those who question evolutionary theory.

In Florida, ID supporters lobbied for a bill that would protect teachers from being "disciplined, denied tenure, terminated, or otherwise discriminated against for objectively presenting scientific views regarding biological or chemical evolution." On 23 April, the state Senate passed it by a vote of 21 to 17. But the House sponsor, D. Alan Hays, replaced the Senate language with a single line that instead would require public schools to provide "a thorough presentation and critical analysis of the scientific theory of evolution." Hays's legislative assistant, Tiffany Rousseau, told *Science* that the change was made due to fears that conferring protection upon teachers "might be unconstitutional."

On 28 April, the House voted 71–43 in favor of Hays's legislation. But attempts at reconciliation failed. Senator Ronda Storms, who sponsored the bill, told the *Florida Baptist Witness* that "the House vehicle [had] veered off of the sure path to our destination."

In Louisiana, state senators voted unanimously that the state school board should promote "open and objective discussion of scientific theories . . . including, but not limited to, evolution, the origins of life, global warming, and human cloning." A House committee was expected to take up the measure this week.

"It has been difficult to rally opposition," says Barbara Forrest, a philosopher at Southeastern Louisiana University in Hammond. Forrest and other educators have formed the Louisiana Coalition for Science in a bid to block the legislation. Backers of the bill include the conservative Louisiana Family Forum.

Groups opposed to teaching creationism are likely to challenge any proposal that becomes law. But they would prefer to defeat the movement earlier. "One can reasonably conclude that the freedom [these bills] are trying to empower teachers with is to present the same material that was found unconstitutional in the Dover case, namely intelligent design," says Eric Rothschild, who represented the plaintiffs in their suit against the Dover, Pennsylvania, school board (*Science*, 6 January 2006, p. 34). But mounting a judicial challenge could be a costly and time-consuming process, Rothschild warns: "It's always better for bad laws to be avoided by legislators themselves."

—YUDHIJIT BHATTACHARJEE

SCIENCESCOPE

FDA Drops Helsinki Rules

Drug companies doing clinical trials outside the United States will no longer have to follow long-standing international ethical guidelines to pass muster with the U.S. Food and Drug Administration (FDA). Agency officials say that the Declaration of Helsinki, adopted in the 1960s, favors available treatments over placebos, which FDA prefers in some circumstances. The periodic amendments to the declaration could create confusion among drug companies, they add. "We're saying that our regulations should not depend on any documents outside our control," says FDA's Rachel Behrman.

In criticizing FDA's decision last week to reject the declaration, Peter Lurie of Public Citizen, a public interest group in Washington, D.C., says the agency is sending a message that the United States is exempt from international guidelines. —JENNIFER COUZIN

The Next Lyme Battle

The Infectious Diseases Society of America (IDSA) is bracing for a new public review of its stance on Lyme disease now that Connecticut Attorney General Richard Blumenthal has ended an investigation of alleged financial conflicts. The society has opposed as dangerous the long-term use of antibiotics, a practice favored by some activists and doctors. Last week, Blumenthal agreed to drop an 18-month probe in return for IDSA's promise to reconsider its treatment guidelines. Disease activists had faulted IDSA members for taking fees from insurance companies. "We hope [last week's settlement] clears the air," says IDSA spokesperson Steven Baragona. The society's next step is setting up a panel of certified conflict-free experts who will reconsider the 2006 guidelines. —ELIOT MARSHALL

Clearing the Air

New York City officials heard a plea last week to turn back an attempt to control the proliferation of environmental monitoring devices. Pending legislation that would require users to obtain a permit and give the police department broad powers of enforcement is a bad idea, environmental and public health organizations and universities told a city council panel. Exempting devices used for teaching, research, and industrial hygiene would help, they said, although retaining emergency authority to confiscate instruments might still impede science.

The bill is an attempt to keep track of devices that might provide early warning of terrorist attacks and to prevent false alarms. —ELSA YOUNGSTEADT

INTELLECTUAL PROPERTY

Chinese Province Crafts Pioneering Law to Thwart Biopiracy

GUIYANG, CHINA—Two years ago, a Chinese company hit upon a winner. The company planned to market a kind of sweet, sticky rice that Kam (Dong) people have cultivated for generations, without using chemical pesticides or fertilizers, on the terraced hillsides of southern China's Guizhou Province. That was the beginning of an entrepreneurial success story—especially for the Kam. Provincial legal experts intervened, helping Kam chieftains trademark the rare organic rice varieties and forcing the company and others to negotiate deals to return a percentage of profits to the Kam.

Guizhou officials are now hoping to build on this concept and head off any future attempts at "biopiracy"—the plunder of natural resources—by enshrining the protection of indigenous knowledge into law. Guizhou Intellectual Property Office (GIPO) in Guiyang, the provincial capital, has dispatched experts to enclaves of Kam, Hmong (Miao), and other ethnic minorities to assemble a compendium of know-how—from medicinal plants to embroidery techniques—that may merit legal protection. Such communities were once isolated and had no need to worry about theft of their traditional knowledge, says Long Yu-Xiao, director of the Chinese Institute for Indigenous Knowledge and Culture Property at Guizhou University in Guiyang. Globalization has changed that, he says. "Pandora's box is open."

Long and other experts are helping GIPO draft China's first legislation that would treat indigenous knowledge as intellectual property (IP). Their inspiration is the 15-year-old Convention on Biological Diversity, or biodiversity treaty, which seeks to balance innovation with the protection of biodiversity and fair compensation for traditional knowledge sources. "The legislation is not idealism, it's not romantic. It's realistic," says Li Fayao, Long's deputy and a researcher at the Guizhou Academy of Social Sciences. The focus is not on future scientific finds but on "actual circumstances in this province."

The effort is one facet of China's ambitious drive to bring its feeble and patchy enforcement of IP rights into line with international norms. Later this month, the State Intellectual Property Office is expected to release a national IP strategy that would strengthen rights of both domestic and foreign companies as well as increase penalties for piracy. And the Supreme People's Court last month announced that foreign experts will now be permitted to testify in patent-infringement cases involving foreign parties.

But by spinning a legal web of protection around indigenous know-how, Guizhou would enter uncharted waters for China. "Guizhou is regarded as an undeveloped province. Its scientific level is relatively low, but it's rich in traditional knowledge. Because we lack the means to turn knowledge into innovation, we have to protect the knowledge for future development," says GIPO vice-director An Shouhai, who trained as a plant physiologist and who initiated the legislation.

Other countries have made similar attempts to reconcile indigenous know-how and IP rights. But Guizhou is an interesting test case, says Shalini Bhutani, an environmental lawyer based in New Delhi for GRAIN, a nonprofit. Hmong, for instance, live in Laos, Thailand, and Vietnam. "What happens with shared knowledge across borders?" she asks. Guizhou's effort is also timely, as the issues provincial authorities are grappling with are at the heart of negotiations over a global regime for sharing traditional knowledge benefits that will be discussed later this month at the 9th conference of parties to the biodiversity treaty in Bonn, Germany. Conferees aim to devise policies that would achieve a target agreed to 6 years ago, to reduce the rate of biodiversity loss by 2010.

GIPO plans to present its legislation for approval in the provincial People's Congress by the end of the year. First, however, legal experts must settle a thorny issue. Which forms of indigenous know-how should be treated as IP? It's a tricky balancing act. "If the protection is too narrow, indigenous people may choose not to share their knowledge or know-how. Then everybody loses," says Zang Xingdong, a law professor at Guizhou University.

The Kam rice experience has helped shape Guizhou's draft legislation. Although most Kam farmers over the years have switched to the more common Indica rice, farmers in two counties—Li Ping and Cong Jiang—have stuck with their traditional varieties. "These villages have the last Kam sweet rice gene pool," says Long. "They have been able to preserve their varieties against genetic contamination from Indica strains."

By helping Kam chieftains register a trademark for "Kgoux Bagx Dangl" rice, Long's group gave the farmers leverage over companies that wanted to market the rice. "Of course the companies resisted," Long says.

CREDIT: P. STONE/SCIENCE

Shared heritage. Who should own the rights to rare rice varieties in Guizhou's terraced hills, or to Hmong costumes?

"But once the Kam acquired this right, they could get capital and work with an outside company without being dominated. They had the power to negotiate." To distribute any income from a marketing deal, Long's group used a new national law on rural development to help Kam farmers organize a cooperative.

Guizhou's draft legislation is, in part, a patchwork of statutes from existing laws on IP, ethnic minorities, and rural development. "We're taking statutes and integrating them in a creative way to build a new legal framework," Long says. A key task has been to define the legal concept of traditional knowledge to the exclusion of other legal concepts that are already protected. "Not all traditional knowledge must be protected," An says. Existing legal regimes cover the protection of cultural relics—legally defined as objects of cultural value made before 1966—and species.

GIPO is putting a heavy emphasis on indigenous medicines. One test case is a medicinal grass called *guanyin cao* that Hmong use to treat coughs and colds. Like many traditional Chinese medicine (TCM) remedies, *guanyin cao* is brewed as a tea. If a company were to identify the active ingredient and develop it as a drug, the innovation would win patent protection and the source of know-how could end up empty-handed. "Companies can misappropriate traditional knowledge by taking advantage of loopholes in the existing legal regime," says Long. Many prescriptions in other countries are based on open publications of TCM ingredients. "In these instances, there's nothing we can do about it; the law cannot protect the original TCM," says An. But Guizhou has a window of opportunity to protect the lesser known medicines of the Hmong and Kam. "That's why we are taking action and working on this pioneering legislation," Long says.

The Guizhou legislation would ensure that any innovation based on traditional know-how would return a portion of profits to the source of the knowledge. That principle is not controversial, although it may take some creativity to figure out how best to divvy up royalties. "One difficulty is how to divide IP rights. Do they belong to the community, the collective?" asks Lei Xiuwu, director of the Ethnic Research Institute in Kaili. "An IP system inherently based on private rights may not have solutions for the 'protection' of traditional knowledge, which is a shared heritage," adds Bhutani.

But the draft legislation may go further and provide legal protection to ancient wisdom—such as the Hmong's insight in the use of *guanyin cao* to treat cough. Guizhou's experts are struggling to determine where to draw the line: what is unique, and what kind of protection it should be afforded. Another issue is whether to regard customs and handicrafts as IP. "In a narrow sense, traditional knowledge only means traditional scientific knowledge. But our understanding is that it also includes traditional culture," says An.

In a courtyard on a misty hilltop in Nanhua, a village in the Hmong heartland in southeastern Guizhou, several young women wheel in sync around a tall wooden totem devoted to a butterfly god. They execute graceful dips and pirouettes under the weight of several kilograms of silver jewelry and ornaments, including elaborate headdresses. A trio of young men steps to the fore, playing a Hmong ballad on bamboo flutes called *lusheng*. Hmong have worn these hand-embroidered garments, danced these dances, and played and sung these songs at festivals since time immemorial. But is the living tradition IP? GIPO thinks so. "All these deserve protection as traditional knowledge," says An.

"Because we lack the means to turn knowledge into innovation, we have to protect the knowledge for future development."

—AN SHOUHAI, GUIZHOU INTELLECTUAL PROPERTY OFFICE

As Lei notes, many museums outside China purchased Hmong dresses decades ago. "But legally acquiring a dress does not mean you own the traditional knowledge. You cannot say the information belongs to that museum. We have to protect the information," he says. "There is no easy formula," adds Long.

If Long and his colleagues succeed, knowledge may not mean power for Guizhou's indigenous peoples, but it might help ensure their survival—or even prosperity—in today's global village.

—RICHARD STONE

CREDIT: R. STONE/SCIENCE

Korea Targets Basic Science

Worried about a widening deficit in high-tech trade, South Korea's President Lee Myung-bak said last week that he wants overall research spending to rise from 3.2% to 5% of the country's gross domestic product by 2012. Insiders say his Administration, which took office in February, wants to lead the way by doubling government spending.

The government currently funds about one-fourth of the $30 billion now spent on research. Private-sector spending is targeted at applications, and 75% of government spending goes to applied areas. Officials in the Lee Administration hope to make basic research half of the government's overall portfolio. Yu Hee-Yol, chair of the governmental Korea Research Council of Fundamental Science & Technology, says the country's scientists and engineers are "very excited about" the new funding targets. —DENNIS NORMILE

Solar Sensor Back on Board

A key climate sensor has been restored to the $12 billion National Polar-Orbiting Operational Environmental Satellite System (NPOESS). The Total Solar Irradiance Sensor (TSIS) had been removed along with four other key climate sensors in 2006 when the Pentagon restructured the program (*Science*, 31 August 2007, p. 1167). But lawmakers and officials who run NPOESS vowed to fix the problem, and last week, managers announced that the sensor will fly on the first NPOESS mission in 2013.

"It's fabulous," says space scientist Judith Lean of the Naval Research Laboratory in Washington, D.C. The last scheduled flight for the sensor had been as part of a NASA payload in 2010. Lean says it's important for TSIS missions to overlap for proper calibration. "Without that important [solar] record, the whole climate field is up for speculation," she says. —ELI KINTISCH

Not So Presidential

The 99 winners of the annual Presidential Award for Excellence in Mathematics and Science Teaching came to Washington, D.C., last week to be feted and to learn about federal efforts to improve science and math education. But for only the second time in his 8-year term, neither President George W. Bush nor his wife, Laura, hosted them at the White House. Coincidentally, the visit overlapped with a symposium in which academic and industrial leaders bashed the government for its inadequate support of science (see p. 728).

—JEFFREY MERVIS

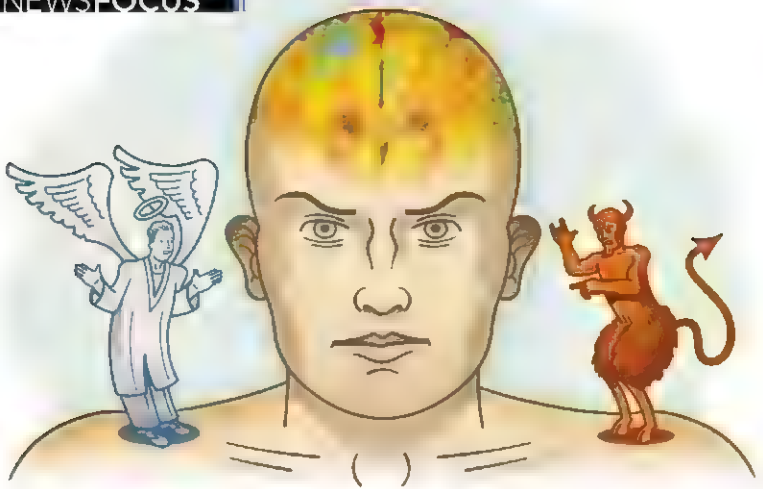

The Roots of Morality

Neurobiologists, philosophers, psychologists, and legal scholars are probing the nature of human morality using a variety of experimental techniques and moral challenges

A team of psychologists recently asked dozens of college students to consider several morally charged situations. In one, a friend lies on his résumé to land a job; in another, survivors of a plane crash consider cannibalizing an injured boy to avoid starvation. Students who pondered these hypothetical scenarios while sitting at a filthy desk with sticky stains and a chewed-up pen rated them as more immoral, than did students who sat at a pristine desk. In another version of the experiment, a nearby trash can doused with novelty fart spray had a similar effect. The findings, in press at *Personality and Social Psychology Bulletin*, demonstrate that emotions such as disgust exert a powerful influence on moral judgments, even when they are triggered by something unrelated to the moral issue, says study co-author Jonathan Haidt, a psychologist at the University of Virginia, Charlottesville.

Haidt is one of a growing number of researchers taking an experimental approach to investigating the nature of human morality. The field has drawn practitioners from diverse backgrounds including philosophy, psychology, and neuroscience. They don't always see eye to eye, but they are united in their belief that the scientific method will yield fresh insights into questions that have vexed philosophers for centuries.

One area of intense interest is the interplay of emotion and reason in moral decision-making. Haidt argues that people rely on gut reactions to tell right from wrong and employ reason mainly when they try to justify their intuitions after the fact, not unlike an art museum visitor who is struck by the beauty of a painting but struggles to explain why. Not everyone accepts this view, but other researchers do see evidence that moral judgments are surprisingly automatic. "I think there is an emerging consensus that things happen pretty quickly and that explicit conscious reasoning is not where the action is," Haidt says.

This automaticity has led some researchers to suggest that the human brain has built-in moral instincts. Cognitive neuroscientists are already hunting for the underlying neural mechanisms. At the same time, psychologists and anthropologists are searching for evidence of universal moral principles shared by all people. Others are interested in how morality differs from culture to culture. They are using techniques that include brain imaging and online questionnaires to probe the roots of morality, and some researchers are viewing the development of moral principles through the lens of evolution.

The work is likely to yield a better understanding of our moral intuitions and where they come from, says Walter Sinnott-Armstrong, a philosopher at Dartmouth College. Philosophers, from the ancient Greeks on, have tried to answer these questions mainly through introspection, an exercise that has often amounted to seeking new arguments for a previously held conviction, says Sinnott-Armstrong, who has recently begun some experimental work of his own. "One thing that's fascinating about science is you don't know where you're going to end up."

CREDIT: PETER HOEY

Dissecting moral cognition

Two 18th century thinkers have had a huge influence on moral philosophy: David Hume, a Scotsman, who argued that passions drive moral judgments, and Immanuel Kant, a German, who countered that dispassionate reason is, or ought to be, the driving force. The clash between these two philosophical titans still reverberates today.

Lately, Hume seems to be gaining an edge, thanks to the work of Haidt and others. In an influential 2001 paper in *Psychological Review*, Haidt describes an experiment in which he and colleagues asked people to consider a hypothetical situation involving a brother and sister who decide to have sex. They use two forms of birth control, enjoy the experiment, but decide not to do it again. Most people took little time to condemn the siblings' actions as morally wrong but then struggled when pressed to explain why. After all, there was virtually no chance of conception and the vignette had made it clear that the siblings were not emotionally scarred by the experience. Many of the volunteers eventually resorted to an explanation along the lines of "I just know it's wrong." If people were reasoning their way to an opinion, Haidt argued, they wouldn't be so dumbfounded when asked to explain it.

In more recent work, Haidt has investigated whether manipulating emotions can alter moral judgments. The messy desk experiment suggests that it can, as does an earlier study in which Haidt and then-graduate student Thalia Wheatley used hypnotic suggestion to trigger a wave of disgust in volunteers as they read vignettes about morally dubious behavior. Volunteers issued harsher moral judgments for vignettes containing a cue word that triggered the hypnotic suggestion than they did for an alternative version with slightly different wording. Wheatley and Haidt reported in 2005 in *Psychological Science*.

Disgust even raised people's moral suspicions when the act described was innocuous. One scenario described a student council member picking topics for faculty-student discussions. When this vignette contained the disgust-triggering cue word, subjects rated the student's activities as less morally appropriate. "It just seems like he's up to something," one wrote.

Other evidence that emotions guide moral judgments comes from work with people who've suffered damage to brain regions that mediate emotion. In a 2007 paper in *Nature*, a team led by Michael Koenigs of the University of Iowa, Iowa City, and Antonio Damasio of the University of Southern California in Los Angeles reported that people with damage to the ventromedial prefrontal cortex made abnormal judgments on hypothetical moral dilemmas that forced them to consider whether it was permissible to sacrifice the life of one person to save several others. These scenarios included variants of the so-called trolley problem, a favorite tool of morality researchers. One version puts the subject behind the wheel of a runaway trolley headed toward five hapless workers, the only way to save the five is to hit a switch on the dashboard that would divert the trolley to a track with just one worker. Healthy volunteers and lesion patients alike tended to say this was acceptable. The two groups differed, however, on a more emotionally charged version of the dilemma in which the only way to save the five is to shove a large man off a footbridge to stop the runaway trolley. Although the same utilitarian logic applies—kill one to save five—healthy subjects found this option harder to stomach: only about 20% said it would be permissible. But twice as many of the brain-damaged subjects said they would shove the man, suggesting that their damaged emotional circuitry made them unusually likely to pick the utilitarian option.

Jorge Moll, a neuroscientist at Labs D'Or Hospital Network, a private medical and research institute in Rio de Janeiro, Brazil, views the ventromedial prefrontal cortex as part of a network of brain regions underlying "prosocial sentiments" such as guilt and compassion. Moll and colleagues reported last year in *Social Neuroscience* that this brain region is activated by viewing morally evocative photographs, such as ones of a hungry child, even when no judgment is required. In a 2006 paper in the *Proceedings of the National Academy of Sciences* (*PNAS*), he and others reported that the same region is activated when volunteers elect to donate money to charity. Moll views prosocial sentiments as the core of morality and thinks they arose from ancient mechanisms that evolved to enable our ancestors to form social attachments and cooperative groups.

The Koenigs study contains hints that emotions aren't the entire story, however, says co-author Marc Hauser, a cognitive scientist at Harvard University. He points out that the lesion patients still made normal judgments in many situations, particularly regarding dilemmas that didn't tug at the emotions and "easier" ones that are emotionally charged but elicit strong consensus among healthy subjects that it's wrong, for example, to earn money to feed your family by allowing your young daughter to appear in a pornographic film, even in hard times. "That rules out the strong version of the hypothesis that emotions are causally necessary for making [all] moral judgments," Hauser says. "That just can't be right."

Don't get all emotional

An alternative view, championed by Joshua Greene, a cognitive neuroscientist and philosopher at Harvard, is that when people grapple with moral dilemmas like the trolley problems, emotion and rationality duke it out in the brain. In Greene's view, the key difference between flipping the switch and shoving the man off the footbridge is that the latter evokes a negative emotional reaction that overrides cold utilitarian logic.

In a 2001 *Science* paper, Greene, then a postdoc with Jonathan Cohen at Princeton University, and colleagues reported that the medial frontal gyrus and other brain regions linked to emotion become more active when people contemplate "personal" moral dilemmas—such as shoving the man onto the trolley tracks or removing a man's organs against his will to save five transplant recipients—compared with when they weigh impersonal moral dilemmas—such as flipping a switch to save the workers or declaring bogus business expenses on a tax return. These impersonal dilemmas preferentially activate a different set of brain regions thought to contribute to abstract reasoning and problem solving. Greene and colleagues reported in a follow-up study, published in 2004 in *Neuron*.

Based on these findings,

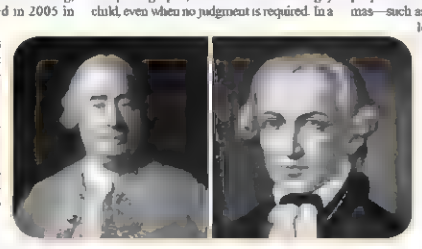

CREDIT: WIKIPEDIA

Philosophical difference. New studies tend to support the view of David Hume (*left*) that emotions drive moral judgments. Immanuel Kant (*right*) argued that reason should be the driving force.

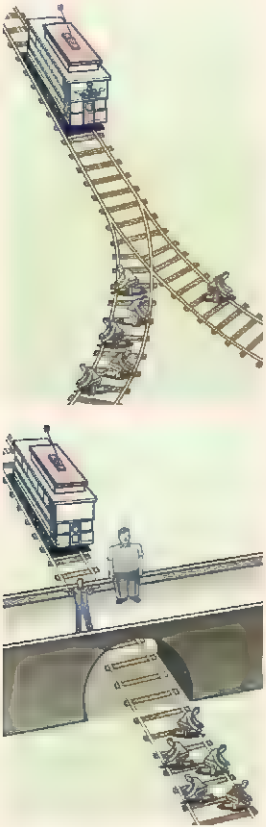

Moral dilemma. Is it morally acceptable to redirect a runaway trolley car hurtling toward five workers onto a track with just one worker? How about pushing a man off a footbridge into the path of the trolley to stop it before it hits the hapless workers? Most people say they would sacrifice one life to save five in the first scenario but not the second. In this case, emotion may trump utilitarian logic.

Greene envisions a tug of war between emotion and cognition in the brain. Emotions tell us we'll feel terrible if we push the man, cognition says: Push him! Five is greater than one. Greene suspects that the arbiter in this conflict may be a brain region called the anterior cingulate cortex. Previous studies have found that this region fires up when people wrestle with many types of internal conflicts, and it did so when subjects in Greene's study faced particularly difficult moral dilemmas.

In a recent study that mirrors Haidt's work with manipulating emotion, Greene and colleagues had college students evaluate moral dilemmas while grappling with an extra cognitive burden: searching for a particular number in a string of characters scrolling across a computer screen. The extra cognitive work slowed response times when students made utilitarian judgments but not emotional ones, the researchers report in an upcoming issue of *Cognition*. Greene sees the study as evidence that cognition is an important part of moral decision-making.

Getting off track?

Some researchers see the trolley problems as too artificial. "We don't have a lot of faith in using these esoteric examples," says Jordan Grafman, a cognitive neuroscientist at the National Institute of Mental Health in Bethesda, Maryland. The situations are so far-fetched that Grafman and others question whether they really engage the neural mechanisms involved in everyday moral reasoning. Everyday moral reasoning is likely to involve a memory component that's missing in Greene's account, Grafman says. "More often than not, we take a situation we've experienced in the past and compare it to the new one," he says. Brain-imaging studies done with more realistic scenarios might catch some of the underlying neural mechanisms, says Grafman, who is gearing up to do such an experiment in collaboration with Ralph Adolphs and colleagues at the California Institute of Technology in Pasadena, who have been collecting hundreds of real-life moral dilemmas experienced by people of different ages, education levels, and socioeconomic backgrounds. In a paper published online by *Science* this week (www.sciencemag.org/cgi/content/abstract/1153651), researchers led by Ming Hsu, now at the University of Illinois, Urbana-Champaign, and colleagues at Caltech report taking a different approach: scanning the brains of volunteers as they tried to decide the fairest way to distribute donations to a real-life Ugandan orphanage.

At the same time, some researchers argue that the emphasis on emotion and reason is too simplistic, akin to placing the ghost of Hume in one network of brain regions and the ghost of Kant in another. "It's like they take 18th century categories and try to do 21st century science," says John Mikhail, a legal scholar at Georgetown University in Washington, D.C. Mikhail, Hauser, and others point out that before emotion and reason can evaluate a given situation, the brain has to first answer questions such as who did what to whom, whether someone got hurt, and whether the harm was intentional.

For example, most people would condemn someone who tried to poison a friend's coffee but accidentally stirred in sugar instead of poison. It's the bad intention that matters, not the outcome. To investigate how the brain makes such distinctions, Hauser and Harvard graduate students Liane Young and Fiery Cushman recently teamed up with Rebecca Saxe, a cognitive neuroscientist at the Massachusetts Institute of Technology (MIT) in Cambridge. When volunteers read vignettes about intentional and unintentional harms, activity increased in the right temporoparietal junction (RTPJ), a brain region involved in sussing out other people's intentions. RTPJ activity was greatest for cases like the bungled poisoning in which someone tried but failed to inflict harm, the researchers reported last year in *PNAS*.

At last month's meeting of the Cognitive Neuroscience Society, Saxe and Young reported that interfering with RTPJ activity using a noninvasive method called transcranial magnetic stimulation caused people to downplay intentions and, for example, judge the attempted poisoning less harshly because ultimately no harm was done. Such findings demonstrate that the cognitive contributions to moral judgments aren't limited to the weighing of harms that's emphasized by trolley problems, Saxe says. Understanding intentions is another crucial component, and the RTPJ findings begin to hint at the neural mechanisms involved, she says.

A moral grammar

Some morality researchers see parallels in the study of language, particularly the

CREDIT: PETER HICKEY

influential work of MIT linguist Noam Chomsky, who has argued that humans have an innate capacity for language and that all languages share common principles—a universal grammar. Could there be an analogous moral capacity in the human brain and a universal moral grammar?

Mikhail began pondering these questions as a philosophy graduate student, during a year he spent working with Chomsky at MIT. To investigate, he administered trolley problems and other moral dilemmas to different groups of people, including children and people from non-Western cultures. If there is universal moral grammar, he reasoned, factors such as gender, age, education level, and cultural background should have little influence on the judgments people make. Preliminary results pointed in that direction, and Mikhail's initial work has been expanded and confirmed by Hauser, Cushman, and Young, who developed an online Moral Sense Test (moral.wjh.harvard.edu) that has been taken by more than 200,000 people from 120 countries. Chinese, Spanish, and Dutch versions are now up and running as well, and Hauser is collaborating with several anthropologists to gather similar data from remote indigenous populations in Guatemala, Papua New Guinea, Tanzania, and Bolivia. It's work in progress, Hauser says, but so far "it's looking like there's a lot of similarity across widely different cultures."

Mikhail, meanwhile, has been studying legal texts for clues to what the elements of a universal moral grammar might be. "The law is the one institution in most societies that's responsible for the practical matter of solving day-to-day moral problems that arise," Mikhail says. "The rules of law that have evolved over time, to my mind, are a really good first approximation of the unconscious rules that people use in moral judgments."

Flavors of morality

Although harm and fairness have been the focus of most research so far on the psychology and neuroscience of morality, some researchers think there's more to the story. Haidt argues for five psychological foundations of morality. He includes harm and fairness and adds loyalty, respect for authority, and spiritual purity (*Science*, 18 May 2007, p. 998). Other scholars have proposed lists of universal aspects of morality, and Haidt identified his five by trying to work out what they all had in common. He hypothesizes that all five exist in every culture but are emphasized to varying degrees. "I see them as being much like the five kinds of taste buds," he says. "If you go around the world, the cuisines differ in how much they rely on each one."

Haidt set up a Web survey (www.YourMorals.org) to evaluate how people weight the five foundations. More than 35,000 people have logged on so far, he says, and the findings suggest cultural differences in how people carve up the moral domain. In more liberal cultures, such as Western Europe and Australia, people emphasize harm and fairness over the others. In more conservative cultures, including South Asia and the Middle East, all five foundations are important. In the United States, which falls in the middle of the spectrum, Haidt and colleagues have found a similar divide between self-described liberals and conservatives. Liberals tend to downplay purity, for example, arguing that something can be indecent without being morally wrong, Haidt says. But it's a matter of degree: Although many liberals wonder why conservatives are so hung up on what types of sexual behavior are right and wrong, they have analogous hang-ups, often more symbolic than rational, about food that was processed in certain ways, or by people seen as either villains or victims. Haidt says he hopes the work will spur his colleagues, most of them two-foundation liberals like himself, to think beyond harm and fairness.

Sinnott-Armstrong agrees that morality is multifaceted. "It's not clear to me at all that all those judgments where we call different types of acts morally wrong are based on the same psychological or neurobiological mechanisms." He has been working on brain-imaging experiments to investigate whether different types of moral scenarios engage different neural circuitry.

Many researchers think moral cognition depends on neural mechanisms that also play roles in other types of social cognition and are likely present to some degree in our primate kin. Primatologists have found hints of a sense of harm and fairness even in monkeys, who will forgo food for days to prevent a neighbor from receiving a shock and will reject a small reward when they've learned that a given task usually earns them a larger one. Haidt speculates that morality is an elaboration of primate social behavior that evolved in part because it helped promote cohesiveness in groups of early humans, giving them an advantage over competing groups. Hauser agrees that morality probably has roots in primate social behavior. But that raises a puzzle about why moral decisions seem to feel somehow different, he says. "One of the problems for our field right now is when you say something is moral, how does the brain know it's moral as opposed to just social?"

The moral brain. Neuroimaging studies have linked several brain regions to moral cognition. Disruptions to the right temporoparietal junction (brown), which is involved in understanding intentions, or the ventromedial prefrontal cortex (green), which processes emotion, have been found to alter moral judgments. Greene and colleagues have suggested that activity in the anterior cingulate cortex (pink) signals conflict between emotion, reflected by activity in the medial frontal gyrus (blue) and other areas (orange, brown), and "cold" cognition, reflected by activity in dorsolateral prefrontal cortex (yellow).

It's too early to know where all of the empirical work on morality will lead. Forced to speculate, researchers can envision brain scans that could determine whether a defendant in a murder case had the mental capacity to tell right from wrong and lawyers who wear perfume formulated to sway the emotions—and verdict—of a jury. Sinnott-Armstrong says he can envision revised sentencing guidelines that take human psychology into account. "If we have a better understanding of morality, we'll have a better understanding of how [lawmakers] get their intuitions about how much punishment is deserved," he says. "We might find that [moral intuitions] are more reliable in some cases than in others."

Most likely of all, perhaps, the work may give us a better understanding of ourselves. However, reducing a noble human attribute such as morality to a matter of natural selection and brain activity may lead us into uncomfortable territory, says Saxe. "Even though we know this in hundreds of ways, it continues to be both fascinating and unsettling to find out that something you thought of as a feature of the self turns out to be a product of your brain." —GREG MILLER

CREDIT: K. SUTHERSHAE/SCIENCE

PLANETARY SCIENCE

To Touch the Water of Mars and Search for Life's Abode

The Phoenix lander will soon arrive at Mars to perform the first analyses of martian water and to probe the rocky polar soil as a habitat for life; it has been a struggle

The fortunes of planetary science had sunk about as low as they could go by the late 1990s. First, Mars Climate Orbiter missed its mark on 11 December 1998 and incinerated itself deep in the martian atmosphere—something about engineers' confusion over metric versus English units of rocket thrust. Then, less than a month later, Mars Polar Lander (MPL) headed in for its blazing atmospheric entry, parachute descent toward the surface, and soft, rocket-aided landing. It was never heard from again; why, no one knows for sure.

Now it's Phoenix's turn. On 25 May, the $420 million mission will attempt the first soft landing on Mars in 30 years on its way to search for what could be "the last viable habitat on Mars," as Phoenix principal investigator Peter Smith of the University of Arizona, Tucson, puts it. As its name suggests, Phoenix will attempt to rise from the ashes of Mars Polar Lander.

Team members inherited much of the mission's hardware and software from MPL and a second, canceled Mars mission, the Mars Surveyor 2001 Lander. Wringing the unseen risks out of flawed hand-me-downs created during NASA's ill-fated "faster, better, cheaper" era proved a challenge, but the team says it's as ready as it ever could be. "We've really worked the kinks out," says team member Caro Stoker of NASA's Ames Research Center in Mountain View, California. "We're really excited."

The excitement comes from the prospect of getting their hands—or at least a robot arm's scoop—on martian water. NASA has long followed the water on Mars in pursuit of life but always arrived billions of years behind its fleeting objective. With Phoenix, researchers expect not only to touch water frozen just beneath the surface but to "taste" and "smell" it using onboard laboratories. And if that ice ever melted long enough to harbor martian life, Phoenix could return evidence of that too. It might even detect the molecular remains of martian life, ancient or modern. But first it has to be ready for its 7 minutes of terror.

Out of the fast lane

Landing on Mars is all about stopping, explains Phoenix project manager Barry Goldstein of the Jet Propulsion Laboratory (JPL) in Pasadena, California. One minute the half-ton spacecraft is doing 20,500 kilometers per hour, and 7 minutes later it's supposed to settle gently on the surface. MPL apparently didn't survive its terrifying arrival at Mars. "We inherited a spacecraft that failed to land properly," says Smith. "We had to be suspicious of what we inherited." The advantage of a big inheritance, he adds, is that the engineering team had almost 4 years to work out the bugs before launch rather than the usual year or so.

A review board investigation in 2000 had concluded that the most likely MPL failure would have come as the lander extended its three legs while still riding its retrorockets down. An onboard computer could have mistaken the jolt of the leg extension for the impact of touchdown, the signal to turn off the rockets. The resulting 40 meters of free fall would have been the end of it. But "nobody could be sure" what the problem really was, Smith notes.

So the Phoenix entry, descent, and landing team tackled every trouble spot identified by the MPL review board and by the return-to-flight review of the eventually canceled 2001 mission. Then the team came up with some potential problems of its own. "We found over 12 particular items that were not on anyone else's list," says Goldstein, and "we've resolved those too." Problem resolution involves analysis and testing in the lab, in computer simulations, and in the field until the root cause of the problem is found.

Resolution did not always come easily. The lander's radar, for example, turned out to have a long list of failure modes, says Smith. The model—one flown on F-16 fighters—was adapted to measure velocities of a very different craft. "We did an enormous amount of testing and analysis," he says, including trying to fool the radar by flying it on a cable beneath a helicopter over a variety of terrains. Flawed computer code made the radar stumble all too easily. Testing it and fixing its problems accounted for much of the mission's $30 million cost overrun.

One problem that turned up late in testing never was solved. The Mars Descent Imager—originally built for the Mars Surveyor Lander—was going to snap downward-looking pictures from the descending lander. But testing showed that sending images to a data-handling component could silence the onboard gyroscope and produce another disaster. Lacking time and money for a redesign, engineers decided to keep the descent imager switched off.

Given all the time and money for testing, "the team feels confident they've done every test they would ever want to do," says Smith. And their efforts have not gone unnoticed. "You may not succeed," Gentry Lee of JPL—chair of one of a number of external review panels—told the team, "but you deserve to succeed."

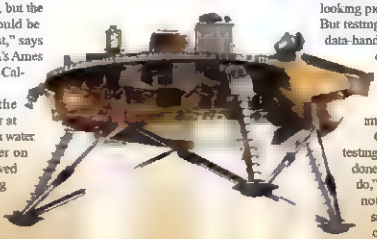

CREDIT: CORBY WAISTE, JET PROPULSION LABORATORY

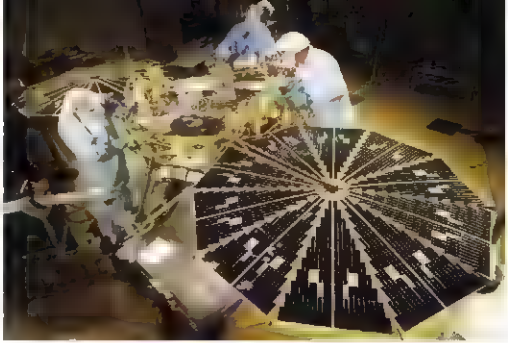

Twice measured, once cut. The Phoenix lander, on its way to analyze martian ice and soil, inherited much of its hardware from previous missions, one disastrous and one canceled. That required exhaustive testing of complex systems like the one for entry, descent, and landing.

Onto a sweet spot

While the engineers were working on getting a lander safely to the surface of Mars, the scientists were looking for a safe surface to land on. Both efforts operated under considerable constraints. The engineers couldn't test the entire landing system under actual martian conditions, only components. And the scientists were in the hunt for landing hazards that they couldn't see. They started by looking at some of the most inviting terrain on the planet, the smooth plains of the northern lowlands. It was there above 60° latitude that instruments on the orbiting Mars Odyssey had detected ice-rich soils (*Science*, 11 April 2003, p. 234).

So Raymond Arvidson of Washington University in St. Louis, Missouri, and other Phoenix team members gathered the usual data returned from Mars orbiters, including imaging to count potentially hazardous rocks. The available imaging could not resolve the smallest rocks that might pose a threat, but extrapolating their numbers from larger rocks had worked well before (*Science*, 16 June 2006, p. 1588). "Everything we had looked good in this region [called] B for 'best,'" says Arvidson. "It all looked pretty benign. We were happily moving along."

Then in November 2006, the HiRISE camera aboard Mars Reconnaissance Orbiter began its imaging mission in earnest. Able to resolve rocks as small as 1 meter, it promptly returned startling images of "boulders the size of minivans," as Smith puts it. Apparently, the repetitive temperature changes that create the distinctive "polygonal" patterning of the icy northern plains also work buried boulders upward to the surface. The rock counters, it turns out, had been counting not individual rocks but clusters of these reworked rocks, says Arvidson.

After 3 months of searching with HiRISE, "we found a good place, one of the few in the northern plains," says Arvidson: a broad blanket of fine-grained, boulder-free debris thrown out of a nearby 10-kilometer-wide impact crater.

Getting wet

Once safely on the surface, Phoenix can finally catch up with the water. At first, the ice itself will be nowhere in sight, even from the lander's camera tower or from the imager on the end of its 2.4-meter, scoop-equipped robot arm. But "there's a lot of ice where we're going," says Smith. "They say we'll hit very hard ice 2 to 6 centimeters down" beneath the loose soil. Researchers reach a similar conclusion whether they are interpreting neutron and gamma-ray remote sensing data from Odyssey, inferring ice depth from the dimensions of the polygonal patterning, or modeling martian water vapor permeating the cold soil and forming ice in its pores.

No one knows just what will turn up once the arm digs down to the ice. The arm will feed soil and ice samples to Phoenix's two analytical instrument packages. One will heat samples to 1000°C and feed the resulting gases to a mass spectrometer for molecular analysis. The other is a miniaturized wet chemistry lab for geochemical analysis.

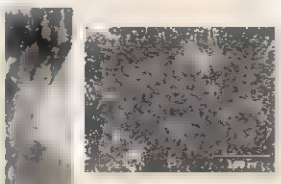

Looks good from here. Phoenix's soil and ice frozen "polygonal" terrain whose crinkliness is here accentuated by long shadows.

The Phoenix science team will combine these analytical capabilities with lander imaging—from instruments ranging from the arm-mounted camera down to an atomic force microscope—to seek out a habitable environment, or at least one habitable in the recent geologic past. Phoenix doesn't carry life-detecting instruments, says Stoker, "but if we found evidence of habitability—liquid water or organic compounds—that would make that environment the target for a future mission. That's what makes the landing site so exciting." If ice had melted during warmer summers thousands or millions of years ago, the liquid water might have left distinctive soil textures or leached salts from the soil and pulled the salts up toward the surface.

Finding life's organic matter could be more problematic. Any organic matter could be the remains of long past life or even of dormant life locked in the ice awaiting the next thaw. But it could also be never-living material carried in by the constant drizzle of meteorites. Back in the 1970s, the Viking landers looked for organic matter down to the parts-per-billion level and found none, not even the meteoritic sort. Mystified, many researchers have since concluded that Mars somehow generates strong oxidizing agents that obliterate any organics on or within the soil. They hope the ice at the landing site has protected the organics long enough for Phoenix to find them.

Phoenix has 90 days in its "nominal" mission to look for a likely place for life. Unlike the two ancient rovers still dragging themselves around the planet, Phoenix will not be operating much beyond its allotted time. It has only a dozen single-use sample vessels between the two instrument packages, and when "winter comes to the north, we're pretty much done," says Smith. Within a few months of the end of the nominal mission, the winter cold will wrap Phoenix in a thick blanket of carbon dioxide frost. If in the martian spring it rose once again from its icy tomb, Smith says, "I'd be absolutely dumbfounded."

–RICHARD A. KERR

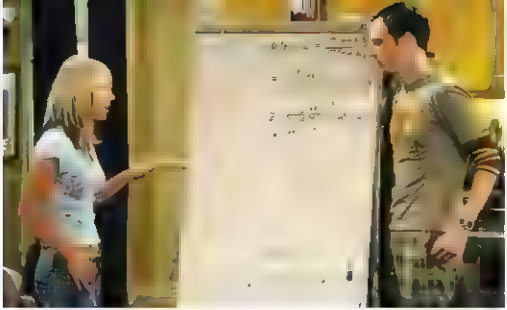

Weird science. Real physics and math make cameos on *The Big Bang Theory*

SCIENCE AND SOCIETY

Talk Nerdy to Me

A surprise hit, the new TV comedy *The Big Bang Theory* plumbs science for laughs, thanks to aid from physicist David Saltzberg and friends

Leonard: *"At least I didn't have to invent 26 dimensions to make the math work"*
Sheldon: *"I didn't invent them. They're there."*
Leonard: *"In what universe?!"*
Sheldon: *"All of them. That's the point."*

Physicists may be notorious for coming up with weird concepts such as alternative universes. But a popular situation comedy based on their work seems almost as fanciful. Yet last October, the American TV network CBS premiered *The Big Bang Theory*, and about 9 million people now watch it each week—enough for CBS to quickly renew the show for another year. The *Washington Post*'s critic Tom Shales calls it "the funniest new sitcom of the season." Apparently, it isn't just quarks that can be strange and charming.

Centering on two male physics postdocs and the blonde bombshell who moves in next door, *The Big Bang Theory* follows the sitcom formula of placing quirky, exaggerated characters in situations both odd and mundane. But where the show breaks the mold is that most of those characters and situations revolve around science, highly accurate science for the most part, thanks to experimental particle physicist David Saltzberg of the University of California, Los Angeles (UCLA), who's been with the show from the initial episode. From making sure lab equipment looks suitably haphazard to supplying the equations displayed on the show, Saltzberg's presence is regularly felt on the set; he even has a director's chair with his name on it. "I can't overestimate his value to what we do," says Bill Prady, who along with Chuck Lorre created the show.

Hollywood has a tradition of exploiting geek humor, from Jerry Lewis's *The Nutty Professor* to the *Revenge of the Nerds* Many current TV shows, particularly forensic crime dramas such as *CSI*, draw regularly on math and science, both for plot elements and the occasional laugh. *Numb3rs*, in which a mathematician helps his FBI agent brother, is even used as the basis for teacher's worksheets provided by Texas Instruments and the National Council of Teachers of Mathematics. Given all of that, working on film or television can be a perk for a Los Angeles–area scientist or physician. Kevin Grazier of NASA's Jet Propulsion Laboratory in Pasadena, for example, consults for three shows.

Online
sciencemag.org
For video clips of *The Big Bang Theory*, visit this story online.

Still, *The Big Bang Theory* is the first time a prime-time comedy has taken science this seriously—and Saltzberg is surely the only particle physicist to advise a sitcom. *Science* recently spoke with him and Prady, and paid a visit to the set of *The Big Bang Theory*, to learn how cutting-edge research gets injected into the show.

The pair defended the show against charges that it has too few women scientists and mocks physicists as Klingon-speaking nerds. Whether giving a talk about the sitcom at the Kavli Institute for Theoretical Physics or simply attending a party, Saltzberg inevitably encounters people offended by the show's putative sexism and nerdism. Most of the show's detractors, he notes, have never seen a whole episode. Prady stresses that *The Big Bang Theory* means no ill will. "If the scientific community is concerned with how we depict them, be gentle and be patient," he says. "We are you, we love you."

Sheldon: *"This is one of those circumstances people unfamiliar with the law of large numbers would call a coincidence"*

Saltzberg got his unusual gig via a friend, a Hawaiian astrophysicist who'd helped on the show's unaired pilot. When the show was picked up by CBS, the producers went searching for a local to vet last-minute changes. Saltzberg generally looks over the scripts in advance and then drives in once a week to Burbank for the show's evening tapings. Saltzberg is "right there to give us the new word we need," Prady says. "A couple of weeks ago, he provided us with a terrific, genuine joke, and it was on the air."

The sitcom features Leonard and Sheldon, the two physicists, and Penny, an actress/waitress who is their bridge to the world of people who don't have a periodic table shower curtain. She's a loyal friend, even attending Leonard's talk on supersolidity—at which she falls asleep. Leonard's subject matter was suggested by the show's "geek of the week," in this case graduate student Matt Mecklenburg, who'd accompanied Saltzberg to the set, as colleagues, friends, and students do every week.

One can argue about whether *The Big Bang Theory* is funny—TV critic Maureen Ryan of the *Chicago Tribune* called its jokes "tired and mean-spirited"—but it's clear that Prady and his writers have scientific chops, accurately incorporating physics terms such as "soft component of cosmic radiation" into dialogue even

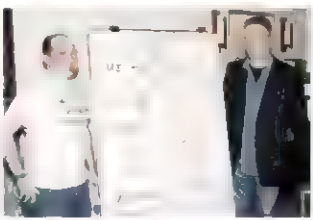

Odd couple. Physicist David Saltzberg (*left*) and Bill Prady, *The Big Bang Theory*'s co-creator.

CREDITS: (TOP TO BOTTOM) WARNER BROS. TELEVISION ENTERTAINMENT

before Saltzberg sees a script. Several years ago, one writer dressed up for a Halloween party as the Doppler effect. The show incorporated the idea, putting Sheldon in a bodysuit with white vertical stripes separated by less and less distance. He made accompanying train noises whose pitch went up and down. To his dismay, no guest got it.

Prady, a self-taught software programmer initially envisioned programmers at the heart of a sitcom. But sitting at a computer all day doesn't make for great physical comedy. Physicists, however, write on whiteboards, and that visual element had appeal. "We realized this was a better way to show somebody working with their mind," Prady says.

Leonard: *"Sounds like a breakthrough, should I ask* Science *to hold the cover?"*
Sheldon: *"It's time travel, Leonard. I will have already done that."*

Some episodes of *The Big Bang Theory* could inspire an evening of studying math or physics. Saltzberg likes to inject scripts with terms such as Casimir effect, molecular positronium, and giant magnetoresistance (the subject of the 2007 Nobel Prize in physics). "I go for stuff that sounds really fake—that you think is Hollywood science but find out not only is it real, it's topical," he says.

Saltzberg views the show as a tool for science education. PBS's *NOVA* with run shots. During an awkward date, Leonard gets an olive to rotate inside a glass—and corrects Penny, and likely most viewers, that centripetal, not centrifugal, force explains the trick.

Leonard, played by Johnny Galecki, is the experimentalist who longs for Penny and has a disastrous fling with Leslie, a brilliant labmate, who spends part of their tryst correcting an equation. In the episode in which Leonard first asks Leslie for a date—"a biosocial exploration with a neurochemical overlay," he calls it—the two test how long it takes a powerful lab laser to heat up soup.

Leslie is the only female researcher on the show, a complaint Prady and Saltzberg hear often from women, whether scientists or journalists. Prady promises that more female scientists will appear. "The [female-male] ratio is actually higher on the show than it is in my part of the field, which is pretty bad," Saltzberg unhappily adds.

The show's writers saw that firsthand when they toured UCLA labs. Prady met a physicist who lies about what she does in social situations, because she feels her career intimidates men. "We're going to have Leslie do that," Prady says. "Whenever anybody says they lie about who they are, there's a rich story to tell there."

The show's other lead character is string theorist Sheldon, played by Jim Parsons as an arrogant, emotionally oblivious, yet endearing, former child prodigy. When Penny complains that a bad relationship lasted 4 years, "as long as high school," Sheldon, perplexed, replies, "It took you 4 years to get through high school?" He's even less tactful to non-Ph.D. engineers, calling them "Oompa-Loompas of science," a knowing jab at the academic pecking order.

Sheldon's lack of social graces and other quirks have led to speculation that he must have Asperger syndrome, an autism spectrum disorder commonly assumed to be prevalent in scientists and computer programmers. Although Prady concedes that Sheldon fits the diagnosis, he rejects the idea that this is the ultimate in negative geek stereotypes, saying the character is an affectionate composite of the programmers he used to know.

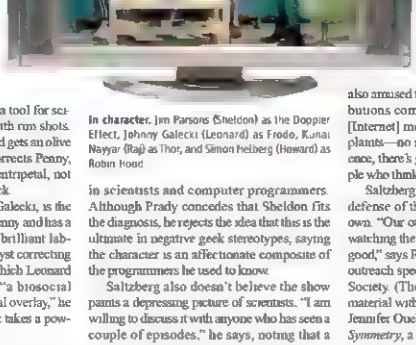

In character. Jim Parsons (Sheldon) as the Doppler Effect, Johnny Galecki (Leonard) as Frodo, Kunal Nayyar (Raj) as Thor, and Simon Helberg (Howard) as Robin Hood.

CREDITS: KMAZUR/GETTY IMAGES; WARNER BROS. TELEVISION ENTERTAINMENT

Saltzberg also doesn't believe the show paints a depressing picture of scientists. "I am willing to discuss it with anyone who has seen a couple of episodes," he says, noting that a UCLA physics student who recently visited the set remarked that she wanted to be just like the show's characters. "This is our attempt to show our own lives," Prady says. "My father-in-law is a brilliant pediatric rheumatologist, but he is capable of saying, 'That's a very interesting story, but who is this Tom Cruise?'"

Sheldon: *"That's my work. It's just some quantum mechanics. A little string theory doodling around the edges. That part there—that's just a joke. It's a spoof of the Born-Oppenheimer approximation."*

UCLA hasn't objected to Saltzberg's spending his free time consulting for the show—he gets an on-air credit and fee—but Warner Bros.' lawyers have stopped on-air disclosure of Sheldon and Leonard's academic home. Still, a slip during the pilot, and its Pasadena setting, obviously hint at Caltech, whose walkways and fountains grace *Numb3rs*'s "CalSci."

Science is vital to the show, but not at the expense of humor, Saltzberg must always remind himself. At a rehearsal, he catches that an equation he provided with accompanying Feynman diagram appears scarily complicated but is actually too basic to cause physics postdocs the terror the scene requires. The writers gamely try out new dialogue, but nothing clicks. They finally ask Saltzberg to provide a new, more challenging equation, with the same solution as the old one so no dialogue has to be changed. Mercifully, before Saltzberg has to improvise, everyone realizes that all it takes is modifying the characters' reactions. It's an engineer who's most frightened.

Although Saltzberg always winces when he realizes he's let something wrong slip in, he's also amused that even his most accurate contributions come off as fake. "If I look on the [Internet] message boards, there's still complaints—no matter how right you get the science, there's going to be some fraction of people who think it's wrong!"

Saltzberg has found scientific allies for his defense of the show—and a few fans of his own. "Our outreach department really enjoys watching the show; the science adviser is very good," says Rebecca Thompson-Flagg, public outreach specialist for the American Physical Society. (The society plans to send the show material with its logo for use.) Science writer Jennifer Ouellette recently penned an op-ed in *Symmetry*, a magazine for particle physicists, calling on its readers to embrace the show. (David Harris, the physicist who is editor of the magazine, loves the show.) "I bought a T-shirt at the American Physical Society that said, 'Flirt harder, I'm a physicist,'" Saltzberg says. "I don't know why we should hold television up to a different standard than we hold ourselves."

–KAREN HEYMAN

Karen Heyman is a freelance writer in Santa Monica, California.

Ready for reentry. Released otters in the Netherlands quickly had a baby boom.

CONSERVATION BIOLOGY

Into the Wild: Reintroduced Animals Face Daunting Odds

Researchers in the emerg[illegible] ... [illegible] ... and poache[illegible] ...

CHICAGO, ILLINOIS—In some ways, the science of reintroducing wildlife to the wild is like staging a reality show. Even after you get the principal actors into the right setting, there's no telling what they will do. Take the case of juvenile male otter A08, released with adult males and females in a peat bog in the Netherlands 3 years ago in an effort to restore a flagship species (*Lutra lutra*) that had gone extinct in the wild in 1998. Once released, A08 was "chased away by the other males," says population geneticist Hans Peter Koelewijn of the Alterra Research Institute in Wageningen, the Netherlands. But a year later, A08 surfaced as the father of half of the 28 young otters born in the wild, shown via genetic analysis of the otters' scat. "Somehow he'd become the dominant male," Koelewijn recalled. With Genghis Khan–like determination, A08 busily impregnated most of the females for the next several litters.

Despite all the baby otters, the effort "seemed doomed to failure," says Koelewijn, because A08's dominance raised the specter of inbreeding. When reports came of otters being hit by cars—their chief cause of mortality—Koelewijn admits that team members would whisper, "Let it be A08." Ultimately, A08 took a natural fall: His sons deposed him.

A08's time in the sun holds a lesson for reintroduction programs, Koelewijn told the audience at a recent meeting here:* "You can have a technical strategy, a scientific strategy, and a socioeconomic strategy, but the animals also have their own strategy."

The young science of reintroduction biology is struggling to map out those strategies for success, as evidenced by the tenor of talks and posters at the reintroduction meeting, organized by the International Union for Conservation of Nature (IUCN) and the Lincoln Park Zoo (LPZ) in Chicago, Illinois. More than 200 scientists and wildlife managers from 31 countries met for the first time, hoping to bring new rigor to sprawling efforts to restore species including the American burying beetle (*Nicrophorus americanus*) on Massachusetts's Nantucket Island and the one-horned rhinoceros (*Rhinoceros unicornis*) in India.

It's a mighty challenge. Early reintroduction efforts often failed, and today, less than half of all such projects are proven successful, says Joanne Earnhardt, an LPZ population biologist. In some cases, reintroduced species do well at first, only to be felled later by the same forces that drove them extinct in the wild in the first place. In other cases, there are simply no data on how reintroduced species are doing. And yet the field is exploding, growing from a total of some 100 reintroduced species in the early 1990s to more than 700 by this year, 74% of them mammals and birds. (Another conference, focused on bird reintroductions, takes place this week at the Zoological Society of London.)

There are some striking success stories. Golden lion tamarins (*Leontopithecus rosalia*) in Brazil now number more than 1500 in the wild, and an astonishing 80% of bird reintroductions in New Zealand have proved successful. Researchers hope there will be more to come, given the long list of species in need. "We are in a time of extinctions, and reintroductions will be key in the 21st century," zoologist Philip Seddon of the University of Otago in Dunedin, New Zealand, said at the conference.

Every reintroduction faces daunting challenges, from assessing the genetic diversity of the animals to ensuring that the habitat can sustain them. "Habitat quality is certainly key," said Debra Shier, a behavioral ecologist with the Zoological Society of San Diego in Escondido, California. "But you have to measure it from the perspective of the animal." In essence, any reintroduction is a "forced dispersal," she explained, and there can be many reasons why an animal won't settle after being released into what humans think is perfect habitat. For example, even after 40 years, red kites in Britain haven't moved into the high-quality habitat scientists had identified for them; instead, they crowd in with other kites in central Wales.

Animals often settle in better if there are signs of their fellows nearby; thus, before translocating black rhinos in South Africa, biologists from the San Diego Zoo spread rhino dung around the new area. "It doesn't seem to matter whose dung it is," said Shier, "just so long as it's black rhino dung." Similarly, playback calls of black-capped vireos in Texas have helped reassure newcomers, and wooden decoys have drawn fairy terns in New Zealand to reestablish old breeding territories.

That behavioral approach has guided the reintroduction of the Puerto Rican parrot (*Amazona vittata*), said wildlife biologist Thomas White of the U.S. Fish and Wildlife Service in Rio Grande, Puerto Rico. Since 2006, 62 parrots have been raised in large cages—designed to help them stay aerobically active—right at the Rio Abajo site where they were to be released; to date, 46 have been set free and another 20 are scheduled to fly

* First International Wildlife Reintroduction Conference, Lincoln Park Zoo, Chicago, 15–16 April 2008.

CREDIT: HUGH JANSMAN

this year. Living in the cages helps "imprint" the habitat, making it more likely that the birds will stay in the vicinity and form a flock with other parrots. "When they're released, they are already 'home,'" said White.

Newly released wildlife may also need to learn other key behaviors, including hunting and parenting. In the case of the parrots, White and his team try to train them to recognize and avoid their chief predator, red tail hawks, by watching managed attacks. With a parrot pair now nesting in the wild, 18 months after release, and about 25 birds still alive, the project may prove successful—although many at the meeting questioned just what "success" means in reintroduction biology.

IUCN defines the term as the establishment of a "self-sustaining population that requires minimal long-term management." Some projects do meet this standard. For instance, dozens of bird species are thriving on their own again in New Zealand, where scientists are now bringing back reptiles, invertebrates, and plants—all the key players in island ecosystems that were lost after rats arrived on European ships. Some of the Kiwis' success is due to the government's "practical approach," says Ian Jamieson, a behavioral ecologist at Otago. Faced with fewer regulations, managers can "just go in and do the job," including removing all invasive species. Elsewhere, as in the United States and Europe, a tangle of government agencies may be involved in any reintroduction, and managers must juggle competing interests.

That's why, for many projects, IUCN's definition of success might "not be grounded in reality," argues biologist Markus Gusset of Germany's Leipzig Zoo. He studied a project in South Africa, which has reestablished several small populations of African wild dogs in conservation areas. There are islands of habitat separated by mostly unsuitable areas where people have moved in. So when the dogs reproduce, they must be trucked from one area to another, "mimicking a dispersal," and put together in new packs. "It's successful in the short-term," Gusset said, because the dogs are reproducing. "But it can only be successful in the long-term if the translocations continue. It's the best we can do."

Indeed, the human hand hovered over every talk and poster at the meeting, and many researchers pointed out that without the support of local communities, reintroduction projects are doomed to fail. Wildlife biologist Andrew Spalton, an adviser on the environment to the Royal Court in Muscat, Oman, described how the once-lauded Oman Arabian oryx reintroduction program rapidly collapsed because of a thriving illegal wildlife trade, which caused the antelope's original decline.

The last wild oryx (*Oryx leucoryx*) was killed in the desert of Oman in 1972, but Operation Oryx, working with the San Diego Zoo, was already breeding the animals in captivity. A decade later, oryx were returned to the wild, and within 13 years, in 1995, there were 450 wild Omani oryx roaming free. But the following year, poachers began capturing the oryx to sell to private collectors with "small zoos or pens in their backyards," said Spalton. Buyers anted up $25,000 for a wild female oryx. Some 100 poachers were arrested and convicted to no avail. Today, there are few wild oryx in Oman. Poaching for meat and catching females to sell was the "cause of the original decline, and it happened again," said Spalton, perhaps because the project's rangers "all came from one community." Those left out were among the first poachers. "We did do the science," Spalton concluded, "but we should have had social scientists on our team," who might have come up with a better response to the poaching.

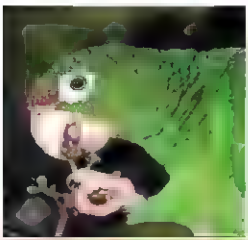

CREDITS (TOP TO BOTTOM): BRET COREY/ROGER WILLIAMS PARK ZOO; ISTOCK, NO NATURE ITEMS

Against the odds. The Puerto Rican parrot (*top*) may yet be reestablished, but the Oman Arabian oryx is almost extinct in the wild.

Digging in. The burying beetle is gaining a toehold on Nantucket.

Even when a project seems successful, in some cases it's hard to be sure of the reasons because the original data are missing or incomplete. "Were Hawaiian crows reintroduced as adults or fledglings? No one really remembers," says Earnhardt. "When you have a high-profile species such as the California condor, every egg that's laid is documented. But for low-profile species such as the brown nuthatch, almost no data" have been collected. To help remedy these problems, Earnhardt unveiled a new LPZ database documenting the 602 releases of 128 avian species (www.lpzoo.org/ARTD), a similar database is being created for amphibians.

An initial baby boom in the wild, like that spurred by A08, is no guarantee of long-term success, either, Seddon and others pointed out, saying that monitoring must continue. Conservation biologist Devra Kleiman of the Smithsonian Institution, who coordinated the tamarin project, now fears that it may be doomed by its own achievements. "It's labeled a 'success,' so everyone thinks we can stop now," she said. "We're having difficulty getting funds to continue the monitoring," leaving the tamarins potentially at risk for a repeat decline. "That's the trap," agrees Seddon. "I'm not sure we can ever take our eye off the ball," especially because climate change may transform environments after animals have been released.

As for the Dutch otters, they may soon be on their own. The government may cut off funding next year. As feared, A08's exuberant mating has led to sister-brother and aunt-nephew couples, and it's not clear what the long-term effects will be. But other otters are mixing it up with more recently released individuals, Koelewijn says. Despite the challenges, he and other researchers are still optimistic that their work will help give the otters and other teetering on the brink species a second chance to make a home in the time of the Anthropocene.

—VIRGINIA MORELL

748 LETTERS | BOOKS | POLICY FORUM

751

757 EDUCATION FORUM | PERSPECTIVES

LETTERS

edited by Jennifer Sills

Lost in Transliteration

THE RANDOM SAMPLES ARTICLE "ONE WEI OR ANOTHER" (15 February, p. 881) addressed the confusion caused in the scientific community by Asian names that use the same English transliteration. This situation becomes more serious as increasing numbers of Asian scientists publish papers in English journals (*1*). To complicate matters even further, about half of the Chinese names have three words, one for the family name and two for the first name. Just like the two-word names (*2*), they sometimes use the same English spelling. For instance, the name "Lixin Wang" is a transliteration of at least 1600 possible Chinese names. The three-word scenario may lead to citation confusion because journals follow different styles. Some journals treat "Lixin Wang" as "L. Wang," whereas others abbreviate it as "LX Wang." Both ways make sense given that the first name "Lixin" includes two words (Li-Xin). However, some major databases (such as Web of Science) misinterpret "L. Wang" and "LX Wang" as two unique names; changing affiliations only add to the confusion.

To be more precise, *Physical Review Letters* allows authors with Asian names to include the original spelling on papers (*2*). It is a good start, but it is still difficult for non-Asian researchers to identify the characters and thus the specific author. Instead of including Asian spellings, I suggest that researchers each adopt a unique identification number, which can be published along with their names (*3*). Scientists with Asian names are not the only ones who would benefit from a more precise naming system.

LIXIN WANG

Department of Environmental Sciences, University of Virginia, Charlottesville, VA 22904, USA.

References and Notes

1. Editorial, *Nature* **447**, 885 (2007).
2. K. W. Barton, *Science* **319**, 881 (2008).
3. One such "ResearcherID" is developed by the Thomson Corporation (www.researcherid.com).

Source of confusion. All of these Chinese names could use the transliteration "Lixin Wang."

Evolution and Faith: Empathy Is Misplaced

FOUND THE NEWS FOCUS STORY "CROSSING THE DIVIDE" (J. COUZIN, 22 February, p. 1034) to be particularly disturbing and unworthy of publication in *Science*. Three full pages were dedicated to paleontologist Stephen Godfrey, who (finally) rejected creationism and embraced evolution and "is still recovering from the traumatic journey." Give me a break! Had *Science* magazine been around during the 17th century, would we have seen such consolatory text for those "traumatized" by the fact that the Sun does not revolve around the Earth? Or earlier, would we have seen such gentle treatment of those "devastated" by the realization that the Earth is not flat? While Dr. Godfrey's escape from the ignorant shroud of Biblical literalism is praiseworthy, *Science* magazine is not the place to give even a hint of respectability to those who would deny the fundamental fact of evolution. There is too much at stake, for our children and our society, to give any credence to those promoting unscientific nonsense (creationism or intelligent design) and justifying irrational beliefs under the guise of religion.

CRAIG W. STEVENS

Department of Pharmacology and Physiology, Oklahoma State University Center for Health Sciences, Tulsa, OK 74107, USA.

Evolution and Faith: Empathy Is Crucial

THE NEWS FOCUS STORY BY J. COUZIN, "CROSSING THE divide" (22 February, p. 1034) accurately and respectfully describes the crux of the challenge that our scientific understanding presents to members of faith communities. With more than 20 years of experience in teaching biology to evangelical undergraduates, I can state with a high degree of confidence that the situation within evangelicalism is to a great extent just as Couzin presented. The worldview in which so many conservative Christians are raised and trained gives them but two stark choices. Either there is a God, the world is a few thousand years old, and therefore evolution cannot have occurred, or the scientific community is correct, evolution occurred, and there is no God. The heart of the matter revolves around meaning in life, not around scientific knowledge. If we can understand the tremendous cognitive and spiritual stress this presents to the faith community, then we as truth-seeking scientists should be willing to listen to the concerns of those holding such positions.

We within the scientific community must continue to present the demonstrable evidence from the physical realm and clearly express how that evidence supports our current interpretations. This effort is not served well at all by dogmatic pronouncements such as "Evolution is fact," even if such statements are accurate. Furthermore, for members of the scientific community to make theological statements in the name of science is philosophically illegitimate, and destructive in our truth-seeking efforts. In this short essay, *Science*

has published the only example I have read in the leading scientific literature that takes the time and effort to understand and express what really drives the concerns of the majority of evangelicals, and does so in a manner that respects the integrity of both the scientific endeavor and the integrity of the faith commitments within the evangelical community.

Allow me to suggest that this serves as a call to us in the sciences to be more humble as we interact with the faith community. We as scientists ought to be those most keenly aware of the tenuous and ever-changing nature of human knowledge, even as we build on that which has stood the test of time. We ought to behave as though the faith community poses no threat to the integrity of science, just as the faith community ought to behave as though science poses no threat to the integrity of faith. That is the challenge to us brought forth so eloquently in this piece, and is a major focus of organizations such as The American Scientific Affiliation. Let us all humbly seek for truth as we respect one another's efforts to do so.

ANDREW WHIPPLE

Department of Biology, Taylor University, Upland, IN 46989, USA.

Data Discrepancies in Solar-Climate Link

CONTRARY TO THE IMPRESSION GIVEN IN J. Pasotta's News of the Week story ("Daggers are drawn over revived cosmic ray–climate link," 11 January, p. 144), neither I nor any of the other climate scientists quoted in the story seek "to strangle the hypothesized climate geomagnetism connection in its crib." However, it is not unreasonable to expect that a hypothesis that neglects well established greenhouse gas and aerosol radiative forcings should at least be based on appropriate and accurately described data.

Courtillot and co-workers (*1*) made two errors that exaggerate the solar-climate correlation (*2*, *3*). First, they showed only the most recent 50 years of a solar irradiance proxy; application of the same data analysis to the readily available full-century record causes the apparent correlation to fall apart. Second, the temperature record used as a basis of comparison was not a global mean temperature or any of the other temperature curves discussed in the paper (*4*) cited as a data source. In (*1*), this temperature curve was labeled "Tglobe," and it was described explicitly as giving a "global temperature trend" at two places in the paper. Furthermore, when Bard and Delaygue raised questions about the data source, the original publicly posted version of Courtillot's response gave the name of a global land and ocean data set. It was only after a further challenge by Bard and Delaygue that the actual data set was revealed, and it turned out to be a record of growing season temperature for Northern Hemisphere extratropical land alone, derived originally for calibrating tree ring proxies, unambiguously described in the data set header as such.

The corrected version of the erroneous figure reproduced in Pasotta's article can be found in (*3*), or compared side by side with the original in (*3*).

J. PECKER

Department of Geophysical Sciences, The University of Chicago, Chicago, IL 60637, USA.

References

1. V. Courtillot *et al.*, *Earth Planet. Sci. Lett.* **253**, 328 (2007).
2. E. Bard, G. Delaygue, *Earth Planet. Sci. Lett.* **265**, 302 (2007).
3. Real Climate (www.realclimate.org/index.php/archives/2007/12/les-chevaliers-de-lyre-2-la-revanche-de-la-lyre-plate-part-ii-courtillots-geomagnetic-excursion/).
4. P. D. Jones *et al.*, *Rev. Geophys.* **37**, 173 (1999).

Living Up to Ancient Civilizations

THE CLASSICAL PERIOD OF GREECE AND Rome lasted more than a thousand years (from about 750 BCE to about 400 AD). By contrast, the modern world, beginning with Columbus's discovery of America, has lasted just over 500 years.

As a result of overpopulation, overconsumption, global warming, and environmental degradation, it now looks increasingly likely that there will be a major societal collapse within the next 200 years. How ironic that a civilization capable of tracing the origin of the universe from 10^{-43} seconds after its formation and putting a lander on Titan does not have the rigor and self-discipline to sustain itself for as long as the ancients managed to do.

GEOFFREY P. GLASBY

Department of Geochemistry, GZG, University of Göttingen, Goldschmidtstrasse 1, D-37077, Germany

CORRECTIONS AND CLARIFICATIONS

Editorial: "New career paths for scientists" by B. Alberts (18 April, p. 289). The page number for *Science* Careers should have referenced the *Science* Online table of contents on page 283. The link to *Science* Careers in the HTML version is correct.

Reports: "Age and evolution of the Grand Canyon revealed by U-Pb dating of water table–type speleothems" by V. Polyak *et al.* (7 March, p. 1377). Reference 8 was incorrect and should have been "L. J. Wiwagrad *et al.*, *Science* **258**, 255 (1992)." The HTML version has been corrected.

Reports: "Evidence for positive epistasis in HIV-1" by S. Bonhoeffer *et al.* (26 November 2004, p. 1547). The HIV sequence studies in this paper were not deposited in GenBank at the time of publication but are now available there. The accession numbers are EU606356 to EU615822.

TECHNICAL COMMENT ABSTRACTS

COMMENT ON "Absence of Cooling in New Zealand and the Adjacent Ocean During the Younger Dryas Chronozone"

Patrick J. Applegate, Thomas V. Lowell, Richard B. Alley

Barrows *et al.* (Reports, 5 October 2007, p. 86) presented cosmogenic exposure dates and data from an ocean sediment core that challenge evidence for glacier advance in New Zealand during the Younger Dryas event. We use modeling of geomorphic processes to argue that their cosmogenic exposure dates are inconclusive.

Full text at www.sciencemag.org/cgi/content/full/320/5877/746d

RESPONSE TO COMMENT ON "Absence of Cooling in New Zealand and the Adjacent Ocean During the Younger Dryas Chronozone"

Timothy T. Barrows, Scott J. Lehman, L. Keith Fifield, Patrick De Deckker

Applegate *et al.* present the results of a moraine degradation model and suggest that the age of the Waihō Loop may be 1000 years older than the age we presented, thus raising the possibility that the moraine is a Younger Dryas landform. We show that this assessment is misleading on a number of grounds.

Full text at www.sciencemag.org/cgi/content/full/320/5877/746e

HISTORY OF SCIENCE

Protesting Scientists

Audra J. Wolfe

At the opening plenary session for this year's annual meeting, outgoing AAAS president David Baltimore endorsed Science Debate 2008 a petition asking the American presidential candidates to debate their positions on science, technology, and the environment (*1*). Baltimore's call for a traditional political debate might at first seem a far cry from his days as a campus radical and antiwar protester. But hard as it is now to believe only 50 years ago activist scientists couldn't even get the AAAS Council to affiliate with a Quaker group that called on scientists to participate in "constructive" research. In *Disrupting Science*, Kelly Moore attempts to explain how scientists' attitudes about the proper role of science and scientists in public life changed so dramatically within two generations.

In the years following World War II, U.S. scientists found themselves deeply enmeshed in military and government contracts. Security clearances and classified work became the norm, particularly for the physicists and chemists associated with nuclear energy. How some of these scientists attempted to limit the destructive powers of their inventions, largely through governmental advising, is a familiar story. Not as well known is the path of activism that less-prominent scientists took when the limits to the physicists' critiques became clear. Moore's well-researched account introduces the pacifists, petition writers, newsletter publishers, and protesters—scientists all—who doggedly drew attention to the ways that militarism was infiltrating the practice of science in the United States.

Disrupting Science asks not only why scientists engaged in such sustained self-examination but also how the different forms these actions took reflected changing notions about individual and collective responsibility, the nature of progress, and the structure of democracy. Moore focuses on three organizations that espoused very different approaches to social action: the Society for Social Responsibility in Science, a Quaker fellowship that encouraged individual scientists to reject military contracts; the Committee for Nuclear Information (CNI), a St. Louis–based group that pioneered information-based advocacy, and Science for the People, a decentralized radical collective that wanted a fundamental reorganization of American science. Given these groups' varied levels of success by traditional measures such as organizational survival and political influence, Moore is at pains to say that their direct impact misses the point. Ultimately, she argues, these movements were important because they greatly expanded the range of options for scientists' political expression.

Moore has a second, more subtle point, perhaps best illustrated through her account of the development and growth of CNI. In the four years following the March 1954 Bravo test of the hydrogen bomb, the American public was presented with a number of competing claims about the dangers of atomic fallout. The Atomic Energy Commission issued several reports designed to allay public fears, claiming, for instance, that x-rays posed a greater threat to human health than atomic fallout. Meanwhile, geneticists such as Curt Stern, A. H. Sturtevant, and Hermann J. Muller publicly expressed concerns that contemporary radiation levels would lead to thousands of mutations in future generations. A fierce televised debate between Edward Teller and Linus Pauling on the scientific merits of a nuclear test ban only muddied the waters. Into this fray stepped Washington University biologist Barry Commoner with a plan to provide the public with more, rather than less, information. When CNI was created in the spring of 1958, its 182 founding members saw their mission as the provision of neutral information that would allow citizens to make their own informed decisions.

This information-provision model was wildly successful, inspiring a number of successor groups such as the Scientists' Institute for Public Information, the Committee for Environmental Information, and the Union of Concerned Scientists. Even so, these groups officially "nonpartisan and formally apolitical" approach fooled no one. In the case of CNI, it was common knowledge that the scientists involved opposed nuclear testing, and all the participants recognized that deciding what information to provide was, in itself, a political decision. At the same time that the authority of scientific knowledge became more enshrined in public consciousness, Moore argues, the authority of individual scientists to speak from beneath the cloak of objectivity was in decline.

Moore (a professor at the University of Cincinnati) is a sociologist rather than a historian, and the book's grounding in social movement theory is its greatest strength. She is particularly interested in countering a tendency in the social studies of science that considers scientists' public actions primarily through the lens of self-interested boundary work, and her examples serve as a welcome reminder that scientists are people, too, with moral and religious convictions that influence their political choices. By ending her account with a nod to the vibrant growth of such new subdisciplines as green chemistry and wildlife ecology that draw on an advocacy base, Moore has written a hopeful book. One could imagine an alternate ending in which she addressed the American scientific community's response (or lack thereof) to the United States's most recent round of military interventions. In choosing to skirt the issue, she leaves us to draw our own conclusions on the lasting legacy of postwar scientists' activism against a militaristic culture.

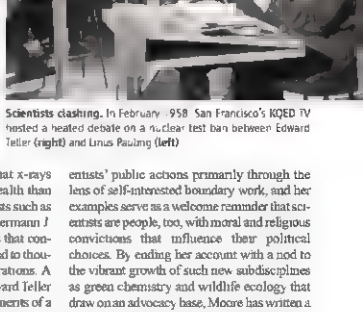

Scientists clashing. In February 1958 San Francisco's KQED TV hosted a heated debate on a nuclear test ban between Edward Teller (**right**) and Linus Pauling (**left**).

The reviewer is at the Chemical Heritage Foundation, 315 Chestnut Street, Philadelphia, PA 19106, USA. E-mail: awolfe@chemheritage.org

Reference

1. www.sciencedebate2008.com.

10.1126/science.1157925

TECHNOLOGY

Designers and Builders

Thomas P. Hughes

Handsomely illustrated, Andrew Saint's *Architect and Engineer: A Study in Sibling Rivalry* offers photographs, drawings, paintings, diagrams, or maps on almost every page. These convey the gist of the book.

The text offers six case studies located in Britain, France, and the United States. The first deals with the roles of engineers and architects within the context of military construction and organization in the 17th, 18th, and 19th centuries. The second and third cases consider the impact of so-called new materials, iron and concrete, on the interactions of engineers and architects. The fourth explores how bridges shaped the relationship. The fifth case, dealing with major projects since the 1930s, reveals that architects and engineers grew closer together. Lastly, Saint (a historian of architecture and the general editor of the Survey of London) covers the training of the two professions in the three countries. He stresses that his cases are not drawn from original research but from his readings in books and articles.

In the opening chapter, Saint expounds on the role of Sebastian Le Prestre, the Marquis de Vauban, history's most famous military engineer, who designed and built for Louis XIV of France The Sun King is remembered chiefly for Versailles, but among contemporaries he was admired and feared in large part because of Vauban's fortifications and siege-warfare. Louis XIV spent three-quarters of his total revenue on war. Saint portrays Vauban as architect and engineer, which at the time were muddled together. Saint suggests that Vauban's work is not simply military engineering, it is architecture—and even more, art. Furthermore, Vauban, according to the author, had a system for his military works, "which his assistants and followers reduced to formulae." Saint admiringly comments that Vauban's citadels are like an orchestral composition.

Saint's canvas is vast. He explores, for instance, the well-known late-19th-century Chicago school of architecture and the Opera House in Sydney. In telling about the Chicago school, he focuses upon Dankmar Adler and Louis Sullivan. They encompassed the tension among efficient engineering, good management, and art. They juxtaposed, Saint claims, structure and ornament, making them "stand for difficult, interlocking paths in modern culture"—a quotation that demonstrates some of the difficulties in following the author's writing and reasoning.

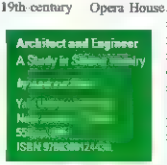

The section on the Opera House (begun 1957; completed 1973) features the Anglo-Danish engineer Ove Arup and the Danish architect Jørn Utzon. Utzon consulted no engineer before submitting his winning design and was subsequently persuaded to work with Arup, whose firm focused on the difficult problem of the concrete "sails" or shells. After having bracked up the door between his and Arup's offices, Utzon resigned from the project in 1966. He accused Arup of destroying the architect's position, by dividing structure and architecture. In the end, Utzon, not Arup—the architect, not the engineer—would be remembered for the Opera House. Saint admires Arup and his approach to combining engineering and architecture, but notes, "For many architects design is all, construction only an aftermath."

In his introduction, Saint promises to reveal a pattern of relationship between the siblings. Yet, he starts his conclusion noting, "The patient reader will find that the answers proffered tend to undermine the questions," which left me puzzled. My understanding was not improved by remarks, shortly afterward, that "'architect' often means the moving force behind any scheme of complexity" and that in common English language, an "engineer is someone who deals with machinery."

Saint does offer helpful subtitles in the conclusion: "Were Architects and Engineers Once the Same?", "How and Why Did Architect and Engineer Separate?", "Have the Professions Been Reconciled?", and "Art, Usefulness and Marriage." Exploring these themes, he argues that in the later Middle Ages the two were the same. He then suggests that their separation during the Enlightenment and the Industrial Revolution was due to more-complex structures, materials, and calculations (including descriptive geometry), with which architects were not trained to cope. In the 19th century, architects and engineers became reconciled because they realized that buildings needed to be seen as wholes.

Unfortunately, rather than revealing a pattern, the author leaves the reader in limbo. For instance, he writes "If it is proper to regard art as a consolation for the stresses and damage imposed upon us by material progress, then the wayward pleasures of architecture can stand as a compensation for the compunctionless efficiencies of engineering." In the end, drawing on Ove Arup, Saint concludes that the interaction between engineering and architecture can be seen as a marriage with the potential for both harmony and conflict.

Architecture and engineering together. Edouard Durandelle recorded the construction of the Eiffel Tower in a series of photographs (1888).

The reviewer is at the Program in Science, Technology, and Society, Massachusetts Institute of Technology, and the Department of History and Sociology of Science, University of Pennsylvania, Philadelphia, PA 19118-3925, USA. E-mail: thughes@sas.upenn.edu

10.1126/science.1157832

PUBLIC HEALTH

Reassessing HIV Prevention

The largest investments in AIDS prevention targeted to the general population are being made in interventions where the evidence for large-scale impact is uncertain

Malcolm Potts,[1]* Daniel T. Halperin,[2]*† Douglas Kirby,[3] Ann Swidler,[4] Elliot Marseille,[5] Jeffrey D. Klausner,[6] Norman Hearst,[7] Richard G. Wamai,[8] James G. Kahn,[5] Julia Walsh[1]

Several decades into the AIDS pandemic, HIV transmission in most of the world remains firmly concentrated among sex workers, men who have sex with men (MSM), injecting drug users (IDUs), and their sex partners (*1*). In some parts of Africa, where over two-thirds of infections occur globally, HIV has expanded outside these high-risk groups, creating generalized, predominantly heterosexual epidemics. In nine southern African countries, more than 12% of adults are infected with HIV. Such devastating epidemics have frequently been attributed to poverty, limited health services, illiteracy, war, and gender inequity. Although these grave problems demand an effective response in their own right, they do not appear to be the immediate causes of generalized epidemics (*2*).

Some assumptions that drive current HIV prevention strategies are unsupported by rigorous evidence. The presumption, for example, that poverty increases vulnerability to HIV infection is challenged by studies such as an analysis of recent Demographic and Health Surveys (DHSs) from Africa, which shows a strong positive correlation between HIV prevalence and wealth in eight countries examined (*3*, *4*) [see supporting online material (SOM)]. Among Kenyan women, HIV prevalence is 3.9% in the lowest economic quintile and 12% in the highest. A study of serodiscordant couples found that, across 12 African nations, the woman was the HIV-infected partner in 34 to 62% of these couples, which suggests that many infections are not, as is commonly assumed, brought into the relationship by the man (*4*, *5*). African regions suffering from conflict, genocide, and rape, such as Rwanda, Congo, and Angola, are much less affected by AIDS than peaceful, wealthier, and more literate countries such as Botswana or Swaziland, which have the world's highest HIV prevalence (*6*).

Where multiple sexual partnerships, especially concurrent ones, are uncommon, and particularly where male circumcision (MC) is common, HIV infection has remained concentrated in high-risk populations (*7*). Niger, a Muslim country where sexual behavior is relatively constrained and MC is universal, has an adult HIV prevalence of 0.7% (*1*), despite being the lowest ranking country in the Human Development Index. Botswana, the second wealthiest country in Sub-Saharan Africa, has high levels of multiple concurrent partnerships among both sexes and lack of MC (*8*), with an HIV prevalence of 25% (*1*) (see SOM).

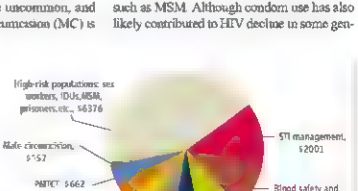

UNAIDS resource allocation estimates to achieve "universal access" to HIV prevention by 2010 (in millions of U.S. dollars). Although interventions for high-risk populations are crucial, the resource allocation recommended by UNAIDS is too small for those approaches likely to have a major impact on generalized heterosexual epidemics. (Note: Much of the funding for categories such as "high-risk populations" would actually go for interventions like condom promotion.)

Several current prevention approaches have value, and the search for new, more effective interventions must continue. However, especially given the severe human resource constraints in Africa, we are arguing for a shift in prevention priorities.

Weaker Evidence for Effectiveness

For generalized epidemics, most emphasis has been placed on the three "established" pillars of HIV prevention: condom promotion and distribution, voluntary counseling and testing (VCT), and treatment of other sexually transmitted infections (STIs) (*4*). Recently, the USA's global AIDS program has also promoted abstinence. Although it can be difficult to assess exactly why HIV prevalence has fallen in some generalized epidemics, two other factors stand out as particularly important: the epidemic's natural progression, as the most susceptible populations become infected and die (*9*), and behavior change, particularly declines in multiple sexual partnerships (*2*, *4*, *7*, *9*–*11*).

Condom use. Condom promotion is effective in epidemics spread mainly through sex work, as in Thailand (*7*, *10*, *11*) and also, to some extent, among other high-risk groups such as MSM. Although condom use has also likely contributed to HIV decline in some generalized epidemics, there is no evidence of a primary role (*2*, *4*, *10*, *11*). This is because consistent condom use has not reached a sufficiently high level, even after many years of widespread and often aggressive promotion, to produce a measurable slowing of new infections in the generalized epidemics of Sub-Saharan Africa. When most transmission occurs within more regular and, typically, concurrent partnerships, consistent condom use is exceedingly difficult to maintain (*2*, *4*, *7*, *10*).

HIV testing. Unfortunately, reviews of many studies have shown no consistent reduction in risk for those who test HIV-negative, although risk reductions in some who test positive have been reported (*4*, *12*, *13*). Several HIV and STI incidence studies in Africa have found no population-level impact of VCT (*12*–*14*). Although a critical link to life-prolonging treatment, HIV testing is therefore unlikely to substantially alter the epidemic's course [the potential for domestic violence against women who test

[1]School of Public Health, University of California at Berkeley, Berkeley, CA 94720, USA. [2]Harvard University School of Public Health, Boston, MA 02115, USA. [3]ETR Associates, Scotts Valley, CA 95066, USA. [4]Department of Sociology, University of California at Berkeley, Berkeley, CA 94720, USA. [5]Philip R. Lee Institute for Health Policy Studies, University of California at San Francisco, San Francisco, CA 94143, USA. [6]San Francisco Department of Public Health, San Francisco, CA 94102, USA. [7]Department of Family and Community Medicine, University of California at San Francisco, San Francisco, CA 94143, USA.

*These authors contributed equally to this work.

†Author for correspondence. E-mail: daniel_halperin@harvard.edu

positive must also be considered (*15*)].

Treatment of other STIs. Six randomized controlled trials (RCTs) to measure the impact of STI treatment on HIV transmission have been published. Although the first study, in Mwanza, Tanzania, found a nearly 40% reduction in HIV when STIs were treated through syndromic management, subsequent trials found no effect on HIV (*16*). Two recent RCTs to prevent HIV acquisition by treating genital herpes have been similarly discouraging (*17*). Although STI treatment remains critical for broader public health programs, the population-level evidence for impact on HIV transmission, especially in generalized epidemics, appears minimal.

Vaccines and microbicides. Work on vaccine development has been sadly disappointing. In 2007, large-scale efficacy trials were stopped prematurely owing to lack of impact or possibly even harm (*17*). Attempts to develop a female-controlled prevention method have been similarly discouraging; several microbicide candidates (and the cervical diaphragm) have failed (*16*). Microbicides would have considerably lower biological effectiveness than condoms and, even if effective, might be unlikely to be used consistently enough, especially in longer-term partnerships, to slow a generalized epidemic.

Abstinence. Abstinence completely prevents sexual transmission, and young people should be encouraged to delay sexual debut (*18*). However, most HIV infections occur among people in their 20s or older, when most are sexually active and, thus, abstinence is unlikely to have a major epidemiological impact (*4*, *11*).

Interventions such as blood screening and preventing maternal-to-child transmission (PMTCT) are clearly effective, but only address a relatively small proportion of total HIV transmission.

What Works

Male circumcision. Over 45 observational, biological, and other studies from the last 20 years have shown that MC significantly reduces the risk of heterosexual HIV infection (*2*, *7*, *19*, *20*). The population-level effect of widespread MC is observed in west Africa, where HIV has been present for many decades, yet prevalence remains relatively low (*1*, *7*, *19*, *20*). All three recent RCTs of MC in Africa were stopped early for ethical reasons when initial findings demonstrated at least 60% reduction in HIV risk (*19*, *20*). The population-level impact, taking into account "herd immunity," could be even greater if a large proportion of men become circumcised (*19*, *20*). Unlike most other interventions, MC is a one-time procedure that confers lifelong protection. Modeling suggests that MC could avert up to 5.7 million new HIV infections and 3 million deaths over the next 20 years in Sub-Saharan Africa, many of these among women (*21*).

A dozen acceptability studies and on-the-ground experience in many high-HIV-prevalence African countries demonstrate that the majority of uncircumcised men and their female partners accept and want MC services (typically for reasons of hygiene and sexual pleasure) (*22*). In Swaziland, men almost rioted because circumcision services were not available (*20*). Studies suggest that up to 80% in high HIV-prevalence countries like Botswana and Swaziland would seek MC if it were safe and inexpensive (*22*).

Donor agencies have the opportunity to be proactive, but African governments and civil society must take the lead, as has begun to occur in several countries (*19*). MC must be combined with behavior change, especially promotion of partner reduction and consistent condom use (*1*, *2*, *19*). Over time MC, which has been called a "surgical vaccine," would probably protect more women, albeit indirectly, than nearly any other achievable HIV prevention strategy (*19*–*21*).

Reducing multiple sexual partnerships. Another preventive measure that has had a powerful impact and that could have even greater effect, if it were more widely and assertively promoted, is partner reduction (*2*, *4*, *7*, *11*, *18*, *23*–*25*). In Uganda, HIV prevalence declined dramatically following the extensive "Zero Grazing" campaign of the late 1980s (*2*, *7*, *11*, *23*). WHO surveys conducted in 1989 and 1995 found a >50% reduction in the number of people reporting multiple and casual partners (*11*, *23*–*25*). In Kenya, partner reduction and fidelity also appear to have been the main behavioral change associated with the recent HIV decline (*2*, *4*, *7*). Similar behavior change has been reported in DHS surveys in Zimbabwe, where HIV has also fallen (*1*, *2*, *7*, *26*), along with Ethiopia (*7*, *11*), Côte d'Ivoire, and urban Malawi (see SOM). In Swaziland, the number of people reporting two or more partners in the past month was halved after an aggressive 2006 campaign focusing on the danger of having a "secret lover" (*7*).

There are, however, few demonstrated replicable approaches to reducing multiple sexual partnerships on a large scale. Nonetheless, mass mobilization of the community, as occurred with gay men in the United States and among heterosexuals in Uganda, can effectively encourage behavior change (*18*, *23*, *25*). And the Ugandan experience suggests that both partner reduction and combating stigma can be successfully achieved (*24*, *25*).

What Can Be Done Now?

Currently, the largest donor investments are being made in interventions for which evidence of large-scale impact is increasingly weak, whereas much lower priority is given to interventions for which the evidence of potential impact is greatest (see figure, page 749). About 1% of total requested funding is for MC, and probably only a fraction of "community mobilization and mass media" and "workplace" efforts would be focused on reducing multiple and concurrent sexual partnerships. This balance needs to be reassessed.

References and Notes

1. UNAIDS, the Joint United Nations Programme on HIV/AIDS, *AIDS Epidemic Update* (UNAIDS Publ. UNAIDS/07.27E/JC1322E, UNAIDS, Geneva, 2007); www.unaids.org/en/KnowledgeCentre/HIVData/EpiUpdate/EpiUpdArchive/2007/default.asp.
2. Southern African Development Community (SDAC), *Expert Think Tank Meeting on HIV Prevention in High-Prevalence Countries in Southern Africa: Report*, Maseru, Lesotho, 10 to 12 May 2006 (SADC, Botswana, 2006); www.sadc.int/downloads/news/SADCPrevReport.pdf.
3. V. Mishra *et al.*, *AIDS* **21** (suppl. 7), S17 (2007).
4. J. D. Shelton, *Lancet* **370**, 1809 (2007).
5. "The not-so-fair sex," *Economist*, 28 June 2007, p. 95; www.economist.com/science/displaystory.cfm?story_id=9401560.
6. P. B. Spiegel *et al.*, *Lancet* **369**, 2187 (2007).
7. D. T. Halperin, H. Epstein, *South African J. HIV Med.* **26**, 19 (2007); www.harvardaidsprp.org/research/halperin&epstein-why-is-hiv-prevalence-so-severe.pdf.
8. M. W. Carter *et al.*, *AIDS Behav.* **11**, 822 (2007).
9. J. D. Shelton, D. T. Halperin, D. Wilson, *Lancet* **367**, 1120 (2006).
10. N. Hearst, S. Chen, *Stud. Fam. Plann.* **35**, 39 (2004).
11. J. D. Shelton *et al.*, *BMJ* **328**, 891 (2004).
12. M. M. Cassell, A. Surdo, *Lancet Infect. Dis.* **7**, 491 (2007).
13. J. A. Denison *et al.*, *AIDS Behav.* **12**, 363 (2008).
14. E. L. Corbett *et al.*, *AIDS* **21**, 483 (2007).
15. S. Maman *et al.*, *AIDS Behav.* **7**, 373 (2003).
16. R. H. Gray, M. Wawer, *Lancet* **370**, 200 (2007).
17. J. Cohen, *Science* **319**, 888 (2008).
18. D. T. Halperin *et al.*, *Lancet* **364**, 1913 (2004).
19. H. A. Weiss *et al.*, *AIDS* **22**, 567 (2008).
20. J. D. Klausner *et al.*, *Future HIV Ther.* **2**, 1 (2008); www.futuremedicine.com/doi/full/10.2217/17469600.2.1.1.
21. B. G. Williams *et al.*, *PLoS Med.* **3**, e262 (2006).
22. N. Westercamp, R. C. Bailey, *AIDS Behav.* **11**, 341 (2007).
23. R. L. Stoneburner, D. Low-Beer, *Science* **304**, 714 (2004).
24. E. C. Green, D. T. Halperin, V. Nantulya, J. A. Hogle, *AIDS Behav.* **10**, 335 (2006); www.springerlink.com/content/h00r4n6521805w27/fulltext.html.
25. H. Epstein, *The Invisible Cure: Africa, the West and the Fight Against AIDS* (Farrar, Straus, and Giroux, New York, 2007).
26. S. Gregson *et al.*, *Science* **311**, 664 (2006).

27. This paper emerged from an HIV prevention experts' meeting sponsored by the Bixby Center for Global Reproductive Health, University of California at Berkeley, and Harvard University in May 2007. We also thank A. Herling, H. Epstein, P. Kilmarx, H. Kinlaw, T. Mah, J. Chin, M. Hanley, J. Howson, H Weiss, G. Woelk, and R. Bailey.

10.1126/science.1153843

Supporting Online Material
www.sciencemag.org/cgi/content/full/320/5877/749/DC1

PHYSICS

Designer Atomic Nuclei

New isotopes with unusual decay modes or number of neutrons are having impacts in areas ranging from astrophysics to medicine

Bradley M. Sherrill

The rise of nanotechnology is garnering much attention for its ability to construct objects with individual atoms and molecules, at a scale roughly a billion times smaller than the objects we encounter in our everyday lives. In parallel to nanotechnology's often astonishing achievements, scientists have started to build a capacity to do useful work on an even more minute scale. During the past decade, chemists and physicists have begun a fabrication process at the scale of the atomic nuclei. It is an emergent means of producing, in sufficient quantities, "designer" atomic nuclei, which are new, rare isotopes with unusual numbers of neutrons or protons, or unusual decay modes (*1*). There are several reasons why a latent demand exists within the scientific community for new isotopes. One is that the properties of particular isotopes often hold the key to understanding some aspect of nuclear science. Another is that the rate of certain nuclear reactions involving rare isotopes can be important for modeling astronomical objects. Finally, the pursuit of ever more exotic isotopes sometimes advances basic understanding of the nuclear landscape, along with unexpected areas of application.

The capacity to produce and study single atoms represents a "technical capability" on the nuclear scale. For example, superheavy isotopes of light elements, such as lithium, have such a high ratio of neutrons to protons that the neutrons have a relatively low binding energy. Quantum mechanically, the wave function of the neutrons can extend far beyond the normal range of the nucleus. In the case of ^{11}Li, the nucleus stretches capaciously to 10 fm (or 10^{-14} m) across, which corresponds to nearly 10 times the volume of a normal ^{6}Li nucleus (*2*) (see the figure). The existence of such nuclei allows researchers to study the interaction of neutrons in nearly pure neutron matter, similar to what exists in neutron stars (*3*). A recent study of the charge radius of ^{11}Li provides key information for ab initio nuclear theory (*4*).

In addition to the discovery of nuclei with very atypical characteristics, such as ^{11}Li, access to key isotopes has shown that the quantum "magic numbers" in nuclei are not always the same, which is contrary to what is observed for electrons in atomic physics. In atomic physics, the filling of quantum orbits means that atoms with an atomic number of 2, 10, 18, 36, 54, or 86 will always be a noble gas. The standard magic numbers for nuclei—2, 8, 20, 28, 50, 82, and 126—are only valid for the stable isotopes found in nature and can change dramatically for very exotic isotopes (*5*). We know, for example, that a nucleus with 28 neutrons is sometimes but not always magic (*6*). However, a change in the magic numbers in rare isotopes is not always found. A recent mass measurement of the rare isotope ^{132}Sn, with a proton number Z of 50 and neutron number N of 82, found it to have the largest measured shell gap, which is the energy difference between the filled shell model orbit and the next unfilled one (*7*).

Atomic nuclei fuel the fusion processes in stars, and their reactions are responsible for the chemical evolution of the universe. The gold found on Earth was probably created in supernovae explosions sometime in the distant past, but the details of how, where, and when are not known. Access to new isotopes can refine our models of stellar processes. Key reactions such as proton capture on radioactive sodium can now be measured (*8*), and production of radionuclides in novae explosions more reliably modeled. Goals in this area include the production of isotopes relevant to nucleosynthesis in supernovae and development of an understanding of the r-process that creates heavier elements. Recent progress in measuring the elements' abundances in old stars has revealed a wealth of information about how the elements are created, but reliable modeling of these processes requires more nuclear physics input (*9*).

Access to unusual nuclei also provides the possibility to study new modes of nuclear decay. A new radioactive decay mode, the emission of two protons from an atomic nucleus, was recently studied in great detail and found to correspond to a three-body decay, as opposed to the emission of a ^{2}He pair (*10*). This experiment was performed by literally photographing the decay of individual, exotic ^{45}Fe nuclei. It is far too early to speculate about any future applications such new nuclear decay modes may provide, but in the past, the discovery of new decay modes formed the basis of

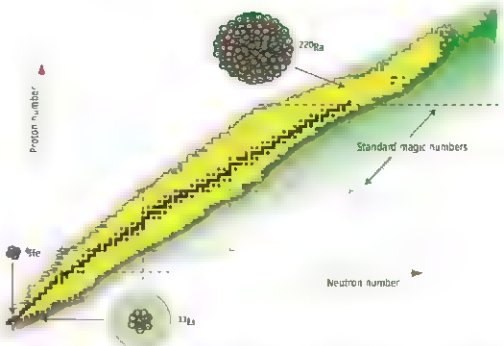

Nuclear landscape. Each isotope is represented by a square at its respective neutron and proton number. Stable isotopes are black, yellow indicates isotopes produced so far, and green represents the possible range of future isotopes that may exist. The rich variety of nuclei is indicated by the depiction of three isotopes: ^{8}He, ^{11}Li, and ^{220}Ra. For example, ^{11}Li has a diffuse surface of neutron matter, unlike normal nuclei, and its size is similar to that of the much heavier ^{220}Ra.

National Superconducting Cyclotron Laboratory, Michigan State University, East Lansing, MI 48824, USA. E-mail: sherri2@msu.edu

techniques such as positron emission tomography (*11*).

There are a host of other potential applications for designer nuclei and the advanced accelerator technology that will create them. A wider range of available isotopes should benefit the fields of biomedicine (by producing an expanded portfolio of radioisotopes), international security (by providing the technical underpinning to nuclear forensics specialists), and nuclear energy (by leading to better understanding of the sort of nuclear reactions that will power cleaner, next-generation reactors).

The scientific opportunities were outlined in a recent report from the National Academies Rare Isotope Science Assessment Committee (*12*).

Approximately 270 isotopes are found naturally on Earth. However, many more isotopes—the number today stands at slightly over 3000—can be produced by particle accelerators or in nuclear reactors. With such an ever-expanding menu of a la carte isotopes, unforeseen applications and insights are surely possible.

References

1. D. F. Geesaman, C. K. Gelbke, R. V. F. Janssens, B. M. Sherrill, *Annu. Rev. Nucl. Part. Sci.* **56**, 53 (2006).
2. A. Tamburini, J. Phys. G Nucl. Part. Phys. **22**, 157 (1996).
3. F. M. Walters, J. M. Lattimer, *Nucl. Phys. A* **763**, 49 (2005).
4. R. Sánchez *et al.*, *Phys. Rev. Lett.* **96**, 033002 (2006).
5. T. Otsuka *et al.*, *Phys. Rev. Lett.* **87**, 082502 (2001).
6. B. Bastin *et al.*, *Phys. Rev. Lett.* **99**, 022503 (2007).
7. M. Dworschak *et al.*, *Phys. Rev. Lett.* **100**, 072501 (2008).
8. S. Bishop *et al.*, *Phys. Rev. Lett.* **90**, 162501 (2003).
9. C. Sneden, J. J. Cowan, *Science* **299**, 70 (2003).
10. K. Allaart *et al.*, *Phys. Rev. Lett.* **99**, 232501 (2007).
11. M. E. Phelps, *Proc. Natl. Acad. Sci. U.S.A.* **97**, 9226 (2000).
12. National Research Council, Rare-Isotope Science Assessment Committee, *Scientific Opportunities with a Rare-Isotope Facility in the United States* (National Academies Press, Washington, DC, 2007).

10.1126/science.1151836

ECOLOGY

How the Sahara Became Dry

A continuous lake record elucidates how Saharan climate changed gradually from humid to today's desert conditions.

Jonathan A. Holmes

About 14,800 years ago, a strengthening of the summer monsoons led to a dramatic increase in North African lakes and wetlands and an extension of grassland and shrubland into areas that are now desert (*1*), creating a "green Sahara" (see the first figure). On page 765 of this issue, Kröpelin *et al.* (*2*) report a lake sediment record that sheds light on how this "African Humid Period" came to an end.

Current knowledge of the climate history of North Africa comes from three main sources. Lake sediments provide information about the size and distribution of former lakes and preserve pollen from past vegetation (*3*). Marine sediments from the equatorial Atlantic also preserve evidence of environments on the adjacent continent (*4*). Finally, climate models (*5*) allow past patterns of precipitation and vegetation to be reconstructed, helping to elucidate the mechanisms underlying change.

However, lake sediments may have uncertain chronologies and are often discontinuous in the drier parts of North Africa. Ocean sediment sequences are often uninterrupted and well dated, but integrate information from a wide area, making it difficult to reconstruct regional patterns. Models reconstruct past climate and vegetation patterns with variable success, and model results must be validated using the geological records.

A different past. This tropical savanna with freshwater wetland in the Sahel is a possible analog for the "green Sahara."

In general, the evidence shows that the African Humid Period came to an end between ~6000 and ~4000 years ago. Beyond this, there is much uncertainty. Kröpelin *et al.* now fill an important gap in our understanding of the past 6000 years of North African climate through their study of a sediment record from Lake Yoa in northern Chad. The record comes from one of the few Saharan lakes in which sediments have accumulated without a break during the Holocene (the past 11,500 years). Despite its hyperarid location, the lake is fed by ancient groundwater and therefore does not dry up. The authors infer the past salinity of the lake—a proxy for effective precipitation—from the remains of diatoms and aquatic invertebrates preserved in its sediments and reconstruct the vegetation history of the surroundings from pollen. Groundwater input has reduced the lake's hydrological sensitivity to climate change, but the reconstructed salinity values still provide a record of changing precipitation. Finally, the authors reconstruct the input of atmospheric dust to the lake using mineral magnetic measurements. dust flux reflects wind regimes and the extent of vegetation cover in the surrounding landscape. The results show that vegetation and dust flux changed gradually over the past 6000 years, accompanied by the slowly weakening monsoon, whereas a rise in lake salinity ~4000 years ago was more abrupt.

Sediments from the equatorial Atlantic suggest that dust export from North Africa increased sharply ~5500 years ago, implying that the end of the African Humid Period was abrupt (see the second figure, panel A) (*4*). This is something of a puzzle, because the reduction in the seasonal contrast in insolation—the fundamental driving force behind the weakening of the African monsoons in the Holocene—has been gradual (see the second figure, panel D). Climate modelers have shown that feedbacks involving changes in vegetation, surface albedo, and sea surface temperature are important in explaining the strong monsoon of the early to mid-Holocene (*5*, *6*). However, the spatial and temporal patterns of change are less faithfully reconstructed by models.

Moreover, there is disagreement about the abruptness of mid-Holocene aridification. Several simulations indicate an abrupt collapse in both vegetation and precipitation

CREDIT: JONATHAN A. HOLMES

Environmental Change Research Centre, Department of Geography, University College London, London WC1E 6BT, U.K. E-mail: j.holmes@ucl.ac.uk

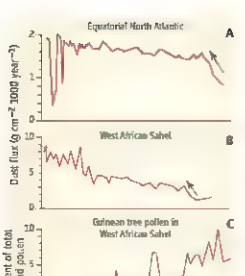

Evolution of mid- to late-Holocene climate of North Africa. Saharan dust flux over the Atlantic (*4*) increased sharply 5500 years ago [arrow in (**A**)], suggesting an abrupt end to the African Humid Period, whereas records from the West African Sahel (*10*) show a later rise [arrow in (**B**)]. A reduction in swamp forest in the Sahel (*9*), indicated by Guinean tree pollen (**C**), accompanied the demise of wetlands and broadly followed changes in insolation (**D**).

between ~6000 and ~4000 years ago that is consistent with the marine dust flux record (*7*). However, various simulations suggest that precipitation changed more gradually, accompanied by vegetation collapse in some models but steadier decline in others (*8*).

Even the continental geological evidence is equivocal. The appearance of abrupt drying of the Sahara might have arisen from the removal of sediments from many basins by the wind following desiccation during the mid-Holocene. Added to this, there is a dearth of well-dated sites in the Sahara, truncated or otherwise (*3*). In the Sahel, the semiarid southern fringe of the present-day Sahara, continuous and well-dated lake-sediment sequences do not support the idea of abrupt drying either; here, changes in vegetation were gradual (*9*) (see the second figure, panel C) and dust flux increased later than 5500 years ago (see the second figure, panel B) (*10*). However, the extent to which these Sahelian records are more widely representative is uncertain.

The evidence from Lake Yoa reported by Kröpelin *et al.* adds a new dimension to the problem. The continuous and well dated pollen record for this site shows no abrupt change in vegetation in the mid-Holocene. The rise in Lake Yoa's salinity was rapid, but this was almost certainly a response to a local threshold being crossed as the lake changed from hydrologically open to hydrologically closed, rather than to abrupt climatic drying. The relatively smooth rise in dust flux is consistent with the gradual reduction in vegetation cover. Kröpelin *et al.* conclude that the vegetation feedbacks that have preoccupied modelers of the African monsoons must have been weaker than previously thought.

The record does not provide the last word on the tempo of Holocene aridification in North Africa, but it does raise important questions about Holocene environmental changes across the area and about the nature of feedbacks in the climate system. There is little point in calling for further continuous records to help resolve these issues: As Kröpelin *et al.* point out, suitable sites probably do not exist. However, improving existing geological records and using these to refine climate models would go a long way toward furthering our understanding.

References

1. P. Hoelzmann *et al.*, *Global Biogeochem. Cycles* **12**, 35 (1998).
2. S. Kröpelin *et al.*, *Science* **320**, 765 (2008).
3. F. Gasse, *Quat. Sci. Rev.* **19**, 189 (2000).
4. J. Adkins *et al.*, *Paleoceanography* **21**, 4203 (2006).
5. J. E. Kutzbach *et al.*, *Nature* **384**, 623 (1996).
6. J. E. Kutzbach, Z. Liu, *Science* **278**, 440 (1997).
7. M. Claussen *et al.*, *Geophys. Res. Lett.* **26**, 2037 (1999).
8. Z. Liu *et al.*, *Quat. Sci. Rev.* **26**, 1818 (2007).
9. M. P. Waller *et al.*, *J. Biogeogr.* **34**, 1575 (2007).
10. F. A. Street-Perrott *et al.*, *Holocene* **10**, 293 (2000).

10.1126/science.1158105

AIDS/HIV

A STEP into Darkness or Light?

The recent failure of a vector-based HIV vaccine may be explained by individual subjects' immune capacity and genetics.

John P. Moore,[1]* P. J. Klasse,[1] Matthew J. Dolan,[2] Smail K. Ahuja[3]*

The outcome of the efficacy trial of an adenovirus serotype 5 (Ad5) vector-based HIV-1 vaccine last November (STEP trial) was unexpected. Not only was the vaccine ineffective at lowering plasma viremia postinfection, but it may have increased the risk of acquiring HIV-1 infection. Although firm conclusions cannot be drawn based on the small number of infections that occurred (49 in the vaccinated patient group, 33 in the placebo group), it has been suggested that vaccine-induced generalized immune activation, which can promote HIV-1 replication, might have increased the infection risk (*1*).

The vector-based vaccine used in the STEP trial was a recombinant Ad5 virus expressing immunogenic HIV-1 proteins. A higher number of HIV-1 infections occurred in the subset of vaccinees with high, preexisting titers of Ad5-specific antibodies, compared with placebo recipients. One possible explanation is that anti-Ad5 antibodies facilitate cellular uptake of the Ad5 vector (perhaps by cells other than the ones normally targeted), inducing an immune response that enhances HIV-1 infection. Although immune responses to viral infections are usually protective, they can also be harmful (as with West Nile, dengue, measles, and respiratory syncytial virus infections). For example, a low titer antibody response to West Nile virus can enhance viral replication and exacerbate disease (*2*). Whether similar events occur after vaccination with an Ad5 or similar viral vector is now something to consider.

One way to examine the apparent effect of anti-Ad5 antibodies is to plot the relative risk of HIV-1 infection in the STEP trial groups as a function of antibody titer (see the figure). Unexpectedly, the higher the anti-Ad5 antibody titer in the placebo group, the lower the HIV-1 infection rate. By contrast, infection risk in the vaccinated group appears similar at high and low titers. Given statistical limitations, a conservative explanation is that these patterns arise by chance. However, because of the need to understand all aspects of the STEP trial, we here consider whether the data patterns are meaningful.

[1]Weill Medical College of Cornell University, New York, NY 10065, USA. [2]Infectious Disease Clinical Research Program, San Antonio Military Medical Center, Ft. Sam Houston and Lackland AFB, TX 78234, USA. [3]Veterans Administration Research Center for AIDS and HIV-1 Infection, South Texas Veterans Health Care System, San Antonio, TX 78229, and University of Texas Health Science Center, San Antonio, TX 78229, USA. *E-mail: jpm2003@med.cornell.edu; ahuja@uthscsa.edu

It seems implausible that Ad5-specific antibodies directly protect against HIV-1 infection, as no reasonable mechanism is apparent. On the other hand, it may be that an individual with a high-titer Ad5-specific antibody response can better resist HIV-1 infection naturally. The anti-Ad5 antibody titer could thus be a surrogate marker for a host genetic constitution that confers reduced susceptibility to HIV-1. Other factors, perhaps including immune activation, might outweigh this effect in Ad5 vaccine recipients.

A possible precedent arises from two earlier HIV-1 vaccine trials with the gp120 glycoprotein protein of HIV-1 (AIDSVAX). The infection rates were almost the same in vaccine and placebo recipients, but the titers of gp120-binding antibodies and the risk of HIV-1 infection were inversely correlated (*3*) (see the figure). It is not likely that this correlation arose because binding antibodies are themselves protective. For the overall trial outcome to be neutral (the vaccine conferred no protection compared to the placebo), if above-average titers of gp120-binding antibodies directly protected against infection, then below-average antibody titers would also have to act directly, to place individuals at a greater risk of infection than placebo recipients. This seems improbable. The authors of this study argued that the ability to mount a strong anti-gp120 antibody response inversely measures susceptibility to HIV-1 infection. This scenario might also apply to high anti-Ad5 antibody titers in the STEP trial. Hence, individuals that can mount strong antibody and possibly other relevant immune responses to pathogen antigens may be inherently more resistant to HIV-1 infection—they have "better immune systems."

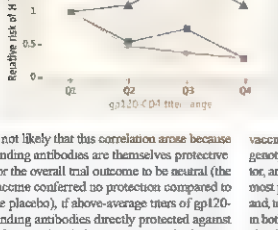

Possible influence of antibody titers on risk of HIV-1 infection. Data from (*3*) show the relative risk of HIV-1 infection in the Ad5-vaccinated (triangles) and placebo (squares) groups from the STEP trial, as a function of the anti-Ad5 antibody titer range. An anti-Ad5 antibody titer of <18 does not mean that an individual has never been exposed to Ad5, as some infected people have subthreshold responses. Data from (*3*) (circles) show the relative risk of HIV-1 infection in recipients of AIDSVAX (gp120) as a function of the titer range of antibodies that block gp120 from binding to CD4, a receptor used by HIV-1 to gain entry into host T cells (other measures of the antibody response to gp120 yield broadly similar plots). The confidence limits on both data sets (not shown) are broad. Both studies are large (5403 participants in the AIDSVAX trial, analysis of the STEP data is based on a subset of 1836 of those enrolled). The statistical significance of the trend shown for the AIDSVAX data is established (*3*), whereas significance of the trend among the STEP data is debatable (*1*). Comparison of the associations is therefore speculative. Not every individual may have been exposed to Ad5 in the STEP trial, whereas in the AIDSVAX trial, every vaccine recipient was given gp120.

There is a modest but significant tendency for individuals with weak antibody responses to one component of a vaccine against measles, mumps, and rubella (MMR) to also respond poorly to the other vaccines (*4*). Moreover, antibody responses to measles and mumps vaccines are influenced by host genetics, including genes encoding antigen-presenting proteins [human leukocyte antigen (HLA)] that are important for immune function, and single-nucleotide polymorphisms in genes encoding cytokines or their receptors, such as interleukin-2 (IL-2), IL-10, and IL-12 receptor β (*5*, *6*). An extrapolation to HIV-1 vaccines suggests that a broad range of host factors, not just those affecting humoral immunity, might influence protection. For example, IL-10 might affect vaccine responses (and susceptibility to infection) by influencing both cellular and humoral immunity (*7*, *8*); gp120 triggers IL-10 production by specific immune cells (dendritic cells) to an extent that varies greatly between individuals (*9*), which may be relevant to understanding the wide range of anti-gp120 antibody titers seen in gp120 vaccinees (*3*).

Host genetic factors may confound HIV vaccine trial evaluation (*10*–*15*). For example, genotypes of CCR5, the major HIV-1 co-receptor, and the gene copy number of CCL3L1, the most potent and HIV-1–suppressive CCR5 ligand, together influence cell-mediated immunity in both HIV-1–negative and –positive individuals (*15*). Genotypes associated with reduced cell-mediated immune responses were similar in the control and HIV-1–infected groups, and predicted an enhanced risk of acquiring HIV-1 and a faster disease course (*15*). Thus, an individual with a "better immune system" might indeed resist HIV-1 infection or partially control replication. This is consistent with observations that pre-seroconversion immune status predicts the rate of HIV-1 infection and rate of immune cell ($CD4^+$ T cell) depletion post-infection (*15*–*17*). A caveat against focusing narrowly upon the antibody response in the STEP trial is supported by the use of cell-mediated immunity–related parameters to define pre-seroconversion immune status in the aforementioned studies (*15*–*17*). Thus, risks for HIV-1 infection may be associated with risks for "a broader spectrum of immunological challenges" that are "reflected in the T cell repertoires of exposed individuals" (*18*).

More complexity is created when the same vaccine is tested in different geographic areas with genetically diverse populations. The STEP trial was conducted mostly in North America and the Caribbean, but a second, now abandoned, trial (PHAMBILI) was initiated in southern Africa. HIV-1 host interactions relevant to the natural history of the epidemic and vaccine responsiveness may be population specific. Indeed, CCR5 genetic determinants influencing AIDS progression rates differ in European Americans and African Americans (*10*). HIV-1 acquisition risk is a product of the susceptibility of uninfected persons and the communicability of HIV-1 from the infected person (*19*, *20*). Communicability is dictated in part by the transmitter's viral load (*19*–*22*), which is influenced by host genetics (*14*, *15*), and also by the genetic makeup of both sexual partners. For example, transmission is more efficient when sexual partners share similar HLA class I alleles (*23*). Thus, even small differences in the frequencies of disadvantageous genetic variants in different vaccine trial cohorts might have a disproportionately large effect on the likelihood that genetically "at-risk" transmitters will encounter similarly "at-risk" recipients. Clinical trial design should take into account the genetically defined individual differences in both susceptibility and transmissibility to better understand puzzling outcomes. Knowledge of population-specific host factors might also help identify what protective effects are attributable to the vaccine or to the host genotype.

Perhaps the STEP trial outcome signals that a step back is needed to seek more information on correlates of protection and susceptibility, rather than initiating trials of broadly similar vaccines (*24*). Additional studies on HIV-1 vaccine cohorts, coordinated with studies of natural infection, might yield useful information about genetic factors influencing both variable vaccine responses and variable susceptibility to infection. Do titers of antibodies to common viral and nonviral

pathogens, including Ad5, correlate with anti-gp120 antibody titers and HIV-1 infection status? What host genetic factors correlate with strong and weak antibody responses? HIV-1 vaccine research must finally step away from its roots in empiricism and embrace new discoveries in immunology and host genetics (*24–26*).

References

1. J. Cohen, *Science* **318**, 1048 (2007).
2. T. C. Pierson *et al.*, *Cell Host Microbe* **1**, 135 (2007).
3. P. B. Gilbert *et al.*, *J. Infect. Dis.* **191**, 666 (2005).
4. J. L. St. Sauver *et al.*, *Vaccine* **19**, 3363 (2001).
5. G. Ovsyannikova *et al.*, *Vaccine* **25**, 3090 (2007).
6. M. Ohman *et al.*, *J. Infect. Dis.* **195**, 21 (2007).
7. H. D. Shin *et al.*, *Proc. Natl. Acad. Sci. U.S.A.* **97**, 14467 [illegible]
8. K. W. Moore *et al.*, *Annu. Rev. Immunol.* **19**, 683 (2001).
9. M. Shen *et al.*, *PLoS Pathog.* **3**, e169 (2007).
10. E. Gonzalez *et al.*, *Proc. Natl. Acad. Sci. U.S.A.* **96**, 12004 (1999).
11. E. Gonzalez *et al.*, *Proc. Natl. Acad. Sci. U.S.A.* **98**, 5199 (2001).
12. S. J. O'Brien, G. W. Nelson, *Nat. Genet.* **36**, 565 (2004).
13. J. Cohen, *Science* **307**, 23 (2005).
14. E. Gonzalez *et al.*, *Science* **307**, 1434 (2005).
15. M. J. Dolan *et al.*, *Nat. Immunol.* **12**, 1324 (2007).
16. F. A. Koning *et al.*, *J. Immunol.* **175**, 6117 (2005).
17. L. Van Asten *et al.*, *AIDS* **18**, 1885 (2004).
18. M. S. Killian *et al.*, *AIDS* **18**, 161 (2004).
19. R. Anderson, M. Hanson, *J. Infect. Dis.* **191** (suppl. 1), S85 (2005).
20. S. Blower, E. J. Schwartz, J. Mills, *AIDS Rev.* **5**, 113 (2003).
21. R. H. Gray *et al.*, *Lancet* **357**, 1149 (2001).
22. T. C. Quinn *et al.*, *N. Engl. J. Med.* **342**, 921 (2000).
23. S. K. Ahuja, G. Catano, *Lancet* **363**, 2109 (2004).
24. R. C. Desrosiers, *Nat. Med.* **10**, 221 (2004).
25. D. R. Burton *et al.*, *Nat. Immunol.* **5**, 233 (2004).
26. R. C. Gallo, *Lancet* **366**, 1894 (2005).

10.1126/science.1154258

BIOCHEMISTRY

Tinkering with Acellular Division

Self organization of proteins involved in bacterial cell division is demonstrated in vitro.

Joe Lutkenhaus

One way to understand a complex biological process is to reconstitute it from purified components. Among many notable successes are the initiation of bacterial DNA replication, protein secretion in prokaryotic and eukaryotic cells, and assembly of the mitotic spindle that segregates chromosomes during eukaryotic cell division. For many other complex processes, reconstitution seems feasible, but for cytokinesis—the last stage of cell division in which the cytoplasm is divided to produce two daughter cells—this seems a formidable task. One might assume that a cell would be necessary to reconstitute such a phenomenon. However, two papers in this issue—by Osawa *et al.* on page 792 (*1*) and by Loose *et al.* on page 789 (*2*)—indicate that bacterial cytokinesis may be achievable in a cell-free system.

Simple and elegant. The oscillation of Min proteins from end to end in a bacterium confines the Z ring (composed of FtsZ protein filaments) to the midcell region, where the final stage of cell division will occur. (Inset) Fluorescently labeled MinD (green) and FtsZ (red) are shown in an *E. coli* cell. [Reprinted from (*18*) with permission from Wiley-Blackwell]

Cytokinesis in almost all bacteria and archaea, and in some organelles (chloroplasts and some mitochondria), uses a cytoskeletal element called the Z ring (*3*), which consists of filaments of polymerized FtsZ protein (see the figure), the bacterial homolog of the eukaryotic cytoskeletal protein tubulin (*4*). The Z ring provides a scaffold to recruit at least 10 additional proteins required for cytokinesis, many of which link the Z ring to synthesis of a new cell wall that accompanies formation of the septum. Though conserved in most bacteria, these proteins are not present in the simplest bacteria that lack a cell wall. In these bacteria, only FtsZ is found, raising the question of whether it is sufficient for constriction of a bacterium lacking a rigid cell wall.

FtsZ does not attach directly to the bacterial membrane but uses a short, conserved carboxyl-terminal tail to bind to other membrane-bound proteins (*5*). Even in bacteria that lack a cell wall, this FtsZ tail is conserved, suggesting that some as yet unknown protein is involved. To circumvent this requirement for membrane attachment in a reconstituted system, Osawa *et al.* replaced the conserved tail with a fluorescent protein and an amphipathic helix borrowed from the bacterial peripheral membrane protein MinD. After mixing this fusion protein with phospholipid vesicles and guanosine 5′-triphosphate (GTP, needed for polymerization of FtsZ), they observed Z rings moving within cylindrical tubes of lipid. Coalescence of faint rings into brighter rings led to partial constriction of the tube. With limiting GTP, constrictions at the Z rings disappeared as the constrictions were resorbed. The study thus reveals that a dynamic Z ring can produce a force capable of initiating a constriction and argues that FtsZ itself (provided it is attached to the membrane) can assemble the Z ring.

FtsZ filaments are thought to be too short to form a complete ring (*6*). One possibility is that the ring is built through lateral interaction of the filaments. Also, the coalescence of faint rings to form the brighter rings that cause constriction suggests that lateral interactions between filaments may be involved. This is somewhat controversial as no contiguous ring of filaments is observed by electron tomography, a technique with high resolution (*7*). Perhaps not all filaments in the ring are preserved with this technique or membrane-tethered filaments are brought together by membrane distortions caused by their lipid anchors.

In the dividing bacterial cell, a Z ring is present long before constriction begins (*8*, *9*). This suggests that one of the roles for the additional cell division proteins is regulatory—to hold the Z ring in check until the appropriate signal for constriction is received. Spatial regulation ensures that the Z ring forms at the cell center (*10*, *11*). In the model bacterium *Escherichia coli*, an important component of spatial regulation is a rapid oscillator that shuttles an inhibitor of Z ring assembly between the ends of the cell. This oscillation occurs many times during the time course of a cell division cycle, resulting in a time-averaged concentration of the inhibitor that is lowest at midcell. The oscillator consists of an adenosine triphosphatase (ATPase) (MinD) and an activator (MinE). The dynamic behavior of these proteins results from the ATP-dependent accumulation of MinD on the membrane followed by its recruitment of MinE (*12*, *13*).

Department of Microbiology, Molecular Genetics and Immunology, University of Kansas Medical Center, Kansas City, KS 66160, USA. E-mail: jlutkenh@kumc.edu

MinE stimulates the ATPase, releasing the proteins from the membrane. A challenge has been to understand how this dynamic interplay with the membrane is translated into a very orderly oscillation in the confines of the cell.

The simplicity of this system has attracted mathematical modelers seeking to determine the essential features necessary to produce the oscillation (*14*). Although none of the models are yet predictive and several variations exist, they suggest possibilities for the underlying mechanisms. A common basis for these models is that interactions between the proteins and the membrane prevent a uniform distribution—so-called dynamic instability. But questions have remained as to whether MinD and MinE are sufficient to generate the oscillations.

As a first attempt to recreate the oscillation, Loose *et al.* added fluorescently labeled MinD, MinE, and an energy source (ATP) to an enclosed system containing a lipid bilayer supported on a mica surface. An initial even distribution of the proteins on the bilayer evolved into waves of MinD and MinE moving across the surface. Each wave consisted of a wide band of MinD with a peak of MinE at the lagging edge of this band—MinE chewing away at the MinD with the released MinD regrouping at the leading edge of the band, resulting in a traveling wave. This wave is reminiscent of the oscillation in vivo where MinE chases MinD from midcell to one end of the cell (*15*–*17*).

The studies by Osawa *et al.* and Loose *et al.* show that two important components of bacterial cell division can self-organize once they are put into a container. So elegant and so simple. With the Z ring and the Min oscillation established in vitro, the next question is whether these systems can be combined to achieve spatial regulation.

References and Notes

1. M. Osawa, D. E. Anderson, H. P. Erickson, *Science* **320**, 792 (2008); published online 17 April 2008 (10.1126/science.1154520).
2. M. Loose, E. Fischer-Friedrich, J. Ries, K. Kruse, P. Schwille, *Science* **320**, 789 (2008).
3. J. Lutkenhaus, S. G. Addinall, *Annu. Rev. Biochem.* **66**, 93 (1997).
4. P. van den Ent, L. Amos, J. Lowe, *Curr. Opin. Microbiol.* **4**, 634 (2001).
5. S. Pichoff, J. Lutkenhaus, *EMBO J.* **21**, 685 (2002).
6. Y. Chen, H. P. Erickson, *J. Biol. Chem.* **280**, 22549 (2005).
7. Z. Lu, M. J. Trimble, Y. V. Brun, G. J. Jensen, *EMBO J.* **26**, 4694 (2007).
8. S. G. Addinall, E. Bi, J. Lutkenhaus, *J. Bacteriol.* **178**, 3877 (1996).
9. M. E. Aarsman *et al.*, *Mol. Microbiol.* **55**, 1631 (2005).
10. L. Rothfield, A. Taghbalout, Y. L. Shih, *Nat. Rev. Microbiol.* **3**, 959 (2005).
11. J. Lutkenhaus, *Annu. Rev. Biochem.* **76**, 539 (2007).
12. Z. Hu, J. Lutkenhaus, *Mol. Cell* **7**, 1337 (2001).
13. Z. Hu, E. P. Gogol, J. Lutkenhaus, *Proc. Natl. Acad. Sci. U.S.A.* **99**, 6761 (2002).
14. K. Kruse, M. Howard, W. Margolin, *Mol. Microbiol.* **63**, 1279 (2007).
15. X. Fu, Y. L. Shih, Y. Zhang, L. I. Rothfield, *Proc. Natl. Acad. Sci. U.S.A.* **98**, 980 (2001).
16. D. M. Raskin, P. A. de Boer, *Proc. Natl. Acad. Sci. U.S.A.* **96**, 4971 (1999).
17. C. A. Hale, H. Meinhardt, P. A. de Boer, *EMBO J.* **20**, 1563 (2001).
18. Y. L. Shih, T. Kawagishi, L. Rothfield, *Mol. Microbiol.* **58**, 917 (2005).

19. J.L.'s work is supported by NIH grant R37GM09764.

10.1126/science.1158463

MATERIALS SCIENCE

High-Frequency Chip Connections

Advanced interconnects will be required to keep pace with the increasing speed of future microelectronics

Todd J. Spencer, Tyler Osborn, Paul A. Kohl

The bandwidth needs for future electronic systems are expected to expand in the next decade because of the large data requirements of multimedia and high-performance computing systems. With the frequency of high-speed input-output (I/O) connections expected to increase from the 2 GHz currently available to more than 67 GHz (*1*), this will require not only fast and reliable processors, but equally fast and reliable data links between system components and the network. We discuss some of the advances that have been achieved and the challenges that lie ahead for high-performance interconnects.

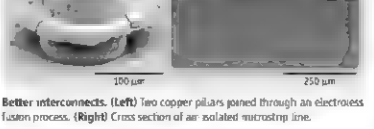

Better interconnects. (Left) Two copper pillars joined through an electroless fusion process. **(Right)** Cross section of an isolated microstrip line.

High-speed communication between microprocessors and other chips or networks depends on both electrical and optical links. Optical links are particularly beneficial over long distances (tens of meters to several kilometers) because of the low loss in optical fibers. Multiple data sets can be transmitted through the same fiber, providing higher data rates than those achievable electrically. Signal-processing techniques can also improve data rates but have disadvantages in circuit complexity and power dissipation. Optical interconnects also perform well at short distances (tens of micrometers to meters) (*2*), but integration is difficult because of the requirements of precise alignment and losses at 90° routing angles. Optical sources and receivers must also be maintained at prescribed temperatures to prevent changes in operating characteristics (such as wavelength and current) that can render the device inoperable.

Electrical connections alleviate many integration challenges in high-performance computing systems but require improvements to reduce the signal loss. An electrical signal falls off exponentially, with a decay constant γ, along the length of a transmission line. This signal decay arises from electrostatic (i.e., capacitive) and magnetic (i.e., inductive) contributions from the circuitry. To achieve low loss, the lines must have insulators that provide low capacitance and inductance. The lines must also be insulated from neighboring lines to prevent cross-talk and undesirable capacitive coupling and inductance that contribute to noise in the circuit.

For more than a decade, the first-level connection between a high-performance chip and the external circuitry has typically been made via solder ball connections between the chip and an epoxy fiberglass substrate. However, solder has many restrictions as the interconnect size continues to shrink. The formation of brittle copper-tin intermetallics can compromise thermomechanical reliability. Solder also has low electromigration resistance, which becomes important as the diameter of interconnects is reduced and current density

School of Chemical and Biomolecular Engineering, Georgia Institute of Technology, Atlanta, GA 30332, USA. E-mail: kohl@gatech.edu

increases. Solder connections are limited to spheres with an aspect ratio of 1.1 (height:diameter), making connections with high aspect ratios (large chip-to-substrate stand-off distances) very difficult to fabricate. This causes difficulties with flow in the placement of underfill (a stress-distributing layer around the solder balls). Fragile on-chip interlayer dielectrics require lower-stress I/O so as not to cause fracture.

The next frontier is an all-copper chip-to-substrate interconnect, which would eliminate many of the problems with solder. Copper has superior electrical properties relative to solder with respect to both electrical conductivity and electromigration resistance. It also has superior mechanical properties, such as yield stress and elastic modulus, that allow for the design of mechanically compliant interconnect structures. Having no tin-based materials present eliminates the formation of brittle intermetallics, thus leading to an improvement in the thermomechanical reliability of the device. Finally, copper interconnects are capable of forming high aspect ratios because they are not melt-cast and therefore don't need to be spherical in shape. This will pave the way for fine-pitch interconnects with higher stand-off distances and complex shapes, such as shielded coaxial structures, which can support high-frequency I/O. Copper-to-copper bonding via methods that are compatible with temperature-sensitive substrate materials has been reported using surface-activated bonding (*3*) and electroless deposition and annealing (*4*). The left panel of the figure shows two (short) copper pillars joined by the all-copper electroless process. Such copper bonding facilitates connections for low-loss high-frequency operation that is not possible with solder.

Substrate and board-level signaling are particularly challenging because of the longer wires that require small γ to maintain adequate voltages. Conventional board-level wires, etched copper traces on fiberglass and epoxy substrates, suffer from large losses due to substrate capacitance and conductance. Improved performance can be achieved with more expensive ceramic substrates that offer comparable capacitance loss while reducing dielectric conductance. Such ceramics offer mechanical benefits due to the lower coefficient of thermal expansion.

Substrate capacitance can be reduced through the use of polymer dielectrics, although this typically is associated with an increase in substrate conductance. Further reduction of the coupling capacitances and conductances can be achieved by incorporating gaseous cavities in the material, via either a porous matrix or a continuous air cavity supported by a dielectric (*5*). At higher frequencies, such nonhomogeneous dielectric layers are undesirable, as propagation at different velocities through different media leads to distortion of the electric field. Copper surface roughness can also degrade performance at high frequencies because of the longer path length along the surface, where charge concentrates at higher frequencies as a result of the skin effect. Surface undulations due to glass fibers in epoxy-fiberglass substrates pose challenges to both electrical and optical systems (*6*).

System-level integration of air-insulated copper lines will remain difficult until a variety of mechanical, thermal, and electrical considerations are addressed. Mechanical integrity of copper lines is important to maintain reliability and prevent failure due to stress and electromigration (*7*). Inclusion of air insulation thus poses a particular challenge, as the lack of confining stress allows copper surface diffusion to proceed with greater ease (*8*). The right panel in the figure shows a microstrip copper signal line on a substrate with its return path separated by an air-polymer gap. Moisture absorption into air cavities is particularly troublesome because it can increase the capacitance and conductance, which may result in short circuits. Air-insulated circuits will require surface treatments or hermetic sealing to circumvent these challenges. Maximized electrical performance ultimately corresponds to minimized thermal performance, as air is also an ideal thermal insulator. This increase in thermal resistance may limit heat removal from the package and prevent further improvements in system performance.

Any advances in integrated circuit performance will need to be matched by performance enhancements at the package level. Work is under way toward providing cost-effective high-speed chip-to-chip communication.

References and Notes

1. International Technology Roadmap for Semiconductors, 2007 (www.itrs.net).
2. H. Cho, K. -H. Koo, P. Kapur, K. C. Saraswat, *IEEE Electron Device Lett.* **29**, 122 (2008).
3. T. H. Kim, M. M. Howlader, T. Itoh, T. Suga, *J. Vac. Sci. Technol. A* **21**, 44 (2003).
4. T. Osborn, A. Ho, N. Galiba, P. A. Kohl, *J. Electrochem. Soc.* **155**, D308 (2008).
5. T. J. Spencer, P. J. Joseph, T. H. Kim, M. Swaminathan, P. A. Kohl, *IEEE Trans. Microwave Theory Tech.* **55**, 1911 (2007).
6. T. K. Gaylord, Y. J. Chang, *Appl. Opt.* **46**, 6476 (2007).
7. B. Li, T. D. Sullivan, T. C. Lee, D. Badami, *Microelectron. Reliabil.* **44**, 365 (2004).
8. Z.-S. Choi, R. Monig, C. V. Thompson, *J. Appl. Phys.* **102**, 083509 (2007).

9. Supported by the Semiconductor Research Corporation through the Focus Center Research Program (Interconnect Focus Center) and GRC programs.

10.1126/science.1157129

BIOGEOCHEMISTRY

News About Nitrogen

M. Claire Horner-Devine[1] and Adam C. Martiny[2]

Discoveries of microbial pathways, players, and population dynamics challenge conventional models of the nitrogen cycle

Understanding of microbial diversity and interactions is crucial for quantifying fluxes in nutrient cycles and forecasting ecosystem responses to global environmental changes. This is particularly true for the nitrogen cycle. In contrast to the carbon cycle, none of the steps in the nitrogen cycle can be measured at a global scale on the basis of satellite data. Instead, global biogeochemical models rely on field measurements of nitrogen concentrations and fluxes, combined with rate constants from a few known organisms, to balance the net flux of nitrogen. Thus, incomplete knowledge of microbial diversity and ecological dynamics may mislead estimates of fluxes in the nitrogen cycle.

Three discoveries illustrate how much scientists are still learning about the nitrogen cycle. First, ammonia oxidation by microbes was thought to proceed only in the presence of oxygen. However, bacteria have been shown to be capable of oxidizing ammonium anaerobically, using nitrite rather than oxygen as the electron acceptor, resulting in the production of N_2 gas (*1*). Although this "anammox" reaction was theoretically predicted, finding anammox organisms has helped to explain deviations between models of the marine nitrogen cycle and observed ammonia concentrations and N_2 production in anaerobic marine environments (*2*).

[1]School of Aquatic and Fishery Sciences, University of Washington, Seattle, WA 98195, USA. [2]Earth System Science and Ecology and Evolutionary Biology, University of California, Irvine, CA 92697, USA. E-mail: mchd@u.washington.edu

Second, archaea—previously thought to inhabit only extreme environments—have been shown to constitute a substantial proportion of marine plankton worldwide (*3*, *4*). Some archaea have the genetic capacity for ammonia oxidation, as evidenced by an archaeal version of the ammonia monooxygenase (*amoA*) gene (*5*, *6*). Perhaps more important, the cultivation of an ammonia-oxidizing archaeon in the laboratory allowed researchers to establish a link between the presence of the *amoA* gene and archaeal ammonia oxidation (*7*). Field studies show that archaea likely contribute substantially to nitrification in marine and terrestrial environments (*8*–*11*).

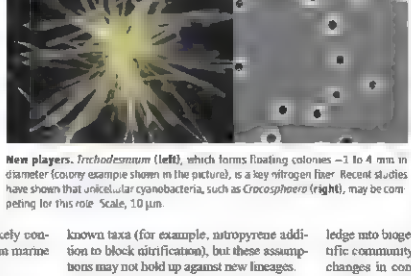

New players. *Trichodesmium* (**left**), which forms floating colonies ~1 to 4 mm in diameter (colony example shown in the picture), is a key nitrogen fixer. Recent studies have shown that unicellular cyanobacteria, such as *Crocosphaera* (**right**), may be competing for this role. Scale, 10 μm.

Third, researchers have found several new lineages responsible for nitrogen fixation *Trichodesmium* (see the figure, left panel) and symbionts of diatoms were long thought to be the major nitrogen fixers or diazotrophs in the open ocean, the discovery of this trait in unicellular cyanobacteria (see the figure, right panel) suggests that this is not the case. Researchers have found novel lineages of N_2 fixers in hot springs, including cyanobacteria and archaea (*12*, *13*). These findings suggest that the ability to fix nitrogen is widely distributed among bacteria and archaea.

From a biogeochemical perspective, one might argue that all this diversity may not matter to our understanding of nutrient fluxes. Microbial ecologists will likely continue to discover new lineages capable of a given reaction, but incorporating all these groups into ecosystem models would be intractable. However, the discovery that such disparate groups are involved in ammonia oxidation, nitrogen fixation, and other steps in the nitrogen cycle calls for a reevaluation of the assumptions made in biogeochemical models and field experiments (*14*). Many rate constants used in models are based on only a few taxa. These rate constants may be very different from those of newly discovered taxa, and some of these new players may have very different nutrient or energy requirements.

For example, two dominant marine N_2 fixers—*Trichodesmium* and unicellular cyanobacteria (see the figure)—may have vastly different phosphate uptake kinetics due to differences in cell size and physiology (*15*). This could be important for predicting the response of diazotrophs to a shift from a nitrogen- to phosphorus-controlled ocean environment in the North Pacific Subtropical Gyre (*16*). In addition, several assays used to measure nitrogen transformation rates were based on known taxa (for example, nitropyrene addition to block nitrification), but these assumptions may not hold up against new lineages.

In addition to new pathways and players, understanding of the global nitrogen cycle has recently benefited from work at a smaller scale of organization: the interaction between populations. Experiments in wastewater bioreactors revealed that the dynamics of two guilds involved in nitrification are tightly linked to nitrogen transformation rates. Guilds of ammonia- and nitrite-oxidizing bacteria were prone to chaotic behavior, resulting in marked temporal variation in nitrification (*17*). Increasing variation in the abundance of ammonia-oxidizing bacteria was associated with large, destabilizing variations in nitrite-oxidizing bacterial abundance, resulting in the extinction of *Nitrospira* and the breakdown of nitrification (*18*). Thus, complexity and dynamics at these small scales of organization can have important consequences for local nitrogen transformation rates.

The above results suggest critical gaps in our knowledge of the relationship between microbial composition and nutrient fluxes. Changes in community composition in a particular microbial functional group can be associated with changes in nutrient cycling rates (*19*–*21*), implying that all microbes in a functional group are not functionally redundant. We must understand when, where, and at what scale of organization it is necessary to consider complex dynamics and shifts in composition in ecosystem models. Nitrogen cycle monitoring and modeling may require more sophisticated representations of microbial communities, as was recently proposed for marine phytoplankton (*22*).

Novel ways of understanding and incorporating new pathways, players, and population dynamics may be particularly pertinent for forecasting nutrient dynamics in the face of human disturbances. Human activities increasingly dominate nitrogen input in many regions of the world. Combined with climate change, these perturbations are globally altering nitrogen dynamics (*23*) and are likely changing microbial community composition and activity (*24*). Our ability to forecast ecosystem responses to human disturbances would benefit from a coordinated effort of both observational and experimental studies and integration of this knowledge into biogeochemical models. The scientific community must better understand how changes in community and population dynamics are related to nitrogen transformation rates and how both the players and the processes respond to disturbances. Only by understanding nitrogen cycling at a range of scales of biological organization can scientists predict how anthropogenic pressures will influence local and global nitrogen dynamics.

References

1. A. Mulder, A. A. Vandegraaf, L. A. Robertson, J. G. Kuenen, *FEMS Microbiol. Ecol.* **16**, 177 (1995).
2. M. M. M. Kuypers *et al.*, *Proc. Natl. Acad. Sci. U.S.A.* **102**, 6478 (2005).
3. J. A. Fuhrman, K. McCallum, A. A. Davis, *Nature* **356**, 148 (1992).
4. E. F. DeLong, *Proc. Natl. Acad. Sci. U.S.A.* **89**, 5685 (1992).
5. J. C. Venter *et al.*, *Science* **304**, 66 (2004); published online 4 March 2004 (10.1126/science.1093857).
6. A. H. Treusch *et al.*, *Environ. Microbiol.* **7**, 1985 (2005).
7. M. Konneke *et al.*, *Nature* **437**, 543 (2005).
8. C. Wuchter *et al.*, *Proc. Natl. Acad. Sci. U.S.A.* **103**, 12317 (2006).
9. S. Leininger *et al.*, *Nature* **442**, 806 (2006).
10. J. M. Caffrey, N. Bano, K. Kalanetra, J. T. Hollibaugh, *ISME J.* **1**, 660 (2007).
11. J. M. Beman, B. N. Popp, C. A. Francis, *ISME J.* **2**, 429 (2008).
12. M. P. Mehta, J. A. Baross, *Science* **314**, 1783 (2006).
13. A. S. Steunou *et al.*, *Proc. Natl. Acad. Sci. U.S.A.* **103**, 2398 (2006).
14. C. Deutsch, J. L. Sarmiento, D. M. Sigman, N. Gruber, J. P. Dunne, *Nature* **445**, 163 (2007).
15. J. A. Sohm, D. G. Capone, *Mar. Ecol. Prog. Ser.* **317**, 21 (2006).
16. D. M. Karl, R. R. Bidigare, R. M. Letelier, *Deep Sea Res. II* **48**, 1449 (2001).
17. D. W. Graham *et al.*, *ISME J.* **1**, 385 (2007).
18. C. W. Knapp, D. W. Graham, *FEMS Microbiol. Ecol.* **62**, 195 (2007).
19. C. V. Hawkes, J. F. Wren, D. J. Herman, M. K. Firestone, *Ecol. Lett.* **8**, 976 (2005).
20. K. M. Carney, P. A. Matson, D. J. N. Bohannan, *Ecol. Lett.* **7**, 684 (2004).
21. G. Webster, T. M. Embley, T. E. Freitag, Z. Smith, J. I. Prosser, *Environ. Microbiol.* **7**, 676 (2005).
22. M. J. Follows, S. Dutkiewicz, S. Grant, S. W. Chisholm, *Science* **315**, 1843 (2007).
23. P. Vitousek *et al.*, *Ecol. Appl.* **7**, 737 (1997).
24. H. P. Horz, A. Barbrook, C. B. Field, B. J. M. Bohannan, *Proc. Natl. Acad. Sci. U.S.A.* **101**, 15136 (2004).

10.1126/science.1147012

Toward an AIDS Vaccine

Bruce D. Walker[1,2]* and Dennis R. Burton[3]*

A quarter century of scientific discovery has been applied to developing an AIDS vaccine, yet this goal remains elusive. Specific characteristics of the virus, including the extreme genetic variability in circulating viral isolates worldwide, biological properties of HIV that impede immune attack, and a high mutation rate that allows for rapid escape from adaptive immune responses, render this a huge challenge. However, evidence of protection against AIDS viruses in animal models and control of HIV in humans under certain circumstances, together with scientific advances in understanding disease pathogenesis, provide a strong rationale and objective paths to continue the pursuit of an effective AIDS vaccine to stem the global epidemic.

Twenty-five years ago, a report in this journal of the discovery of a pathogenic human retrovirus (*1*) led to great optimism that a solution to an emerging lethal epidemic was at hand. This discovery, along with subsequent key confirmatory reports the following year (*2*–*5*), firmly established human immunodeficiency virus (HIV) as the causative agent of AIDS and prompted then U.S. Health Secretary Margaret Heckler to publicly proclaim at a news conference on April 23, 1984, that a preventive HIV vaccine could be expected to be available for testing within 2 years.

A quarter of a century later, HIV continues to wreak havoc on a global scale, with the most devastating consequences seen in the most impoverished nations. Despite tremendous advances in the development of life-extending anti-HIV medications and an understanding of how HIV causes disease, there have already been more than 25 million deaths. Nearly a billion dollars is spent globally on HIV/AIDS research annually, and yet the sobering reality is that at present there are no promising candidates for an HIV vaccine. The most recently tested vaccine, a collaboration between Merck and the National Institutes of Health (NIH), is only the second candidate HIV vaccine to complete efficacy testing in humans, despite considerable hope, the outcome may have been worse than simple failure. Not only did the vaccine not protect against infection, nor contain virus replication in those who became infected, apparently it increased susceptibility to infection in persons who had preexisting antibodies to the adenovirus vector used to deliver the HIV vaccine antigens (*6*). The failure of this vaccine has led some leaders in the field to question whether an AIDS vaccine is feasible given what is currently known (*6*).

This review will address the quest for an HIV vaccine in the broader context of why collective efforts and steady progress by two generations of committed scientists have failed to deliver on the early promise of an effective AIDS vaccine and suggest paths forward to attain this elusive goal.

Vaccines That Work and Why

Since Edward Jenner's success with smallpox immunization in 1796, there have been dramatic immunization related reductions in disease incidence for a number of viral diseases including polio, measles, mumps, rubella, hepatitis B, and influenza. For each of these, protection has been achieved by mimicking infection with the pathogen and thereby establishing immunologic memory that can rapidly respond should an actual infection occur. This has been perhaps best achieved with the use of live attenuated virus vaccines, such as the mumps and measles vaccines, which infect the host but do not cause disease and elicit strong and long-lasting immune responses. A second successful approach involves the use of killed virus vaccines, an example of which is the original Salk killed poliovirus vaccine, used in the first widespread polio vaccination campaigns in the mid 20th century. A third approach employs exposure of the immune system to recombinant viral proteins alone, as in the current highly successful hepatitis B vaccine.

The goal of each of these vaccination strategies is to have an immunologic barrier in place that will prevent infection or, failing that, minimize symptoms of disease caused by virus infection. Successful vaccines have typically been generated against pathogens for which the immune response thwarts serious disease in a substantial fraction of those infected. Remarkably, knowledge of how vaccine barriers function to protect against infection and/or disease remains limited. What is known is largely built upon observations from animal models but, although these are widely accepted as relevant to human vaccines, direct mechanistic evidence for how any vaccine works in humans is sparse.

The main gatekeeper in most vaccination strategies is thought to be neutralizing antibody (Fig. 1). Preexisting serum or mucosal antibody induced by an earlier infection or through vaccination can bind to free virus particles, prevent viral entry to host cells ("neutralization"), and therefore prevent the establishment of infection. Even if some host cells are infected, antibody can bind to such cells, trigger their elimination via host effector systems, and perhaps contribute to aborting infection. Immunity generated in these types of scenarios is termed "sterilizing," and neutralizing antibodies administered intravenously or mucosally can alone provide sterilizing immunity against several viruses in experimental animal models. Realistically, for most human

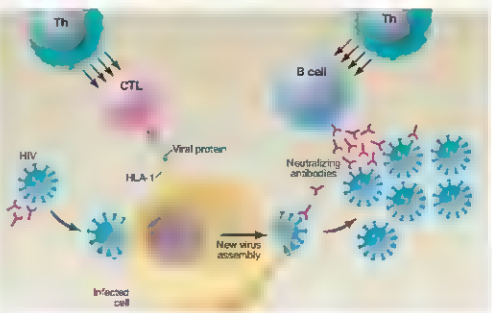

Fig. 1. Adaptive immune responses in HIV infection. HIV infection of cells can be prevented by antibodies that can neutralize free virus before progeny viruses are produced, can neutralize newly released virions from infected cells, and can act against infected cells. CTLs act once a cell becomes infected by recognizing processed viral proteins presented in the context of HLA class I molecules at the cell surface through the T cell receptor of the CTL. Coordination of CTL and neutralizing antibody responses is mediated by $CD4^+$ T helper (Th) cells.

[1]Massachusetts General Hospital and Harvard Medical School, Boston, MA 02129, USA. [2]Howard Hughes Medical Institute, Chevy Chase, MD 20815, USA. [3]The Scripps Research Institute, La Jolla, CA 92037, USA.

*To whom correspondence should be addressed. E-mail: bwalker@partners.org, burton@scripps.edu

vaccines, antibodies are unlikely to provide sterilizing immunity; rather, they limit the initial burst of virus replication such that it can then be contained by ongoing immune responses without substantial disease symptoms—the most likely mechanism for most successful vaccines.

The most important second line of defense is the cellular immune response, particularly cytotoxic T lymphocytes (CTLs). Immunization with the appropriate T cell–inducing vaccine generates a population of memory T cells that can rapidly expand in the first days after infection. These expanding CTLs kill infected cells by recognizing foreign viral proteins that bind to developing human leukocyte antigen (HLA) class I molecules and are displayed at the cell surface, providing a signal that the cell should be eliminated (Fig. 1). Lysis of a virus-infected cell before the assembly of mature progeny virions leads to elimination of the virus, which undergoes rapid degradation in the extracellular milieu in the absence of the protective outer envelope. CTLs also release antiviral cytokines, which may act to limit the impact of progeny virions already produced (*7*). Many live attenuated vaccines elicit both neutralizing antibodies and CTL, the combination of which is likely to be necessary for rapid elimination of the virus or successful immunologic containment preventing the development of disease. CTL can also be induced by killed virus and recombinant protein vaccines through cross-priming when these vaccine antigens are taken up by professional antigen-presenting cells. Even in the case of vaccines that induce neutralizing antibodies, CTL may also be induced by the infection and contribute to preventing symptomatic disease. Optimal coordination of both neutralizing antibody and CTL responses requires induction of virus-specific CD4 T cell responses (Fig. 1).

Unique Challenges for HIV Vaccination

The tremendous global success with other viral vaccines raises the question as to why HIV vaccine development has been so difficult. Many of the difficulties lie in distinct properties of this virus compared with other viruses (Table 1). Foremost among these is HIV's enormous sequence diversity. Because of an error-prone reverse transcriptase, a high propensity for recombination, and an extremely rapid turnover in vivo, HIV's capacity for mutation and adaptation is enormous (*8*). There are three different groups of HIV globally (M, N, and O), and group M is further subdivided into nine distinct subtypes and numerous additional circulating recombinant forms. Viruses even within the same HIV-1 subtype may differ by up to 20%, and in places such as Africa where there are multiple subtypes, circulating viruses can differ within the highly variable envelope protein by up to 38% (Fig. 2). Indeed, the amount of HIV diversity within a single infected individual can exceed the variability generated over the course of a global influenza epidemic, the latter of which results in the need for a new vaccine each year. With more than 33 million people currently infected with HIV, and the need for a vaccine that simultaneously protects against all potential exposures, HIV sequence diversity alone represents a staggering challenge.

A further hurdle to AIDS vaccine development is that HIV is an infection of the immune system, specifically targeting $CD4^+$ T lymphocytes. Within days of exposure, massive infection and loss of memory $CD4^+$ T cells ensues, particularly within the gut-associated lymphoid tissue (*9*, *10*) where most of these cells reside. The loss of these cells, which are critical for coordinating effective immune responses, results in considerable immune impairment within the first weeks of HIV infection. Furthermore, bacterial translocation across a damaged intestinal mucosa may even help to drive ongoing $CD4^+$ T cell activation and facilitate viral replication, which is most efficient in activated cells (*11*).

Yet another challenge is that HIV has evolved strategies to avoid immune elimination. Particularly notable examples include the accessory protein Nef, which down-regulates molecules of the major histocompatibility complex (MHC) that are crucial for T cell recognition of infected cells (*12*, *13*), and surface envelope proteins, which incorporate multiple features to avoid antibody recognition (*14*). HIV also rapidly establishes a latent reservoir of infected lymphocytes by inte-

Table 1. Properties of HIV that hinder vaccine development.

Sequence diversity
Infection of critical immune cells
Immune avoidance
Masking of neutralization epitopes
MHC down-regulation
Immune escape through viral mutation
Counter-immunoregulatory mechanisms
Latency

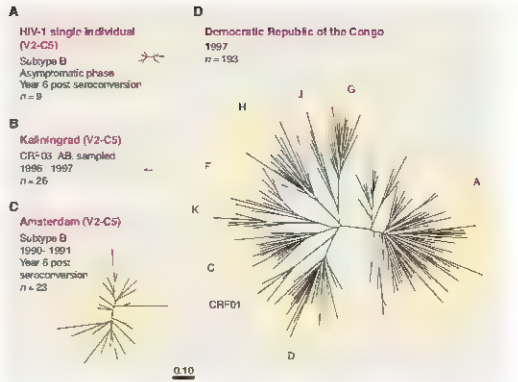

Fig. 2. Representations of HIV diversity under differing circumstances. A comparison of the evolutionary distances of DNA encoding HIV-1 partial envelope gene sequences (C2-V5) through phylogenetic analysis is shown in a "tree" representation. (**A**) Tree based on nine sequences taken from an asymptomatic individual 73 months after seroconversion of a subtype B infection. This tree is the result of a typical example of sampling of intrapatient diversity at one time point. (**B**) Tree based on HIV-1 circulating recombinant form CRF03_AB sequences derived from samples taken from 26 Kaliningrad individuals. The Kaliningrad epidemic represents a unique situation in which a recombinant form of the virus spread explosively through a population of intravenous drug users and all viruses were extremely closely related to their most recent common ancestor. These samples were collected in 1997 to 1998, less than a year after the strain had been introduced to the population. Drawn at this scale, the tree appears as a dot because of the lack of diversity. (**C**) Tree based on sequences representing a subtype B epidemic, sampled from 23 individuals residing in Amsterdam in 1990 to 1991. (**D**) Tree based on HIV-1 V2-C5 sequences sampled in 1997 from 193 individuals residing in the Democratic Republic of the Congo. This is a remarkably diverse set. The HIV-1 subtypes are labeled, and the full spectrum of diversity found in the HIV-1 M group is represented by the epidemic occurring in this region. All panels show maximum likelihood trees generated using a REV model and allowing for rate variation at different sites (*23*). The genetic distance scale bar is shown. [From (*8*, *52*)].

gration of its genetic material into the host chromosome. This represents one of the greatest challenges because this is an irreversible process that occurs immediately after infection and ends only with the death of the infected cell (*15*). The virus is immunologically silent in this latent reservoir, but production of infectious virus particles may be subsequently initiated if cells become activated at a later time. The stability of this reservoir means that lifelong infection of the host is maintained, even in the face of potent anti-HIV medication.

All of these features of the virus mean that an optimal HIV vaccine will need to recognize a huge array of diverse viruses, and with sufficient speed to prevent the establishment of a latent reservoir. Failing this, it will need to augment natural immune responses so as to prevent the early wholesale destruction of the CD4 cell population and immunologically suppress virus for the lifetime of the individual, without allowing for immune escape. Such enormous challenges are made even more important by the lack of understanding of the immune responses that can control HIV replication.

The Neutralizing Antibody Problem

A huge gap in HIV vaccine development is the failure to generate an immunogen to elicit effective neutralizing antibodies. Only one antibody-based AIDS vaccine has been taken through efficacy trials thus far, using the gp120 subunit protein as an immunogen, and this vaccine candidate did not elicit antibodies neutralizing field isolates of HIV, did not prevent infection, and did not affect subsequent viral load (*16*).

Why has there been so much difficulty in generating an immunogen able to elicit neutralizing antibodies to HIV? To be effective, antibodies must bind to structures on the surface of the virus known as spikes, composed of the gp41 transmembrane protein and the heavily glycosylated gp120 surface protein, which exhibit enormous sequence variation among different viruses (Fig. 3). An effective vaccine must therefore induce antibodies able to bind and neutralize not just one or a few viral species, as might be the case with poliovirus, for example, but the millions of different viruses representative of the global pandemic (*8*). To date, no immunogens have been developed that elicit such broadly neutralizing antibodies (bNAbs). In fact, natural infection, in most cases, does not do much better. Antibodies generated in natural infection clearly exert selection pressure, yet are typically unable to cross neutralize variants that rapidly arise in vivo (*17*, *18*). On the other hand, a few human monoclonal antibodies (mAbs) that neutralize a broad spectrum of circulating HIV isolates in vitro have been derived from infected persons. When these mAbs are passively administered, either systemically or topically, to monkeys that are subsequently challenged with a hybrid AIDS virus that bears HIV spikes and is infectious for monkeys [i.e., simian-human immunodeficiency virus (SHIV)], complete protection against mucosal challenge can be achieved, although the amounts of antibody required are generally high (*19*).

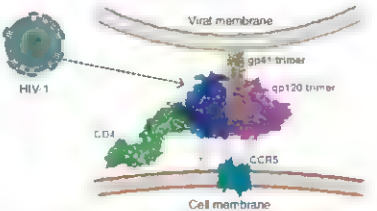

Fig. 3. Schematic of the HIV-1 envelope spike interacting with its cellular receptors on a target cell. Gp120 of the spike interacts with CD4 (shown in green) on T cells leading to conformational changes that allow interaction with the chemokine receptor CCR5. Further conformational changes are triggered in the spike leading to fusion of viral and target cell membranes and transmission of viral genetic material into the target cell. Neutralizing antibodies interrupt the viral entry process by binding to the envelope spike before CD4 binding or after CD4 binding but before fusion. [Modified from (*53*)].

Broadly neutralizing antibodies appear to be very difficult to induce through immunization because of the molecular nature of the HIV surface spike. This is a compact structure heavily camouflaged by sugars in which conserved surfaces, like the CD4 binding site that interacts with the viral envelope and is a target of bNAbs, are either buried and very difficult for antibodies to access or only form through conformational changes after gp120 binding. In addition, the viral spike is an unstable structure that is difficult to generate in recombinant form. Indeed, many of the antibodies generated in natural infection target virion debris that forms after disintegration of the mature envelope trimer (*20*, *21*). The ability to generate bNAbs with vaccines has been so poor thus far that most vaccinologists agree that an HIV vaccine able to induce sterilizing immunity will not be possible without some fundamental new breakthroughs. Currently, there are no neutralizing antibody vaccine candidates in advanced clinical trials.

T Cell Immunity and an HIV Vaccine

The second major gap in HIV vaccine development is a failure to identify the nature of T cell responses that could best contribute to vaccine protection against HIV. Should the antibody gatekeepers fail to completely prevent infection, as seems likely, then an effective T cell response will probably be required to control infection. Because the set-point level of viremia after infection predicts both disease progression and the likelihood of subsequent transmission, a vaccine that did not protect against infection could still be effective if it induced sufficient immune responses to dramatically lower the steady-state viral load should a vaccinee become infected (Fig. 4). Indeed, at a set-point plasma viral load of 1000 to 2000 RNA copies/ml (lower by a factor of about 30 than the median viral set point after infection), the chances of disease progression and of transmission are markedly diminished [reviewed in (*22*)]. In the absence of vaccines that induce a neutralizing antibody response, it is understandable that the field has focused on exploring vaccines to induce T cell responses alone ("T cell–only vaccine").

The rationale for a T cell–based AIDS vaccine stems from data in monkey models and in humans indicating that CTLs play a role in control of HIV. Although these cells do not prevent infection because they only target virus after a cell becomes infected, their effects on infection are considerable. For example, depletion of CTLs in monkeys with acute or chronic simian immunodeficiency virus (SIV) infection has been shown to lead to a marked increase in viral load (*23*). In infected humans, there are strong linkages between certain HLA class I alleles and viral control, whereas other class I alleles are associated with more rapid disease progression (*24*, *25*). Because CTLs recognize infected cells by interaction with viral peptides bound to surface HLA class I molecules, the association between HLA alleles and disease outcome has provided strong evidence that CTL responses contribute substantially to immune control during infection. CTL responses exert sufficient pressure on the virus to lead to the emergence of "escape" viruses that have mutations occurring within or adjacent to the peptide sequences recognized (*26*–*28*). Further evidence for the importance of the anti-HIV activity of CTLs comes from studies that indicate that CTLs from infected persons can effectively contain HIV replication in vitro (*7*, *29*, *30*). Crucial for the evolution of the HIV vaccine field were studies that showed strong protection by T cell–based vaccines in a particular monkey model (SHIV 89.6P). Whereas control animals rapidly developed disease on virus challenge, vaccinated animals that had a vaccine-induced CTL response, as measured by assays quantifying surrogate markers of CTL function such as interferon-γ (IFN-γ) Elispot, became infected but had a relatively low set-point level of viremia, with most not progressing to disease

(*31*, *32*). Together these findings provided a rationale for exploring a T cell–only vaccine.

The STEP Trial and the Future of AIDS Vaccines

Based on the monkey model results, the STEP trial (*6*), the first test of efficacy of a T cell–only vaccine, was initiated in 2004 using recombinant adenoviruses to express HIV Gag, Pol, and Nef proteins. Why the vaccine failed to provide evidence of protection has been widely debated. The simplest explanation is that the vaccine-induced CTL responses were of insufficient magnitude and/or breadth to substantially impact HIV replication in humans. It is worth noting that the hybrid SIV/HIV virus used for challenge, as well as the selection for particular MHC alleles in the monkey model used to support the STEP trial, was considered by some not to be representative of human infection (*33*, *34*). Indeed, an alternative model that had been thought more representative, using animals of differing MHC types and challenge with a pathogenic SIV strain, failed to show protection even for homologous challenge, i.e., when the vaccine and challenge strain are identical (*35*). In humans, of course, challenge is heterologous.

It should also be noted that the strength of vaccine-induced CTL responses, as estimated in surrogate assays such as the IFN-γ Elispot used in the STEP trial, may not provide a robust indication of functional antiviral activity as compared with more direct measurement of antiviral activity: the cytotoxic killing of cells by CTL. Not only does the IFN-γ Elispot assay fail to directly assess CTL function, but it uses peptide-pulsed cells, meaning that the multiple steps in antigen processing and presentation normally required to sensitize infected cells in vivo, or the effects of viral proteins on these processes, are not taken into account. Numerous population-based studies have shown that IFN-γ Elispot responses in infected humans have no correlation with control of viremia (*36*, *37*), raising questions about its suitability as a sole correlate for moving T cell–based vaccines forward. Furthermore, monkeys protected against a robust SIV challenge with live attenuated SIV vaccines have only modest CTL responses when assayed by IFN-γ Elispot assays, underscoring the lack of understanding of immune responses required for an effective vaccine (*38*).

Overall, it appears that there is still much to be learned about what constitutes functional CTL responses and how to elicit such responses. Other immunologic parameters that are more burdensome to assess may be critical for immune control and may not have been assessed in the STEP trial. In phase I studies preceding the STEP trial, the breadth of the CTL responses induced by the vaccine was quite narrow, with a median of one Gag peptide epitope targeted per vaccinee and a median of three responses per person when responses to all three expressed vaccine proteins were examined, far less than the median of 14 observed in the context of natural infection, which fail to prevent disease progression (*37*). Moreover, the specificity of responses may matter. The breadth of the Gag-specific response, but not other responses, is associated with lowering of viral load in chronic infection (*39*). Studies in infected humans suggest that avidity (the amount of viral peptide required at the cell surface to sensitize cells for lysis) may be key, with lower avidity responses lacking potent antiviral function and being less effective at killing infected cells (*29*). A function of CTLs that has been associated with in vivo containment of virus replication is the ability of these cells to proliferate when they encounter cognate antigen (*40*). Also important may be the breadth and magnitude of responses at the mucosal level, which may also have been suboptimal in the STEP trial. Given the many limitations described above, the STEP trial does not provide a definitive answer regarding the potential utility of the T cell–only vaccine concept. Perhaps most crucially, the STEP trial provides little insight regarding the potential success of a vaccine that induces both bNAbs and functional CTLs.

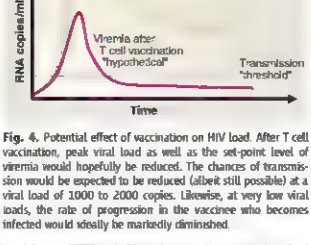

Fig. 4. Potential effect of vaccination on HIV load. After T cell vaccination, peak viral load as well as the set-point level of viremia would hopefully be reduced. The chances of transmission would be expected to be reduced (albeit still possible) at a viral load of 1000 to 2000 copies. Likewise, at very low viral loads, the rate of progression in the vaccinee who becomes infected would ideally be markedly diminished.

Recommendations for Immediate Attention

The unique challenges posed by HIV, the lack of clear understanding of what constitutes an effective immune response, the inadequacy of current assays to evaluate these responses, and the HIV vaccine failures of the past emphasize that the route forward to developing an effective vaccine is by no means straightforward. Some would argue it is probable that a vaccine will not be available for use for many years to come. Nevertheless, there is room for optimism. First, for example, long-term vaccine-mediated protection from AIDS virus infection has been achieved in animal models, albeit with live attenuated AIDS virus vaccines considered too dangerous to pursue in humans (*41*, *42*) but demonstrating nonetheless that durable control is attainable. Second, there are some infected individuals who do generate broadly cross-reactive neutralizing antibodies, and these antibodies have been shown to be able to provide sterilizing immunity when infused in animal models of mucosal AIDS virus challenge (*19*). Finally, there is a subset of infected persons, who have been termed "elite controllers," who maintain virus load below the limits of detection by the most sensitive commercial assays available, some now for more than 25 years (*22*). How this is achieved in these individuals is still being investigated but is likely associated with immune control of virus. There are thus reasons to be hopeful.

Several critical issues can be identified to accelerate the development of an effective vaccine.

Solve the neutralizing antibody problem. This problem has not yielded to the more conventional approaches, meaning that a more rational approach based on molecular understanding of the HIV envelope spike structure and its interaction with bNAbs might be the way forward. Key components of this strategy are (i) determination of the specificities responsible for broad neutralization in a wide selection of different individuals, (ii) isolation and characterization of panels of monoclonal bNAbs, (iii) determination of the structure of intact functional HIV spikes alone and in complex with bNAbs, and (iv) rational design and high throughput evaluation of immunogens until a useful set, able to induce serum antibodies capable of neutralizing a majority of circulating viruses, is derived. Such an approach will entail an understanding of the relationship between antigenicity and immunogenicity at a level far deeper than currently exists. There are many variants of this approach, and alternate strategies should also be explored in parallel.

Define the correlates of T cell–mediated control of HIV. Although the first efficacy trial of a T cell–based vaccine failed, despite the induction of HIV-specific CTLs, this does not mean that the entire concept is flawed. Rather, it may be that the T cells induced were suboptimal in their antiviral effect. A critical next step is to develop methods to assess the antiviral efficacy of CTL, akin to the antibody neutralization assay, rather than relying on IFN-γ Elispot assays (*30*). Not all CTL responses are created equally in terms of the ability to inhibit virus replication (*29*, *43*, *44*), and it is critical to define the antigens that elicit the most potent responses. Efforts also need to be expanded to define the role of virus-specific CD4 T helper cell responses in durable HIV containment. Further, given concerns from the recent Merck/NIH vaccine trial, it must be determined

to which extent such responses induced by a vaccine, either directed at HIV or at a vaccine vector, may add fuel to the fire by causing CD4 T cell activation

Determine mechanisms of HIV control in cases where these occur. Apparent durable control of HIV occurs in about one in 300 persons infected with HIV, and control of SIV occurs in macaques vaccinated with attenuated virus or treated with antiretroviral drugs shortly after infection. Despite some evidence for the involvement of CTL responses, there is strikingly little that is definitively known about mechanisms of control in these cases. Unraveling the mechanisms involved in these cases should be a high priority because this may facilitate the design of immunogens able to elicit the corresponding protective responses.

Define the role of innate immunity in viral containment. The innate immune response also serves as an important first line of defense against viruses, but little is known about its contribution to vaccine success. Accelerated efforts to define the contribution of the innate immune response to HIV control and to determine how innate immune mechanisms can be exploited for adjuvant development and to induce immunologic memory with a vaccine must be a clear priority.

Make best use of animal, particularly monkey, models. There is still no consensus about the most appropriate animal model for HIV vaccine evaluation. Although the SIV mac239/macaque model correctly predicted the failure of the STEP trial (*45*), it would need to predict a success to be a fully validated model. Nevertheless, a strong argument can be made that this is the best available model at this time, and a reasonable current requirement for any immunogen seeking to be advanced into human trials is that it be able to suppress viral load by a minimum of about 1 to 2 logs (peak and set point) compared with control animals in this model (*46*). At the same time, vigorous exploration of immunization and protection should proceed in macaques and other animal models to further understanding of potential vaccine candidates.

Define the mechanisms of action of successful human vaccines. Remarkably, there is little consensus as to the precise mechanisms that create a vaccine-induced barrier to infection and/or disease for any of the current successful human vaccines. Antibody induction has been used as a surrogate for immunogenicity, and neutralizing antibodies are presumed to be involved, but the relative contributions of neutralization versus other effector arms remain undefined. Substantial additional work needs to be done on the science of immunization and in exploring the roles of molecules such as interleukin 10 (IL-10) and other immunoregulatory mechanisms in controlling the magnitude of immune responses (*47*, *48*).

Explore alternative approaches to "vaccination." Traditional vaccine approaches have failed thus far, and although rational design toward a traditional vaccine must be pursued, novel approaches should also be encouraged. The possibility of nonclassical routes to antibody mediated protection, such as inducing antibodies to the chemokine coreceptor or providing bNAbs passively via a viral vector or stem cell transformation, should also be considered, as should efforts to reverse the integration process (*49*).

Test candidate vaccine efficacy in humans only when well-defined criteria are met, and test in smaller cohorts. It is critical for the field to establish firm go/no-go criteria to advance products into human efficacy testing. Only vaccines that are clearly superior in immunogenicity and in animal protection studies to previous failed vaccines should be advanced into efficacy trials. Moreover, vaccine candidates should be tested in small screening test of concept (STOC) trials (*50*) that are by necessity performed in areas of high HIV incidence, requiring a global commitment to this strategy.

Support innovation, interdisciplinary research, and new blood. Given the lack of success thus far, one of the most important issues to address is the need for innovation. The current constraints on NIH funding have a negative impact on innovative research, as study sections tend to take fewer informed risks when funding is tight, despite potential greater rewards. This is particularly a problem for more junior investigators attempting to obtain their first funding. Given the expected long route to an AIDS vaccine, it is critical not to lose this next generation of committed scientists. Funding agencies have the critical task of continuing to support basic innovative scientific discovery and to guard against investing in premature product development. Moreover, restrictions imposed by foundations funding AIDS vaccine research can have an unintended impact of thwarting innovation, to the extent that funding is highly project and milestone driven, which may inhibit rapid changes in direction needed to adapt to an ever-changing body of knowledge. We believe great success would result from a model in which the investment is made in people rather than projects, particularly including scientists from diverse fields not currently engaged in HIV vaccine research, allowing them to focus totally on the task at hand. Given the magnitude of the global crisis, an approach free from traditional academic and private sector constraints seems highly warranted.

Conclusions

With few exceptions, even the most critical and skeptical of scientists, who have stressed the difficulties of developing an HIV vaccine, feel that this is no time to give up (*51*). However, far more selectivity than hereto in advancing immunogens to large-scale clinical trials is required. The mantra of "the only way we will know if it is likely to be effective is to try it in humans" is not appropriate given the current state of knowledge. Trust in science, making full use of the tool kit that is provided by modern molecular biology, immunology, virology, structural biology, chemistry, and genomics is crucial. There is a critical need to understand how other vaccines work with a level of detail that has never been necessary for pathogens less adapted to immune evasion. The way forward is without question very difficult and the possibility of failure high, but the global need is absolutely desperate, and this is an endeavor that must be pursued, now with greater passion than ever.

References

1. F. Barre-Sinoussi *et al. Science* 220, 868 (1983).
2. R. C. Gallo *et al., Science* 224, 500 (1984).
3. M. Popovic, M. G. Sarngadharan, E. Read, R. C. Gallo, *Science* 224, 497 (1984).
4. J. Schupbach *et al., Science* 224, 503 (1984).
5. M. G. Sarngadharan, M. Popovic, L. Bruch, J. Schupbach, R. C. Gallo, *Science* 224, 506 (1984).
6. R. Steinbrook, *N. Engl. J. Med.* 357, 2653 (2007).
7. O. O. Yang *et al., J. Virol.* 71, 3120 (1997).
8. B. Korber *et al., Br. Med. Bull.* 58, 19 (2001).
9. J. M. Brenchley *et al., J. Exp. Med.* 200, 749 (2004).
10. S. Mehandru *et al., J. Exp. Med.* 200, 761 (2004).
11. J. M. Brenchley *et al., Nat. Med.* 12, 1365 (2006).
12. S. Le Gall *et al., Immunity* 8, 483 (1998).
13. O. O. Yang *et al., J. Virol.* 76, 1626 (2002).
14. R. Wyatt, J. Sodroski, *Science* 280, 1884 (1998).
15. T. W. Chun *et al., Nature* 387, 183 (1997).
16. M. M. Flynn *et al., J. Infect. Dis.* 191, 654 (2005).
17. D. D. Richman, T. Wrin, S. J. Little, C. J. Petropoulos, *Proc. Natl. Acad. Sci. U.S.A.* 100, 4144 (2003).
18. X. Wei *et al., Nature* 422, 307 (2003).
19. D. R. Burton *et al., Nat. Immunol.* 5, 233 (2004).
20. P. W. Parren, D. R. Burton, Q. J. Sattentau, *Nat. Med.* 3, 366 (1997).
21. J. P. Moore, D. D. Ho, *AIDS* 9 (suppl. A), S117 (1995).
22. S. G. Deeks, B. D. Walker, *Immunity* 27, 406 (2007).
23. J. E. Schmitz *et al., Science* 283, 857 (1999).
24. R. A. Koup *et al., Nat. Med.* 2, 405 (1996).
25. M. Carrington *et al., Science* 283, 1748 (1999).
26. C. B. Moore *et al., Science* 296, 1439 (2002).
27. P. Klopfleis *et al., Nature* 432, 769 (2004).
28. Z. L. Brumme *et al., PLoS Pathog.* 3, e94 (2007).
29. M. S. Bennett, P. L. Ng, M. Dagarag, A. An, O. O. Yang, *J. Virol.* 82, 4973 (2007).
30. A. Saez-Cirion *et al., Retrovirology* 3, 81 (2006).
31. J. W. Shiver *et al., Nature* 415, 331 (2002).
32. D. H. Barouch *et al., Nature* 415, 335 (2002).
33. M. B. Feinberg, J. P. Moore, *Nat. Med.* 8, 207 (2002).
34. J. D. Lifson, M. A. Martin, *Nature* 415, 272 (2002).
35. D. R. Casimiro *et al., J. Virol.* 79, 15547 (2005).
36. M. R. Betts *et al., J. Virol.* 75, 11983 (2001).
37. M. M. Addo *et al., J. Virol.* 77, 2081 (2003).
38. K. Mansfield *et al., J. Virol.* 82, 4235 (2008).
39. P. Klopfleis *et al., Nat. Med.* 13, 46 (2007).
40. S. A. Migueles *et al., Nat. Immunol.* 3, 1061 (2002).
41. M. D. Daniel, F. Kirchhoff, S. C. Czajak, P. K. Sehgal, R. C. Desrosiers, *Science* 258, 1938 (1992).
42. M. S. Wyand *et al., J. Virol.* 73, 8356 (1999).
43. O. O. Yang *et al., J. Exp. Med.* 197, 1365 (2003).
44. J. B. Sacha *et al., J. Immunol.* 178, 2746 (2007).
45. D. R. Casimiro *et al., J. Virol.* 78, 13434 (2004).
46. D. Watkins, *Nat. Med.*, in press (2008).
47. D. G. Brooks *et al., Nat. Med.* 12, 1301 (2006).
48. M. Ejrnaes *et al., J. Exp. Med.* 203, 2461 (2006).
49. L. Sarkar, J. Hauber, J. Hauber, F. Buchholz, *Science* 316, 19, 2 (2007).
50. J. L. Excler, W. Rida, F. Priddy, P. Fast, W. Koff, *AIDS* 21, 2259 (2007).
51. D. Baltimore, paper presented at the AAAS Annual Meeting, Boston, MA, 14 to 18 February 2008; www.aaas.org/meetings/Annual_Meeting/2008_boston/program/lecture.
52. B. D. Walker, B. T. Korber, *Nat. Immunol.* 2, 473 (2001).
53. G. B. Karlsson Hedestam *et al., Nat. Rev. Microbiol.* 6, 143 (2008).

54. The authors' laboratories are supported by funding from NIH and the International AIDS Vaccine Initiative.

10.1126/science.1152622

Climate-Driven Ecosystem Succession in the Sahara: The Past 6000 Years

S. Kröpelin,[1]* D. Verschuren,[2] A.-M. Lézine,[3] H. Eggermont,[2] C. Cocquyt,[2,4] P. Francus,[5,6] J.-P. Cazet,[3] M. Fagot,[2] B. Rumes,[2] J. M. Russell,[7] F. Darius,[1] D. J. Conley,[8] M. Schuster,[9] H. von Suchodoletz,[10,11] D. R. Engstrom[12]

Desiccation of the Sahara since the middle Holocene has eradicated all but a few natural archives recording its transition from a "green Sahara" to the present hyperarid desert. Our continuous 6000-year paleoenvironmental reconstruction from northern Chad shows progressive drying of the regional terrestrial ecosystem in response to weakening insolation forcing of the African monsoon and abrupt hydrological change in the local aquatic ecosystem controlled by site-specific thresholds. Strong reductions in tropical trees and then Sahelian grassland cover allowed large-scale dust mobilization from 4300 calendar years before the present (cal. yr B.P.). Today's desert ecosystem and regional wind regime were established around 2700 cal yr B.P. This gradual rather than abrupt termination of the African Humid Period in the eastern Sahara suggests a relatively weak biogeophysical feedback on climate.

One of the most prominent environmental changes of the past 10,000 years is the transition of northern Africa from a "green Sahara" (*1*) during the early Holocene "African Humid Period" (*2*) to the world's largest warm desert today. Detailed knowledge of the tempo and mode of this transition is crucial for understanding the interaction between tropical and mid-latitude weather systems (*3–6*) and the multiple impacts of mineral aerosols exported from the Sahara on global climate (*7–10*) and distant ecosystems (*11–13*). The distinct lack of high-quality paleoenvironmental records covering the past four to five millennia from within the Sahara desert (*14*) (SOM text 1) has directed substantial effort to the modeling of African monsoon dynamics in response to orbital insolation changes (e.g., *15*, *16*), and of the influence of surface temperature changes in the adjacent tropical ocean (e.g., *4*) and biogeophysical feedbacks between climate and vegetation (*1*, *17–20*). Modeling results suggest that a strong positive biogeophysical feedback between rainfall and vegetation (*18*) appear to be supported by the record of terrigenous (land-eroded) dust deposited in deep-sea sediments downwind from the Sahara, which shows a sudden increase at 5500 calendar years before the present (cal yr B.P.) (*2*, *21*). As a result, the Holocene drying of the Sahara (i.e., termination of the "African Humid Period") is widely believed to have been an abrupt event, completed within a few hundred years (e.g., *22*, *23*). In turn, this abrupt event of possible continental scale is regarded as a prime example of catastrophic regime shifts in natural ecosystems (e.g., *24*, *25*).

In this context, we present a continuous and accurately dated paleo-environmental record covering the past 6000 years from within the Sahara, using multiple proxies and indicators preserved in a finely laminated lake-sediment sequence from northern Chad. High-resolution sedimentological and geochemical data coupled with biological indicators (pollen, spores, and the remains of aquatic biota) permit a precise reconstruction of terrestrial and aquatic ecosystem response to climate-driven moisture-balance changes in the now hyperarid core of the east-central Sahara desert.

Study site and material. Lake Yoa is one of a handful of permanent lakes occupying Pleistocene deflation basins in Ounianga, situated halfway between the Tibesti- and Ennedi mountains (Fig. 1). The subtropical desert climate of this area is characterized by high daytime temperatures, negligible rainfall, and dry northeasterly trade winds blowing almost year-round through the Tibesti-Ennedi corridor (Fig. 1C) (SOM text 2). The Ounianga lakes are maintained against this extremely negative water balance by groundwater inflow from the Nubian Sandstone Aquifer, which was last recharged during the early Holocene (*26*). This stable groundwater input ensured permanence of the aquatic ecosystem throughout the dry late-Holocene period but dampened its hydrological sensitivity to climate. Sediments in Lake Yoa are finely laminated throughout the sampled upper 7.47 m of the sequence (*27*). Sections with annual lamination (varves) (Fig. 2D) show an average sedimentation rate of 1.3 mm per year, in support of the age-depth model constructed from 12 accelerator mass spectrometry radiocarbon dates and the 1964 caesium marker of nuclear bomb testing (*27*) (table S1).

The Lake Yoa record documents dramatic changes through time in three important components of the Saharan paleoenvironment. First, it traces the evolution of the local aquatic ecosystem from a dilute freshwater habitat to the present-day hypersaline oasis. Second, it reveals the establishment of today's terrestrial desert ecosystem as the result of continuous vegetation succession between 5600 and 2700 cal yr B.P. Third, it shows the changing regional wind regime, culminating in establishment of today's almost year-round northeasterly winds around 2700 cal yr B.P.

Evolution of the aquatic ecosystem. The most prominent feature in the recorded history of Lake Yoa is its relatively rapid transition, between 4200 and 3900 cal yr B.P., from a seemingly stable freshwater habitat (surface-water conductivity of 300 to 500 μS/cm) to a true salt lake (>10,000 μS/cm) in which only specialized fauna and flora can survive (Fig. 2A and figs. S2 to S4) (*27*). In reality, the ecology of Lake Yoa evolved continuously during the past 6000 years, in response to changes in water chemistry, nutrient dynamics, and substrate availability driven by changing lake hydrology and water balance (SOM text 3 and 4). In brief, organic matter deposition (Fig. 2C) (SOM text 5) and the stratigraphy of phytoplankton species (figs. S2 and S3) indicate that Lake Yoa switched from a less to a more productive aquatic ecosystem ~5600 cal yr B.P. Lake productivity remained high after the fresh-to-saline transition until ~3300 cal yr B.P., when conductivity rose above 20,000 μS/cm (Fig. 2A), and also the most salt-tolerant freshwater biota disappeared (fig. S4). From that moment on, both primary productivity (percentage organic matter) (Fig. 2C) and secondary productivity (represented by fossil chironomid abundance) (fig. S4) gradually declined, until by 2700 cal yr B.P. they stabilized at ~50 to 70% lower values. This transition coincided with a virtually complete collapse of the Lake Yoa diatom flora [biogenic SiO_2 (Fig. 2B); diatom cell counts (fig. S3)]. This fairly unproductive, hypersaline aquatic ecosystem then acquired its modern-day biology with establishment of the

[1]Africa Research Unit, Institute of Prehistoric Archaeology, University of Cologne, Jennerstraße 8, D-50823 Köln, Germany. [2]Limnology Unit, Department of Biology, Ghent University, K. L. Ledeganckstraat 35, B-9000 Gent, Belgium. [3]Laboratoire des Sciences du Climat et de l'Environnement, CNRS-CEA-UVSQ UMR 1572, L'Orme des Merisiers, F-91191 Gif-Sur-Yvette, France. [4]National Botanic Garden of Belgium, Domein van Bouchout, B-1860 Meise, Belgium. [5]Institut National de la Recherche Scientifique, Centre Eau, Terre et Environnement, 490 Rue de la Couronne, Québec, Québec G1K 9A9, Canada. [6]GEOTOP, Geochemistry and Geodynamics Research Centre, C.P. 8888, Université du Québec à Montréal, Succursale, Centre-Ville, Montréal, Québec H3C 3P8, Canada. [7]Geological Sciences, Brown University, Box 1846, Providence, RI 02912, USA. [8]GeoBiosphere Centre, Department of Geology, Lund University, Sölvegatan 12, SE-22362 Lund, Sweden. [9]Institut International de Paléoprimatologie, Paléontologie Humaine, Evolution et Paléoenvironnements, CNRS-UMR 6046, Université de Poitiers, 40 Avenue du Recteur Pineau, F-86022 Poitiers, France. [10]Geoforschungszentrum Potsdam, Telegrafenberg, D-14473 Potsdam, Germany. [11]Lehrstuhl für Geomorphologie, Universität Bayreuth, Universitätsstraße 30, D-95440 Bayreuth, Germany. [12]St. Croix Watershed Research Station, Science Museum of Minnesota, Marine on St. Croix, MN 55047, USA.

*To whom correspondence should be addressed. E-mail: s.kroepelin@uni-koeln.de

salt-loving hemipteran *Anisops* as the dominant macrozooplankton species ~2700 cal yr B.P and appearance of brine flies (*Ephydra*) 1500 cal yr B.P (fig. S2).

Evolution of the terrestrial ecosystem. Palynological and lithological indicators describe a more progressive evolution of the terrestrial ecosystem surrounding Lake Yoa. Throughout the last 6000 years, the regional vegetation was dominated by grasses (Poaceae), in association with scattered *Acacia* trees (Fig. 2G). Before 4300 cal yr B.P the regional landscape was an open grass savannah complemented with modest but indicative populations of tropical (Sudanian) trees (e.g., *Piliostigma*, *Lannea*, and *Flueggea virosa*), which today commonly occur in wooded grasslands and dry forests at least 300 km to the south. Their co-occurrence with ferns (Fig. 2G) suggests that these trees formed streambank communities in temporarily flooded river valleys (wadis). The savannah also included tropical herb species (e.g., *Mitracarpus* and *Spermacoce*). This mid-Holocene pollen assemblage was completed by the mountain shrub *Erica arborea*, now restricted to a few small areas above 2900 m altitude in the Tibesti. Substantial input of *Erica* pollen throughout the period with abundant humid plant indicators may suggest that a river from the Tibesti flowed at least seasonally into Lake Yoa until 4300 cal yr B.P. Drying of this exotic river may have partly accounted for the negative water balance that terminated the lake's fresh water ecosystem shortly thereafter. The first evidence of ecosystem drying in the Ounianga region, however, is already observed at 5600 cal yr B.P., with increasing *Acacia* and the expansion of plants typifying semidesert environments (e.g., *Boerhavia* and *Tribulus*). The demise of tropical trees, accelerating after 4800 cal yr B.P., was initially compensated by expansion of Sahel type trees and shrubs (e.g., *Commiphora* and *Balanites*), of which the northern limit today does not extend beyond the Enneđi (Fig. 1C). This Sahelian vegetation component, although substantive, was relatively short lived, because by ~4300 cal yr B.P *Commiphora* dwindled to a sporadic occurrence.

General deterioration of the terrestrial ecosystem of northern Chad 4800 to 4300 cal yr B.P is also reflected in a dramatic fall in grass pollen influx, which we interpret to indicate that grass cover became sparse or discontinuous at the landscape scale (despite grass still contributing ~50 to 55% to the pollen sum) (Fig. 2G). This observation is confirmed by the rise in magnetic susceptibility above background values of 2 to 10 $\times 10^{-6}$ SI units from 4300 cal yr B.P., reflecting increased input of wind-blown dust (Fig. 2E) (*27* and SOM text 6). The gradual rise of fine sand (75 to 150 μm) in the upper half of the sequence, above background values of 1 to 5% (Fig. 2F), indicates that from 3700 cal yr B.P onward, winds also increasingly entrained sand. A first (semi-)desert plant community developed between 3900 and 3100 cal yr B.P with expansion of herbs such as *Biepharis*, *Boerhavia* (Fig. 2G) and *Tribulus* (scarce), followed at ~2700 cal B.P by vegetation found today both in the immediate vicinity of Ounianga and throughout the central Sahara (*28*): *Artemisia*, *Cornulaca*, and Amaranthaceae-Chenopodiaceae, with scattered *Salvadora persica* and *Ephedra* trees (Saharan plant taxa, Fig. 2G), as well as *Acacia*.

The near-synchronous immigration of true desert plant types at ~2700 cal yr B.P is associated with a marked increase in the influx of grass pollen (Fig. 2G), despite our inference of a by now mostly barren desert landscape (SOM text 7). This switch coincides with magnetic susceptibility reaching a plateau value of ~40 $\times 10^{-6}$ SI units, followed by a modest, gradual decline toward the present (Fig. 2E). We interpret this coincidence to reflect the establishment around 2700 cal yr B.P of the modern regional wind regime, with strong northeasterly trade winds blowing almost year-round (Fig. 1A). In this interpretation, the greater pollen influx mostly reflects enhanced long-distance transport from a now much expanded pollen source area, including scrubland and steppe at the northern fringe of the Sahara. This interpretation is supported by the occurrence after 2700 cal yr B.P of pollen from plant species (e.g., *Quercus*) (Fig. 2G) that likely originate from the Mediterranean coast (Fig. 1A) (*29*). The expanded pollen source area implies that average northeasterly wind strength must have increased during this time, either because wintertime trade-wind circulation intensified or because a change in the mean position of the Libyan high-pressure cell now channeled low-level northeasterly flow more effectively through the Tibesti-Enneđi corridor. After passing through the Ounianga region, these surface winds continue into the Bodélé depression of the northern Lake Chad basin, the single most important source of Saharan dust (*9*, *30*). Important topographic control by the Tibesti and Enneđi on the generation of erosive Bodélé low-level jet winds (*31*, *32*) implies that our timing of the onset of the modern wind regime in northeastern Chad

Fig. 1. Location of Lake Yoa (19.03° N, 20.31° E, 380 m above sea level (asl)) at continental and regional scales. (**A**) Map of Africa north of the equator highlighting land >1000 m asl, the natural distribution of vegetation zones (*29*), and synoptic climatology. Arrows: moist tropical Atlantic monsoon circulation (blue) and dry northeasterly trades (light yellow) in relation to the position of the Intertropical Convergence Zone (ITCZ) during Northern Hemisphere summer and winter [adapted from (*9*)]. Vegetation zones, from north to south: Mediterranean evergreen forest (pink), Mediterranean scrubland (light yellow), desert (ochre, with relief), Sahelian wooded grassland (yellow), Sudanian wooded grassland (green), tropical dry forest (blue-green), and tropical rainforest (dark blue); mountain ranges are shown in dark brown. (**B**) Quickbird satellite image of Lake Yoa (4.3 km^2, 26 m deep), bounded to the south and west by sandstone cliffs and to the north and east by dunes of quartz sand. These accumulate in low-wind zones beneath the dissected rim of the Ounianga escarpment, and their progressive migration into the lake has now reached its modern depositional center. *Typha* (cattail) stands develop near groundwater inflow along the northern and eastern lakeshore. Also shown are the locations of sediment cores collected in 2003 and 2004, which together form the studied sediment sequence (*27*). (**C**) Landsat 7 Geocover mosaic satellite image of the Ounianga region showing the main geomorphological features and the northern limit of Saheuan grassland (dotted line) (*28*).

has direct bearing on the history of Saharan dust production and export. We interpret the slightly decreasing dust flux (magnetic susceptibility) at Ounianga since 2700 cal yr B.P to indicate that deflation during the preceding 1900 years had by that time removed all loose soil laid bare through the loss of vegetation cover (SOM text 6). From that moment on, the mineral dust flux became limited by its rate of erosion from dried-out lake basins and exposed bedrock. Redeposition of sand mobilized in this process led to dune development at the foot of the Ounianga escarpment. The rising sand content after 2700 cal yr B.P (Fig. 2F) may reflect the gradual migration of these dunes into Lake Yoa (Fig. 1B) and their approach of the midlake coring site.

The record of *Typha* (cattail) pollen (Fig. 2G) illustrates the temporal linkages between the evolution of terrestrial and aquatic ecosystems at Ounianga over the past six millennia.

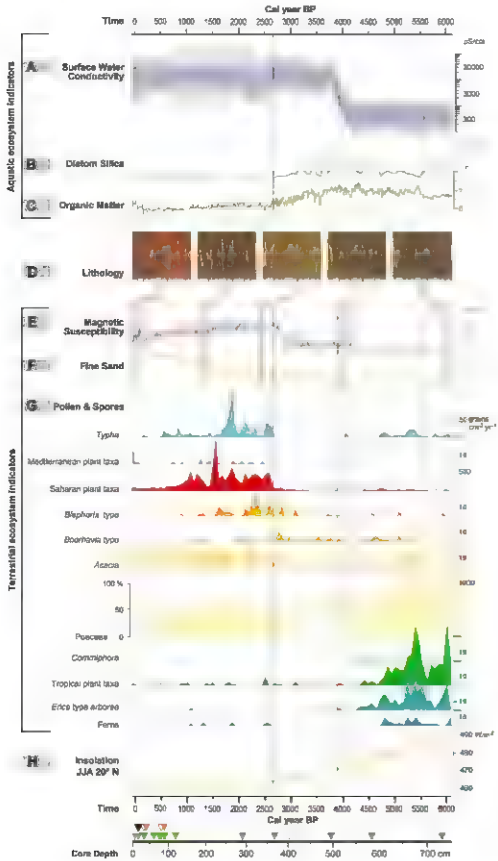

Fig. 2. Evolution of aquatic and terrestrial ecosystem components over the past 6000 years, with episodes of marked change highlighted with stippled vertical lines. The aquatic ecosystem of Lake Yoa is described by paleosalinity reconstructions based on fossil chironomids and diatoms (**A**); and diatom silica in weight percent of SiO_2 (**B**) and bulk organic matter (**C**) as indicators of primary productivity. Core lithology is illustrated by sections of laminated sediment representative for lower, middle, and upper portions of the cored sequence (**D**). The terrestrial ecosystem of the Ounianga region is described by the magnetic susceptibility record of eolian dust input (**E**), the dry-weight fraction of fine sand (**F**), and the influx rate (**G**, right axes) and percentage (**G**, left axis, Poaceae only) of pollen or spores from principal plant taxa. (**H**) shows local summer insolation over the past 6000 years (44). The age-depth model (fig. S1) is constrained by the sediment-water interface (2003 AD), the ^{137}Cs marker of peak nuclear bomb testing (1964 AD, purple) and 17 ^{14}C dates on bulk organic matter (green; open triangles are outliers), with a lake-carbon reservoir correction based on paired ^{14}C dating of bulk organic matter and either charred grass (brown) or 1918 AD in varve years (black) (27).

Two episodes of expanded *Typha* swamp occurred at 5500 to 4700 cal yr B.P. and 2700 to 600 cal yr B.P. The first of these coincides with the first recorded evidence for a drying terrestrial ecosystem (Fig. 2G), as well as with indicators of increasing aquatic productivity (Fig. 2C) and community turnover in the phytoplankton (fig. S2). We interpret these data to indicate that by 5600 to 5500 cal yr B.P. climatic deterioration of the regional moisture balance caused parts of the rocky Ounianga plateau to develop drought-tolerant vegetation and forced a lake-level decline that both intensified lake nutrient dynamics and allowed *Typha* swamp to develop along gently sloping shorelines. *Typha* expansion at 2700 cal yr B.P. coincides with the establishment of today's desert plant community and of Lake Yoa as a relatively unproductive, hypersaline desert lake (Fig. 2). We interpret these indicators to signal the stabilization of Lake Yoa at its present elevation, set by the hydrological balance between a hyperarid climate regime, wind-enhanced evaporation, and fossil groundwater input.

Timing and mode of climate change. Arid climatic conditions in the Sahara since ~4300 cal yr B.P. have eradicated all but a few permanent aquatic environments. Paleoenvironmental records covering this period with similar data quality (SOM text 5) are unlikely to exist anywhere else in the arid climate belt of North Africa. Our multiple-indicator reconstruction illustrates the complex relationship between Saharan ecosystems and climate throughout the period of aridification. It gives no indication for abrupt mid-Holocene climate change, or for alternation between marked dry and wet episodes that allowed the vegetation to recover to previous ecological conditions (SOM text 8). Most important, our data do not show an abrupt collapse of the early Holocene terrestrial ecosystem, but a gradual reduction in the abundance of tropical vegetation components followed by loss of grass cover and establishment of the modern desert plant community.

The combined paleoenvironmental evidence indicates that annual rainfall in the Ounianga region was reduced from ~250 mm at 6000 cal yr B.P. to <150 mm by 4300 cal yr B.P., followed by somewhat slower evolution to present-day hyperarid conditions (<50 mm annually) by 2700 cal yr B.P. (SOM text 9). Terrestrial and aquatic ecosystems experienced both gradual evolution and relatively rapid, threshold-type changes, progressing through a predictable sequence of interconnected system responses to climate-driven deterioration of the regional water balance. At the landscape scale this reduction in moisture was effected through decreasing and more intermittent rainfall, lowering of the groundwater table, and the drying out of surface waters. For example, the fairly rapid fresh-to-saline transition of Lake Yoa probably reflects its switch from a hydrologically more open lake system before 4300 cal yr B.P., when substantial surface or subsurface outflow prevented concentration of dissolved salts, to a hydrologically closed system with water output only through evaporation, and a consequent concentration of dissolved salts. The exact timing of this transition depended on a site-specific threshold in the evolving balance between summed inputs (rain, local runoff, groundwater, and river inflow) and outputs (evaporation and subsurface outflow), rather than the timing and rate of regional climate change. Plant community response to climate is also often nonlinear (*25*, *33*), because it is governed by the physiological tolerance of key species to water scarcity and/or osmotic stress (e.g., *34*), by soil moisture thresholds for vegetation persistence, or by the role of vegetation and its spatial patterning in promoting infiltration (*35*) and preventing soil erosion or nutrient loss (*36*, *37*). If mid-Holocene climate change had been concentrated in a relatively short period, the long process of ecological succession and species turnover between "green" and "desert" Sahara states would not have been recorded or would have collapsed into a time window lasting a few centuries rather than the 2.5 millennia observed in our data.

In summary, the Lake Yoa record supports archaeological (*38*) and geological (*14*) data from the eastern Sahara as well as palynological data from the West African Sahel (*39*, *40*) that the iconic record of Saharan dust deposition in the tropical Atlantic Ocean (*2*) is not representative for landscape history throughout dry northern Africa. It is also consistent with climate modeling output (*20*) showing a mostly gradual mid-Holocene precipitation decline over the eastern Sahara (SOM text 8), in line with monsoon-proxy records from elsewhere (*41*–*43*) that indicate a close link between the hydrological cycle in northern subtropical regions and orbital insolation forcing (Fig. 2I). Disagreement with modeling results indicating abrupt mid-Holocene vegetation collapse (*18*, *20*) suggests that the implicated biogeophysical climate-vegetation feedback may have been relatively weak (*6*) and that nonlinear vegetation response to moisture-balance variability superimposed on the long-term drying trend, although certainly affecting individual species distributions, did not lead to abrupt vegetation collapse at the landscape scale.

References and Notes

1. M. Claussen, V. Gayler, *Glob. Ecol. Biogeogr.* **6**, 369 (1997).
2. P. B. deMenocal *et al.*, *Quat. Sci. Rev.* **19**, 347 (2000).
3. COHMAP Members, *Science* **241**, 1043 (1988).
4. J. E. Kutzbach, Z. Liu, *Science* **278**, 440 (1997).
5. A. Ganopolski, C. Kubatzki, M. Claussen, V. Brovkin, V. Petoukhov, *Science* **280**, 1916 (1998).
6. P. Braconnot *et al.*, *Clim. Past* **3**, 279 (2007).
7. A. S. Goudie, N. J. Middleton, *Earth Sci. Rev.* **56**, 179 (2001).
8. J. M. Prospero, P. J. Lamb, *Science* **302**, 1024 (2003).
9. S. Engelstaedter, I. Tegen, R. Washington, *Earth Sci. Rev.* **79**, 73 (2006).
10. Y. J. Kaufman, D. Tanre, O. Boucher, *Nature* **419**, 215 (2002).
11. E. A. Shinn *et al.*, *Geophys. Res. Lett.* **27**, 3029 (2000).
12. T. D. Jickells *et al.*, *Science* **308**, 67 (2005).
13. I. Koren *et al.*, *Environ. Res. Lett.* **1**, 10.1088/1748-9326/1/1/014005 (2006).
14. P. Hoelzmann *et al.*, in *Past Climate Variability Through Europe and Africa*, R. W. Battarbee, F. Gasse, C. E. Stickley, Eds. (Kluwer, Dordrecht, Netherlands, 2004), pp. 219–256.
15. J. E. Kutzbach, B. L. Otto-Bliesner, *J. Atmos. Sci.* **39**, 1177 (1982).
16. S. Joussaume *et al.*, *Geophys. Res. Lett.* **26**, 859 (1999).
17. V. Brovkin, M. Claussen, V. Petoukhov, A. Ganopolski, *J. Geophys. Res. Atmos.* **103**, 31613 (1998).
18. M. Claussen *et al.*, *Geophys. Res. Lett.* **26**, 2037 (1999).
19. H. Renssen, V. Brovkin, T. Fichefet, H. Goosse, *Quat. Int.* **150**, 95 (2006).
20. Z. Y. Liu *et al.*, *Quat. Sci. Rev.* **26**, 1818 (2007).
21. J. Adkins, P. Demenocal, G. Eshel, *Paleoceanography* **21**, PA4203 10.1029/2005PA001200 (2006).
22. R. B. Alley *et al.*, *Science* **299**, 2005 (2003).
23. J. A. Rial *et al.*, *Clim. Change* **65**, 11 (2004).
24. M. Scheffer, S. Carpenter, J. A. Foley, C. Folke, B. Walker, *Nature* **413**, 591 (2001).
25. J. A. Foley, M. T. Coe, M. Scheffer, G. L. Wang, *Ecosystems (N.Y., Print)* **6**, 524 (2003).
26. International Atomic Energy Agency, Report RAF/8/036 (IAEA, Vienna, 2007).
27. Materials and methods are available as supporting material on *Science* Online.
28. R. Capot-Rey, *Mem. Inst. Rech. Sahar.* **5**, 65 (1961).
29. F. White, *The Vegetation of Africa* (UNESCO, Paris, 1983).
30. R. Washington, M. Todd, N. J. Middleton, A. S. Goudie, *Ann. Assoc. Am. Geogr.* **93**, 297 (2003).
31. J. Maley, *Global Planet. Change* **26**, 121 (2000).
32. R. Washington *et al.*, *Geophys. Res. Lett.* **33**, L09401 (2006).
33. M. Maslin, *Science* **306**, 2197 (2004).
34. M. Sankaran *et al.*, *Nature* **438**, 846 (2005).
35. S. C. Dekker, M. Rietkerk, M. F. P. Bierkens, *Glob. Change Biol.* **13**, 671 (2007).
36. J. van de Koppel, M. Rietkerk, F. J. Weissing, *Trends Ecol. Evol.* **12**, 352 (1997).
37. S. Kefi *et al.*, *Nature* **449**, 213 (2007).
38. R. Kuper, S. Kröpelin, *Science* **313**, 803 (2006).
39. J. Salzmann, P. Hoelzmann, I. Morczinek, *Quat. Res.* **58**, 73 (2002).
40. M. P. Waller, F. A. Street-Perrott, H. Wang, *J. Biogeogr.* **34**, 1575 (2007).
41. G. H. Haug, K. A. Hughen, D. M. Sigman, L. C. Peterson, J. Rohl, *Science* **293**, 1304 (2001).
42. D. Fleitmann *et al.*, *Science* **300**, 1737 (2003).
43. Y. J. Wang *et al.*, *Science* **308**, 854 (2005).
44. A. Berger, M. F. Loutre, *Quat. Sci. Rev.* **10**, 297 (1991).

45. This research was sponsored by the Deutsche Forschungsgemeinschaft through SFB 389 (ACACIA), the Research Foundation of Flanders (FWO Vlaanderen, Belgium) and the Centre National de la Recherche Scientifique (France). We thank B. Mallaye of the Centre National d'Appui à la Recherche of Chad for research permission, J. George for support of test coring in 1999, J. Karstens, A. Moren, A. Alcantara, J. F. Crémer, G. Kabihogo, K. Van Damme, A. Myrbo, and M. Blaauw for assistance with data collection, processing, and analysis, and M. Claussen, D. Fleitmann, H. Goosse, Z. Liu, M. Maslin, J.-B. Stuut, and J. van de Koppel for discussion. Cores were logged and archived at the National Lacustrine Core Repository, University of Minnesota, Minneapolis, USA.

Supporting Online Material
www.sciencemag.org/cgi/content/full/320/5877/765/DC1
Materials and Methods
SOM Text
Figs. S1 to S4
Tables S1 and S2
References

7 January 2008; accepted 20 March 2008
10.1126/science.1154913

Controlled Phase Shifts with a Single Quantum Dot

Ilya Fushman,[2]* Dirk Englund,[2]* Andrei Faraon,[2]* Nick Stoltz,[2] Pierre Petroff,[2] Jelena Vučković[2]†

Optical nonlinearities enable photon-photon interaction and lie at the heart of several proposals for quantum information processing, quantum nondemolition measurements of photons, and optical signal processing. To date, the largest nonlinearities have been realized with single atoms and atomic ensembles. We show that a single quantum dot coupled to a photonic crystal nanocavity can facilitate controlled phase and amplitude modulation between two modes of light at the single-photon level. At larger control powers, we observed phase shifts up to $\pi/4$ and amplitude modulation up to 50%. This was accomplished by varying the photon number in the control beam at a wavelength that was the same as that of the signal, or at a wavelength that was detuned by several quantum dot linewidths from the signal. Our results present a step toward quantum logic devices and quantum nondemolition measurements on a chip.

Photons are attractive candidates for quantum bits, because they do not interact strongly with their environment and can be transmitted over long distances. They are well suited for carrying information by means of polarization or photon number, and can be manipulated with great precision by optical elements (*1*). In addition, photonic qubits can be used to interconnect atom-like qubits realized in various systems (*2*–*6*). Quantum logic with photons requires a gate that facilitates an interaction between two coincident photons (*7*). A controlled-phase gate, which can be realized by an atom in a high-quality (Q) cavity (*2*), performs this function. In this gate, the accumulated phase of one beam is dependent on the total number of photons interacting with the atom, and the presence of other photons can be measured without destroying them (*8*–*10*).

Our nonlinear medium consisted of a three-hole–defect photonic crystal (PC) cavity (*11*) with a coupled InAs quantum dot (QD) (Fig. 1A). Because of the presence of a distributed Bragg reflector underneath the PC membrane, we treated the PC cavity as a one-sided system. The structure was thermally isolated, allowing us to control the cavity and QD resonances with a heating laser (*12*). The cavity field decay rate was $\kappa/2\pi \approx 16$GHz, corresponding to a quality factor $Q \approx 10{,}000$. The QD had an estimated spontaneous emission rate of $\gamma/2\pi \approx 0.2$GHz. In the described experiments, we employed two QDs: a strongly coupled QD with a vacuum Rabi frequency $g/2\pi \approx 16$ GHz and a weakly coupled QD with $g/2\pi \approx 8$ GHz.

We measured the phase of cavity-reflected photons by interfering them with a reference beam of known amplitude and phase (Fig. 1A). The reflectivity of the linearly polarized cavity was isolated from background laser scatter by means of a cross-polarized setup (*13*, *12*). The reference beam was introduced by inserting a quarter wave plate (QWP) between the beam-splitter and the cavity. The QWP converted the linearly polarized signal into an elliptically polarized beam with components parallel and orthogonal to the cavity polarization. After reflection from the sample, these two components acquired a relative phase. The detected signal I_s is an interference between the cavity-reflected component and the reference field

$$I_s(\omega) = A(\theta)\left|r(\omega) + e^{i\Psi(\theta)}\right|^2 \quad (1)$$

where $A(\theta)$ is a coefficient that depends on the QWP angle θ relative to the vertical polarization of the polarizing beam splitter (PBS), $r(\omega)$ is the frequency and power-dependent cavity reflectivity, and $\Psi(\theta)$ is the reference phase delay. $A(\theta)$, $r(\omega)$, and $\Psi(\theta)$ are given in the supporting online material (SOM).

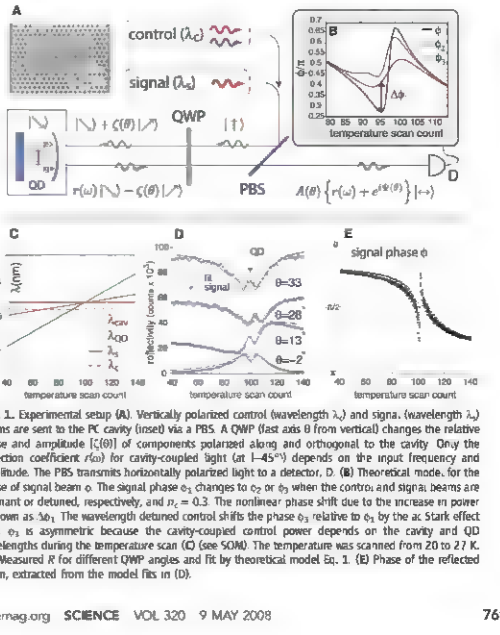

Fig. 1. Experimental setup (**A**). Vertically polarized control (wavelength λ_C) and signal (wavelength λ_S) beams are sent to the PC cavity (inset) via a PBS. A QWP (fast axis θ from vertical) changes the relative phase and amplitude [$\zeta(\theta)$] of components polarized along and orthogonal to the cavity. Only the reflection coefficient $r(\omega)$ for cavity-coupled light (at I–45°) depends on the input frequency and amplitude. The PBS transmits horizontally polarized light to a detector, D. (**B**) Theoretical model, for the phase of signal beam ϕ. The signal phase ϕ_1 changes to ϕ_2 or ϕ_3 when the control and signal beams are resonant or detuned, respectively, and $n_c = 0.3$. The nonlinear phase shift due to the increase in power is shown as $\Delta\phi_1$. The wavelength detuned control shifts the phase ϕ_3 relative to ϕ_1 by the ac Stark effect (*19*). ϕ_2 is asymmetric because the cavity-coupled control power depends on the cavity and QD wavelengths during the temperature scan (**C**) (see SOM). The temperature was scanned from 20 to 27 K. (**D**) Measured R for different QWP angles and fit by theoretical model Eq. 1. (**E**) Phase of the reflected beam, extracted from the model fits in (**D**).

[2]Applied Physics, Stanford University, Stanford, CA 94305, USA. [2]Electrical and Computer Engineering, University of California, Santa Barbara, CA 93106, USA. [2]Electrical Engineering, Stanford University, Stanford, CA 94305, USA.

*These authors contributed equally to this work.
†To whom correspondence should be addressed. E-mail: jesa@stanford.edu

We first performed phase measurements on a single (signal) beam reflected from the cavity with a QD. Interference between the QD-scattered field and the incident signal resulted in the rapidly varying feature in Fig. 1D. As the phase of the reference beam increased from 0° to 3.3°, this interference evolved from destructive to constructive, and the dip at $\theta = 0°$ changed to a peak at $\theta = 3.3°$. We find that this interference is only explained by coherent light scattering from the QD. The experimental data are fit well by Eq. 1, as shown in Fig. 1D. Each fit gives the signal phase $\phi = \arctan(\Im m[r(\omega)]/\Re e[r(\omega)])$, where $\Re e[r(\omega)]$ and $\Im m[r(\omega)]$ are the real and imaginary parts of the cavity reflectivity $r(\omega)$. The phase fits for 11 scans with different QWP angles θ are superposed in Fig. 1E. As the signal wavelength traverses the cavity resonance, ϕ changes from 0 to $-\pi$. An additional phase modulation occurs at the QD resonance, where the phase varies by almost π over the dot bandwidth ($2g^2/\kappa = 2\pi \times 32$ GHz).

When measuring the controlled-phase shifts, we first considered the cases in which the control and signal have the same wavelength (they potentially could be distinguished by polarization or incident direction). When the control and signal are at the same wavelength, the nonlinear interaction between them (Fig. 2, A and B) arises from the saturation of the QD in the presence of cavity-coupled photons (*12*). Saturation occurs when the average photon number inside the cavity reaches approximately one photon per modified QD lifetime, given by κ/g^2. The cavity photon number is $n_c = \eta P_{in}/[2 \times \hbar\omega_c]$, given the input power P_{in}, control frequency ω_c, and coupling efficiency $\eta \approx 2$ to 5% in our experimental setup. The observed QD-induced dip does not fully reach zero at low powers, as expected from theory (*12*, *14*), because of QD-wavelength jitter and blinking (see SOM).

We observed a phase modulation of 0.24π (43°) when the control photon number was increased from $n_c = 0.08$ to 3 and the wavelength was set 0.014 nm ($g/3.5$) away from the anti-crossing point (Fig. 2C). The reflectivity amplitude R normalized by the cavity reflectivity without a dot R_0 is shown for the same detuning in Fig. 2E and changed from 50 to 100% at saturation. The excitation powers were 40 nW and 1.3 μW, measured before the objective lens (corresponding to n_c of 0.08 and 3, respectively), and indicate a coupling efficiency of up to 5%. However, the coupling efficiency fluctuated because of sample drift during the experiment. Therefore, we estimate control powers from fits to the data, and give power levels measured before the objective lens for reference.

In the context of quantum gates (*2*, *15*, *16*), we are interested in the signal photon's phase change caused by a single control photon. When the control and signal have the same wavelength ($\lambda_c = \lambda_s$) and the same duration, the change is given by the difference between the phase evaluated at n_c and $2n_c$ (Fig. 2C). We measured a maximum differential phase shift of 0.07π (12°) when $n_c = 0.1$. The differential amplitude is maximized at a higher $n_c = 0.43$, where it changes by 15% when n_c is increased to $2n_c$ (Fig. 2E). Theoretically, we estimate a maximum of 0.15π (27°) for phase and 20% amplitude modulation with our system parameters.

Conventionally, the intensity-dependent refractive index n_2 or the Kerr coefficient $\chi^{(3)}$ describes the strength of a nonlinear medium in which the nonlinearity is proportional to the photon number (*17*). The cavity-embedded QD is highly nonlinear and is not well described as a pure Kerr medium. However, for weak excitations, we can still approximate the nonlinear index and susceptibility from the relationship between the acquired signal phase shift ϕ_s and n_2 given by $\phi_s = (2\pi n_2/\lambda_c)(P_{in}/A_{cav})(c/2\kappa\pi)$, where $A_{cav} = (\lambda/n)^2$ is the cavity area, and $c/2\kappa\pi$ gives the propagation length in GaAs with refractive index $n = 3.5$. From our experimental data at very low values of control power, we infer $n_2 \approx 2.7 \times 10^{-5}$ cm^2/W and $\chi^{(3)} \sim 2.4 \times 10^{-6}$ m^2/V^2. This value is many orders of magnitude larger than most fast optical nonlinearities in solid-state materials.

Spontaneous emission from the QD into modes other than the cavity reduces the performance of quantum gates because of photon losses. In Fig. 2D, we show a 1% photon loss due to incoherent fluorescent emission from the QD, which is driven 0.014 nm away from resonance by the signal laser. Fluorescence loss is expected to scale as $F_{PC}/(F + F_{PC}) \approx 0.15\%$, where $F = 160$ is the QD Purcell factor in the PC cavity and $F_{PC} \approx 0.25$ is the suppression of the QD radiative rate due to the PC lattice (*18*). The observed 1% is higher than the expected value for losses, but within error, because F_{PC} strongly depends on the dot position and can at most be unity. Radiation from nearby emitters cannot be excluded from this signal and therefore fluorescence losses from the addressed QD may be lower (*18*).

For applications such as quantum nondemolition (QND) detection and optical control, it is advantageous to spectrally separate the control and signal beams. We detuned the control beam by $\Delta\lambda = -0.027$ nm (1.2g) with respect to the signal beam, which again was aligned to the QD-cavity intersection (Fig. 3A). The number of signal photons per QD lifetime (n_s) was fixed and the control photon number (n_c) was varied. In these measurements, a weakly coupled QD with $g/2\pi \approx \kappa/4\pi = 8$ GHz was used. Saturation power scaled with the modified spontaneous emission

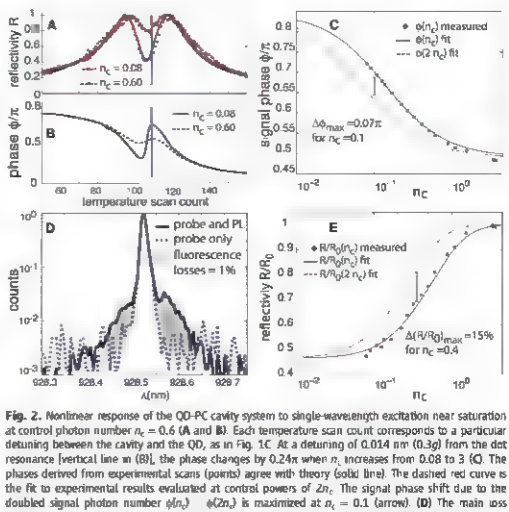

Fig. 2. Nonlinear response of the QD-PC cavity system to single-wavelength excitation near saturation at control photon number $n_c = 0.6$ (**A** and **B**). Each temperature scan count corresponds to a particular detuning between the cavity and the QD, as in Fig. 1C. At a detuning of 0.014 nm (0.3g) from the dot resonance [vertical line in (**B**)], the phase changes by 0.24π when n_c increases from 0.08 to 3 (**C**). The phases derived from experimental scans (points) agree with theory (solid line). The dashed red curve is the fit to experimental results evaluated at control powers of $2n_c$. The signal phase shift due to the doubled signal photon number $\phi(n_s)$ – $\phi(2n_s)$ is maximized at $n_c = 0.1$ (arrow). (**D**) The main loss mechanism due to fluorescence from the QD corresponds to ~1% photon loss. (**E**) Reflectivity power dependence. Points correspond to experimental data for reflectivity (R) normalized by the calculated value of R from a cavity with no QD (R_0).

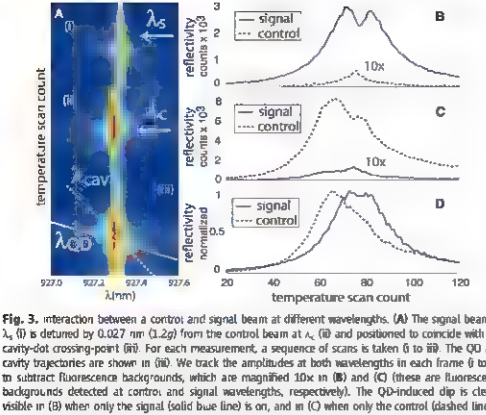

Fig. 3. Interaction between a control and signal beam at different wavelengths. (**A**) The signal beam at λ_S (i) is detuned by 0.027 nm (1.2g) from the control beam at λ_C (ii) and positioned to coincide with the cavity-dot crossing-point (iii). For each measurement, a sequence of scans is taken (i to iii). The QD and cavity trajectories are shown in (iii). We track the amplitudes at both wavelengths in each frame (i to iii) to subtract fluorescence backgrounds, which are magnified 10× in (**B**) and (**C**) (these are fluorescence backgrounds detected at control and signal wavelengths, respectively). The QD-induced dip is clearly visible in (**B**) when only the signal (solid blue line) is on, and in (**C**) when only the control (dashed line) is on. This feature disappears when both beams are on in (**D**). In (**D**), the spectra are normalized to clearly show saturation. The signal and control powers were 100 nW and 200 nW measured before the lens, corresponding to cavity-coupled signal and control photon numbers $n_S \approx 0.2$ and $n_C \approx 0.3$, respectively.

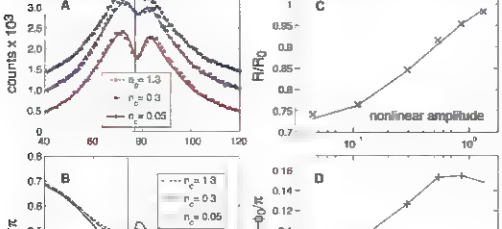

Fig. 4. Nonlinear response of a weakly coupled QD inside the cavity to excitation with control and signal beam wavelengths separated by 0.027 nm (1.2g). The reflectivity of a signal beam with $n_S = 0.2$ photons per cavity lifetime is shown in (**A**) for three values of the control beam photon number n_C. The QD saturates almost completely when $n_C = 1.3$, which corresponds to a power of 1 μW measured before the objective lens. The data are fit with a full quantum model, which allows us to extract the signal phase shown in (**B**). In (**C**), the amplitude of the reflected signal beam when it is 0.009 nm (0.4g) away from the dot resonance [vertical line in (**A**) and (**B**)] is shown as a function of control-beam photon number n_C. In (**D**), we show the difference between the phase shift of the signal beam when the control beam is on (ϕ_1) and when it is off (ϕ_0) as a function of n_C at the same time point as in (**C**).

rate g^2/κ, and so the smaller g value permitted lower control powers and reduced background noise. In Fig. 3, we show the principle of the measurement. First, the signal and control were tuned on independently; the QD dip is visible in Fig. 3, B and C. The dip disappeared when the two beams were tuned on simultaneously and interacted (Fig. 3D). For better visibility at high control powers, the signal power in Fig. 4 was set to 100 nW before the objective lens, corresponding to $n_S = 0.2$ signal photons in the cavity per cavity lifetime.

In Fig. 4, we show experimental results for phase shifts with control and signal beams at different wavelengths. Here, the signal phase was affected by the saturation of the QD and a frequency shift of the QD due to the ac Stark effect (*17*), which can be used to realize large phase shifts (*19*). The signal reflectivity and phase as functions of control-beam photon number are shown in Fig. 4, A and B. We fit both the signal and control data by a full quantum simulation and derived the underlying signal phase shift as a function of the control photon number (*20*) (see SOM). The reflectivity at the signal wavelength saturated completely when the control photon number reached $n_C = 1.3$, which corresponds to 1 μW of power measured before the objective lens. The associated phase modulation was 0.13π at the signal detuning of 0.009 nm (0.4g) from the dot resonance. The phase behavior in Fig. 4B is asymmetric with respect to the center of the QD-induced dip because the coupling of the control beam changed with the temperature scan.

We fixed the signal wavelength at 0.009 nm (g/3) away from the QD resonance and determined the phase and amplitude modulation for a range of values of n_C. The signal phase $\phi(n_C)$ relative to the signal phase with no control $\phi_0 = \phi(n_C = 0)$ is shown in Fig. 4D. The maximum observed phase shift when $n_C = 1$ was 0.16π (28.8°). The largest nonlinear phase change was observed for $n_C = 0.05$, for which $\phi(n_C) - \phi(0) = 0.05\pi$ (9°). These values give a nonlinear index of $n_2 \approx 1.8 \times 10^{-5}$ cm^2/W, or $\chi^{(3)} \approx 1.6 \times 10^{-10}$ m^2/V^2, for a detuning of 0.027 nm (1.2g) between the signal and control. This value is similar to that of the QD with larger g. Numerical simulations indicate that the relative magnitude of nonlinearities due to these two QDs strongly depends on the laser frequency. The nonlinearities for the two cases are summarized in Table 1.

The current implementation of the QD/cavity system is already promising for low-power and QND photon detection (*8*–*10*). We have shown that the phase and amplitude of the signal strongly depend on the control photon number when the signal and control photons are spectrally separated. Furthermore, the magnitude and bandwidth of the Kerr nonlinearity $\chi^{(3)}$ observed in this experiment are rivaled only by measurements in atomic ensembles (*21*, *22*).

To realize useful quantum logic gates, controlled π phase shifts are necessary (*23*). This will require repeated interactions. Such cascading

Table 1. Nonlinear parameters and phase modulation derived from experimental data for the strongly (first row) and weakly (second row) coupled QDs. $\Delta\phi$ is a maximum differential phase shift ($\Delta\phi = \phi(n_c) - \phi(0)$), which is achieved at the intracavity photon number n_c in the last column.

$g/2\pi$ (GHz)	$\lambda_p - \lambda_{QD}$ (nm)	$\lambda_p - \lambda_c$ (nm)	n_2 (cm^2/W)	$\chi^{(3)}$ (m^2/V^2)	$\Delta\phi$	n_c
16	0.014 (0.3g)	0	2.7×10^{-5}	2.4×10^{-10}	0.015π	0.01
8	0.009 (0.4g)	0.027	1.8×10^{-5}	1.6×10^{-10}	0.05π	0.05

requires coupling efficiencies that are higher than the observed 2 to 5%. This technical challenge can be overcome. We have already demonstrated architecture for a QD cavity-waveguide–coupled quantum network (*24*) with coupling efficiency above 50% between two nodes, and cavity waveguide couplers (*25*) with coupling efficiency reaching 90%. The observed fluorescence losses are already sufficiently low to allow scalable computation (*26*), and can be further improved with increases in cavity Q. The ability to tailor photon-QD interactions by PC fabrication makes this a highly versatile platform for a variety of quantum optics experiments and has great potential for compact scalable quantum devices.

References and Notes

1. E. Knill, R. Laflamme, G. J. Milburn, *Nature* **409**, 46 (2001).
2. Q. Turchette, C. Hood, W. Lange, H. Mabuchi, H. J. Kimble, *Phys. Rev. Lett.* **75**, 4710 (1995).
3. T. Wilk, S. C. Webster, A. Kuhn, G. Rempe, *Science* **317**, 488 (2007).
4. J. Majer *et al.*, *Nature* **449**, 443 (2007).
5. A. C. Santori *et al.*, *Phys. Rev. Lett.* **97**, 247402 (2006).
6. M. V. Gurudev Dutt *et al.*, *Science* **316**, 1312 (2007).
7. D. P. DiVincenzo, *Fortschr. Phys.* **48**, 771 (2000).
8. M. Imoto, H. A. Haus, Y. Yamamoto, *Phys. Rev. A* **32**, 2287 (1985).
9. J. P. Poizat, P. Grangier, *Phys. Rev. Lett.* **70**, 271 (1993).
10. G. Nogues *et al.*, *Nature* **400**, 239 (1999).
11. Y. Akahane, T. Asano, B. S. Song, S. Noda, *Nature* **425**, 944 (2003).
12. D. England *et al.*, *Nature* **450**, 857 (2007).
13. H. Alnis, J. Vučković, *Opt. Lett.* **30**, 982 (2005).
14. E. Waks, J. Vučković, *Phys. Rev. Lett.* **96**, 153601 (2006).
15. I. L. Chuang, Y. Yamamoto, *Phys. Rev. A* **52**, 3489 (1995).
16. K. M. W. J. Nemoto, T. Spiller, *Int. J. Phys.* **7**, 137 (2005).
17. R. Boyd, *Nonlinear Optics* (Academic Press, New York, ed. 2, 2003).
18. D. England *et al.*, *Phys. Rev. Lett.* **95**, 013904 (2005).
19. E. Waks, J. Vučković, *Phys. Rev. A* **73**, 041803 (2006).
20. S. M. Tan, www.qo.phy.auckland.ac.nz/qonotebook.html
21. S. Harris, J. Field, A. Imamoğlu, *Phys. Rev. Lett.* **64**, 1107 (1990).
22. K. J. Boller, A. Imamoğlu, S. E. Harris, *Phys. Rev. Lett.* **66**, 2593 (1991).
23. M. A. Nielsen, I. L. Chuang, *Quantum Computation and Quantum Information* (Cambridge Univ. Press, Cambridge, UK, 2000).
24. D. Englund, A. Faraon, B. Zhang, Y. Yamamoto, J. Vučković, *Opt. Express* **15**, 5550 (2007).
25. A. Faraon, E. Waks, D. Englund, I. Fushman, J. Vučković, *Appl. Phys. Lett.* **90**, 073102 (2007).
26. E. Knill, *Nature* **434**, 39 (2005).

27. Financial support was provided by the Multidisciplinary University Research Initiative Center for photonic quantum information systems (Army Research Office/Intelligence Advanced Research Projects Agency Program DAAD19-03-1-0199), Office of Naval Research Young Investigator Award, and NSF grant CCF-0507295. D.E. and J.F. were also supported by a National Defense Science and Engineering Graduate Fellowship. Part of the work was performed at the Stanford Nanofabrication Facility of the National Nanotechnology Infrastructure Network supported by the NSF under grant ECS-9731293.

Supporting Online Material

www.sciencemag.org/cgi/content/full/320/5877/769/DC1
SOM Text
Figs. S1 and S2
References and Notes

26 December 2007; accepted 1 April 2008
10.1126/science.1154643

Conditional Dynamics of Interacting Quantum Dots

Lucio Robledo,[1] Jeroen Elzerman,[1] Gregor Jundt,[1] Mete Atatüre,[2] Alexander Högele,[1] Stefan Fält,[1] Atac Imamoglu[1]*

Conditional quantum dynamics, where the quantum state of one system controls the outcome of measurements on another quantum system, is at the heart of quantum information processing. We demonstrate conditional dynamics for two coupled quantum dots, whereby the probability that one quantum dot makes a transition to an optically excited state is controlled by the presence or absence of an optical excitation in the neighboring dot. Interaction between the dots is mediated by the tunnel coupling between optically excited states and can be optically gated by applying a laser field of the right frequency. Our results represent substantial progress toward realization of an optically effected controlled–phase gate between two solid-state qubits.

Self-assembled semiconductor quantum dots (QDs) (*1*) can be manipulated and probed optically, enabling ultrafast coherent control (*2*) and rendering them model systems for solid-state quantum optics (*3*). Particularly promising are quantum dots deterministically charged with a single electron, because the electron spin state is robust against relaxation and decoherence (*4*). In such systems, single-electron spin states can be optically prepared (*5*) and read out (*6*, *7*), allowing demonstrations of optically detected electron spin resonance (*8*) and coherent spin dynamics (*9*). These results established QD spins as promising candidates for solid-state qubits and motivated our research aimed at demonstrating conditional interactions, which is required for implementing two-qubit quantum gates.

In electrically defined QDs, the exchange interaction (*10*) has been used to demonstrate such controlled conditional coupling between electron spins (*11*). However, this mechanism requires fast electrical control over the exchange splitting, which is not feasible in self-assembled QDs (*12*–*14*). An alternative mechanism that has been proposed for coherent coupling of self-assembled QDs (*15*) is based on dipole-dipole interaction (*16*), which can be switched on in sub-picosecond time scales by optically exciting both QDs (*17*). However, for standard vertically coupled QDs, the bare dipole-dipole interaction is typically too weak (smaller than the linewidth of a QD transition) to allow for the accumulation of large conditional phase shifts.

We present an experimental realization of a strong optically gated interaction between a neutral and a single-electron–charged QD. The interaction mechanism, which relies on the tunnel coupling between the dots (*12*–*14*), is tunable and can be much larger than the dipole-dipole interaction. The experiments were performed in a GaAs device (grown by molecular beam epitaxy), containing two layers of self-assembled InGaAs QDs with a nominal separation of 15 nm. QDs in the top layer tend to grow directly on top of QDs in the bottom layer because of the strain field produced by the latter (*14*), resulting in stacks of vertically coupled QDs (CQDs). These QD stacks are embedded in a field-effect structure consisting of an n^+ doped GaAs layer acting as an electron reservoir (with a 25-nm tunnel barrier to the bottom QD layer) and a 4-nm-thick semi-transparent Ti top gate (Fig. 1A). By varying the gate voltage, we can deterministically charge the two dots and tune their relative energy. In order to reach a regime where the electronic energy levels of a stack can be brought into resonance, the size of the bottom QDs has been reduced during growth, leading to an increase of their recombination energy. In the following, we refer to the QDs of a stack as the blue QD (bottom) and the red QD (top). The relatively thick tunnel barrier between the dots [compared with the CQDs used in (*12*, *13*)] assures that

[1]Institute of Quantum Electronics, Eidgenössische Technische Hochschule (ETH)–Zürich, CH-8093 Zürich, Switzerland. [2]Cavendish Laboratory, University of Cambridge, J. J. Thomson Avenue, Cambridge CB3 0HE, UK.
*To whom correspondence should be addressed. E-mail: imamoglu@phys.ethz.ch

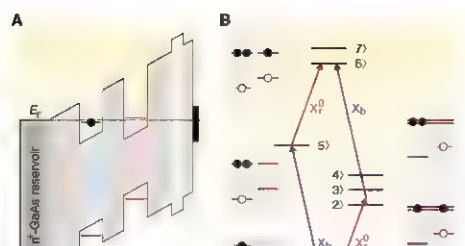

Fig. 1. Conditional interaction in a CQD. **(A)** Schematic band structure of the device, showing the lowest energy levels for electrons and holes confined in the top (red) and bottom (blue) QD. The voltage applied between the gate (black) and the n⁺-GaAs reservoir tilts the bands and thereby controls the charge state of the dots and their detuning, allowing the electronic energy levels to be brought into resonance. **(B)** Schematic energy level diagram representing the relevant elementary optical excitations in both dots. The ground state consists of a single electron in the blue dot. X_b^0 corresponds to the creation or recombination of one electron-hole pair in the otherwise empty red dot; $X_{b,r}$ to the creation or recombination of an electron-hole pair in the blue dot in the presence of a resident electron. Note that X_r^0 is split because of the bare electron-hole exchange interaction (levels 6⟩ and 7⟩) or because of the exchange interaction plus additional mixing with the interdot exciton (levels 2⟩, 3⟩, and 4⟩).

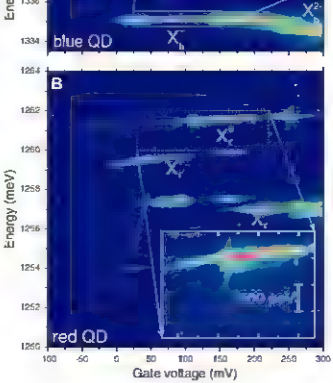

Fig. 2. Low-temperature photoluminescence (in logarithmic color scale) versus gate voltage. **(A)** Recombination involving a hole in the blue dot. PL from the sequence of successively charged exciton complexes leads to the plateaus indicated by the labels. (Inset) The X_b transition shifts abruptly by ~100 μeV because of charge sensing of the red QD. **(B)** Recombination involving a hole in the red dot. (Inset) Anticrossing of intradot and interdot recombination for the X_r^0 transition. The normally dark exciton transition is also visible, ~250 μeV below the bright exciton.

tunnel coupling is only substantial near a resonance condition, that is, around specific gate voltages and for specific charge configurations.

This system allows us to realize the conditional scheme depicted in Fig. 1B. In the ground state ⟨1⟩, the blue dot contains a single electron and the red dot is empty (as indicated in the corresponding level diagram). Upon absorption of a photon with the proper energy, a negatively charged exciton ⟨5⟩ is created in the blue dot (X_b transition); if a second photon that is resonant with the red X_r^0 transition from state ⟨5⟩ is absorbed, an exciton is created in the red dot as well. Because of electron-hole exchange, the X_r^0 transition is in fact split into two transitions with orthogonal linear polarization, $X_{r,x}^0$ and $X_{r,y}^0$ (*18*, *19*), associated with two slightly nondegenerate states, ⟨6⟩ and ⟨7⟩, respectively. In all of these states (⟨1⟩, ⟨5⟩, ⟨6⟩, and ⟨7⟩), there is no resonance between the electron levels in the blue and the red dot, thus, the tunnel coupling is not effective (*20*). In contrast, if no photon is absorbed in the blue dot but only in the red dot, then the relevant states ⟨2⟩ and ⟨3⟩ (again split because of electron-hole exchange) are near resonance with the indirect exciton state ⟨4⟩, in which both electrons are in the blue dot. Therefore, the tunnel coupling is able to mix states ⟨2⟩, ⟨3⟩, and ⟨4⟩, leading to a shift of their energies. As a result, a photon of the bare energy $X_{r,x}^0$ or $X_{r,x}^0$ can only be absorbed if there is an optical excitation present in the blue dot; this scheme thus describes a conditional operation.

To implement this conditional scheme experimentally, we first characterize a particular stack of two CQDs by performing nonresonant photoluminescence (PL) measurements at 4 K. The substantial blue shift of the bottom QD layer enables us to assign all PL peaks to recombinations either involving a hole in the blue QD (Fig. 2A) or involving a hole in the red QD (Fig. 2B). The two QDs behave to a large extent as individual dots because of the relatively thick tunnel barrier between them, so that gate voltage–dependent PL spectra exhibit the characteristic charging plateaus (*21*) labeled in the figure. For the blue dot, the presence of its red partner only manifests itself in charge sensing (Fig. 2A inset), resulting in a ~100-μeV shift of the negatively charged blue transition (X_b^-) when the red QD charge changes from singly positive (a long-lived metastable state) to neutral (*14*).

The PL spectra for the red QD (Fig. 2B) are considerably more complex. In addition to the standard intradot recombination (between an electron and a hole in the same dot), which exhibits a small Stark shift, we also observe interdot recombination (electron and hole in different dots), which shows a much larger slope because of the relative energy detuning of the dots with gate voltage. For certain gate voltages clear anticrossings appear, indicating mixing between intradot and interdot recombination. The region relevant for this experiment is highlighted in the Fig. 2B inset. In this voltage range,

the lowest energy state of the blue QD has a single excess electron, whereas the red QD ground state is uncharged. The fact that in this region we see evidence of tunnel coupling only for X_b^0 recombination but not for X_r^0 tells us unambiguously that the tunnel coupling occurs in the optically excited X_r^0 state but not in the X_b^0 state or the ground state. This situation thus corresponds to the mixing between states |2⟩, |3⟩, and |4⟩ that was described in Fig. 1B (*22*).

To probe the conditional behavior of the CQD, we need precise control over the excitons that are created in the system. We used a tunable laser to resonantly excite one of the dots and detected the absorption of the laser by the CQD device with use of the technique of differential transmission (*23*). We can now resolve the 35-μeV electron-hole exchange splitting of the bright neutral exciton in the red QD into the two orthogonal linearly polarized $X_{r,y}^0$ and $X_{r,x}^0$ resonances (compare the rightmost parts of Fig. 3, B and C). For gate voltages around 125 mV (*24*), these two states mix with the indirect trion state, leading to an anticrossing as depicted schematically in Fig. 3D, with a tunnel splitting of 100 μeV. In addition to shifting the transition energies, the mixing also leads to a gradual change in the polarization character of each of the two exchange-split resonances. In contrast to the red dot, the negatively charged exciton transition in the blue dot (X_b^-) shows no indications of tunnel coupling in this voltage range (Fig. 3A), confirming that the tunnel coupling is only present in the excited state of the red dot.

Although single-laser absorption measurements map out the transitions available from the CQD ground state, two simultaneous lasers are required to reveal the effects an optical excitation in one QD has on the states of the partner QD, establishing the conditional interaction of the dots. We measured the absorption of the "red" probe laser (Fig. 3, B and C) but now in the presence of a second "blue" pump laser that is kept on resonance with the X_b^- transition for all gate voltages. In this case, the pump laser can create an optical excitation in the blue dot, giving rise to an extra absorption resonance for each polarization direction of the red laser (blue lines in Fig. 3, E and F). Both of these extra lines follow the linear Stark shift of X_r^0, indicating that they correspond to absorption of a red photon in the absence of tunneling, that is, when the tunnel coupling has been effectively switched off by exciting the blue dot. The appearance of the extra lines (transitions from state |5⟩ to state |6⟩ or |7⟩ in Fig. 1B) thus directly demonstrates the shift of the red QD levels conditional on the state of the blue dot. The original absorption lines of Fig. 3, B and C, are still visible (red lines in Fig. 3, E and F) because the blue dot remains in its ground state at least half of the measurement time, even in the presence of a strong resonant blue laser.

To illustrate the conditional nature of this new resonance more clearly, we present in Fig. 4A the absorption of the red probe laser when the blue pump laser is tuned through the X_b^- resonance of the blue dot (*25*). Both lasers are y-polarized, and the gate voltage is fixed at 130 mV, where the effect of the tunnel coupling is substantial. The two tunnel-split resonances already seen in Fig. 4C now show up as two horizontal lines (indicated by the top and bottom horizontal arrows). When the blue laser is resonant with the X_b^- transition (vertical arrow), we again see the strong 30-μeV conditional shift of the red resonance (solid horizontal arrow) and the corresponding strong decrease of the unshifted absorption (*26*).

To verify our interpretation of the experimental data, we modeled the system by using a density-matrix approach, only taking into account the five levels from Fig. 1B that are relevant for y-polarized lasers. The energies and lifetimes of these levels were taken from the experiment (*27*), and the absorption was calculated by solving the master equation in Lindblad form in the steady state, as a function of red and blue laser detuning (*28*). The results (Fig. 4B) reproduce all relevant features of the experiment very well. This, in combination with the results of a control experiment in which the roles of the red and blue dot are reversed (fig. S3, B and D), confirms the validity of our model for the conditional interaction

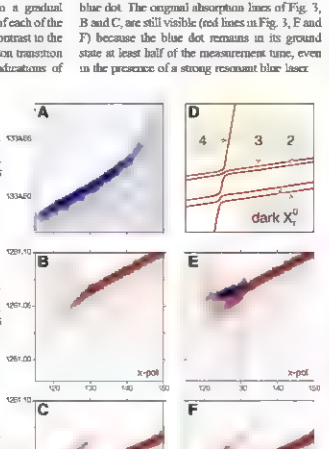

Fig. 3. High-resolution laser absorption mapping out the CQD levels versus gate voltage. (**A**) The X_b^- transition depends linearly on the gate voltage (V_g) below 140 mV, showing no evidence of tunnel coupling. (**B**) Absorption of an x-polarized laser reveals the x-polarized branch ($X_{r,x}^0$) of the red neutral exciton. (**C**) The y-polarized branch ($X_{r,y}^0$), split from $X_{r,x}^0$ because of the electron-hole exchange interaction, is revealed with a y-polarized laser. Both resonances anticross with the indirect exciton for $V_g \sim 125$ mV. (**D**) Schematic energy diagram versus gate voltage around the anticrossing. The states are labeled according to the diagram in Fig. 1B. The region relevant for the experiment is indicated in the box. (**E** and **F**) Single-laser absorption as in (**B**) and (**C**) in the presence of a second (undetected) blue pump laser, which is kept on resonance with the X_b^- transition for every gate voltage inside the dashed region. This reveals the $X_{r,y}^0$ and $X_{r,y}^0$ when the tunnel coupling has been turned off (blue lines) upon absorption of a blue laser photon, in addition to the original transitions that experience tunnel coupling (red lines). Outside the dashed region, the original data from (**B**) and (**C**) are shown.

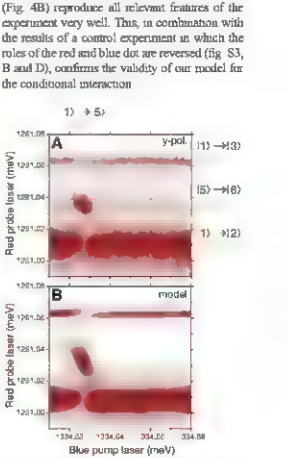

Fig. 4. Two-laser experiment showing conditional interaction in a CQD. Gate voltage is fixed at 130 mV, with y-polarized red and blue lasers. (**A**) Absorption of red probe laser in the presence of a strong (undetected) blue pump laser shows a conditional shift of the red QD transition energy when the blue laser is resonant with the X_b^- transition (vertical arrow). (**B**) Calculated absorption for the experiment depicted in (**A**).

We have demonstrated a method to realize conditional dynamics in a system of two CQDs. The interaction mechanism relies on the tunnel coupling, which can lead to conditional energy shifts that are much larger than those provided by dipole-dipole interactions. More importantly, this tunnel-coupling–mediated interaction can be effectively tuned by changing the energy level detuning via the gate voltage, and it can be optically gated in sub-picosecond time scales by creation of an exciton.

References and Notes

1. P. M. Petroff, A. Lorke, A. Imamoglu, *Phys. Today* **54**, 46 (2001).
2. X. Li *et al.*, *Science* **301**, 809 (2003).
3. M. O. Scully, M. S. Zubairy, *Quantum Optics* (Cambridge Univ. Press, Cambridge, 1997).
4. R. Hanson, L. P. Kouwenhoven, J. R. Petta, S. Tarucha, L. M. K. Vandersypen, *Rev. Mod. Phys.* **79**, 1217 (2007).
5. M. Atatüre *et al.*, *Science* **312**, 551 (2006); published online 5 April 2006 (10.1126/science.1122978).
6. J. Berezovsky *et al.*, *Science* **314**, 1916 (2006); published online 9 November 2006 (10.1126/science.1133862).
7. M. Atatüre, J. Dreiser, A. Badolato, A. Imamoglu, *Nat. Phys.* **3**, 101 (2007).
8. M. Kroner *et al.*, preprint available at http://arxiv.org/abs/0710.4901.
9. M. H. Middelsen, J. Berezovsky, N. G. Stoltz, L. A. Coldren, D. D. Awschalom, *Nat. Phys.* **3**, 770 (2007).
10. D. Loss, D. P. DiVincenzo, *Phys. Rev. A* **57**, 120 (1998).
11. J. R. Petta *et al.*, *Science* **309**, 2180 (2005); published online 1 September 2005 (10.1126/science.1116955).
12. H. J. Kreimer *et al.*, *Phys. Rev. Lett.* **94**, 057402 (2005).
13. E. A. Stinaff *et al.*, *Science* **311**, 636 (2006); published online 11 January 2006 (10.1126/science.1121138).
14. S. Fält *et al.*, *Phys. Rev. Lett.* **100**, 106401 (2008).
15. T. Calarco, A. Datta, P. Fedichev, E. Pazy, P. Zoller, *Phys. Rev. A* **68**, 012310 (2003).
16. C. Hettich *et al.*, *Science* **298**, 385 (2002); published online 5 September 2002 (10.1126/science.1076061).
17. T. Unold, K. Mueller, C. Lienau, T. Elsaesser, A. D. Wieck, *Phys. Rev. Lett.* **94**, 137404 (2005).
18. M. Bayer *et al.*, *Phys. Rev. B* **65**, 195315 (2002).
19. D. Gammon, E. S. Snow, B. V. Shanabrook, D. S. Katzer, D. Park, *Phys. Rev. Lett.* **76**, 3005 (1996).
20. In principle, states (1) or (5) or (6) and (7) could be split because of electron tunneling, but each of these resonances will only occur at substantially different gate voltages because of the fact that the tunneling strength is much smaller than the relevant Coulomb interaction energies.
21. R. J. Warburton *et al.*, *Nature* **405**, 926 (2000).
22. In the inset, the mixing of the bright X_0^B with the indirect exciton is hardly resolved. Clearly visible is the anticrossing of the indirect exciton with the dark X_0^D, which becomes bright because of the mixing (14).
23. B. Alén, F. Bickel, K. Karrai, R. J. Warburton, P. M. Petroff, *Appl. Phys. Lett.* **83**, 2235 (2003).
24. The gate voltage scale for the absorption measurements is slightly different from that of PL because of technical reasons (28).
25. To illustrate the observed effect clearly, the intensity of the probe laser is chosen such that it saturates the corresponding ground state transition, whereas the pump laser is set to five times the saturation intensity.
26. In addition to the strong shifted red absorption that occurs for a resonant blue laser (around 1334.6 meV), we also see a weak red absorption around 1261.04 meV even when the blue laser is not resonant. This effect, which is not present when the blue laser is turned off, indicates that even a nonresonant blue laser has a small probability to fill the tunneling resonance between states (2), (3), and (4). This is most likely due to the creation of charges in nearby impurity sites, which can shift the effective gate voltage felt by the CQD. Also, a faint diagonal absorption line is visible around the shifted resonance, which is due to two-photon resonance between states (2) and (6).
27. We have assumed that all excited states are lifetime-broadened.
28. Materials and methods are available on *Science* Online.
29. This work is supported by National Centre of Competence in Research Quantum Photonics (NCCR QP) research instrument of the Swiss National Science Foundation (SNSF), and European Union Research Training Network Engineering, Manipulation, and Characterization of Quantum States of Matter and Light (EMALI). The authors thank K. Weiss for experimental assistance.

Supporting Online Material

www.sciencemag.org/cgi/content/full/320/5877/772/DC1
Materials and Methods
Figs. S1 to S4
References

18 January 2008; accepted 1 April 2008
10.1126/science.1155374

Subnanometer Motion of Cargoes Driven by Thermal Gradients Along Carbon Nanotubes

Amelia Barreiro,[1] Riccardo Rurali,[2] Eduardo R. Hernández,[3]* Joel Moser,[1] Thomas Pichler,[4] László Forró,[5] Adrian Bachtold[1]*

An important issue in nanoelectromechanical systems is developing small electrically driven motors. We report on an artificial nanofabricated motor in which one short carbon nanotube moves relative to another coaxial nanotube. A cargo is attached to an ablated outer wall of a multiwalled carbon nanotube that can rotate and/or translate along the inner nanotube. The motion is actuated by imposing a thermal gradient along the nanotube, which allows for subnanometer displacements, as opposed to an electromigration or random walk effect.

There is a growing effort in the scientific community to design and fabricate ever more versatile nanoelectromechanical systems (NEMS) (*1*). Because carbon nanotubes are very small, mechanically robust, and chemically inert, they have attracted considerable interest as NEMS components. In addition, their one-dimensional tubular shape offers a natural track for motion. This tubular shape restricts the motion (typically translation or rotation) to only a few degrees of freedom, much as bearings do in everyday machines. The tubular track has been the key component for the fabrication of nanotube-based switches (*2*), rotors (*3*, *4*), and mass conveyors (*5*–*7*).

A second generation of nanotube-based motors has been envisaged that takes advantage of the atomic corrugation for a new class of tracks (*8*, *9*). Because the atoms in a nanotube can be arranged in many different configurations, as defined by its chirality, such motors are expected to be quite versatile. For example, a gold nanoparticle confined inside a nanotube is expected to move along a helical orbit around the nanotube axis; this orbit can take different angles and periodicities, which are controlled by the nanotube chirality (*10*, *11*).

The motion of two coaxial nanotubes relative to one another offers additional possibilities, because it combines a pair of chiralities. The track is given by the mutual atomic interaction between the nanotubes. In some cases, the track follows energy minima that can consist of helical orbits ranging from pure rotation to pure translation. In other cases, it contains local minima and maxima, which can be arranged, for example, as a twisted chessboard-like pattern (see some examples in Fig. 1, D to F) (*8*). This flexibility of the energy surface for motion is expected to provide the framework to explore various motion-related phenomena at the nanoscale, such as the ratchet effect (*12*, *13*), vanishingly small friction (*14*), friction resonances (*15*, *16*), and thermal gradient–induced motion (*10*, *11*). However, nanotube motors controlled by the atomic corrugation remain to be experimentally demonstrated.

We report two advances on a nanotube-based motor designed so that motion occurs between two coaxial nanotubes. First, the atomic interaction between the nanotubes is shown to generate distinct kinds of motion for different devices, namely, rotation and/or translation along the nanotube axis. Second, we show that the motion is driven by a thermal gradient. More specifically, the thermal gradient generates a phononic current in one nanotube that hits and drags the second tube. Both findings hold promise for practical use in future NEMS.

[1]Centre d'Investigacions en Nanociencia i Nanotecnologia (Consejo Superior de Investigaciones Científicas–Institut Català de Nanotecnologia) and Centro Nacional de Microelectrónica, Campus de la Universitat Autònoma de Barcelona (UAB), E-08193 Bellaterra, Spain. [2]Departament d'Enginyeria Electrònica, UAB, E-08193 Bellaterra, Spain. [3]Institut de Ciència de Materials de Barcelona, Campus UAB, E-08193 Bellaterra, Spain. [4]Faculty of Physics, University of Vienna, Strudlhofgasse 4, 01090 Wien, Austria. [5]École Polytechnique Fédérale de Lausanne, CH-1015 Lausanne, Switzerland.

*To whom correspondence should be addressed. E-mail: adrian.bachtold@cnm.es (A.B.), ehe@icmab.es (E.R.H.)

Devices were constructed by means of standard nanofabrication techniques. Multiwalled carbon nanotubes (MWNTs), synthesized by arc-discharge evaporation, were deposited onto an oxidized silicon substrate. Electron-beam lithography and Cr/Au evaporation were used to attach electrodes to an individual nanotube and to pattern a plate in the middle of the nanotube that plays the role of the cargo. A few outer walls of the MWNT were selectively removed via the electrical-breakdown technique, which consists of passing a large current through the MWNT (*17*, *19*). The device is completed by suspending the nanotube and the cargo by means of a wet etching step.

This fabrication process created a motor that consists of a mobile element, which can move along and/or rotate around the axis of the suspended nanotube. The mobile metal cargo is attached to at least one short shell that can slide with respect to the other shells (Fig. 1C). The electrical-breakdown technique does not remove the shell(s) below the metal cargo, probably because the metal plate efficiently absorbs the heat generated in this portion of the tube, which prevents or at least delays the tube oxidation in this part. This mode of attachment can be inferred, because it is possible to move the metal cargo several times back and forth by means of an atomic force microscope (AFM) (Fig. 1, A and B). In contrast, the devices not engineered with the electrical-breakdown technique do not allow for such a manipulation (*20*). The cargo stays immobile until it is suddenly detached from the nanotube when the force applied by the tip becomes too large. Further discussion is provided in (*21*) and elsewhere in the supporting online material (SOM).

The motion of the cargo can also be driven by passing an electron current through the nanotube (without intervention of an AFM). The current has to be large (~0.1 mA) to make this happen. High currents likely cause sufficient dissipation to clean the surface from contaminants and help prevent dangling bonds from obstructing the motion. Previous experiments have shown that the presence of such contaminants alters the motion in a stochastic way (*4*, *22*, *23*). In our case, once the mobile element is free to move, the motion is often observed to be markedly regular and to be oriented toward a specific direction. For some devices, the cargo rotates around the nanotube (Fig. 2); for others, it moves along the nanotube axis (Fig. 3). The SOM contains a selection of videos (movies S2 to S4) and a summary table (table S1) on the motion observed for 11 different devices.

These results can be understood by considering the energy barrier for the relative motion between two coaxial nanotubes. As discussed above, the interaction between atoms of the two tubes generates an energy surface that restricts the motion along specific tracks, which can be translational and rotational (Fig. 1, D to F). In the general case, the easy direction will have both components. However, the motion appears most often to be purely rotational even if it is not, because a small rotation component generates a large deflection of the cargo, whereas a small translation component does not.

Occasionally, the cargo moves in a stepwise fashion, such as the rotational motion shown in Fig. 2. The angle of rotation is markedly constant for the different steps [about 7° (Fig. 2B)], which corresponds to a displacement $a_0 \approx 0.4$ nm along the track of the nanotube, given that its diameter is 7 nm. Such stepwise motion suggests that the cargo must overcome a series of periodic barriers (Fig. 2C). The observed motion is always toward the same direction, which differs from the motion of the ratchet effect (*13*, *24*) that is often used to describe molecular motors. There, the direction of motion fluctuates in time (a net directed displacement is obtained on average).

The energy of the periodic barriers can be estimated by noting that the temperature of the nanotube is very high. The high current flowing through the nanotube results in a high dissipation, which increases the temperature (*25*). The gold cargo, which initially has a rectangular shape, is often observed to melt and to transform into a ball, as shown in Fig. 3 (see also fig. S3). This result suggests that the temperature T approaches the melting temperature of gold (about 1300 K). We can obtain a rough estimate of the barrier height ΔE as

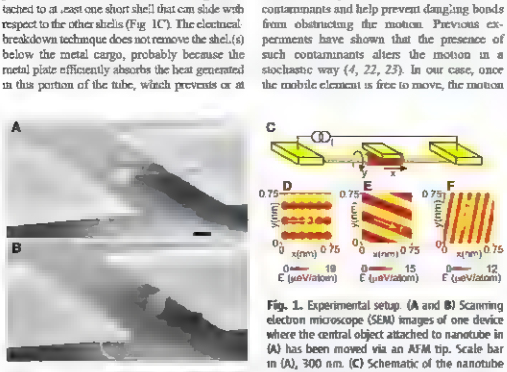

Fig. 1. Experimental setup. **(A** and **B)** Scanning electron microscope (SEM) images of one device where the central object attached to nanotube in **(A)** has been moved via an AFM tip. Scale bar in (A), 300 nm. **(C)** Schematic of the nanotube motor and its degrees of freedom. The outer (red) nanotube moves with respect to the inner (yellow) nanotube. *I*, the current. **(D** to **F)** Shape of the energy barrier for the relative motion between two coaxial nanotubes: (5,5)/(10,10), (29,9)/(38,8), and (27,12)/(32,17), respectively. The diameters of the inner tubes are 0.67, 2.7, and 2.7 nm, respectively. The white arrows indicate the easy axis of motion (*y*). The motion is modulated by a series of small periodic barriers in (D) and (F), whereas vanishingly small friction is expected in (E).

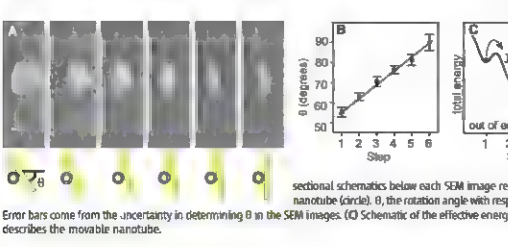

Fig. 2. Rotational motion. **(A)** Top-down SEM images where the gold cargo lying on the movable nanotube is rotating stepwise. The average time for a stepwise rotation to occur is 2.3 s (movie S3). The motion is driven by a 0.07-mA current through the nanotube, and the voltage is 2.3 V. Images are obtained with 10-keV electrons at a pressure of 10^{-6} mbar. Scale bar, 100 nm. The cross-sectional schematics below each SEM image represent the rotation of the plate (rectangle) around the nanotube (circle). θ, the rotation angle with respect to the horizontal. **(B)** Angle of rotation for each step. Error bars come from the uncertainty in determining θ in the SEM images. **(C)** Schematic of the effective energy barriers along the easy axis of motion. The red ball describes the movable nanotube.

follows. If we assume that the motion is in the hindered regime under the conditions present in our experiments, and if we neglect entropic contributions caused by the atomic motion (*26*), we have

$$\Gamma \approx \frac{\omega}{2\pi} e^{-\Delta E/kT} \quad (1)$$

with motion rate Γ and attempt frequency ω, where k is Boltzmann's constant. The precise values of Γ and ω are not important, because they appear as logarithmic terms in ΔE. Taking $\Gamma \approx 1$ Hz, using the approximation $\omega = \sqrt{\frac{\Delta E / \sqrt{2}}{m}}$ with the mass m of the cargo, and using the result that the barrier height is proportional to the contact area (*8*), we obtain a barrier height of ~17 μeV per atom.

We now analyze the observed stepwise motion described above in light of the interaction between two coaxial nanotubes. As discussed previously, the direction of motion follows a main valley of minimum energy. Along this valley, the energy can be either roughly constant or periodically modulated by a series of barriers (Fig. 1, D to F) (*8*). In the former case, the friction is expected to be vanishingly small when neglecting the vibrational motion of the atoms, whereas in the latter case, the motion can be stepwise. For example, as for the (27,12) and the (32,17) nanotubes shown in Fig. 1F, a series of local minima appears along the valley at regular intervals of 0.26 nm, separated by a barrier height of 3 μeV per atom. The stepwise motion observed in Fig. 2 is attributed to such a periodic modulation of the energy along the easy direction of motion. Note that the actual values of the separation and the barrier height are chirality- and diameter-dependent. In addition, the effective barrier that we obtain from our experiments contains an entropic contribution from the vibrational motion of the atoms, which is not considered in this simple model.

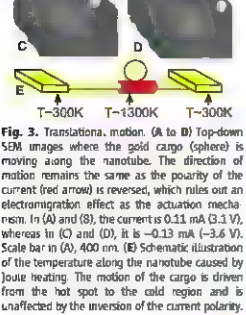

Fig. 3. Translational motion. (**A** to **D**) Top-down SEM images where the gold cargo (sphere) is moving along the nanotube. The direction of motion remains the same as the polarity of the current (red arrow) is reversed, which rules out an electromigration effect as the actuation mechanism. In (**A**) and (**B**), the current is 0.11 mA (3.1 V), whereas in (**C**) and (**D**), it is −0.13 mA (−3.6 V). Scale bar in (**A**), 400 nm. (**E**) Schematic illustration of the temperature along the nanotube caused by Joule heating. The motion of the cargo is driven from the hot spot to the cold region and is unaffected by the inversion of the current polarity.

Let us now discuss the underlying mechanism of the actuation. At first glance, it may be natural to attribute the driving force to the electrical current, as in electromigration, where electrons move atomic impurities through collisions and momentum transfer. However, upon reversing the direction of the current, the cargo continues to displace in the same direction as before (Fig. 3 and movie S4). This finding rules out an electromigration effect as the source of the observed dynamics. We emphasize that the rotational motion is neither the result of the magnetic field induced by the current passing through the nanotube—because the rotation can be right-handed or left-handed, depending on the device (*21*)—nor the result of a stray electric field effect, because the metal plate stays immobile for high-resistive devices even if a high voltage is applied (*21*).

We attribute the driving mechanism to the large thermal gradient along the nanotube. As previously discussed, the gold cargo is often observed to melt, which is indicative of a very high temperature. Nevertheless, the nanotube does not heat up homogeneously, because the heat is evacuated through the electrodes (Fig. 3E). The hottest spot of the device is at (or near) the midpoint of the suspended nanotube, whereas the temperature at the interface with the electrodes is expected to be near room temperature, as was recently measured by Begtrup *et al.* (*27*, *28*). Assuming that the temperature varies between 1300 and 300 K along the nanotube, the thermal gradient is as high as 1 K/nm, given the typical dimensions of our devices.

In the presence of a thermal gradient along the nanotube, there will be a net current of phononic excitations traveling from the hot spot toward the cooler regions; that is, from the midpoint of the suspended nanotube toward the electrodes. These phononic excitations will interact with and transfer momentum to the mobile element, and as a consequence, the cargo will move toward the closest electrode (*29*). Notice that the shape of the thermal gradient is independent of the direction of the electron current, which explains why the cargo does not change direction upon reversing the electron polarity.

This process can be regarded as the reverse of the heat dissipation that occurs in friction. When two objects slide in contact, some of the kinetic energy is dissipated as phononic excitations caused by the interface corrugation. In our experimental setting, in contrast, we induce a net current of phononic excitations that collides with the mobile element. In this scattering process, some of the vibrational energy is transformed into kinetic energy of the mobile element.

In order to substantiate our claim that the thermal gradient is indeed the driving mechanism, we have performed molecular dynamics simulations (Fig. 4A). We take the inner nanotube to be long and subject to a temperature gradient (typically a few kelvin degrees per nanometer), whereas the outer nanotube is short (typically 5 nm) and plays the role of the mobile element. Following the methodology of Saito *et al.* (*8*), we model the inter-nanotube atomic interactions by means of a simple Lennard-Jones pair potential and the intra-nanotube interactions by means of the Tersoff potential for carbon (*30*). Care is taken so that, initially, the outer nanotube has no net center-of-mass velocity, in order to avoid any bias in its dynamics. Full details of our simulations are provided in (*21*). In all our calculations, considering different combinations of inner-outer nanotubes and different diameters, we invariably find a net displacement toward the cold region. In addition, the simulations show that, depending on the nanotube pair, the motion can be translation, rotation, or a mixture of both (Fig. 4, B and C).

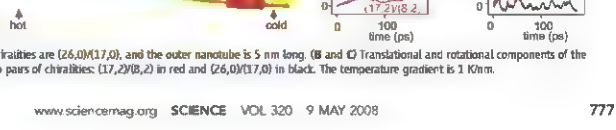

Fig. 4. Molecular dynamics simulations describing the thermal gradient actuation. (**A**) Snapshots of the device that show the motion of the outer (red) nanotube toward the cold end. The temperature gradient along the inner (yellow) nanotube is 7 K/nm, which is imposed by keeping the cold end at 300 K and the hot end at 1000 K. The snapshots are separated by 80 ps, the chiralities are (26,0)/(17,0), and the outer nanotube is 5 nm long. (**B** and **C**) Translational and rotational components of the motion as a function of time for two pairs of chiralities: (17,2)/(8,2) in red and (26,0)/(17,0) in black. The temperature gradient is 1 K/nm.

The motion in these simulations can be markedly fast, up to about 10^6 μm/s. By comparison, the velocity of kinesin-propelled microtubules is typically about 1 μm/s, whereas actin mobility can reach speeds up to 10 μm/s (*31*). However, the velocity that we observe experimentally is only up to about 1 μm/s (*21*). The large difference in velocity between the experiments and simulations is attributed to the difference in the system dimensions. Considering that the number of atoms of the outer nanotube used in the experiments is about 100 times as large as the number of atoms of the nanotube used in the simulations, and taking Eq. 1 with typical values for the temperature and the barrier height (for example, 1300 K and 17 μeV per atom), we obtain a factor of about eight orders of magnitude difference for the velocity, which is consistent with the mismatch between the experiments and simulations. Because our calculation capabilities do not allow speeds down to 1 μm/s to be reached, a direct comparison of the experiments and simulations cannot be made.

Although the temperature in our experiments may appear to be high, it should be possible to reduce it, which would be convenient for certain applications. To achieve this goal, researchers must make the dimensions of the movable nanotube narrower and shorter in order to reduce the barrier height. Another possible solution would be to selectively excite specific phonon modes, so that the average temperature of the phonon bath is lower. Indeed, not all of the phonon modes are expected to interact in the same way with the movable nanotube, and some are likely to be more effective in transferring momentum, such as the breathing modes.

The actuation by means of thermal gradients has obvious potential for NEMS applications. Thermal gradients could be used to drive the flow of fluids inside nanotubes or in nanofluidic devices or used for drug delivery by nanosyringes. The thermal gradient actuation may also be applied to bioengineered nanopores via, for example, the heat generated from the hydrolysis of adenosine triphosphate molecules. Using methods to align nanotubes on substrates, researchers should be able to fabricate arrays of orientationally ordered nanotube-based thermal motors.

References and Notes

1. M. ... Roukes, *Phys. World* **14**, 25 (2001).
2. V. V. Deshpande *et al. Nano Lett.* **6**, 1092 (2006)
3. A. M. Fennimore *et al. Nature* **424**, 408 (2003).
4. B. Bourlon, D. C. Glattli, C. Miko ... Forro, A. Bachtold, *Nano Lett.* **4**, 709 (2004).
5. B. C. Regan, S. Aloni, R. O. Ritchie, U. Dahmen, A. Zettl, *Nature* **428**, 924 (2004).
6. K. Svensson, H. Olin, E. Olsson, *Phys. Rev. Lett.* **93**, 145901 (2004)
7. D. Golberg *et al., Adv. Mater.* **19**, 1937 (2007).
8. R. Saito, R. Matsuo, T. Kimura, G. Dresselhaus, M. S. Dresselhaus, *Chem. Phys. Lett.* **348**, 187 (2001)
9. Yu. E. Lozovik, A. V. Belikov, A. M. Popov, *Phys. Lett. A* **313**, 112 (2003)
10. P. A. E. Schoen, J. H. Walther, S. Arcidiacono, D. Poulikakos, P. Koumoutsakos, *Nano Lett.* **6**, 1910 (2006).
11. P. A. E. Schoen, J. H. Walther, D. Poulikakos, P. Koumoutsakos, *Appl. Phys. Lett.* **90**, 253115 (2007)
12. Z. C. Tu, X. Hu, *Phys. Rev. B* **72**, 033404 (2005).
13. R. D. Astumian, P. Hanggi, *Phys. Today* **55**, 33 (2002).
14. A. N. Kolmogorov, V. H. Crespi, *Phys. Rev. Lett.* **85**, 4727 (2000).
15. P. Tangney, M. L. Cohen, S. G. Louie, *Phys. Rev. Lett.* **97**, 195501 (2006).
16. J. Servantie, P. Gaspard, *Phys. Rev. B* **73**, 125428 (2006).
17. P. G. Collins, M. S. Arnold, Ph. Avouris, *Science* **292**, 706 (2001).
18. P. G. Collins, M. Hersam, M. Arnold, R. Martel, Ph. Avouris, *Phys. Rev. Lett.* **86**, 3128 (2001)
19. B. Bourlon *et al., Phys. Rev. Lett.* **92**, 026804 (2004).
20. Most of the low-resistive devices engineered with the electrical-breakdown technique can be actuated with an electron current, although this is never the case for the non-engineered devices (*21*)
21. Materials and methods are available as supporting material on Science Online.
22. M. F. Yu, B. ... Yakobson, R. S. Ruoff, *J. Phys. Chem. B* **104**, 8764 (2000).
23. A. Kis, K. Jensen, S. Aloni, W. Mickelson, A. Zettl, *Phys. Rev. Lett.* **97**, 025501 (2006).
24. F. R. Kay, D. A. ...ingh, F. Zerbetto, *Angew. Chem. Int. Ed.* **46**, 72 (2007)
25. S. Chen *et al., Appl. Phys. Lett.* **87**, 263107 (2005).
26. G. S. Kottas, L. I. Clarke, D. Horinek, J. Michl, *Chem. Rev.* **105**, 1281 (2005).
27. G. E. Begtrup *et al. Phys. Rev. Lett.* **99**, 155901 (2007).
28. We do not observe any change of the electron resistance when comparing samples with and without gold cappers. As a result, we do not expect a substantial modification of the spatial temperature profile in these two configurations. A direct consequence of this temperature profile is that the speed of the cargo is not constant along the nanotube. It is highest near the midpoint of the tube and lowest near the contacts (Fig. 5Z
29. The temperature profile is likely to be slightly asymmetric with respect to the middle of the nanotube resulting from, for example, different contact resistances. As a result, the mobile element can move even if it is placed exactly in the middle of the nanotube.
30. J. Tersoff, *Phys. Rev. Lett.* **61**, 2879 (1988).
31. M. G. ... van den Heuvel, C. Dekker, *Science* **317**, 333 (2007).
32. We thank J. Jobst, G. Rius, and X. Borrise for valuable help with the experiments, as well as P. Ordejon and M. Monthioux for discussions. Financial support from a European Young Investigator grant, the European Union–funded project FP6-IST-021285-2 (the grants FIS2006-12117-C04 and TEC2006-13731-C02-01 from the Ministerio de Educación y Ciencia, a Ramón y Cajal Fellowship, and the grant 2005SGR683 from Agencia de Gestió d'Ajuts Universitaris i de Recerca is acknowledged. The work in Lausanne was supported by the Swiss NSF and its National Centres of Competence in Research "Nanoscale Science."

Supporting Online Material

www.sciencemag.org/cgi/content/full/1155559/DC1
Materials and Methods
Figs. S1 to S5
Tables S1 and S2
References
Movies S1 to S5

22 January 2008; accepted 31 March 2008
Published online 10 April 2008.
10.1126/science.1155559
Include this information when citing this paper

Fracture Propagation to the Base of the Greenland Ice Sheet During Supraglacial Lake Drainage

Sarah B. Das,[1*] Ian Joughin,[2] Mark D. Behn,[1] Ian M. Howat,[2,3] Matt A. King,[4] Dan Lizarralde,[1] Maya P. Bhatia[5]

Surface meltwater that reaches the base of an ice sheet creates a mechanism for the rapid response of ice flow to climate change. The process whereby such a pathway is created through thick, cold ice has not, however, been previously observed. We describe the rapid (<2 hours) drainage of a large supraglacial lake down 980 meters through to the bed of the Greenland Ice Sheet initiated by water-driven fracture propagation evolving into moulin flow. Drainage coincided with increased seismicity, transient acceleration, ice-sheet uplift, and horizontal displacement. Subsidence and deceleration occurred over the subsequent 24 hours. The short-lived dynamic response suggests that an efficient drainage system dispersed the meltwater subglacially. The integrated effect of multiple lake drainages could explain the observed net regional summer ice speedup.

The Greenland Ice Sheet flows outward from its interior through a combination of internal deformation and basal sliding, losing mass around its edges through meltwater runoff and iceberg calving. Recent observations show that ice flow along the western margin accelerates during the summer when surface meltwater lubricates sliding at the ice-bedrock interface (*1*, *2*). Aside from theoretical predictions (*3*–*5*) and observations on small icecaps (*6*), it has not been established how surface meltwater penetrates through thick, subfreezing ice (*7*, *8*). Ice-sheet models used to predict future sea-level rise typically do not include the impact of surface meltwater on ice dynamics. Attempts to include the effects of enhanced basal lubrication within these models suggest that increased meltwater may substantially accelerate ice-sheet mass loss, but confidence in these results is limited by a poor understanding of ice-sheet hydrology (*9*). Key unknowns in determining Greenland's potential response to climate forcing are the time scales and pathways through which meltwater reaches the ice sheet's base and its consequent effect on basal motion (*10*).

For surface meltwater to reach the ice-sheet bed, a through-ice conduit is required. Theoretical models of fracture propagation through ice suggest that once initiated, water-filled crevasses will propagate rapidly downward through the full ice thickness to the bed (3–5). In such models, the rate of crack propagation is limited only by the meltwater supply needed to keep the crack full (3, 4). Supraglacial lakes (11–13) can provide the large volumes of water required to propagate fractures to the bed (7); thus, these lakes are likely critical for establishing a through-ice conduit (moulin). Furthermore, moulins that form in lake basins lie near the confluence of meltwater streams and will continue to be supplied with surface melt water after the lake drains, routing water to the bed and delaying closure while sufficient meltwater production continues throughout the summer.

To investigate lake drainage and the ensuing ice-sheet response, we established study sites at two large (~2-km diameter) lakes on the ice sheet's western margin at locations with thick (~980 m) (14), subfreezing ice (15). During July 2006, our northernmost study lake (68.72°N, 49.50°W) drained rapidly in an event captured by local Global Positioning System (GPS), seismic, and water level sensors (Fig. 1) (16). A similar, although less well documented, drainage event occurred at this lake again in 2007 (fig. S1).

The lake began filling in early July 2006, reaching its maximum extent around 00:00 (UTC) on 29 July 2006, with a surface area of 5.6 km^2 and a volume of 0.044 ± 0.01 km^3 (16). The lake level then began to fall slowly and steadily at 1.5 cm/hour. At ~16:00 UTC the same day, the lake level began dropping rapidly, reaching a maximum drop rate of 12 m/hour between 16:40 and 17:00 (Fig. 2). Extrapolation of the depth-logger data (Fig. 2) indicates that the entire lake drained in ~1.4 hours. The average drainage rate (8700 m^3/s) during this rapid-drainage phase exceeded the average flow rate over Niagara Falls.

Local vertical and horizontal movement of the ice sheet occurred coincident with the lake drainage. A GPS station located ~0.5 km north of the lake (Fig. 1) recorded both rapid uplift (1.2 m) and northward horizontal motion (0.8 m), with the maximum surface displacement occurring between 17:15 and 17:30 UTC (Fig. 2). This northward motion was substantially faster and orthogonal to the mean westerly velocity of 93 m/year. The following 24-hour period was characterized by gradual subsidence and return to the mean westerly motion accompanied by a transient speedup in the downflow direction. In total, the event resulted in a net westerly surface displacement of 0.5 m in excess of the average daily displacement of 0.25 m (Fig. 2C and fig. S2).

A seismometer located ~0.7 km north of the lake (Fig. 1) recorded elevated activity beginning around 15:30 UTC, ~30 min before the period of rapid lake drainage. The maximum amplitude in seismic energy occurred between 16:45 and 18:00 UTC, during and slightly after the period of rapid lake drainage (fig. S3).

Site visits provided observations of predrainage (July 2006) and postdrainage (July 2007) surface features. We found several km-scale fractures running through the lake basin in 2007. Many were closed at depth (water filled) and no longer draining. Two large moulins were found along the fractures, actively draining the area in 2007 (Fig. 1). A dominant topographic feature in 2007 was an uplifted section of the ice sheet roughly centered over the lake bottom, forming a flat-topped block of ice ~6 m high and 750 m wide (Fig. 1). This block likely was uplifted as water was rapidly injected to the base of the ice sheet near the lake's center during the 2006 drainage event (16). The block's southern edge lay along a ~3.2-km fracture visible from the air and in synthetic aperture radar (SAR) imagery spanning the lake basin's full width, the northern edge lay along a similarly visible fracture (Fig. 1).

The observed fractures and rapid drainage, synchronous with uplift and horizontal acceleration, are strong evidence that water-driven fracture propagation likely established a hydrological connection to the bed. These observations suggest that hydrologic connectivity occurs in four stages: slow initial drainage, connection to the bed and rapid lake drainage through an extensive fracture system, moulin formation and closure of fractures, and subsequent moulin-routed drainage of daily surface meltwater to the ice-sheet bed.

The 16-hour initial drainage stage was characterized by a slow, steady drop in lake level, elevated seismicity in the 30 min before rapid

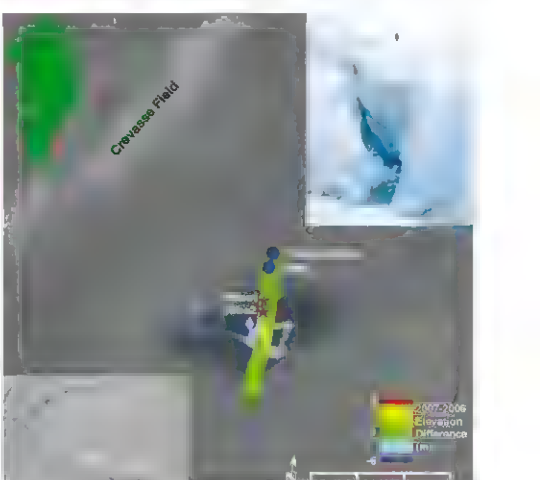

Fig. 1. Early October 2006 SAR image (gray-scale background) overlaid with a semi-transparent image recorded by NASA's Moderate Resolution Imaging Spectroradiometer (MODIS) showing the lake extent (blue) on 29 July 2006. Red stars show the water-pressure logger locations and blue circles show the GPS/seismometer locations. Block uplift (lower-left inset) is revealed by 2006 to 2007 elevation differences (colored swath) recorded by NASA's Airborne Topographic Mapper (ATM) in May of both years. A large fracture is visible in the SAR image as a long, bright linear feature with ends marked by green arrows. Solid blue diamonds indicate locations where sonar and ATM measurements found large "holes" in the lake bed before drainage in 2006. The upper-right inset shows a 1.8-m-tall person standing above a similar hole (open blue diamond) located after the 2007 lake drainage.

[1]Department of Geology and Geophysics, Woods Hole Oceanographic Institution, Woods Hole, MA 02543, USA. [2]Polar Science Center, Applied Physics Lab, University of Washington, 1013 NE 40th Street, Seattle, WA 98105-6698, USA. [3]School of Earth Sciences and Byrd Polar Research Center, The Ohio State University, 1090 Carmack Road, Columbus, OH 43210-1002, USA. [4]School of Civil Engineering and Geosciences, Newcastle University, Newcastle upon Tyne, NE1 7RU, UK. [5]Department of Geology and Geophysics, Massachusetts Institute of Technology/Woods Hole Oceanographic Institution Joint Program, Woods Hole, MA 02543, USA.

*To whom correspondence should be addressed. E-mail: sdas@whoi.edu

drainage (fig. S3), and little or no acceleration or uplift at the GPS site (Fig. 2). This initial phase may have coincided with water filled fracture propagation beneath the lake through the kilometer-thick ice. The main crack's 3.2-km length (Fig. 1) could have stored a volume of water corresponding to the initial lake-level drop, assuming a 0.5-m-wide average opening. Alternatively, the predrainage may have started as the lake began spilling over a low drainage divide where the main fracture intersects the western shoreline, filling an existing dry crack at the lake edge so that it hydro-fractured into and through the ice beneath the lake. Surface strain rates from satellite derived-velocities ($\dot{\varepsilon}$) are tensile ($\dot{\varepsilon}_{xx}$ = 0.003 year^{-1}, x directed along flow) along this western shoreline, favoring crevasse formation, whereas strain rates near the lake's center are compressive ($\dot{\varepsilon}_{xx}$ = −0.004 year^{-1}). At neighboring lakes, we observed similar situations in which lakes spilled over into shoreline cracks, creating moulins. Where the fracturing ran adjacent to rather than through the lake basin, drainage occurred over weeks as overflow melted and deepened the spillover channel leading to the moulin. For either hypothesis, the low seismicity, lack of uplift and acceleration, and the slow drainage rate suggest that little or no water reached the bed of the ice sheet during this first stage.

The second stage began when the fractures breached the full ice thickness, establishing a direct connection to the basal hydrological system. Rapid lake drainage (1.4 hours) was accompanied by an increase in seismic energy (fig. S3) and synchronous surface displacement of the adjacent shoreline up (1.2 m) and away (0.8 m) from the lake center (Fig. 2). The short duration between the drop in lake level and shore-based surface motion indicates rapid and direct transport of water to the bed. Uplift at the center of the lake was likely larger than the 1.2 m observed nearby on shore, and probably coincided with uplift of the large block at the lake's center. The synchronous uplift indicates a nearly vertical path to the bed, as well as the formation of a transient subglacial lake that displaced the overlying ice. The high drainage rate and the presence of rafted ice blocks observed along lake-bed fractures suggest that drainage occurred along most of the fractures' length. The turbulent water flow during the rapid discharge would have melted the fracture walls through frictional heating, concentrating flow paths and leading to the development of larger-diameter openings at points where inflow was greatest (6).

We hypothesize that during the third stage, which lasted a few days after the rapid lake drainage, most of the fractures closed at depth and discrete moulins formed. The surface water flow (~24 m^3/s) previously filling the lake provided inflow into the areas still connected to the bed. Melt widening at locations where inflow was greatest (e.g., at the ends of surface streams), competing with the tendency of overburden pressure to close the no-longer water-filled fractures, probably produced and maintained a few discrete moulins that remained open throughout the remainder of the melt season (fourth stage), similar to those we observed after drainage in 2007 (Fig. 1).

Also during the third stage, the transient subglacial lake drained over a ~24-hour period, as suggested by the GPS-measured vertical subsidence and horizontal southward motion (Fig. 2 and fig. S2). The relatively rapid subglacial lake drainage suggests the presence of an efficient subglacial hydrological system. Increased ice fracturing likely occurred during this stage as well, possibly explaining the elevated seismic energy in the 1 hour period immediately following the lake drainage (fig. S3).

Throughout the melt season, the onshore GPS recorded fluctuations in ice-sheet velocity of 50 to 100% that correlate well with calculations of daily melt intensity and regional ice-sheet flow (*1*). Other than the ~24-hour period following the drainage (Fig. 2 and fig. S2), the character of the pre- and postdrainage speed fluctuations did not differ appreciably (*1*). Thus, the opening of a new moulin draining a large daily melt volume (24 m^3/s) had little apparent lasting effect on the local ice-sheet velocity. Instead, we hypothesize that this event contributed to the collective formation of a network of regionally distributed moulins supplying meltwater to the bed that modulated ice flow both before and after the drainage event. Such modulation implies the presence of a well-connected subglacial drainage system capable of receiving water inflow at discrete locations and dispersing it uniformly beneath the ice sheet. This creates what appears to be partial ice-bed decoupling associated with a distributed subglacial hydrological system. These indirect observations highlight how much remains to be learned about the subglacial environment beneath the Greenland Ice Sheet.

Our lake-drainage observations provide evidence for a fracture-driven process opening a 1 km-deep through-ice conduit and injecting a large volume of surface meltwater directly beneath the ice sheet. Although fracturing established the initial connection, additional melting from energy dissipation during the turbulent flow of water in its 1-km descent likely played a role in widening and maintaining discrete moulins that stayed open throughout the remainder of the melt season. Thousands of lakes are formed on the ice sheet's surface throughout the ablation season, and although we have detailed observations from only a single lake, we do not believe the lake drainage we observed was an isolated or unique event. Other Greenland supraglacial lakes have previously been observed to disappear from the surface in 1 day (*12*). During ground and aerial surveys in 2006 and 2007, we investigated more than 10 surrounding lake basins near our study site and detected numerous streams draining into moulins across the ice sheet's surface. These systems were observed both where lakes had drained completely and also where lakes cut overflow channels that later drained into nearby fractures and moulins. In addition, all of the postdrainage lake basins that we observed had fractures running

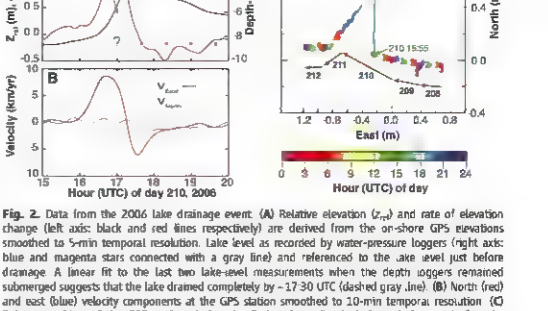

Fig. 2. Data from the 2006 lake drainage event. (**A**) Relative elevation (z_{xx}) and rate of elevation change (left axis: black and red lines respectively) are derived from the on-shore GPS elevations smoothed to 5-min temporal resolution. Lake level as recorded by water-pressure loggers (right axis: blue and magenta stars connected with a gray line) and referenced to the lake level just before drainage. A linear fit to the last two lake-level measurements when the depth loggers remained submerged suggests that the lake drained completely by ~17:30 UTC (dashed gray line). (**B**) North (red) and east (blue) velocity components at the GPS station smoothed to 10-min temporal resolution. (**C**) Relative position of the GPS station during the 5 days immediately before, during, and after the drainage event showing the rapid translation of the surface as it floats up and away from the lake center, and subsequently returns. The color-bar indicates the hour of day, and the bold black arrows delineate each day's net motion.

across their surface, supporting the fracture-based mechanism for rapid drainage that we have described for our study lake.

Thus, we have shown that water-driven fracture enabled by the large volume of water stored in supraglacial lakes provides a means by which hydrologic surface-to-bed connections are established through thick ice. Climate warming would lead to earlier and expanded surface lake formation and, as a result, connections to the bed may occur earlier in the melt season and over a larger area, although further work is needed to constrain the limits of this area. This would increase the annual subglacial throughput of meltwater and may substantially impact Greenland Ice Sheet dynamics (*1*).

References and Notes

1. I. Joughin *et al.*, *Science* **320**, 781 (2008); published online 17 April 2008 (10.1126/science.1153288).
2. H. J. Zwally *et al.*, *Science* **297**, 218 (2002).
3. C. J. van der Veen, *Geophys. Res. Lett.* **34**, L01501 (2007).
4. R. B. Alley, T. K. Dupont, B. R. Parizek, S. Anandakrishnan, *Ann. Glaciol.* **40** (2005).
5. J. Weertman, in *Symposium on the Hydrology of Glaciers*, Cambridge, 7 to 13 September 1969 (International Association of Hydrologic Sciences, Cambridge, 1973), pp. 139–145.
6. S. Boon, M. Sharp, *Geophys. Res. Lett.* **30**, 1916 (2003).
7. J. L. Bamber, R. B. Alley, I. Joughin, *Earth Planet. Sci. Lett.* **257**, 1 (2007).
8. S. J. Marshall, *Earth Planet. Sci. Lett.* **240**, 191 (2005).
9. B. R. Parizek, R. B. Alley, *Quat. Sci. Rev.* **23**, 1013 (2004).
10. IPCC, *Climate Change 2007: The Physical Science Basis. Contribution of Working Group I to the Fourth Assessment Report of the Intergovernmental Panel on Climate Change* (Cambridge Univ. Press, Cambridge and New York, 2007).
11. M. McMillan, P. Nienow, A. Shepherd, T. Benham, A. Sole, *Earth Planet. Sci. Lett.* **262**, 484 (2007).
12. J. E. Box, K. Ski, *J. Glaciol.* **53**, 257 (2007).
13. M. Lüthje, L. T. Pedersen, N. Reeh, W. Greuell, *J. Glaciol.* **52**, 608 (2006).
14. S. Gogineni *et al.*, *J. Geophys. Res.* **106**, 33761 (2001).
15. R. Greve, *J. Clim.* **10**, 901 (1997).
16. Methods are available as supporting material on *Science* Online.

17. Support was provided jointly by NSF and NASA through ARC-0520077 (S.B.D., M.P.B., I.M.H.) and ARC 520382 (I.J.). The Woods Hole Oceanographic Institution Ocean and Climate Change Institute and Clark Arctic Research Initiative provided additional support to S.B.D., M.D.B., and D.L., and a Natural Environment Research Council (UK) Research Fellowship supported M.A.K. Logistical and instrumental support was provided by VECO Polar Resources, PASSCAL, and UNAVCO. Early conversations with R.B. Alley helped initiate this project. Comments from two anonymous reviewers substantially improved the content and clarity of the manuscript. The ATM data were kindly provided by B. Krabill and S. Manizade.

Supporting Online Material
www.sciencemag.org/cgi/content/full/1153360/DC1
Methods
Figs. S1 to S3
References

26 November 2007; accepted 31 March 2008
Published online 17 April 2008;
10.1126/science.1153360
Include this information when citing this paper.

Seasonal Speedup Along the Western Flank of the Greenland Ice Sheet

Ian Joughin,[1*] Sarah B. Das,[2] Matt A. King,[3] Ben E. Smith,[1] Ian M. Howat,[1]† Twila Moon[1]

It has been widely hypothesized that a warmer climate in Greenland would increase the volume of lubricating surface meltwater reaching the ice-bedrock interface, accelerating ice flow and increasing mass loss. We have assembled a data set that provides a synoptic-scale view, spanning ice-sheet to outlet-glacier flow, with which to evaluate this hypothesis. On the ice sheet, these data reveal summer speedups (50 to 100%) consistent with, but somewhat larger than, earlier observations. The relative speedup of outlet glaciers, however, is far smaller (<15%). Furthermore, the dominant seasonal influence on Jakobshavn Isbrae's flow is the calving front's annual advance and retreat. With other effects producing outlet-glacier speedups an order of magnitude larger, seasonal melt's influence on ice flow is likely confined to those regions dominated by ice-sheet flow.

Along its western margin, the Greenland Ice Sheet melts at rates that can exceed 2.5 m/year (*1*) as ice flows seaward at speeds of roughly 100 m/year. Embedded within the ice sheet are faster-flowing (200 to 12,000 m/year) outlet glaciers that discharge ice directly to the ocean. When the combined loss from melt and ice discharge, which now act in roughly equal proportions, removes more ice than is replaced by annual snowfall, the excess ice lost to the ocean contributes to sea-level rise.

Glacial motion results from a combination of internal deformation of ice under its own weight, sliding at the ice-bed interface, and deformation of underlying sediments. Basal sliding over a well-lubricated bed is often the source of fast (e.g., >100 m/year) ice motion (*2*). Seasonal fluctuation in the drainage of rainfall and surface meltwater to the bed modulates the sliding speed of many alpine glaciers (*3*–*5*). Greenland's large coastal melt rates have prompted widespread speculation both in the popular media (*6*) and in the scientific literature (*7*, *8*) that a warmer climate will increase melting, which in turn will enhance basal lubrication and hasten ice-sheet retreat. Poor knowledge of this process is one of the limitations on prediction of future ice-sheet contributions to sea-level rise that was noted by the Intergovernmental Panel on Climate Change (*9*).

The few studies of seasonal speedup in Greenland are equivocal about the importance of this lubrication effect. An early study of western Greenland's largest outlet glacier, Jakobshavn Isbrae, found no measurable seasonal speedup (*10*). One outlet glacier in northern Greenland, however, did undergo a short-term speedup, apparently in response to the drainage of a supraglacial lake (*11*). On the slow-moving ice sheet at Swiss Camp (Fig. 1), located just north of Jakobshavn Isbrae, a time series of Global Positioning System (GPS) observations showed seasonal speedups of 5 to 28% that correlated well with summer melt rates (*7*).

To better determine the influence of surface melting on ice-sheet flow, we have assembled a comprehensive set of interferometric synthetic aperture radar (InSAR) and GPS observations (*12*). These data include 71 (September 2004 to August 2007) InSAR velocity maps along two partially overlapping RADARSAT tracks that include Jakobshavn Isbrae, several smaller marine-terminating outlet glaciers, and a several-hundred-kilometer long stretch of the surrounding ice sheet. We also collected GPS observations from July 2006 to July 2007 at sites near two supraglacial lakes (Fig. 1) south of Jakobshavn Isbrae.

Figure 1 shows the August 2006 speedup measured with InSAR speckle tracking. Although there are coverage gaps, the data show a relatively uniform speedup extending over the bare-ice zone. To simplify the analysis, we used a 150-m/year threshold to partition the area into slower-moving "ice-sheet" and faster-moving "outlet-glacier" regions. Under this rough classification, the ice sheet sped up by 36 m/year (48%) above its 76-m/year mean speed, demonstrating increases over a broad area that are substantially larger than measured earlier at Swiss Camp (28%) (*7*). On the outlet glaciers, the 51-m/year speedup was larger, but this was only 8.6% faster than the 594-m/year mean. Although the InSAR coverage (not shown) is less complete, mid-July 2006 speedups were 71 (97%) and 77 m/year (14%) for the ice-sheet and outlet-glacier regions, respectively. Similar speedups occurred in summer 2007 (e.g., fig. S1).

Although RADARSAT provides good spatial coverage, its temporal resolution (24 days) is limiting. Two-day temporal resolution is available with GPS observations (Fig. 2) from two locations (North Lake and South Lake, Fig. 1). These data reveal periods of generally higher speeds (~50%) during two melt seasons, punctuated by several additional short-term speedups (~100%). The minimum velocity occurs with the late-summer cessation of melt, and speed then slowly increases through the winter before the late-spring large melt-induced speedup.

The GPS sites at both lakes show similar short- and long-term variation in speed, consistent with

[1]Polar Science Center, Applied Physics Lab, University of Washington, 1013 NE 40th Street, Seattle, WA 98105–6698, USA. [2]Department of Geology and Geophysics, Woods Hole Oceanographic Institution, Woods Hole, MA 02543, USA. [3]School of Civil Engineering and Geosciences, Newcastle University, Newcastle upon Tyne NE1 7RU, UK.

*To whom correspondence should be addressed. E-mail: ian@apl.washington.edu

†Present address: The Ohio State University, 1090 Carmack Road, Columbus, OH 43210–1002, USA.

the spatial uniformity visible at longer time scales (Fig. 1). A notable exception is the local speedup on day 210 at the North Lake site (Fig. 2), which coincides with this lake's rapid drainage to the bed (*13*). Another local speedup occurred when a moulin, a surface-to-bed conduit, likely opened along the South Lake's overflow channel and began draining on day 217. Other than these local lake-drainage events, the velocity peaks coincide well with high-melt periods inferred from positive-degree-days recorded at each site.

We also examined InSAR-measured speed at 10 locations (Fig. 1) on eight marine-terminating outlet glaciers (Fig. 3A), which cover a range of flow speeds. We selected these points to sample the full range of variability for fast flowing regions (e.g., areas both near and far from the calving front). Eight of these locations showed coincident speedups of 40 to 200 m/year during the 2006 and 2007 melt seasons. Speed at locations 6 and 8, which were near their respective calving fronts, fluctuated erratically without a distinct seasonal pattern. Speed was considerably more regular at location 9, several km upstream on the same glacier as location 8, suggesting the anomalous behavior seen at locations 6 and 8 was driven by the dynamics near the calving front.

Figure 3A does not include the region of Jakobshavn Isbræ flowing faster than 1500 m/year, which continues to evolve following its speedup that began in 1998 (*14*, *15*). To evaluate seasonal variation in speed on this glacier's fast-moving region, we have removed a linear trend with time at three locations designated A through C (Fig. 1). At location A, 4 to 10 km behind the seasonally varying calving front, the speed varies by ±1000 m/year from its 8500-m/year mean (Fig. 3B). Farther upstream (location B), the annual variation diminishes to roughly ±400 m/year (around a 5200-m/year mean). The seasonal variation at these two sites is distinctly different from the melt-related speedup visible elsewhere (Fig. 3A). Instead, peak speeds occur near the melt season's end, after seasonal speedups on other glaciers have ended. In addition, the main trunk's elevated speeds persist past the end of the melt season, taking several months to reach their mid-winter lows. This variation appears negatively correlated with the calving front's position, which fluctuated annually by ~6 km from 2004 to 2007 (Fig. 3B). At location C, the variation (±200 m/year) is an apparent mixture of melt- and ice-front–driven effects.

The InSAR data indicate that seasonal speedup is widespread across much of the bare-ice zone. When averaged over 24 days, the speedup is spatially uniform to a notable degree, particularly given the expected variation in melt intensity with elevation. This spatial uniformity is consistent with motion over a well-distributed drainage network rather than a network of sparsely distributed large tunnels (*4*, *16*).

On Jakobshavn Isbræ's fastest-moving parts (>4000 m/year), the seasonal speedup is in phase with changes in the ice-front position rather than surface meltwater. This region accelerates through spring and summer, likely in response to a decline in back-stress as the calving front retreats [e.g., (*17*)]. Conversely, minimum speeds occur as the ice front extends to form a short floating ice tongue each winter. This apparent back-stress modulation of speed is consistent with the initial speedup in 2000, which was about a factor of 3 larger than the current annual variation and coincided with the disintegration of a much larger section of the ice tongue (*14*, *17*). The current large seasonal variation also is consistent with earlier observations of little or no seasonal variation (*10*, *15*) when the ice-front position was much less variable (*18*).

Although our observations indicate substantial (≥50%) ice-sheet speedup, the melt induced speedup averaged over a mix of several tidewater outlet glaciers is relatively small (<10 to 15%). When factoring in the short melt-season duration, the total additional annual displacement attributable to surface meltwater amounts to a few percent on glaciers moving at several hundred meters per year. Although conditions might yield a greater sensitivity to melt for some glaciers outside our study area, the limited seasonal observations elsewhere in Greenland suggest a low sensitivity to summer melt similar to that which we observe (*19*–*21*). Because of this low sensitivity, it is unlikely that recent outlet-glacier speedups (*14*, *19*–*21*) were directly caused by increased surface meltwater lubrication during recent warmer summers. Instead, these large speedups were likely driven by processes that caused ice front retreat and reduced back stress (*17*, *19*, *20*, *22*), such as declining sea-ice extent near calving fronts (*18*). The recent period of warmer summers (*23*) might also enhance ice-front retreat through increased hydro-fracturing in water-filled crevasses near the calving front (*18*), which represents a process whereby surface meltwater influences glacial flow through means other than directly enhancing basal lubrication.

Smoother beds beneath outlet glaciers, caused by strong erosion, should yield less sensitivity to water-pressure variation (*3*), which may explain some of the insensitivity of outlet-glacier flow to surface meltwater. Additionally, basal shear-heating under the outlet glaciers produces a steady source of

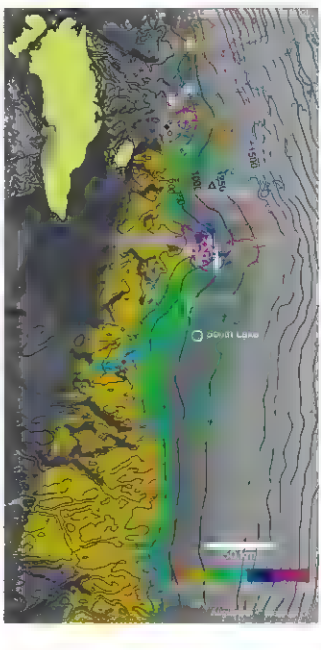

Fig. 1. The August 2006 speedup (color) relative to the September 2004 to December 2006 mean speed displayed over SAR imagery (gray scale). Speeds are determined using overlapping tracks that span two 24-day intervals centered on 5 and 13 August. Mean annual speed is shown with blue, 50-m/year (50 to 150 m/year), and magenta, 200-m/year (200 to 1000 m/year) contours. Contours for speeds greater than 1000 m/year are omitted. Colored/numbered symbols indicate the locations referenced in Fig. 3. We situated our GPS receivers next to two supraglacial lakes at the locations indicated with white circles. The colors within these circles correspond to the values from the GPS observations to allow comparison with the surrounding InSAR speedup values for the same period. Surface elevation is contoured at 250-m intervals (black).

meltwater that could maintain water-filled cavities year-round. In contrast, the water-filled cavities under the ice sheet may drain and collapse over the winter, resulting in a more pronounced speedup once spring melt reaches the bed (e.g., (24)). Another contributor may be that the outlet glaciers are narrow and deep so that their lateral margins have comparable area to their beds. With this geometry, the lateral resistive stresses should be comparable to or even greater than the basal resistive stresses, potentially making outlet glaciers less sensitive to variations in basal lubrication.

Surface meltwater–enhanced basal lubrication has been invoked previously as a feedback that would hasten the Greenland Ice Sheet's demise in a warming climate (*6–8*). Our results show that several fast-flowing outlet glaciers, including Jakobshavn Isbrae, are relatively insensitive to this process. Previously reported acceleration and near-doubling of speed of many outlet glaciers from other effects such as back stress reduction are more than an order of magnitude greater (*14*, *19–21*) than the observed melt-induced acceleration. South of Jakobshavn, however, the ice sheet's western flank is comparatively free of outlet glaciers, and ice loss is largely due to melt. Numerical models appropriate to this type of sheet flow and that include a parameterization of surface meltwater–induced speedup predict 10 to 25% more ice loss in the 21st century than models without this feedback (*8*). Thus, surface meltwater–induced speedup may influence large regions of the ice sheet in a warming climate. Although our data provide the most comprehensive observations to date, more data are needed to quantify the relative importance of melt- and calving front–induced changes in ice flow in controlling near-future ice-sheet mass balance. Our results thus far suggest that surface meltwater–enhanced lubrication likely will have a substantive but not catastrophic effect on the Greenland Ice Sheet's future evolution.

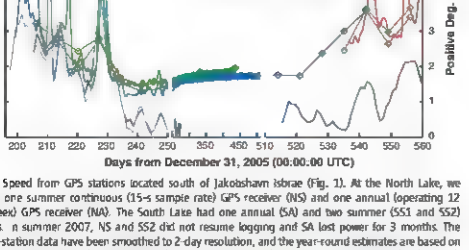

Fig. 2. Speed from GPS stations located south of Jakobshavn Isbrae (Fig. 1). At the North Lake, we installed one summer continuous (15-s sample rate) GPS receiver (NS) and one annual (operating 12 hours/week) GPS receiver (NA). The South Lake had one annual (SA) and two summer (SS1 and SS2) receivers. In summer 2007, NS and SS2 did not resume logging and SA lost power for 3 months. The summer-station data have been smoothed to 2-day resolution, and the year-round estimates are based on weekly positions. Positive-degree-day (PDD) values are included for both sites in 2006 and for the South Lake in 2007. Gray shading indicates when the North Lake drained in 2006 (*13*).

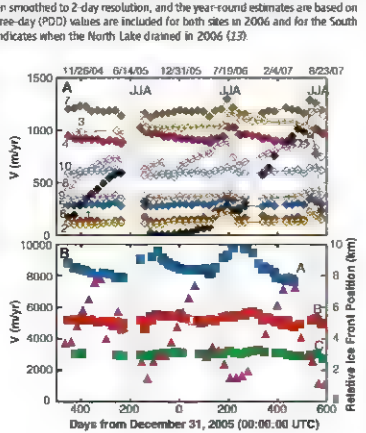

Fig. 3. (**A**) nSAR-determined speed from September 2004 through August 2007 at 10 outlet-glacier locations. The gray shading indicates the months of June, July, and August (JJA). (**B**) Detrended (1Z) speeds (squares) at three locations (A, B, and C) on Jakobshavn Isbrae and relative ice-front position (triangles). Figure 1 shows sampled locations with corresponding colored and numbered/lettered symbols.

References and Notes

1. J. E. Box *et al.*, *J. Clim.* **19**, 2783 (2006).
2. W. S. B. Paterson, *The Physics of Glaciers* (Pergamon, Oxford, ed. 3, 1994).
3. A. Iken, *J. Glaciol.* **27**, 407 (1981).
4. A. Iken, H. Rothlisberger, A. Flotron, W. Haeberli, *J. Glaciol.* **29**, 28 (1983).
5. B. Kamb *et al.*, *J. Geophys. Res.* **99**, 15231 (1994).
6. A. Gore, *An Inconvenient Truth: The Planetary Emergency of Global Warming and What We Can Do About It* (Rodale, Emmaus, PA, 2006).
7. H. J. Zwally *et al.*, *Science* **297**, 218 (2002).
8. B. R. Parizek, R. B. Alley, *Quat. Sci. Rev.* **23**, 1013 (2004).
9. IPCC, *Climate Change, 2007: The Physical Science Basis. Contribution of Working Group I to the Fourth Assessment Report of the Intergovernmental Panel on Climate Change*, S. Solomon *et al.*, Eds. (Cambridge Univ. Press, Cambridge and New York, 2007).
10. K. Echelmeyer, W. D. Harrison, *J. Glaciol.* **36**, 82 (1990).
11. I. Joughin, S. Tulaczyk, M. Fahnestock, R. Kwok, *Science* **274**, 228 (1996).
12. Methods are available as supporting material on *Science* Online.
13. S. B. Das *et al.*, *Science* **320**, 778 (2008); published online 17 April 2008 (10.1126/science.1153529).
14. I. Joughin, W. Abdalati, M. Fahnestock, *Nature* **432**, 608 (2004).
15. A. Lucchitta, T. Murray, *Geophys. Res. Lett.* **32**, L08501 (2005).
16. A. Iken, R. A. Bindschadler, *J. Glaciol.* **32**, 101 (1986).
17. R. H. Thomas *et al.*, *J. Glaciol.* **49**, 231 (2003).
18. H. G. Sohn, K. C. Jezek, C. J. van der Veen, *Geophys. Res. Lett.* **25**, 2699 (1998).
19. I. M. Howat, I. Joughin, S. Tulaczyk, S. Gogineni, *Geophys. Res. Lett.* **32**, L22502 (2005).
20. A. Luckman, T. Murray, R. de Lange, E. Hanna, *Geophys. Res. Lett.* **33**, L03503 (2006).
21. E. Rignot, P. Kanagaratnam, *Science* **311**, 986 (2006).
22. I. M. Howat, I. Joughin, T. A. Scambos, *Science* **315**, 1559 (2007).
23. P. Clarke, M. K. Dubey, G. Lesins, *Geophys. Res. Lett.* **33**, L11707 (2006).
24. J. T. Harper, N. F. Humphrey, W. T. Pfeffer, B. Lazar, *Geophys. Res. Lett.* **34**, L12503 (2007).
25. Support was provided jointly by NSF and NASA through ARC-0520382 (I.J.), ARC-0520077/ARC-0531345 (S.B.D., M.H., and T.A.), and NNG06GE55G (B.E.S.). A National Environment Research Council (UK) Research Fellowship supported M.A.K. Early conversations with R. B. Alley helped initiate this project. SAR data were acquired by the Canadian Space Agency and distributed by the Alaska Satellite Facility. We acknowledge VECO Logistics support. UNAVCO (GPS) and PASSCAL (seismometers). Comments by the two anonymous reviewers led to substantial improvements in the manuscript.

Supporting Online Material

www.sciencemag.org/cgi/content/full/1153288/DC1
Methods
Fig. S1
References

26 November 2007; accepted 31 March 2008
Published online 17 April 2008;
10.1126/science.1153288
Include this information when citing this paper

Monte Verde: Seaweed, Food, Medicine, and the Peopling of South America

Tom D. Dillehay,[1]* C. Ramírez,[2] M. Pino,[3] M. B. Collins,[4] J. Rossen,[5] J. D. Pino-Navarro[6]

The identification of human artifacts at the early archaeological site of Monte Verde in southern Chile has raised questions of when and how people reached the tip of South America without leaving much other evidence in the New World. Remains of nine species of marine algae were recovered from hearths and other features at Monte Verde II, an upper occupational layer, and were directly dated between 14,220 and 13,980 calendar years before the present (~12,310 and 12,290 carbon-14 years ago). These findings support the archaeological interpretation of the site and indicate that the site's inhabitants used seaweed from distant beaches and estuarine environments for food and medicine. These data are consistent with the ideas that an early settlement of South America was along the Pacific coast and that seaweeds were important to the diet and health of early humans in the Americas.

Most scholars now accept that people entered the Americas through Beringia before 16,000 calendar years ago (*1*–*3*). After entering, it is not known whether people colonized the hemisphere by moving along the Pacific coast, through interior routes, or along both areas. Early coastal migrants probably obtained much of their food from the sea, including sea mammals, shellfish, and seaweed (*4*, *5*). Convincing data have not yet been recovered to support the coastal model, although a few early littoral sites have been reported (*6*–*11*). A coastal route along which resources are similar would more easily explain the rapid movement of people into South America and their presence at Monte Verde II, Chile, the upper layer of the Monte Verde site, dated at ~14,600 calendar years before the present (cal yr B.P.) (*12*, *13*) [supporting online material (SOM) text, section 2]. Here we report the recovery of three marine, two estuarine, and one terrestrial shoreline algae species new to the site and three additional stone artifacts, one with the remains of seaweed on a worked edge, that suggest a strong reliance on coastal resources for food and medicine.

Monte Verde II is buried in the terraces of a small creek in the Maullin river basin, located midway between the Pacific coast and the Andean mountains. Today, the area is characterized by a cool temperate climate, by wetlands composed of various hydrophytic communities and their successive species, and by remnants of a partly deciduous rainforest (*12*). During the late Pleistocene, temperatures were cooler, the site was drier, and the coast was situated ~90 km to the west, where sandy beaches, rocky shores, and delta estuaries offered a wide variety of marine and brackish water resources (Fig. 1). The inland marine bay of Seno de Reloncaví, dominated by a rocky shoreline, was ~15 km to the south. Monte Verde was ~120 m above sea level at the time of human occupation (SOM text, section 1). Today, the sea is ~55 km west and ~11 km south of the site and ~59 m below it.

At Monte Verde II, organic remains are well preserved under a peat stratum that covers the ~14,600 cal yr B.P. archaeological layer. Previous research recovered wood tent remains, hut foundations and floors, hearths and braziers, wooden lances, mortars and digging sticks, medicinal and edible plants, animal bones, hide and soft tissue, human footprints, numerous stone tools, and other materials demonstrating human occupation (*13*). This evidence suggests that the site was occupied year round

[1]Department of Anthropology, Vanderbilt University, Nashville, TN 37265, USA, and Instituto de Ciencias Sociales, Universidad Austral de Chile, Valdivia, Chile. [2]Instituto de Botánica, Universidad Austral de Chile, Valdivia, Chile. [3]Instituto de Geociencias, Universidad Austral de Chile, Valdivia, Chile, and Núcleo Forest Ecosystemic Services to Aquatic Systems Under Climatic Fluctuations (FORECOS) Millennium Science Initiative, Chile. [4]Texas Archeological Research Laboratory, University of Texas, Austin, TX 78712, USA. [5]Department of Anthropology, Ithaca College, Ithaca, NY 14850, USA. [6]Centro de Estudios Ambientales, Universidad Austral de Chile, Valdivia, Chile.

*To whom correspondence should be addressed. E-mail: tom.d.dillehay@vanderbilt.edu

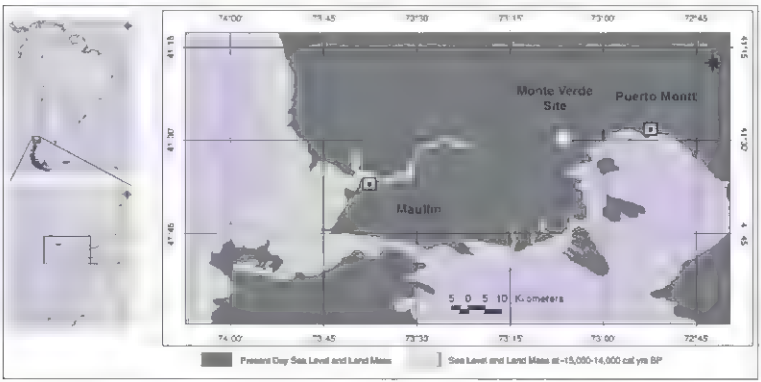

Fig. 1. Map of the Monte Verde area showing the location of the sea level and coastline at ~15,000 to 14,000 cal yr B.P. and at the present day.

and that resources were exploited from a wide variety of habitats, including the coast and the mountains. Fifteen species of aquatic plants from freshwater marshes of the distant Maullín floodplain and from coastal dunes and brackish water estuaries of the delta, along with gomphothere (*Cuvieronius tarma* Casamiquela) and paleocamelid (*Paleolama* sp.) meat, wild potatoes (*Solanum maglia*), and 45 other plant species from inland forests and wetlands provided the bulk of the Monte Verdeans' diet (*12*, *13*). Included in the plant inventory were four previously reported varieties of seaweed, *Durvillaea Antarctica* (*cochayuyo*), *Porphyra* sp. (*luche*), *Gracilaria* sp. (*pelillo*), and *Sargassum* sp., from sandy and rocky shorelines (*14*–*16*). All of these species are edible and have important medicinal properties. Also recovered were the remains of 19 other probable medicinal species, 5 of which came from coastal environments (*14*–*16*). Other coastal resources collected from beaches and transported to the site were discoidal pebbles made into stone tools, bitumen used as adhesive to attach tools to wooden shafts, and marine fossils (*12*, *13*).

Our new analyses are from 27.2 liters of previously excavated but unstudied sediment fill from 24 hearths and braziers in the floors of two structures thought to be the remains of a medicinal hut and a residential tent. We recovered the remains of seaweed and other economically important plants (SOM text, section 2, and table S1) and three stones, one of which is a flake tool. Identified were *Porphyra* sp. and *Durvillaea Antarctica* (Fig. 2) and five new species of seaweed: *Gigartina* sp. (*luga roja*); *Mazzaella* sp. (*luga cuchara*); *Porphyra columbina*, probably *Sarcothalia crispata* (*luga negra*, Fig. 3); and *Macrocystis pyrifera* (*huiro*) (*13*). We also recovered *Trentepohlia* sp., an algae that is available exclusively on trees (*Aextoxicon punctatum* and *Griselinia jodinifolia*) and rocks in the littoral zone. The excellent preservation of the specimens allowed species-level identification based on cellular structure, plant morphology, and color. Two accelerator mass spectrometry radiocarbon dates derived from fragments of *Gigartina* sp. on the floor of a wishbone-shaped hut and from *Mazzaella* sp. in a brazier on a tent floor are respectively between 14,190 and 13,990 cal yr B.P. (~12,290 ± 60 C^{14} yr B.P., Beta Analytic radiocarbon dating service sample number 238355) and 14,220 and 13,980 cal yr B.P. (~12,310 ± 40 C^{14} B.P., Beta Analytic sample number 239650). These dates agree with those derived from wood artifacts and charcoal in hearths at Monte Verde II, which range between 14,600 and 14,200 cal yr B.P. (*13*).

It was difficult to count the soft remains of the 10 species of algae because many were fragmented and mixed with other plants in masticated cuds, thought to be representative of an ancient pharmacopeia (*14*, *15*) (SOM text, section 3, and fig. S1), or were trampled and embedded in hut floors. However, the dry weight total of all excavated seaweed remains was ~125 g. Several algae fragments were partially burned, suggesting that they had been dried,

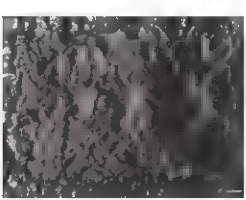

Fig. 2. Microscopic view of an archaeological specimen of *Durvillaea antarctica* from a hearth matrix located in the remains of a domestic hut. Scale bar, ~100 μm.

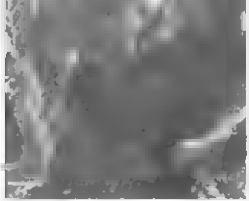

Fig. 3. Microscopic view of an archaeological specimen of *Sarcothalia crispata* from a hearth matrix located in the remains of a domestic hut. Scale bar, ~ 200 um.

Fig. 4. Microscopic view of *Sargassum* sp. from the floor of the wishbone-shaped hut. Scale bar, ~100 μm.

probably for transport from the coast or for storage, or were cooked. The fragility of soft leafy seaweeds, their unlikely preservation in archaeological sites, and yet their widespread dispersion in hearths and braziers across the site and their combination with other medicinal plants in the form of masticated cuds suggest their value for both food and medicinal purposes.

The seaweeds represent contrasts in environment and seasonal availability. Four genera (*Durvillaea*, *Porphyra*, *Mazzaella*, and *Sarcothalia*) derive from rocky coastlines and intertidal pools located west and south of Monte Verde (*16*, *17*), whereas three (*Gracilaria*, *Gigartina*, and *Macrocystis*) originate only from sandy coastlines west of the site. The peak availability of three (*Mazzaella*, *Gigartina*, and *Sarcothalia*) occurs from early spring to early summer, one (*Gracilaria*) is available from late spring to early summer, one (*Porphyra*) is found in mid-summer, and one (*Durvillaea*) occurs in late summer to early fall (*18*–*21*). *Sargassum* sp. (Fig. 4) is a warm-water species with a wide Pacific natural range. Its growth anywhere in Chile, where the cold Humboldt Current sweeps the coast, is doubtful (*17*, *22*). *Sargassum* probably reached Chile through violent storms or major El Niño events, or perhaps the configuration of ocean currents was different at the time of site occupation. *Trentepohlia* sp. is available year-round along the littoral. Seaweed collection by Monte Verdeans was thus conducted at various coastal locales from early spring to early fall. Today, the tidal range of the sea varies from 6.5 m near Puerto Montt in the Reloncaví Bay to 4 m at the mouth of the Maullín River, in both areas producing a wide and abundantly available resource-rich intertidal beach. With the exception of *Sargassum* sp., moderate quantities of all varieties of seaweeds are deposited along the shoreline during storm surges. All nine seaweed species recovered at Monte Verde II are excellent sources of iodine, iron, zinc, protein, hormones, and a wide range of trace elements, particularly cobalt, copper, boron, and manganese (*23*–*29*). Secondary beneficial effects of these seaweeds include aiding cholesterol metabolism, increasing the calcium uptake of bones, antibiotic effects, and increasing the body's ability to fight infection. These species have medicinal uses that closely correspond to common contemporary health problems in the study area today (SOM text, section 3). Two species, *Gigartina* and *Sargassum*, are non-edible and were evidently used exclusively for medicinal purposes. Collectively, the seaweeds and 10 other plant species at Monte Verde II suggest a medicinal stock derived from the cool temperate environment of the region. These same species are used today as medicinal plants by local indigenous populations.

We also recovered a total of 268 edible seeds, fruits, and other plant parts (SOM and table S1) from the processed feature fills, which correspond with the genera previously reported

from the site (*13–16*). Also recovered were three stone tools, one of which exhibits microparticles of *Gigartina* sp. on a used edge (SOM text, section 4, and fig. S2), suggesting that it was used for cutting and preparing seaweed. Fragments of *Porphyra* sp. and *Sargassum* sp. were reported previously on other stone tools (*13*). The remaining two stones show indeterminate human modification (SOM and figs. S4 to S6).

Not known is whether people arrived at Monte Verde through an interior or coastal route. However, these new data indicate that the people inhabiting Monte Verde II were accustomed to frequently exploiting coastal resources year round, which, coupled with interior foods, allowed them to remain in the area. Prior evidence suggests that the Monte Verdeans also regularly moved up and down the Maullín basin to exploit resources and/or to exchange them with other people living in the area (*13, 16*). Assuming that other late Pleistocene people operated under similar subsistence and settlement practices, our data imply that if groups traveled along the Pacific coast, they may have migrated slowly and exploited the interior resources of the hundreds of river basins descending the long mountain chain from Alaska to Tierra del Fuego to the sea. Several recent archaeological findings support the idea of early coastal migration and specialized maritime sites, but this evidence also indicates contacts with interior people or transhumance between coastal and interior areas and thus broad-spectrum economies (*7, 8, 10, 11*).

References and Notes

1. J. Dixon, *Bones, Boats, and Bison* (Univ. of New Mexico Press, Albuquerque, NM, 1999).
2. T. D. Dillehay, *A New Prehistory: Settlement of the Americas* (Basic Books, New York, 2000).
3. D. Meltzer, *Dev. Quat. Sci.* **1**, 539 (2003).
4. K. R. Fladmark, *Am. Antiq.* **44**, 55 (1979).
5. R. Gruhn, in *Methods and Theory for Investigating the Peopling of the Americas*, R. Bonnichsen, D. G. Steele, Ed. (Oregon State Univ. Press, Corvallis, OR, 1994), pp. 24–256.
6. D. Lavallée *et al.*, *Bull. Inst. Fr. Etudes Andines* **28**, 13 (1999).
7. A. L. Martinez, *Am. Antiq.* **44**, 309 (1979).
8. D. Jackson, C. Méndez, R. Seguel, A. Maldonado, G. Vargas, *Curr. Anthropol.* **48**, 725 (2007).
9. J. Erlandson, in *The First Americans: The Pleistocene Peopling of the New World*, N. Jablonski, Ed. (Memoirs of the California Academy of Sciences 27, Univ. of California Press, Berkeley, CA, 2002), pp. 52–93.
10. D. K. Keefer *et al.*, *Science* **281**, 1833 (1998).
11. D. H. Sandweiss *et al.*, *Science* **281**, 1830 (1998).
12. T. D. Dillehay, *Monte Verde: A Late Pleistocene Settlement in Chile, Vol. 1* (Smithsonian Institution Press, Washington, DC, 1989).
13. T. D. Dillehay, *Monte Verde: A Late Pleistocene Settlement in Chile, Vol. 2* (Smithsonian Institution Press, Washington, DC, 1997).
14. C. Ramírez, in (*12*), pp. 147–169.
15. B. Ugent, D. R. Tindall, in (*12*), pp. 911–914.
16. J. Rossen, T. D. Dillehay, in (*13*), pp. 331–350.
17. J. D. Pino-Navarro, *Informe Etnográfico para la Interpretación de los Posibles Usos de Algas Halladas en el Sitio Arqueológico Monte Verde, Valle del Río Maullín, X Región de los Lagos* (manuscript on file at Vanderbilt Univ., Nashville, TN, 2007).
18. M. Ramírez, B. Santelices, *Catálogo de las Algas Marinas Bentónicas de la Costa Temperada del Pacífico de Sudamérica* (Monografías Biológicas 5, Pontificia Univ. Católica, Santiago, Chile, 1991).
19. B. Santelices, *Algas Marinas de Chile: Distribución, Ecología, Utilización, Diversidad* (Ediciones Univ. Católica de Chile, Santiago, Chile, 1989).
20. J. Varela, B. Santelices, J. Correa, M. Arroyo, *J. Appl. Phycol.* **18**, 827 (2006).
21. R. Westermeier, A. Aguilar, J. Sigüel, J. Quintanilla, J. Morales, *Hydrobiologia* **398-399**, 137 (1999).
22. J. C. Castilla *et al.*, *Biol. Invasions* **7**, 213 (2005).
23. E. B. Damonte, M. C. Matulewicz, A. S. Cerezo, *Curr. Med. Chem.* **11**, 2399 (2004).
24. H. Noda, H. Amano, K. Arashima, K. Nisizawa, *Hydrobiologia* **204-205**, 577 (1990).
25. A. Buschmann *et al.*, *J. Appl. Phycol.* **13**, 255 (2001).
26. B. Matsuhiro, E. Zúñiga, M. Jashes, M. Guacucano, *Hydrobiologia* **321**, 77 (1996).
27. D. McHugh, *Hydrobiologia* **221**, 19 (1991).
28. A. Smit, *J. Appl. Phycol.* **16**, 245 (2004).
29. N. J. Turner, H. Clifton, in *Eating and Healing: Traditional Food as Medicine*, A. Pieroni, L. Leimar Price, Eds. (Haworth Press, NY, 2005), pp. 153–178.
30. We thank NSF for sponsoring this research and the Consejo de Monumentos Nacionales, Chile, for supporting it. We are especially grateful to R. Westermeier for identifying the species of some algae specimens and for providing invaluable information on the seaweeds in south Chile. J.D.P.-N.'s work was supported by FONDECYT grant number 1060111. M.P.'s work was supported by the Millennium Science Nucleus FORECOS, grant number P04-065-F. The stone specimens were drawn by P. Headrick and digitally imaged and photographically composed by S. Gardner. P. Sikox aided in formatting all figures. P. Romero drafted the digital map in Fig. 1. The authors are solely responsible for any mistakes.

Supporting Online Material
www.sciencemag.org/cgi/content/full/320/5877/784/DC1
SOM Text
Figs. S1 to S6
Table S1
References

15 February 2008; accepted 8 April 2008
10.1126/science.1156533

DNA from Pre-Clovis Human Coprolites in Oregon, North America

M. Thomas P. Gilbert,[1*] Dennis L. Jenkins,[2*] Anders Götherstrom,[3] Nuria Naveran,[4] Juan J. Sanchez,[5] Michael Hofreiter,[6] Philip Francis Thomsen,[1] Jonas Binladen,[1] Thomas F. G. Higham,[7] Robert M. Yohe II,[8] Robert Parr,[8] Linda Scott Cummings,[9] Eske Willerslev[1]†

The timing of the first human migration into the Americas and its relation to the appearance of the Clovis technological complex in North America at about 11,000 to 10,800 radiocarbon years before the present (^{14}C years B.P.) remains contentious. We establish that humans were present at Paisley 5 Mile Point Caves, in south-central Oregon, by 12,300 ^{14}C years B.P., through the recovery of human mitochondrial DNA (mtDNA) from coprolites, directly dated by accelerator mass spectrometry. The mtDNA corresponds to Native American founding haplogroups A2 and B2. The dates of the coprolites are >1000 ^{14}C years earlier than currently accepted dates for the Clovis complex.

The timing, route, and origin of the first human migration into the Americas remain uncertain. Some archaeological (*1*) and genetic [reviewed by (*2*)] evidence has been used to argue for a settlement by 30,000 years ago (ka) (calendar years) or even earlier, but both lines of evidence remain controversial. The most widely accepted dates of occupation relate to the Clovis complex, ~11,000 to 10,800 ^{14}C years before the present (yr B.P.) (13.2–13.1 to 12.9–12.8 ka), a distinct technology that appears to have originated and spread throughout North America in as little as 200 to 300 years (*3*).

The oldest directly dated human osteological remains from the Americas are no more than 11,000 ^{14}C yr B.P. (~12.9 ka) (*3, 4*) and appear to be congruent with the "Clovis-first" model of colonization (*5, 6*). However, this theory is complicated by Monte Verde, in southern Chile, which contains artifacts dated to ~12,500 ^{14}C yr B.P. (~13.9 to 13.8 ka) that exhibit little technological connection to Clovis (*7*). Although a number of pre-Clovis occupation sites have been reported from North America (*8*), their age and cultural origins remain controversial, primarily because of the lack of directly dated human remains or artifacts (*9*).

Here we present evidence for human presence in North America before the Clovis complex, through the identification and genetic profiling of coprolites directly dated to 12,300 ^{14}C yr B.P. (~14.27 to 14.0 ka) at the Paisley 5 Mile Point Caves in south-central Oregon (Fig. 1A). The Paisley Caves are wave-cut shelters located on the highest shoreline of pluvial Lake Chewaucan, which once filled the Summer Lake–Chewaucan–Lake Abert basins (Fig. 1A). As the lake level fell since the last glacial maximum (*10, 11*), the caves began filling with aeolian-transported silt and sand, gravel, roof spall, and organic material (bones, coprolites, plant remains, and artifacts) deposited by humans and animals. Sheltered from moisture, these extremely dry deposits contain perishable human artifacts, manufactured threads of sinew and plant fibers, hide, basketry, cordage, rope, and wooden pegs, as well as animal bones and diverse kinds of feces, in an un-

broken stratigraphic sequence spanning the late Pleistocene and Holocene (*12*). Stone tool and debitage assemblages are small, suggesting that site occupations were generally brief. Pleistocene assemblages contain few chronologically diagnostic artifacts. The few projectile point fragments recovered are morphologically consistent with lanceolate, Western Stemmed, and folsate types common in the Younger Dryas (10,200 to 10,700 ^{14}C yr B.P.) and early Holocene archaeological sites of the region. However, the stratigraphic distribution of artifacts and radiocarbon dating of likely butchered bones suggest that the site may have been occupied as early as 12,400 and 12,000 ^{14}C yr B.P.

Fourteen coprolites recovered from the lowest levels of Paisley Caves are morphologically human (based on size, shape, constituents, and color). In initial screening using a multiplex polymerase chain reaction (PCR) and nonsequencing assay, all 14 were positive for human mitochondrial DNA (mtDNA) (*13*). This result is not surprising, because the coprolites had not been excavated under sterile conditions and could be expected to contain DNA derived from the excavation team (*14*, *15*). Although all of the coprolites contained single-nucleotide polymorphisms (SNPs) diagnostic of European populations (which is consistent with contamination), independently generated cloned and pyrosequenced PCR products from six samples reproducibly yielded SNPs diagnostic of Native American founding mtDNA haplogroups (Hgs) A2 and B2, (Table 1; supporting online material (SOM) text; fig. S1; and tables S1, S5, S7, and S9) (*16*). The absence of PCR amplifiable Native American mtDNA in the remaining eight samples may be due to differences in DNA survival across specimens or the possibility that these coprolites are nonhuman; or, what is more likely, the ratio of contaminant to endogenous DNA was too great for endogenous mtDNA detection using our techniques.

Human ancient DNA studies are extremely prone to contamination that may occur during sampling or subsequent laboratory analyses (*14*, *15*). To exclude laboratory-based contamination, the Hg A and B results were independently confirmed with several different DNA typing and sequencing methods (*13*) in multiple laboratories (in Copenhagen, Denmark; Uppsala, Sweden; and Leipzig, Germany) (Table 1). Furthermore, to ensure that the Hg A and B results were not the result of contamination during the excavation, we mitotyped the 55 individuals (students, instructors, and visitors) who had been present at the site during the two-season excavation (*13*). Additionally, we mitotyped the 12 researchers present in the principal DNA laboratory (*13*). This was performed regardless of whether an individual played an active role in the excavation or in the genetic analysis of the coprolites. For example, although 55 people had been present at the archaeological site, only 14 were actively involved in the excavation of the six coprolites reported here, and only two of those could have come in contact with all six specimens. The results show that none of the individuals tested are the sources of the Hg A and B mtDNA (*13*) (table S4). Because the coprolites had been stored in sealed plastic bags from the time of excavation until the genetic analyses were undertaken, it is difficult to explain the results by other sources of post-excavation contamination. To provide additional confirmation for a human origin of the coprolites, we submitted part of the four oldest samples (as material allowed) for protein residue (crossover immunoelectrophoresis) and reconstitution analyses (trisodium phosphate solution analyses) (*13*). The results of these tests confirmed the results of the morphological and genetic analyses that the coprolites are of human origin (Table 1 and SOM text).

The leaching of DNA from younger to older stratigraphic layers may be a problem in relatively wet, temperate cave settings (*17*). Although it is unlikely that leaching would be able to pro-

[1]Centre for Ancient Genetics, University of Copenhagen, Universitetsparken 15, 2100 Copenhagen, Denmark. [2]Museum of Natural and Cultural History, 1224 University of Oregon, Eugene, OR 97403-1224, USA. [3]Department of Evolutionary Biology, Uppsala University, Norbyvagen 18D, 74236 Uppsala, Sweden. [4]Instituto de Medicina Legal, Facultad de Medicina, University of Santiago de Compostela, San Francisco s/n 15782, Santiago de Compostela, Spain. [5]National Institute of Toxicology and Forensic Science, Canary Islands Delegation, 38320 Tenerife, Spain. [6]Max Planck Institute for Evolutionary Anthropology, Deutscher Platz 6, 04103 Leipzig, Germany. [7]Research Laboratory for Archaeology and the History of Art, Dyson Perrins Building, South Parks Road, Oxford, OX1 3QY, UK. [8]Department of Sociology/Anthropology, California State University, 9001 Stockdale Highway, Bakersfield, CA 93311, USA. [9]Palaeo Research Institute, 2675 Youngfield Street Golden, CO 80401, USA.

*These authors contributed equally to this work.
†To whom correspondence should be addressed. E-mail: ewillerslev@bio.ku.dk

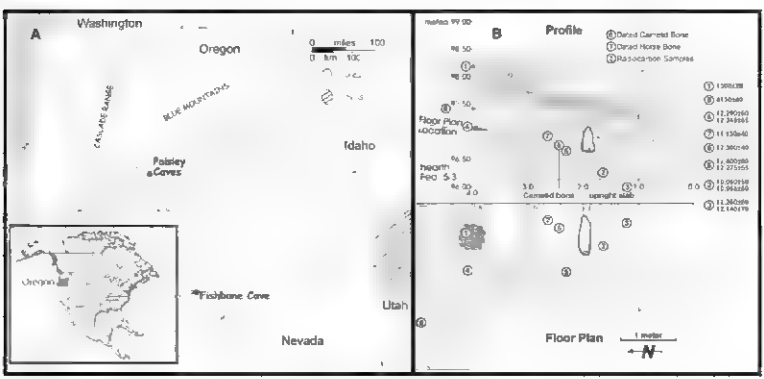

Fig. 1. Geographical and stereographical information on Paisley 5 Mile Point Caves. (**A**) The location of Paisley 5 Mile Point Caves in Oregon and location of Oregon in the United States (inset). (**B**) Horizontal, vertical, and stratigraphic distribution of five of the human coprolites. Sample 1374-PC-1/2A-2B (Table 1) was excavated from another cave (Cave 1) and thus is not shown. Also indicated are a dated camelid astragalus, a horse phalange, and sample 8, a coprolite found out of context, indicating some stratigraphic disturbance. For further details, see SOM text.

vide crossover immunoelectrophoresis false positives, because of the relatively large amounts of proteins needed, we conducted two additional tests for DNA leaching. Wood rat (*Neotoma lepida*) fecal pellets are a major constituent of the strata in the Paisley 5 Mile Point Caves and were found in direct contact with the six coprolites in question (table S9). Thus, we screened the six coprolites for *Neotoma* mtDNA (*13*). To account for any possible differences in *Neotoma* species inhabiting the caves in the past, we used primers designed to amplify mtDNA from all members of the genus. Control *Neotoma* fecal samples from the caves gave positive results for *Neotoma* DNA (table S6). However, all six coprolites testing positive for human DNA tested negative for *Neotoma* DNA. We additionally screened 14 control sediment samples and two long bones morphologically identified as *Spermophilus lateralis* (golden-mantled ground squirrel), recovered from around the coprolites, for the Hg A and B SNPs (*13*) (table S6). Although 8 out of the 16 samples were positive for human mtDNA (presumably derived from the excavation team), none of the samples were positive for the Native American SNPs (table S6). Additionally, primers specific for *S. lateralis* gave positive results for the two long bones, demonstrating that DNA survived in noncoprolite specimens from the Paisley Caves for long times also. The results strongly suggest that leaching of DNA is not a concern in the Paisley Caves and are in agreement with empirical and theoretical evidence suggesting that substantial amounts of liquid water are required to move free DNA molecules between strata (*17*, *18*).

Three of the six coprolites also contained canid 16S mtDNA with high similarity to red fox (*Vulpes vulpes*, one substitution difference), coyote (*Canis latrans*, one substitution difference), or domestic dog or wolf (*Canis familiaris* or *C. lupus*, 100% match) (Table 1) (*13*). In light of the nongenetic tests showing a human origin of the coprolites and the findings of diverse canid bones in the strata, the most likely explanations for these results are that humans may have eaten canids or that canids living in the caves during periods of nonhuman occupation urinated directly onto human feces.

Accelerator mass spectrometry (AMS) radiocarbon dating of bone collagen from a canid astragalus, recovered in stratigraphic association (stratum LU1b) with three of the oldest human coprolites, produced an age of 12,300 ^{14}C yr B.P. (Fig. 1B). To ensure reliable ages of the coprolites, the five specimens from the deepest layers were submitted for direct dating by AMS at two independent laboratories, Beta Analytic (Florida, USA) and the Oxford Radiocarbon Accelerator Unit (University of Oxford, UK). Although each laboratory used different methodologies (*13*), all specimens except one (sample 1294 PC-5/6B-40) produced consistent dates, ranging from approximately 1300 to 12,300 ^{14}C yr B.P., and three of the coprolites pre-dated 11,000 ^{14}C yr B.P.

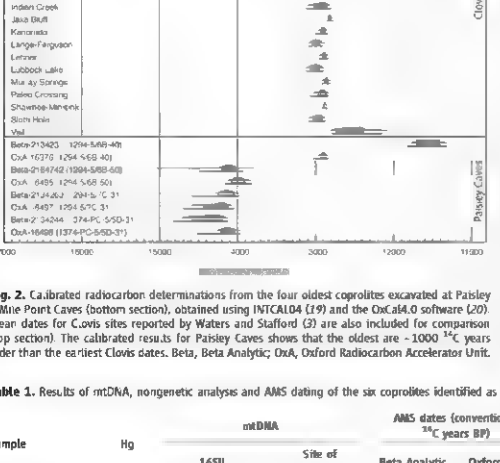

Fig. 2. Calibrated radiocarbon determinations from the four oldest coprolites excavated at Paisley 5 Mile Point Caves (bottom section), obtained using INTCAL04 (*19*) and the OxCal4.0 software (*20*). Mean dates for Clovis sites reported by Waters and Stafford (*3*) are also included for comparison (top section). The calibrated results for Paisley Caves shows that the oldest are ~1000 ^{14}C years older than the earliest Clovis dates. Beta, Beta Analytic; OxA, Oxford Radiocarbon Accelerator Unit.

Table 1. Results of mtDNA, nongenetic analyses and AMS dating of the six coprolites identified as of Native American origin.

Sample	Hg	mtDNA		AMS dates (conventional ^{14}C years BP)		Cave	Fig. 1B no.#	CIE**	TP††
		16S‖	Site of replication	Beta Analytic	Oxford Univ.				
1294 PC 5/7D-4	B2*	*C. latrans*	Uppsala	Not tested	1,308 ± 28	5	1		n/a
1374 PC 1/2A 28	B2†		Uppsala	6,640 ± 40	6,608 ± 35	1		–	n/a
1294 PC 5/6B 40	B2†	*C. lupus/ familiaris*¶	Uppsala	10,050 ± 50	10,965 ± 50	5	2	Human	n/a
1294-PC-5/6B 50	A2‡	*V. vulpes*	Uppsala	12,260 ± 60	12,140 ± 70	5	3	Human	Human
1294 PC 5/7C 31	B5,§§		Uppsala/Leipzig	12,290 ± 60	12,345 ± 55	5	4	Human	Human
1374 PC 5/5D 31‖	B2†		Uppsala	12,400 ± 60	12,275 ± 55	5	5	–	Human

Mitochondrial DNA Hgs were identified with different techniques across laboratories as follows. *Copenhagen SNaPshot, Uppsala Pyrosequenced, Uppsala cloned; †Copenhagen SNaPshot, Copenhagen cloned, Uppsala Pyrosequenced, Uppsala cloned and sequenced; ‡Copenhagen SNaPshot, Uppsala Pyrosequenced; §Copenhagen SNaPshot, Uppsala Pyrosequenced, Leipzig cloned and sequenced. Although Hgs A and B are based on independently replicated results, sub-Hgs A2 and B2 are in general based on single laboratory analyses. For details, see SOM text. ‖Canid sequences detected with generic mammalian 16S mtDNA primers. ¶Sequences are indistinguishable over generic marker. #Sample identification in Fig. 1B. **Result of crossover immunoelectrophoresis analysis. (–) no result: recovered because of poor protein preservation in the sample (see SOM text for more discussion). ††Result after reconstitution in trisodium phosphate solution. n/a, sample not assessed. §§Insufficient DNA was available to further resolve the haplogroup. ‖ Fig. S1.

(Table 1 and Fig. 2). Thus, our data show that humans were present in North America before the Clovis complex. Analyses of complete Native American mtDNA genomes imply that the Hgs A2 and B2 originated at 13.9 ± 2.0 and 16.5 ± 2.7 ka, respectively (*16*). The coprolites at Paisley may thus derive from among the earliest members of these Hgs. The Paisley Caves contain only small, pre-Clovis lithic tool assemblages, and thus the cultural and technological associations of the early site occupants and their relationship to the later Clovis technology are uncertain.

References and Notes

1. P. C. Orr, *Prehistory of Santa Rosa Island* (Santa Barbara Museum of Natural History, Santa Barbara, CA, 1968).
2. J. A. Eshleman, R. S. Malhi, D. G. Glenn-Smith, *Evol. Anthropol.* **12**, 7 (2003).
3. M. R. Waters, T. W. Stafford Jr., *Science* **315**, 1122 (2007).
4. J. M. Adovasio, D. R. Pedler, in *Entering America: Northeast Asia and Beringia before the Last Glacial Maximum*, D. B. Madsen, Ed. (Univ. of Utah Press, Salt Lake City, UT, 2004), chap. 5.
5. E. J. Dixon, *Quat. Sci. Rev.* **20**, 277 (2001).
6. M. J. Hamilton, B. Buchanan, *Proc. Natl. Acad. Sci. U.S.A.* **104**, 15625 (2007).
7. T. D. Dillehay, *Monte Verde: A Late Pleistocene Settlement in Chile, Vol. 2* (Smithsonian Institution Press, Washington, DC, 1997).
8. T. Falk, *Science* **305**, 550 (2004).
9. A. C. Roosevelt, J. Douglas, L. Brown, in *The First Americans: The Pleistocene Colonization of the New World*, N. G. Jablonski, Ed. (Memoirs of the California Academy of Sciences, San Francisco, 2002), vol. 27, chap. 3.
10. L. S. Allison, *Geology of Pluvial Lake Chewaucan, Lake County, Oregon* (Studies in Geology 11, Oregon State Monographs, Oregon State Univ. Press, Corvallis, OR, 1982).
11. J. M. Lorrain, *J. Quat. Sci.* **16**, 545 (2001).
12. D. L. Jenkins, in *Paleovindian or Paleoarchaic, Great Basin Human Ecology at the Pleistocene-Holocene Transition*, K. Graf, D. Schmitt, Ed. (Univ. of Utah Press, Salt Lake City, UT, 2007), chap. 4.
13. Materials and methods are available as supporting material on *Science* Online.
14. E. Willerslev, A. Cooper, *Proc. Biol. Sci.* **272**, 3 (2005).
15. M. T. P. Gilbert, H. J. Bandelt, M. Hofreiter, I. Barnes, *Trends Ecol. Evol.* **20**, 541 (2005).
16. F. Tamm *et al.*, *PLoS ONE* **2**, e829 (2007).
17. J. Malhi *et al.*, *Mol. Biol. Evol.* **24**, 982 (2007).
18. A. J. Hansen *et al.*, *Genetics* **173**, 1175 (2006).
19. P. J. Reimer *et al.*, *Radiocarbon* **46**, 1029 (2004).
20. C. Bronk Ramsey, *Radiocarbon* **43**, 355 (2001).

21. We thank T. B. Brand, B. Kemp, T. J. Connolly, and L. Davis for assistance and comments. The Lakeview and Vale District offices of the Bureau of Land Management provided funding for the field work through the direction of W. J. Cannon (Lakeview) and D. Pritchard (Vale). G. Skelton and P. Chodoczot of the Klamath Tribes assisted in the coordination of the Paisley Caves archaeological project. Financial support for the project was provided by the Museum of Natural and Cultural History, University of Oregon, and the Association of Oregon Archaeologists (O.J.). and the Marie Curie Actions 025082 "ORAMAPLEX (M.T.P.G.) and MEST-CT-2004-007909 GENETAKE (E.W. and N.N.) grants. GenBank accession numbers are as follows: EU579350 for the *H. fossilis* 16S mtDNA and EU579351 for the *S. latentifer* 16S mtDNA.

Supporting Online Material

www.sciencemag.org/cgi/content/full/1154116/DC1
Materials and Methods
SOM Text
Figs. S1 to S5
Tables S1 to S9
Cloned DNA Sequence Alignments

13 December 2007; accepted 19 March 2008
Published online 3 April 2008;
10.1126/science.1154116
Include this information when citing this paper

Spatial Regulators for Bacterial Cell Division Self-Organize into Surface Waves in Vitro

Martin Loose,[1,2] Elisabeth Fischer-Friedrich,[3] Jonas Ries,[1] Karsten Kruse,[4]* Petra Schwille[1,2]*

In the bacterium *Escherichia coli*, the Min proteins oscillate between the cell poles to select the cell center as division site. This dynamic pattern has been proposed to arise by self-organization of these proteins, and several models have suggested a reaction-diffusion type mechanism. Here, we found that the Min proteins spontaneously formed planar surface waves on a flat membrane in vitro. The formation and maintenance of these patterns, which extended for hundreds of micrometers, required adenosine 5′-triphosphate (ATP), and they persisted for hours. We present a reaction-diffusion model of the MinD and MinE dynamics that accounts for our experimental observations and also captures the in vivo oscillations.

How macroscopic order can emerge from local molecular interactions is a general problem of cell biology. Organization can emerge from a limited number of constituents that diffuse and locally interact with each other, provided that the system is out of equilibrium (*1*). A reaction-diffusion mechanism of pattern formation has been observed in a number of systems (*2*, *3*) and has also been suggested to lead to spatial protein organization in vivo (*4*–*7*).

The oscillations of the Min system in *Escherichia coli* are a strong candidate for a reaction-diffusion system in vivo (*6*). This system consists of the proteins MinC, MinD, and MinE (*8*), which oscillate between the poles of the rod-shaped bacterium (*9*, *10*) and thereby select the cell center as the site for division septum formation (*11*). The Min proteins are crucial for accurate cell division. Mutants lacking the Min system are prone to divide asymmetrically, which gives rise to DNA-free minicells. MinD is an adenosine triphosphatase (ATPase) that dimerizes in the presence of adenosine 5′-triphosphate (ATP) and binds to the lipid membrane via amphipathic helices (*12*). In the cell, MinD assembles on the cytoplasmic membrane covering roughly half of the cell. MinE binds to membrane-bound MinD and induces ATP hydrolysis by MinD (*13*). Subsequently, both proteins detach from the membrane, and MinD reassembles in the opposite half of the cell. MinE is predominantly located at the rim of the MinD domain and forms a ring close to the cell center (*14*). MinC follows the movement of MinD directly and is not required for the oscillations (*9*, *10*). However, it prevents the assembly of FtsZ, which is known to be the first protein to localize at the future site of cell division (*15*). By inhibiting FtsZ assembly at the cell poles, the Min system restricts the formation of the division septum to the cell center.

Various theories have been suggested to explain the Min oscillations (*6*). Some models

Fig. 1. Min-protein surface waves in vitro. Confocal images of self-organized protein waves on a supported lipid membrane, MinD (1 μM), doped with 20% Bodipy-labeled MinD (green), MinE (1 μM), doped with 10% Alexa647-labeled MinE (red). Scale bar, 50 μm.

[1]Biotechnologisches Zentrum der Technischen Universität Dresden, Tatzberg 47-51, 01307 Dresden, Germany. [2]Max Planck-Institute for Molecular Cell Biology and Genetics, Pfotenhauerstrasse 108, 01307 Dresden, Germany. [3]Max Planck-Institut für Physik komplexer Systeme, Nöthnitzer Strasse 38, 01187 Dresden, Germany. [4]Theoretische Physik, Universität des Saarlandes, Postfach 151150, 66041 Saarbrücken, Germany.

*To whom correspondence should be addressed. E-mail: petra.schwille@biotec.tu-dresden.de (P.S.); k.kruse@physik.uni-saarland.de (K.K.)

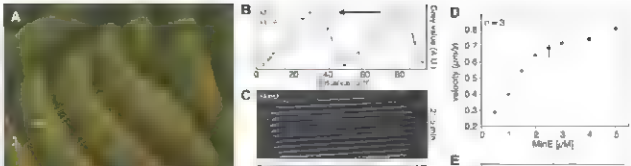

Fig. 2. Quantitative characterization of protein waves. (**A**) Confocal image of Min protein waves on a lipid membrane. MinD (1 μM), green channe., MinE (1.5 μM), red channel. Scale bar, 50 μm. (**B**) Intensity profile plots for MinD and MinE waves along the rectangular area shown in (A). Arrows in (A) and (B) indicate direction of wave propagation. (**C**) Kymographs for MinD and MinE along the rectangular area shown in (A). Surface wave velocity (**D**) and wavelength (**E**) as a function of MinE concentration (MinD at 1 μM). Data of the velocities fitted to Hill equation yielded V_{max} = 0.94 μm/s (left). Each data point has been obtained from $n = 3$ independent measurements. Error bars in (D) and (E) indicate SD.

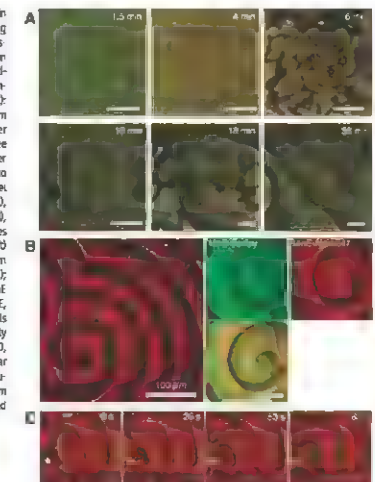

Fig. 3. nitiation of protein surface waves. (**A**) Starting from a homogenous distribution of MinD (1.5 min after addition of MinE), addition of MinE led to dynamic instability (4 to 38 min): First, MinD detached from the membrane, and after reattachment, protein-free ripples in the protein layer eventually synchronized to a regular pattern of parallel surface waves. MinD (1 μM), green channel; MinE (1.5 μM), red channel. (**B**) Spiral waves formed by Min proteins. (Left) Only labeled MinE is shown (MinD, 1 μM; MinE, 1 μM); (right) labeled MinD and MinE are shown (MinD, 1 μM; MinE, 1 μM). (**C**) Double spirals formed by Min proteins; only labeled MinE is shown (MinD, 1 μM; MinE, 0.5 μM). The star marks the center of the double spiral. Scale bar, 50 μm if not differently indicated (movies in SOM).

propose that no spatial markers are required to generate this pattern (*6*) and that spontaneous oscillations will form even from a uniform initial state, a phenomenon called dynamic instability. Thus, Min-protein self organization should not be restricted to living bacteria, but could also be tested in vitro (*16*). We designed an experimental approach with a minimal number of components to systematically explore the Min system.

Our in vitro system was based on a supported lipid bilayer to mimic the cell membrane, which was immersed in buffer containing the fluorescently labeled proteins MinE (Alexa647) and MinD (Bodipy FL) (*17*). In the presence of ATP, MinD attached to the membrane, forming a dense, homogeneous protein layer. When we added MinE to the buffer, planar surface waves formed on the membrane within 1 hour (Fig. 1 and movie S1). These waves moved in a distinct direction across the membrane and persisted for several hours. They were composed of spatially periodic bands of MinD and MinE, separated by troughs devoid of protein. The fluorescence intensities indicated a characteristic protein-density distribution parallel to the propagation direction (Fig. 2, A and B, and movie S2). From the leading edge of the wave, the density of MinD increased and decreased sharply toward the trailing edge. The MinE density displayed a similar intensity profile, but with a shallow linear rise in fluorescence and a sharp decrease at the trailing edge. In a propagating wave, the density maximum of MinE followed the maximum of MinD and formed a sharp line along the trailing edge of the wave. This pattern resembles the situation in the cell, where a dynamic MinE ring moves toward the pole, detaching MinD from the cell membrane (*14*).

The dynamics of the waves were influenced by the concentration of MinE. For given concentrations of MinD and MinE, waves moved at constant velocity and wavelength (Fig. 2C). When we increased the MinE concentration from 0.5 to 5 μM, the average propagation velocity changed from 0.28 μm/s to a value of 0.8 μm/s (Fig. 2D). At the same time, the average wavelength decreased from 100 to 55 μm (Fig. 2E). At concentrations below 0.2 μM, waves still formed erratically, but the system did not settle into a well-defined state (see movie S3). Wave formation crucially depended on the hydrolysis of ATP. Consistent with previous investigations (*15*), MinD did not attach to the membrane in the absence of ATP, and wave formation could not be observed. When we supplied the nonhydrolyzable ATP analog, adenosine 5′-*O*-(3-thiotriphosphate) (ATP-γ-S), MinD formed a homogeneous protein layer on the membrane. MinE attached to membrane-bound MinD, but was not able to induce wave formation (fig. S6). These findings confirmed that surface waves were only formed when energy was dissipated.

Without MinE, MinD was homogenously distributed on the membrane. How did the

presence of MinE lead to planar surface waves? One to 5 min after addition of MinE, the dense layer of MinD on the membrane became unstable and depletion zones appeared, which coincided with regions of high MinE density (Fig. 3A, at 4 min, and movie S4). These areas without membrane-bound MinD increased in size at constant MinE concentration in the buffer and were delimited by a continuous line of MinE. Depletion zones merged as they grew and encountered each other. MinE borders coalesced, leaving only MinD islands, which eventually disappeared (Fig. 3A, at 6 min). Subsequently, MinD reattached to the protein-free parts of the membrane with MinE distributed inhomogeneously around the newly formed MinD layer (Fig. 3A, at 10 min). Discrete protein-free ripples moved independently from each other across the membrane. The direction of motion of a ripple was governed by the asymmetry of MinE distribution, with MinE mainly located as a sharp line at the leading edge (see Fig. 3A and movies S4 and S5). When two ripples collided they fused and formed a larger protein-free area, which then moved in one direction. After about 1 hour all discrete ripples had synchronized into a highly regular pattern of parallel moving protein bands (Fig. 3A, at 18 and 38 min, see movie S5). In some instances, we observed rotating spirals of Min proteins (Fig. 3, B and C, and movies S6 to S8). The wavelengths and velocities of the waves emanating from a spiral did not vary with the distance from the spiral center and were the same as for the planar waves. When waves from two neighboring counter-rotating spirals collided, they fused to form parallel protein bands (Fig. 3C and movie S9). This might be the reason why we most frequently observed parallel waves.

To further investigate the mobility of the proteins during wave propagation, we performed fluorescence photobleaching experiments. The bleached area of MinF or MinD remained at its original position on the membrane, while the wave was propagating (figs. S9 and S10). This implies that the waves were not the result of protein translocation in the plane of the membrane, but were generated by sequential rounds of detachment and reattachment of proteins from the soluble pool.

The waves we observed experimentally were qualitatively different from the behavior predicted by existing theories (*6*) (see movies S12 and S13). These theories are either based on a classical reaction-diffusion mechanism (*18*, *19*), where cooperative MinD binding to the membrane is essential to generate oscillations, or they assume attractive interactions between MinD molecules bound to the membrane (*20*). From the observation that regions of high MinE densities initiated MinD detachment and eventually pattern formation (Fig. 3A), we developed a computational model [see supporting online material (SOM) text] that includes cooperative effects during MinE binding to the membrane, similar to those suggested in (*18*, *21*). MinE cooperativity proved to be crucial to reproduce the dynamic patterns observed experimentally (Fig. 4 and movies S10 to S11). Our theory also captured a similar protein density distribution within a protein band (Fig. 4B), as well as the dependencies of the wavelengths and velocities on the MinE concentration (Fig. 4D).

Several features of the in vitro structures of the Min system are strongly reminiscent of the Min oscillations in vivo: MinD was distributed homogenously on the membrane in the absence of MinE, whereas dynamic patterns could be observed only in the presence of MinE; MinE was found predominantly localized at the trailing edge of a moving MinD band (*14*, *22*). We characterized the velocity and wavelength of the surface waves as a function of MinE concentration and conclude that the frequency of the oscillations increases with an increasing MinE/MinD ratio (*14*). An explanation for the different length scales of the patterns observed in vitro and in vivo is given by our theoretical description. When we used lower values for the diffusion constants of the membrane-bound proteins in our model, we could also reproduce the Min oscillations observed in the cell (*23*) (see SOM text). One possible reason for lower diffusion constants in vivo could be molecular crowding in the cytoplasmic membrane of *E. coli*. Thus, the mechanism generating the surface waves in vitro may also drive the Min oscillations in vivo. By extending the experiments to the rod-shaped geometry of an *E. coli* cell, it could be possible to reconstitute pole-to-pole oscillations as observed in vivo or, eventually, even the whole prokaryotic cell division machinery. Here, we have shown that complex biological behavior can emerge from a limited number of components, namely, two proteins, a membrane, and ATP.

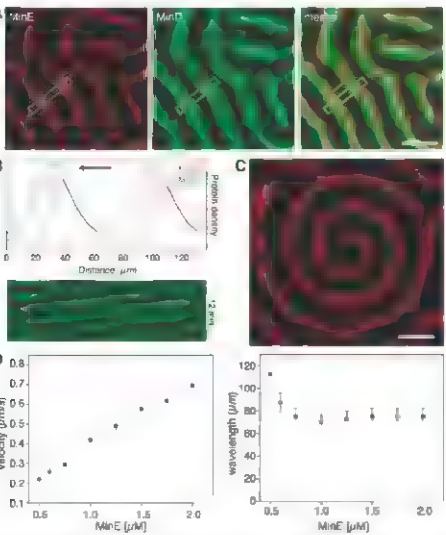

Fig. 4. Computational model of Min-protein dynamics. **(A)** Planar surface wave solutions of the dynamic equations (see SOM). **(B)** Profile plots and kymographs for MinD and MinE waves along the rectangular area shown in (A). Arrows indicate direction of wave propagation. Maxima of the MinE distribution follow maxima in the MinD distribution. **(C)** Spiral soution for the same parameter values as in (A). **(D)** Dependence of the velocity and wavelength of the surface waves on the MinE concentration. Whereas the velocity increases markedly with increasing MinE concentrations, the wavelength shows a moderate decrease. In all simulations, periodic boundary conditions have been used. The size of the domains in the simulations were 900 μm × 900 μm, extracts are shown in (A) and (B). Scale bar, 100 μm. Error bars in (D) and (E) indicate SD. Parameter values are given in the SOM text.

References and Notes

1. A. M. Turing, *Bull. Math. Biol.* **52**, 153 (1990).
2. M. C. Cross, P. C. Hohenberg, *Rev. Mod. Phys.* **65**, 851 (1993).
3. G. Nicolis, I. Prigogine, *Self-Organization in Nonequilibrium Systems: From Dissipative Structures to Order Through Fluctuations* (John Wiley & Sons, New York, 1977).
4. M. Caudron, G. Bunt, P. Bastiaens, E. Karsenti, *Science* **309**, 1373 (2005).
5. J. Meyers, J. Craig, D. J. Odde, *Curr. Biol.* **16**, 1685 (2006).
6. K. Kruse, M. Howard, W. Margolin, *Mol. Microbiol.* **63**, 1279 (2007).
7. F. Karsenti, *Nat. Rev. Mol. Cell Biol.* **9**, 255 (2008).
8. P. A. de Boer, R. E. Crossley, L. Rothfield, *Cell* **56**, 641 (1989).
9. Z. Hu, J. Lutkenhaus, *Mol. Microbiol.* **34**, 82 (1999).
10. D. M. Raskin, P. A. de Boer, *Proc. Natl. Acad. Sci. U.S.A.* **96**, 4971 (1999).
11. J. Lutkenhaus, *Annu. Rev. Biochem.* **76**, 539 (2007).
12. Z. Hu, J. Lutkenhaus, *Mol. Microbiol.* **47**, 345 (2003).
13. Z. Hu, E. P. Gogol, J. Lutkenhaus, *Proc. Natl. Acad. Sci. U.S.A.* **99**, 6671 (2002).
14. C. A. Haba, H. Meinhardt, P. A. de Boer, *EMBO J.* **20**, 1563 (2001).
15. E. F. Bi, J. Lutkenhaus, *Nature* **354**, 161 (1991).
16. E. Fischer-Friedrich, R. M. van Yen, C. Kruse, *Phys. Biol.* **4**, 38 (2007).
17. Materials and methods are available as supporting material on *Science* Online.
18. H. Meinhardt, P. A. de Boer, *Proc. Natl. Acad. Sci. U.S.A.* **98**, 14202 (2001).
19. K. C. Huang, Y. Meir, N. S. Wingreen, *Proc. Natl. Acad. Sci. U.S.A.* **100**, 12724 (2003).
20. G. Meacci, K. Kruse, *Phys. Biol.* **2**, 89 (2005).
21. This model, however, considered protein synthesis and degradation as an essential element, which has been shown to be unimportant for the Min oscillations in *E. coli* and was absent in our in vitro experiments.
22. D. M. Raskin, P. A. de Boer, *Cell* **91**, 685 (1997).
23. G. Meacci *et al.*, *Phys. Biol.* **3**, 255 (2006).
24. We thank W. Margolin for his generous gift of the plasmid; J. Howard, E. Paluch, F. Nédélec, and all members of the Schwille laboratory for help and discussions; and M. Meyer, M. Krishnan, and S.W. Grill for critically reading earlier versions of the manuscript. M.L. would like to thank H. Keller, T. Dirr, A. Baumann, and J. Müller for advice and experimental help. E.F. thanks T. Reichenbach, E. Nicola, and B. Friedrich for interesting discussions on the modeling. M.L. received a scholarship from the Studienstiftung des deutschen Volkes. This work was supported by the Max Planck Society (M.L., P.S., E.F.).

Supporting Online Material

www.sciencemag.org/cgi/content/full/320/5877/789/DC1
Materials and Methods
SOM Text
Figs. S1 to S13
Table S1
References and Notes
Movies S1 to S13

20 December 2007; accepted 18 March 2008
10.1126/science.1154413

Reconstitution of Contractile FtsZ Rings in Liposomes

Masaki Osawa, David E. Anderson, Harold P. Erickson*

FtsZ is a tubulin homolog and the major cytoskeletal protein in bacterial cell division. It assembles into the Z ring, which contains FtsZ and a dozen other division proteins, and constricts to divide the cell. We have constructed a membrane-targeted FtsZ (FtsZ-mts) by splicing an amphipathic helix to its C terminus. When mixed with lipid vesicles, FtsZ-mts was incorporated into the interior of some tubular vesicles. There it formed multiple Z rings that could move laterally in both directions along the length of the liposome and coalesce into brighter Z rings. Brighter Z rings produced visible constrictions in the liposome, suggesting that FtsZ itself can assemble the Z ring and generate a force. No other proteins were needed for assembly and force generation.

FtsZ is the primary cell division protein in almost all bacterial and archaeal species. In vitro, FtsZ assembles into short, one-stranded protofilaments, averaging 30 subunits and 125 nm in length (*1*). In the bacterial cell, these are further assembled into a long, thin filamentous structure attached to the inner bacterial membrane. Normally this filament forms a single Z ring at the center of the cell but sometimes the ring separates into a close-packed helix (*2*, *3*). Conventional electron microscopy (EM) has failed to resolve any structure of the Z ring in vivo, but a recent study with the use of cryo-EM tomography has resolved the arrangement of protofilaments in the Z ring of *Caulobacter crescentus* (*4*). These images showed individual protofilaments scattered in a narrow band around the circumference of the cell. Figure 1A depicts a model of how these protofilaments can be arranged to make the Z ring, consistent with the cryo-EM and earlier indirect analyses (*1*, *5*). This model raises two fundamental questions: (i) How are protofilaments connected to each other to make the very long and thin ring or helix? (ii) How are the protofilaments attached to the membrane? The first question still has no answer, but the second question was recently answered by Pichoff and Lutkenhaus (*6*), who demonstrated that FtsZ is tethered to the membrane by FtsA. Specifically, the C-terminal peptide of FtsZ binds FtsA, and the C terminus of FtsA forms an amphipathic helix that inserts into the membrane (Fig. 1B).

In addition to FtsZ and FtsA, the Z ring contains nearly a dozen other proteins that are essential for cell division. These proteins appear to function in later steps, especially in remodeling the peptidoglycan wall. Z ring assembly requires only FtsZ and either FtsA or ZipA (*6*, *7*). We have suggested earlier that FtsZ, in addition to providing the cytoskeletal framework, may also generate the constriction force (*8*). However, it has remained an open question whether force requires interactions with other proteins.

In the present study, we asked whether FtsZ could form a Z ring without FtsA if we provided a direct tether to the membrane. To test this possibility, we removed the FtsZ peptide that binds FtsA and ZipA and replaced it with an amphipathic helix, producing membrane-targeted FtsZ (FtsZ-mts) (Fig. 1C). We then expressed FtsZ-mts in the *Escherichia coli* strain JKD7 1(pKD3), in which the native FtsZ can be suppressed by growth at 42°C (*9*, *10*). The depletion of FtsZ blocked cell division and caused the cells to grow into long filaments. In these filamentous cells, the FtsZ-mts formed abundant Z rings and helical structures, which are very similar to native Z rings (Fig. 2). We concluded that Z ring assembly does not require FtsA, but only the membrane-targeting amphipathic helix.

Having achieved the reconstitution of the Z rings in *E. coli*, we next attempted reconstitution in a liposome system in vitro. We made large multilamellar vesicles (*11*), which were initially mostly spherical, with a tendency to aggregate into irregular clumps. We then mixed the liposomes with FtsZ and guanosine 5′-triphosphate (GTP) (GTP is necessary for polymerization), put a drop on a slide, and placed a coverslip on it. Initially, the FtsZ-mts was on the outside of the vesicles, but

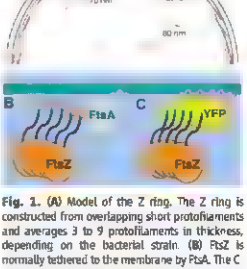

Fig. 1. (A) Model of the Z ring. The Z ring is constructed from overlapping short protofilaments and averages 3 to 9 protofilaments in thickness, depending on the bacterial strain. **(B)** FtsZ is normally tethered to the membrane by FtsA. The C-terminal peptide (orange) of FtsZ binds FtsA, and FtsA binds the membrane by its amphipathic helix (purple). **(C)** In FtsZ-mts, the FtsA-binding peptide is replaced with yellow fluorescent protein (YFP) and an amphipathic helix.

Department of Cell Biology, Duke University Medical Center, Durham, NC 27710–3709, USA.

*To whom correspondence should be addressed. E-mail: h.erickson@cellbio.duke.edu

during these manipulations tubular liposomes formed and some of these incorporated FtsZ-mts inside. We do not know how this process occurs.

Inside the liposomes, the FtsZ-mts spontaneously assembled into multiple Z rings, almost all of them being closed rings perpendicular to the axis of the tube (Fig. 3). The liposomes frequently showed indentations or constrictions at the site of the brighter Z rings. The constrictions usually distorted the entire wall of the thick, multilamellar liposome (Fig. 3A) but sometimes appeared to detach the inner layers (Fig. 3B). In some cases, a constriction already present in our first image constricted further a few minutes later (Fig. 3C). We have not observed any convincing cases of constrictions proceeding all the way to liposome division. The limited constriction is perhaps due to the rigidity of the thick walls of the multilamellar liposomes, we have not yet succeeded in producing tubular liposomes with thinner walls.

Movie S1 depicts a tubular liposome observed over a period of 10 min. Initially the liposome contained multiple dim Z rings and no membrane constrictions (fig. S1, 0 and 100 s). These dim Z rings were found to slide back and forth along the length of the tube. When Z rings collided, they coalesced and produced brighter Z rings, and visible constrictions of the liposome wall appeared over them (fig. S1, 200 and 300 s). The constrictions in movie S1 are slight (see Figs. 3 and 4 and movies S2 and S3 for more prominent constrictions), but fig. S1 (taken from movie S1) illustrates that constrictions (i) appear only after the formation of bright Z rings and (ii) coincide with the locations of Z rings. We also observed that when dim Z rings coalesce to make bright ones, they never reemerge. This may be because the Z ring material is generating a constriction force, making it unfavorable to move uphill toward the larger diameter and away from the constriction.

Whereas Fig. 3, movie S1, and fig. S1 show constrictions developing at the sites of bright Z rings, Fig. 4 illustrates an example of the opposite. In this experiment, we reduced the GTP from 400 to 100 μM, and we estimated that the GTP should be exhausted in ~20 min. The liposome in Fig. 4 showed a deep constriction centered on a bright Z ring at early time points (Fig. 4, 50 and 250 s). Eight minutes later, the constriction relaxed slightly for ~20 s (Fig. 4, 450 s) and then abruptly relaxed completely (Fig. 4, 460 s; this abrupt expansion is much more dramatic in movie S2). The Z ring did not collapse or disassemble but expanded uniformly to the larger diameter. The expansion occurred in less than 10 s and remained stable for more than 20 min. A second Z ring in the liposome abruptly relaxed its constriction 2 min later (movie S2). The remaining dim Z rings mostly disappeared over the next 20 min, consistent with the exhaustion of GTP. This series suggests that the early constrictions were maintained by a Z ring–dependent force and relaxed when these Z rings lost their ability to maintain the force. Movie S3 depicts another series where initially weak constrictions deepened over 10 min and then relaxed as the GTP was depleted. We also tested assembly in guanosine 5′-[(α,β)-methyleno] triphosphate (GMPCPP), which is hydrolyzed 3 to 10 times more slowly than GTP (*12*). GMPCPP supported the assembly of Z rings in the liposomes, and these liposomes had small constrictions.

Some tubular liposomes had Z rings, and others did not. This provided an additional opportunity to test the association of Z rings with constrictions. We measured by eye the frequency of visible indentations in tubular liposomes with inside diameters of <2.5 μm. In liposomes that did not contain Z rings, we counted 32 visible indentations over a total length of 2222 μm. In

Fig. 2. FtsZ-mts was expressed in *E. coli* depleted of wild-type FtsZ, which forms long filaments because division is blocked. FtsZ-mts formed numerous Z rings and tight-pitch helices.

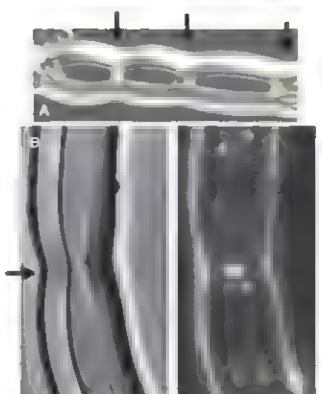

Fig. 3. FtsZ-mts and GTP were mixed with liposomes. Although the FtsZ-mts was initially outside the liposomes, some tubular, multilamellar liposomes were formed that enclosed FtsZ-mts and GTP. The FtsZ assembled into Z rings in these tubular liposomes. **(A)** A liposome with three bright Z rings, each centered on a constriction. The fluorescent FtsZ is shown in yellow, superimposed on the differential interference contrast image of the liposome. Arrows indicate Z rings. **(B)** The bright Z ring near the middle (indicated by the arrow) is forming a visible constriction and on the right side appears to have detached some inner layers of the multilamellar wall. **(C)** A liposome is shown here with a visible constriction at the Z ring when first observed, 5 to 10 min after making the specimen. Six minutes later the constriction has narrowed markedly. See movie S1 for a 10-min series showing Z rings coalescing into brighter ones, which generate constrictions.

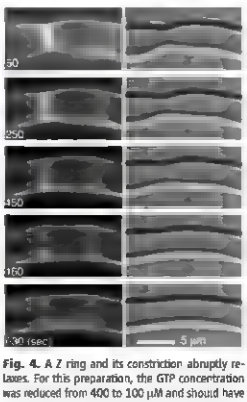

Fig. 4. A Z ring and its constriction abruptly relaxes. For this preparation, the GTP concentration was reduced from 400 to 100 μM and should have been exhausted in ~20 min. The first image was obtained ~10 min after mixing liposomes with FtsZ-mts and GTP, and images were taken every 10 s for another 60 min. Elapsed times after the first image are indicated on the frames. See movie S2 for the complete time series.

liposomes that contained Z rings, we counted 44 indentations over a total length of 575 μm. These indentations almost always coincided with a bright Z ring. Indentations or constrictions were thus five times more frequent in tubular liposomes that contained Z rings than in those without Z rings.

If the Z rings are generating a constriction force in the liposomes, they are doing this without a motor molecule. What could be the mechanism of force generation? We have previously reported that FtsZ can switch from a straight protofilament in GTP to a highly curved conformation in guanosine diphosphate (*8*, *13*, *14*). This conformational change is a candidate for force generation by FtsZ alone. Li *et al.* (*4*) also suggested that individual protofilaments may be generating a constriction force on the membrane segments to which they are attached.

A notable feature of the reconstituted Z rings is their strong tendency to form perfect closed rings that are oriented perpendicular to the axis of the tube. These features are consistent with the generation of a constriction force. If a filament grew longitudinally while attached to the membrane, in the absence of any force it might assume a loose helical shape or even more irregular course. If it is generating a constriction force, it would tend toward a minimum diameter, which would be a ring perpendicular to the axis (*15*).

The images of Li *et al.* (*4*) show individual protofilaments with few contacts between them. This raises the possibility that the assembly of protofilaments to form the long, thin Z ring is not propagated by direct lateral contacts between FtsZ protofilaments. An alternative mechanism is that a protofilament, by inserting amphipathic helices and exerting a force on the membrane, may produce distortions of the membrane that favor the attachment of additional protofilaments near the ends. This assembly, which would favor the formation of closed rings, might also be a source of constriction force.

Because FtsA is an actin homolog and is known to form dimers or oligomers (*16*, *17*), we initially thought that FtsA self-association might play an essential role in Z ring assembly. However, our reconstitution shows that neither FtsA nor downstream division proteins are required for Z ring assembly. FtsZ, a membrane tether, and the interior curved surface of a tubular liposome are sufficient for this assembly and the generation of a constriction force.

The earliest cellular life forms probably contained a replicating system of macromolecules surrounded by a lipid membrane. A mechanism would be needed to divide this living liposome. Our simple system may recapitulate the primordial division machine (*18*).

References and Notes

1. Y. Chen, H. P. Erickson, *J. Biol. Chem.* **280**, 22549 (2005).
2. S. Thanedar, W. Margolin, *Curr. Biol.* **14**, 1167 (2004).
3. P. C. Peters, M. D. Migliozzi, C. Thoni, E. J. Harry, *Mol. Microbiol.* **64**, 487 (2007).
4. Z. Li, M. J. Trimble, Y. V. Brun, G. J. Jensen, *EMBO J.* **26**, 4694 (2007).
5. D. E. Anderson, F. J. Gueiros-Filho, H. P. Erickson, *J. Bacteriol.* **186**, 5775 (2004).
6. S. Pichoff, J. Lutkenhaus, *Mol. Microbiol.* **55**, 1722 (2005).
7. S. Pichoff, J. Lutkenhaus, *EMBO J.* **21**, 685 (2002).
8. H. P. Erickson, *Trends Cell Biol.* **7**, 362 (1997).
9. R. Dai, J. Lutkenhaus, *J. Bacteriol.* **173**, 3500 (1991).
10. S. D. Redick, J. Stricker, G. Briscoe, H. P. Erickson, *J. Bacteriol.* **187**, 2727 (2005).
11. Methods are available as supporting material on *Science* Online.
12. L. Romberg, M. Simon, H. P. Erickson, *J. Biol. Chem.* **276**, 11743 (2001).
13. H. P. Erickson, D. W. Taylor, K. A. Taylor, D. Bramhill, *Proc. Natl. Acad. Sci. U.S.A.* **93**, 519 (1996).
14. C. Lu, M. Reedy, H. P. Erickson, *J. Bacteriol.* **182**, 164 (2000).
15. S. S. Andrews, A. P. Arkin, *Biophys. J.* **93**, 1872 (2007).
16. A. Feucht, L. Lucet, M. D. Yudkin, J. Errington, *Mol. Microbiol.* **40**, 115 (2001).
17. B. Lara *et al.*, *Mol. Microbiol.* **55**, 699 (2005).
18. H. P. Erickson, *Bioessays* **29**, 668 (2007).
19. This work was supported by NIH grant GM66014.

Supporting Online Material

www.sciencemag.org/cgi/content/full/1154520/DC1
Materials and Methods
Fig. S1
References
Movies S1 to S3

21 December 2007; accepted 25 February 2008
Published online 17 April 2008
10.1126/science.1154520
Include this information when citing this paper

Architecture of a Charge-Transfer State Regulating Light Harvesting in a Plant Antenna Protein

Tae Kyu Ahn,[1,2]* Thomas J. Avenson,[2,3]* Matteo Ballottari,[4] Yuan-Chung Cheng,[2] Krishna K. Niyogi,[2,3] Roberto Bassi,[4]† Graham R. Fleming[1,2]†

Energy-dependent quenching of excess absorbed light energy (qE) is a vital mechanism for regulating photosynthetic light harvesting in higher plants. All of the physiological characteristics of qE have been positively correlated with charge transfer between coupled chlorophyll and zeaxanthin molecules in the light-harvesting antenna of photosystem II (PSII). We found evidence for charge-transfer quenching in all three of the individual minor antenna complexes of PSII (CP29, CP26, and CP24), and we conclude that charge-transfer quenching in CP29 involves a delocalized state of an excitonically coupled chlorophyll dimer. We propose that reversible conformational changes in CP29 can "tune" the electronic coupling between the chlorophylls in this dimer, thereby modulating the energy of the chlorophyll-zeaxanthin charge-transfer state and switching on and off the charge-transfer quenching during qE.

The photosynthetic apparatus in higher plants is designed to perform two seemingly opposing tasks: to efficiently harvest sunlight and transfer excitation energy to the reaction center (RC), but also to rapidly dissipate excessively absorbed light energy harmlessly as heat to avoid deleterious photodamage. Because highly reactive chemical species are inevitable by-products of photosynthesis, various regulatory processes are critical for the robustness of photosynthesis and for plant survival (*1*). Regulation of light harvesting is predominantly mediated by energy-dependent quenching (qE) (*2*, *3*), a phenomenon that depends on the transthylakoid pH gradient (ΔpH) (*4*), zeaxanthin (*Z*) (*5*), and the photosystem II (PSII) antenna-associated protein PsbS (*6*). However, precisely how and where within PSII these components interact to mediate qE at the molecular level is still not well understood. Identification of the precise molecular architecture that is responsible for this vital regulatory process could provide insight into the design principles of photoprotection in natural photosynthesis and could inspire approaches to engineer more robust artificial systems for solar energy conversion (*7*–*9*).

Two different mechanisms, which are not mutually exclusive, have been proposed recently to explain qE (*10*, *11*). According to Ruban *et al.* (*11*), qE occurs in the peripheral, trimeric antenna of PSII called LHCII (*12*), and its molecular mechanism involves energy transfer from chlorophyll *a* to a low-lying excited state of a carotenoid (lutein 1) in LHCII (*11*). A change in the conformation of a different carotenoid (neo-

[1]Physical Biosciences Division, Lawrence Berkeley National Laboratory, Berkeley, CA 94720, USA. [2]Department of Chemistry and QB3 Institute, University of California, Berkeley, CA 94720, USA. [3]Department of Plant and Microbial Biology, 111 Koshland Hall, University of California, Berkeley, CA 94720, USA. [4]Department of Science and Technology, University of Verona, 37134 Verona, Italy.

*These authors contributed equally to this work.
†To whom correspondence should be addressed. E-mail: grfleming@lbl.gov (G.R.F.); bass@sci.univr.it (R.B.)

xanthin) was identified spectroscopically and correlated with LHCII quenching in vitro, and this conformational change was in turn correlated with qE in vivo (*11*). On the other hand, we have proposed a charge-transfer (CT) mechanism for qE on the basis of quantum chemical calculations (*13*) and ultrafast pump-probe experiments (*10*, *14*). The CT mechanism involves energy transfer from the chlorophylls bound to the PSII LHCII supercomplex to a chlorophyll-Z heterodimer. The chlorophyll-Z heterodimer then undergoes charge separation followed by recombination, thereby transiently producing a Z radical cation ($Z^{\bullet+}$). Formation of $Z^{\bullet+}$ in thylakoids depends on the three components that are necessary for qE in vivo (*10*, *14*). In PSII, an inner layer of monomeric (minor) antenna proteins connects the peripheral LHCII trimers to the RC core complex (*15*, *16*). Evidence for CT quenching was recently demonstrated in a composite mixture of isolated minor antenna components (CP29, CP26, and CP24), whereas no trace of $Z^{\bullet+}$ formation signal could be found in isolated LHCII trimers (*14*). Thus, it is possible that different qE mechanisms are operating in different parts of the PSII antenna. Although each of these mechanisms has been proposed to account fully for qE (*11*, *14*), their relative contributions to qE in vivo remain to be determined.

To investigate the molecular architecture of CT quenching and to identify precisely which of the minor complexes are capable of mediating CT quenching, we carried out ultrafast transient absorption experiments in the spectral region of $Z^{\bullet+}$ absorption (*14*, *17*) using all three of the individual, isolated minor complexes. We expressed recombinant apoproteins of CP29, CP26, and CP24 in bacteria and reconstituted them in vitro with chlorophylls (a and b), lutein, and either Z or violaxanthin (V). In plants and isolated thylakoids, the reversible enzymatic conversion of V to Z is correlated with qE (*5*), and previous work has shown that CT quenching is associated with the presence of Z in intact systems (*10*) and in isolated proteins (*14*), whereas V-bound complexes are inactive. Herein we refer to the CP29 complexes reconstituted with Z and V as CP29-Z and CP29-V, respectively (table S1 and fig. S1). We excited the samples at 650 nm and probed the near infrared (NIR) region where carotenoid radical cation species ($Car^{\bullet+}$) exhibited strong absorption (*10*, *14*).

Figure 1A shows the transient absorption profile for CP29-V as compared to that of CP29-Z. Both exhibit rapid rise components followed by exponential decays. However, relative to the CP29-V kinetics, the CP29-Z kinetic profile shows a larger initial amplitude rise, the component dynamics of which are clearly evident in the NIR transient absorption difference trace (Fig. 1A). For example, the difference profile is characterized by both very rapid (<500 fs) and slower (~5.5 ps) rise components, followed by single-exponential decay with a time constant of ~238 ps. Such a profile is indicative of transient $Car^{\bullet+}$ formation and is a signature of CT quenching (*10*, *14*). The spectrum reconstructed from a series of such difference profiles obtained by probing from 880 to 1080 nm exhibits a broad absorption band with a maximum at ~980 nm (Fig. 1B), in good agreement with the established $Z^{\bullet+}$ absorption characteristics (*10*, *14*). Similarly, the NIR transient absorption kinetics for CP26 and CP24 reconstituted with Z were also characterized by transient $Z^{\bullet+}$ formation. These combined results suggest that CT quenching (e.g., involving a chlorophyll-Z species that undergoes charge separation followed by recombination) occurs within all three minor complexes. This finding is consistent with the results of genetic and spectroscopic analyses showing that no single antenna protein is specifically required for qE (*14*, *18*–*20*).

To further explore the molecular details of CT quenching in CP29, we studied a series of mutant CP29 complexes that each lacked a specific chlorophyll. According to the previously reported homology structural model (*21*, *22*), CP29 contains eight chlorophyll-binding sites referred to as A1, A2, A3, A4, A5, B3, B5, and B6, along with two carotenoid-binding sites referred to as L1 and L2 (Fig. 2). Versions of CP29 with mutated ligands to each chlorophyll were reconstituted in vitro with chlorophylls (a and b), lutein, and either V or Z, and stable complexes each lacking specific chlorophylls were recovered except for the A1 mutant. These complexes are referred to as, for example, $CP29_{A2}$, where the subscript denotes the missing chlorophyll (table S2 and figs. S2 to S5). Note that it has been established experimentally that Z binds specifically to the L2 domain, therefore, we can exclude the likelihood that chlorophyll A1 is directly involved in CT quenching (*23*, *24*).

The difference NIR transient absorption kinetic profile (blue trace) for $CP29_{B3}$ is characterized by both rise and decay components that are signatures of $Z^{\bullet+}$ evolution during CT quenching (Fig. 3A), implying that CT quenching is active in the absence of chlorophyll B3. Likewise, the difference profiles for $CP29_{A2}$, $CP29_{A3}$, $CP29_{A4}$, and $CP29_{B6}$ also exhibit evidence of CT quenching irrespective of some variation in $Z^{\bullet+}$ signal that might derive from pleiotropic effects on protein structure (fig. S6). These data show that CT quenching in CP29 is not eliminated by the removal of chlorophylls A2, A3, A4, B3, or B6, thus excluding the likelihood of their participation in CT quenching. In contrast,

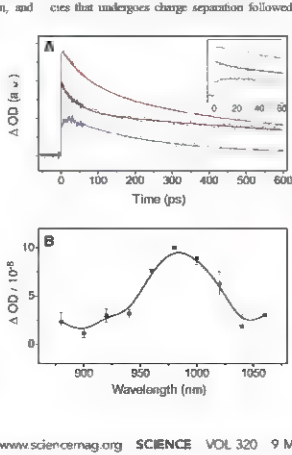

Fig. 1. NIR transient absorption kinetics for the CP29 minor complexes probed at 980 nm. **(A)** NIR transient absorption profiles for isolated CP29 complexes with excitation at 650 nm (chlorophyll b Q_y transition) and probing at 980 nm. The red and black profiles represent kinetics for CP29 complexes bound by Z and V, respectively. Note that the samples are prepared so that they have the same absorbance (0.3) at 650 nm, and these kinetic traces have not been normalized in any way. The difference kinetic trace (blue curve) is obtained by subtraction of the V-kinetic profiles from the Z-kinetic profiles. Inset: Transient absorption profiles over a shorter time region (0 to 60 ps). **(B)** NIR transient absorption spectrum for the isolated CP29 complexes. The spectrum was constructed from a series of NIR transient difference profiles obtained 15 ps after excitation by probing every 20 nm from 880 to 1080 nm. Error bars represent SE of five trials. The solid curve represents a b-spline interpolation among the experimental data points.

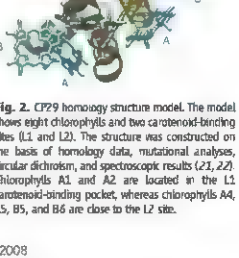

Fig. 2. CP29 homology structure model. The model shows eight chlorophylls and two carotenoid-binding sites (L1 and L2). The structure was constructed on the basis of homology data, mutational analyses, circular dichroism, and spectroscopic results (*21*, *22*). Chlorophylls A1 and A2 are located in the L1 carotenoid-binding pocket, whereas chlorophylls A4, A5, B5, and B6 are close to the L2 site.

the kinetic profiles for CP29 $_{A5}$, whether reconstituted with Z or V, are characterized solely by decay features attributable to chlorophyll excited-state absorption, and the transient absorption difference profile reveals no amplitude change relative to the noise level (Fig. 3B). The interpretation of this result is complicated by the fact that mutation of the amino acid residue that coordinates chlorophyll A5 also results in the loss of chlorophyll B5, specifically in Z-bound CP29 complexes (table S2). However, the kinetic profiles for CP29 $_{B5}$ (a complex lacking chlorophyll B5 only) are also characterized solely by chlorophyll excited-state absorption dynamics and no measurable Z^{+} formation signal (Fig. 3C), which clearly indicates that CT quenching in CP29 involves chlorophyll B5. According to the homology structural model (Fig. 4), chlorophyll B5 is placed farther away from Z (~13 Å) than is chlorophyll A5 (~6 Å). The chlorophyll A5-B5 pair is positioned within the L2 domain and chlorophyll A5 is orientated roughly cofacial to, and centered along the axis of, the Z binding site, which is in good agreement with the requirements for CT quenching previously predicted by quantum chemistry calculations (*13*). Furthermore, chlorophylls A5 and B5 are reported to be strongly coupled (*22*, *25*), and both are important for the regulation of chlorophyll excited states (*21*, *22*). Therefore, we conclude that CT quenching in CP29 most likely depends on both chlorophylls A5 and B5, and rather than a simple chlorophyll-Z heterodimer, the molecular site of CT quenching in CP29 comprises Z and a strongly coupled chlorophyll pair (A5 and B5).

What is the importance of this CT site architecture? Our finding indicates that the primary event of CT quenching in CP29 involves electron transfer from Z to a strongly coupled chlorophyll dimer in the A5-B5 pocket of CP29, rather than from Z to a monomeric chlorophyll molecule (*26*). Relative to a monomeric chlorophyll, a coupled chlorophyll dimer would be more favorable for CT quenching because the charge delocalization over the two chlorophylls will make the product CT state more stable. As a result, controlling the coupling strength between chlorophylls A5 and B5 in CP29, either by changing the distance between them or by altering their orientations, would modulate the reduction potential of the chlorophyll dimer and therefore could be used to switch on and off the CT quenching. This CT switching mechanism provides a potential molecular basis for the regulation of CT quenching during qE in the higher plant antenna.

The rapid reversibility of qE at the physiological level is thought to result from changes in the trans-thylakoid ΔpH that occur, for example, during fluctuations in incident solar flux density. It has been proposed that two thylakoid lumen-exposed glutamate residues of the PsbS protein sense these changes in pH (*27*) and induce protein conformational changes that control qE. Moreover, PsbS has recently been shown not to bind pigments (*28*) but to interact with CP29 (*29*). Therefore, we propose that pH-dependent protein conformational changes that are transduced from PsbS to CP29 (and possibly other minor antenna complexes) can alter the coupling strength between chlorophylls A5 and B5 in CP29 and induce CT quenching during qE. Experiments that can directly probe the efficiency of CT quenching while modulating the electronic coupling between chlorophylls A5 and B5 can test this proposal.

Converging results based on theoretical calculations, molecular genetic analysis, and ultrafast spectroscopy have shown that the mechanism involving CT quenching in minor complexes is emerging as a key component of qE. Our results show that CT quenching can occur in all three minor antenna complexes, which are positioned between LHCII and the RC, a perfect setting for regulating excitation energy transfer to the RC.

References and Notes

1. C. Külheim, J. Ågren, S. Jansson, *Science* **297**, 91 (2002).
2. P. Horton, A. V. Ruban, R. G. Walters, *Annu. Rev. Plant Phys.* **47**, 655 (1996).
3. K. K. Niyogi, *Annu. Rev. Plant Phys.* **50**, 333 (1999).
4. J. M. Bricantais, C. Vernotte, M. Picaud, G. H. Krause, *Biochim. Biophys. Acta* **548**, 128 (1979).
5. B. Demmig-Adams, *Biochim. Biophys. Acta* **1020**, 1 (1990).
6. X.-P. Li *et al.*, *Nature* **403**, 391 (2000).
7. R. Bassi *et al.*, *Proc. Natl. Acad. Sci. U.S.A.* **103**, 5343 (2006).
8. A. Hagfeldt, M. Grätzel, *Acc. Chem. Res.* **33**, 269 (2000).
9. T. A. Moore, A. L. Moore, D. Gust, *Philos. Trans. R. Soc. London Ser. B* **357**, 1481 (2002).
10. N. E. Holt *et al.*, *Science* **307**, 433 (2005).
11. A. V. Ruban *et al.*, *Nature* **450**, 575 (2007).
12. Z. Liu *et al.*, *Nature* **428**, 287 (2004).
13. A. Dreuw, G. R. Fleming, M. Head-Gordon, *Phys. Chem. Chem. Phys.* **5**, 3247 (2003).
14. T. J. Avenson *et al.*, *J. Biol. Chem.* **283**, 3550 (2008).
15. E. J. Boekema *et al.*, *Proc. Natl. Acad. Sci. U.S.A.* **92**, 175 (1995).
16. K. H. Rhee *et al.*, *Nature* **389**, 522 (1997).
17. S. Amarie *et al.*, *J. Phys. Chem. B* **111**, 3481 (2007).
18. J. Andersson, R. G. Walters, P. Horton, S. Jansson, *Plant Cell* **13**, 1193 (2001).
19. J. Andersson *et al.*, *Plant J.* **35**, 350 (2003).
20. L. Kovács *et al.*, *Plant Cell* **18**, 3106 (2006).
21. R. Bassi, R. Croce, D. Cugini, D. Sandona, *Proc. Natl. Acad. Sci. U.S.A.* **96**, 10056 (1999).
22. G. Cinque, R. Croce, A. Holzwarth, R. Bassi, *Biophys. J.* **79**, 1706 (2000).

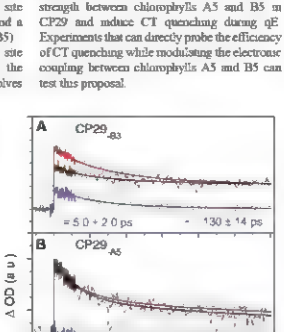

Fig. 3. NIR transient absorption kinetics for CP29 mutants lacking the ligands binding to chlorophylls B3, A5, and B5. Transient absorption profiles were measured using CP29 $_{B3}$ (**A**), CP29 $_{A5}$ (**B**), and CP29 $_{B5}$ (**C**). Other conditions are the same as Fig. 1A.

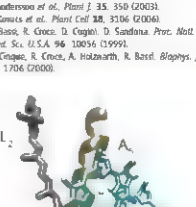

Fig. 4. Molecular details of the CT quenching site in CP29. Molecular sites responsible for CT quenching in CP29, including the Z bound in the L2 site and chlorophylls A5 and B5, are shown. On the basis of the homology model, the center-center distances for chlorophyll A5 to Z, chlorophyll A5 to chlorophyll B5, and chlorophyll B5 to Z are estimated to be ~6 Å, ~10 Å, and ~13 Å, respectively. The dihedral angle between chlorophylls A5 and B5 is about 41°. The structure indicates that chlorophylls A5 and B5 are strongly coupled to each other.

23. J. P. Connelly *et al.*, *Biochemistry* **36**, 281 (1997).
24. T. Morosinotto, S. Caffarri, L. Dall'Osto, R. Bassi, *Physiol. Plant.* **119**, 347 (2003).
25. H. van Amerongen, R. van Grondelle, *J. Phys. Chem. B* **105**, 604 (2001).
26. Formation of a delocalized chlorophyll dimer would depend on occupancy of both A5 and B5 sites by chlorophyll a. Although the A5 site exclusively binds chlorophyll a, B5 is a mixed site of chlorophylls a and b in minor complexes (CP29, CP26, and CP24) (22). Therefore, a delocalized chlorophyll a dimer can form within the A5 and B5 sites in CP29. Moreover, this dimer structure could also explain why $Z^{\cdot+}$ formation is not favored in LHCII (14), in which the A5 and B5 sites specifically bind chlorophylls a and b, respectively (22). Because the large spectral absorbance gap (~700 cm^{-1}) between chlorophylls a and b prohibits delocalization over a chlorophyll heterodimer, no CT state can be produced in the L2 site of LHCII. One additional factor of specificity is that the capacity of LHCII to undergo exchange of V to Z in site L2 in vivo is very low relative to minor complexes (22).
27. X.-P. Li *et al.*, *J. Biol. Chem.* **279**, 22866 (2004).
28. G. Bonente *et al.*, *J. Biol. Chem.* **283**, 8434 (2008).
29. E. Teardo *et al.*, *Biochim. Biophys. Acta* **1767**, 703 (2007).

30. We thank D. Zigmantas for helpful discussions. Supported by Korea Research Foundation grant KRF 2006-214-C00037 funded by the Korean Government (T.K.A.); USDA National Research Initiative competitive grant 2006-03279 (T.J.A.); Office of Basic Energy Sciences, Chemical Sciences Division, U.S. Department of Energy contract DE-AC03-76SF000098 (G.R.F. and K.K.N.); and Italian Basic Research Foundation contract RBLA0345SF and Trento Research Council contract SAMBA (R.B.).

Supporting Online Material
www.sciencemag.org/cgi/content/full/320/5877/794/DC1
Materials and Methods
Figs. S1 to S6
Tables S1 and S2
References

3 January 2008; accepted 7 April 2008
10.1126/science.1154800

Phosphorylation of Retinoblastoma Protein by Viral Protein with Cyclin-Dependent Kinase Function

Adam J. Hume,[1] Jonathan S. Finkel,[2] Jeremy P. Kamil,[3] Donald M. Coen,[3] Michael R. Culbertson,[2] Robert F. Kalejta[1]*

As obligate intracellular parasites, viruses expertly modify cellular processes to facilitate their replication and spread, often by encoding genes that mimic the functions of cellular proteins while lacking regulatory features that modify their activity. We show that the human cytomegalovirus UL97 protein has activities similar to cellular cyclin–cyclin-dependent kinase (CDK) complexes. UL97 phosphorylated and inactivated the retinoblastoma tumor suppressor, stimulated cell cycle progression in mammalian cells, and rescued proliferation of *Saccharomyces cerevisiae* lacking CDK activity. UL97 is not inhibited by the CDK inhibitor p21 and lacks amino acid residues conserved in the CDKs that permit the attenuation of kinase activity. Thus, UL97 represents a functional ortholog of cellular CDKs that is immune from normal CDK control mechanisms.

Cyclin–cyclin-dependent kinase (CDK) complexes are found in all eukaryotes and control cell cycle progression and other processes (*1*). In higher eukaryotes, a major target of the CDKs is the retinoblastoma (Rb) tumor-suppressor protein that controls progression through G_1 phase of the cell cycle. The pathway controlled by Rb may be aberrant in most human cancers (*2*). Unphosphorylated Rb binds to E2F transcription factors, thus inhibiting the expression of genes required for DNA replication and arresting cell cycle progression in G_0 or G_1 phase. During normal cell cycle progression, Rb is functionally inactivated by multiple phosphorylations mediated sequentially by a series of CDK complexes (*3*). Phosphorylation of Rb disrupts complexes with E2Fs, allowing for cell cycle progression into S phase. To create an advantageous cellular environment for viral replication, viruses can inactivate Rb through direct binding of viral proteins to Rb and the consequent disruption of Rb-E2F complexes, by causing Rb degradation, or through constitutive activation of cellular CDKs by virally encoded cyclin proteins (*4*, *5*). Here, we describe a virally encoded protein kinase that directly phosphorylates Rb, and we show that this kinase can substitute for CDKs during cell cycle regulation.

[1]Institute for Molecular Virology and McArdle Laboratory for Cancer Research, University of Wisconsin–Madison, Madison, WI 53706, USA. [2]Laboratories of Genetics and Molecular Biology, University of Wisconsin–Madison, Madison, WI 53706, USA. [3]Department of Biological Chemistry and Molecular Pharmacology, Harvard Medical School, Boston, MA 02115, USA.

*To whom correspondence should be addressed. E-mail: rfkalejta@wisc.edu

Upon infection of quiescent cells with human cytomegalovirus (HCMV), unphosphorylated Rb is first degraded by pp71 (*6*) and then phosphorylated (*7*, *8*) (Fig. 1A and fig. S1). Phosphorylated Rb migrates more slowly during SDS-polyacrylamide gel electrophoresis than does the unphosphorylated form of the protein, and it can be detected in lysates from HCMV-infected cells within 4 hours after infection (Fig. 1A). Three small-molecule inhibitors of CDK activity (roscovitine, olomoucine, and flavopiridol) inhibited Rb phosphorylation induced by serum stimulation, but not phosphorylation induced by HCMV infection (Fig. 1B). Additional experiments with a panel of 20 kinase inhibitors (table S1) revealed that only 2, Gö6976 and NGIC-I, inhibited Rb phosphorylation during HCMV infection (Fig. 1C). These drugs inhibit both cellular protein kinase C (PKC) and the HCMV protein kinase UL97 (*9*). However, Gö7478, an inhibitor of PKC that does not inhibit UL97, did not reduce Rb phosphorylation in HCMV-infected cells (Fig. 1C). Because an HCMV mutant lacking the UL97 gene (*10*) did not induce Rb phosphorylation (Fig. 1, D and E) and because of the presence of three potential Rb-binding motifs in UL97 (fig. S2), we suspected that UL97 was required for Rb phosphorylation during HCMV infection.

Phosphorylation of Rb on Ser^{780}, Ser^{807}, Ser^{811}, and Thr^{821} inactivates the cell cycle–inhibitory and tumor suppressor functions of Rb by disrupting Rb-E2F complexes (*3*). All of these residues are phosphorylated in HCMV-infected cells (Fig. 2A). Residues not known to modify Rb function upon phosphorylation, such as Ser^{249} and Thr^{252}, were not phosphorylated in HCMV-infected cells but were phosphorylated in serum-stimulated cells (Fig. 2A). A recombinant HCMV in which the wild-type (WT) UL97 gene was replaced with an allele encoding a UL97 protein substituted at the active site Lys ($Lys^{355} \rightarrow Gln^{355}$; K355Q) failed to induce phosphorylation of Rb, but a WT revertant virus derived from the K355Q mutant did induce the phosphorylation of Rb (Fig. 2B). The UL97 K355Q mutant virus exhibited a growth defect similar to that of the UL97-null virus, and the growth defect was rescued in the revertant virus (fig. S3). The CDK inhibitor flavopiridol again failed to prevent HCMV-induced phosphorylation of Rb in HCMV-infected cells, but two drugs that inhibit UL97 kinase activity (Gö6976 and maribavir) did inhibit such phosphorylation (fig. S4). Thus, in HCMV-infected cells, kinase activity of UL97 is necessary for Rb phosphorylation on residues that inactivate its function. Rb degradation and phosphorylation in HCMV-infected cells are independent events (fig. S1).

We also tested whether UL97 alone is sufficient to induce Rb phosphorylation. Transfection of expression plasmids for epitope-tagged wild type [but not a catalytically inactive ($Lys^{355} \rightarrow Met^{355}$; K355M) mutant (*11*)] induced the phosphorylation of cotransfected Rb on inactivating residues (Fig. 3A) in Saos-2 cells that are intrinsically unable to phosphorylate Rb. Drugs that inhibit UL97 partially suppressed Rb phosphorylation when added to UL97-expressing

Saos-2 cells, but those that inhibit the CDKs or only PKC did not (Fig. 3B). The K355M mutant protein was readily detected by protein immunoblotting, but WT UL97 was consistently expressed in lower amounts. Inhibition of kinase activity of WT UL97 with drugs also seemed to allow accumulation of more protein (Fig. 3B), perhaps indicating that active UL97 is toxic to mammalian cells. Nevertheless, UL97 expression was sufficient to induce Rb phosphorylation. Purified UL97 phosphorylated an Rb fragment in vitro, as assayed by the incorporation of ^{32}P (Fig. 3C), or with an antibody that specifically recognized Rb phosphorylated on Ser^{807} and Ser^{811} (Fig. 3D). Autophosphorylation was also detected (fig. S5). UL97 showed the same spectrum of sensitivity to kinase inhibitors in vitro as was observed for Rb phosphorylation in HCMV-infected cells (Fig. 3, C and D), and purified catalytically inactive (K355Q) UL97 failed to phosphorylate Rb in vitro (Fig. 3, C and D). These results make it unlikely that a copurifying insect kinase phosphorylated Rb in this assay.

UL97 directly phosphorylates Rb on multiple residues, an activity shared by cellular CDKs. Therefore, we tested whether UL97 represents a functional CDK ortholog by testing if

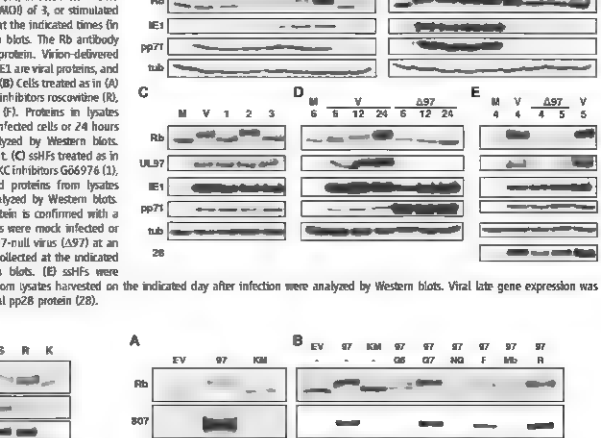

Fig. 1. Requirement of viral UL97 protein kinase, but not cellular CDKs, for Rb phosphorylation in HCMV-infected cells. **(A)** Subconfluent human fibroblasts deprived of serum (ssHFs) were mock-infected (M), infected with HCMV (V) at a multiplicity of infection (MOI) of 3, or stimulated with serum (S). Lysates prepared at the indicated times (in hours) were analyzed by Western blots. The Rb antibody (4H1) detects all forms of the protein. Virion-delivered pp71 (71) and newly synthesized IE1 are viral proteins, and tubulin (tub) is a loading control. **(B)** Cells treated as in (A) were also incubated with the CDK inhibitors roscovitine (R), olomoucine (O), or flavopiridol (F). Proteins in lysates harvested at 6 hours from virus-infected cells or 24 hours from uninfected cells were analyzed by Western blots. Dashes indicate no drug treatment. **(C)** ssHFs treated as in (A) were also incubated with the PKC inhibitors Gö6976 (1), Gö7874 (2), or NGIC-I (3), and proteins from lysates collected after 6 hours were analyzed by Western blots. Expression of the viral UL97 protein is confirmed with a UL97 specific antibody. **(D)** ssHFs were mock infected or infected with WT HCMV or a UL97-null virus (Δ97) at an MOI of 1. Proteins from lysates collected at the indicated hour were analyzed by Western blots. **(E)** ssHFs were treated as in (D), and proteins from lysates harvested on the indicated day after infection were analyzed by Western blots. Viral late gene expression was confirmed by detection of the viral pp28 protein (28).

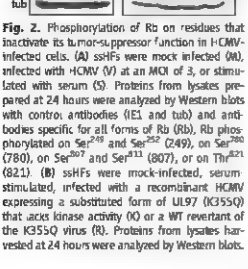

Fig. 2. Phosphorylation of Rb on residues that inactivate its tumor-suppressor function in HCMV-infected cells. **(A)** ssHFs were mock infected (M), infected with HCMV (V) at an MOI of 3, or stimulated with serum (S). Proteins from lysates prepared at 24 hours were analyzed by Western blots with control antibodies (IE1 and tub) and antibodies specific for all forms of Rb (Rb), Rb phosphorylated on Ser^{249} and Ser^{252} (249), on Ser^{780} (780), on Ser^{807} and Ser^{811} (807), or on Thr^{821} (821). **(B)** ssHFs were mock-infected, serum-stimulated, infected with a recombinant HCMV expressing a substituted form of UL97 (K355Q) that lacks kinase activity (K) or a WT revertant of the K355Q virus (R). Proteins from lysates harvested at 24 hours were analyzed by Western blots.

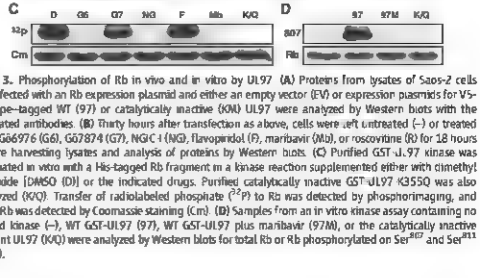

Fig. 3. Phosphorylation of Rb in vivo and in vitro by UL97. **(A)** Proteins from lysates of Saos-2 cells transfected with an Rb expression plasmid and either an empty vector (EV) or expression plasmids for V5-epitope–tagged WT (97) or catalytically inactive (KM) UL97 were analyzed by Western blots with the indicated antibodies. **(B)** Thirty hours after transfection as above, cells were left untreated (–) or treated with Gö6976 (G6), Gö7874 (G7), NGIC-I (NG), flavopiridol (F), maribavir (Mb), or roscovitine (R) for 18 hours before harvesting lysates and analysis of proteins by Western blots. **(C)** Purified GST-UL97 kinase was incubated in vitro with a His-tagged Rb fragment in a kinase reaction supplemented either with dimethyl sulfoxide (DMSO (D)) or the indicated drugs. Purified catalytically inactive GST-UL97 K355Q was also analyzed (K/Q). Transfer of radiolabeled phosphate (^{32}P) to Rb was detected by phosphorimaging, and total Rb was detected by Coomassie staining (Cm). **(D)** Samples from an in vitro kinase assay containing no added kinase (–), WT GST-UL97 (97), WT GST-UL97 plus maribavir (97M), or the catalytically inactive mutant UL97 (K/Q) were analyzed by Western blots for total Rb or Rb phosphorylated on Ser^{807} and Ser^{811} (807).

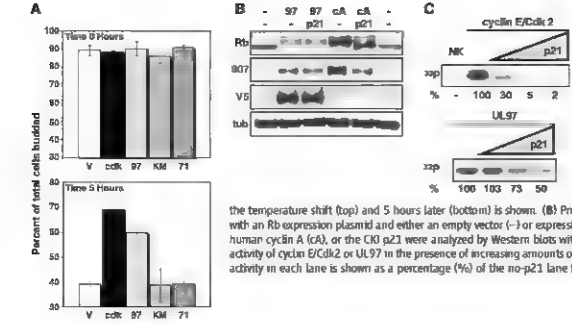

Fig. 4. CDK-like activity of HCMV UL97. (**A**) Saturated cultures of the yeast temperature-sensitive strain carrying *cdc28-13* and harboring a plasmid without a transgene (V) or one expressing WT UL97 (97), catalytically inactive UL97 (KM), HCMV pp71 (71), or cellular Cdk1 (CDK), each under the control of a galactose-inducible promoter, were diluted into galactose-induction medium for one doubling at the permissive temperature and then switched to the restrictive temperature. The number of budded cells [presented as a percentage of total cells with SDs (error bars), present at the time of the temperature shift (top) and 5 hours later (bottom)] is shown. (**B**) Proteins from lysates of Saos-2 cells transfected with an Rb expression plasmid and either an empty vector (–) or expression plasmids for V5-epitope–tagged WT UL97, human cyclin A (cA), or the CKI p21 were analyzed by Western blots with the indicated antibodies. (**C**) In vitro kinase activity of cyclin E/Cdk2 or UL97 in the presence of increasing amounts of p21 was determined as in Fig. 3C. The kinase activity in each lane is shown as a percentage (%) of the no-p21 lane for each set of reactions. NK, no kinase.

UL97 could rescue the cell cycle defect of yeast lacking CDK activity. A yeast mutant (*13*) with a temperature-sensitive allele of the single CDK gene (*cdc28-13*) arrests in G_1 as unbudded cells at the restrictive temperature (Fig. 4A and fig. S6). Expression of human Cdk1 or WT UL97 allowed the cells to remain cycling at the restrictive temperature (Fig. 4A). Catalytically inactive UL97, or the viral pp71 protein (*6*), failed to rescue the cell cycle defect. UL97 also stimulated the cell cycle of mammalian cells (fig. S7). The functional properties presented here lead us to conclude that UL97 is a viral CDK functional ortholog.

We expanded an alignment (*13*) of the kinase subdomains of UL97 with four cellular Ser/Thr kinases (including Cdk2) to include the intervening sequences (fig. S8). Our analysis suggested that UL97 is not subject to the regulatory mechanisms that control CDK activity (*14*), and we confirmed that prediction. UL97 lacks most of the residues of Cdk2 that make contacts with cyclin A, including the conserved PSTAIRE (*15*) helix required for cyclin binding (*16*), indicating that UL97 is unlikely to bind to cyclins. Because cyclins did not copurify with UL97 during tandem affinity purification (*17*) and because of the high activity of UL97 on Rb in vitro (Fig. 3, C and D) in the absence of a cyclin, we conclude that UL97 does not require cyclin binding for activity. The affinity of CDKs for cyclins is enhanced by CDK activating kinase (CAK)–mediated phosphorylation (*18*) of CDKs on Thr[160]. Neither the Thr nor any of the three Arg residues of CDKs that coordinate the phosphate (*16*) are conserved in UL97 (fig. S8). Because flavopiridol and roscovitine, both CAK inhibitors (*18*), do not inhibit the ability of UL97 to phosphorylate Rb in vivo (Figs. 1B and 3B and fig. S4), we conclude that CAK-mediated phosphorylation does not activate UL97. CDK activity is attenuated by phosphorylation on Tyr[15] during G_2 phase of the cell cycle and in response to radiation (*19*). UL97 has a Phe substitution (fig. S8) and thus cannot be phosphorylated at this site. UL97 (fig. S8) lacks most of the conserved CDK residues (*1*, *14*) that interact with members of both classes of CDK inhibitors (CKIs): p21, a potent CKI (*20*), did not efficiently inhibit UL97-mediated phosphorylation of Rb in vivo (Fig. 4B) or in vitro (Fig. 4C).

UL97 is a viral CDK ortholog that is immune from normal cellular control mechanisms that attenuate CDK activity and represents a previously unknown mechanism through which viruses regulate the cell cycle. The remote sequence similarity between CDKs and conserved herpesvirus protein kinases (CHPKs) such as UL97 led others to speculate that CHPKs may mimic CDK function (*13*). We provide direct experimental evidence that UL97 is functionally orthologous to cellular CDKs. UL97 is a target for anti-HCMV therapies because it phosphorylates (and thus activates) the antiviral drug ganciclovir (*21*) and because it is inhibited by maribavir (*22*). UL97 may also be useful as a tool to study the inactivation of the Rb pathway by phosphorylation, to identify other critical substrates of CDKs, and to probe the evolutionary relationships between viral and host cell kinases.

References and Notes

1. D. O. Morgan, *Annu. Rev. Cell Dev. Biol.* **13**, 261 (1997).
2. R. A. Weinberg, *Cell* **81**, 323 (1995).
3. P. D. Adams, *Biochim. Biophys. Acta* **1471**, M123 (2001).
4. A. M. Heil, D. A. Galloway, *Carcinogenesis* **24**, 359 (2003).
5. E. W. Varnum, N. Jones, G. I. Evan, *J. Gen. Virol.* **85**, 1347 (2004).
6. N. F. Kalejta, J. T. Bechtel, T. Shenk, *Mol. Cell. Biol.* **23**, 1885 (2003).
7. F. M. Jault *et al.*, *J. Virol.* **69**, 6697 (1995).
8. Materials and methods are available as supporting material on Science Online.
9. M. Marschall *et al.*, *J. Gen. Virol.* **82**, 1439 (2001).
10. M. M. Prichard *et al.*, *J. Virol.* **73**, 5663 (1999).
11. M. M. Prichard, W. J. Britt, S. L. Daily, C. B. Hartline, E. R. Kern, *J. Virol.* **79**, 15494 (2005).
12. C. Wittenberg, K. Sugimoto, S. I. Reed, *Cell* **62**, 225 (1990).
13. D. Romanos *et al.*, *J. Mol. Biol.* **287**, 821 (1999).
14. M. P. Paudelich, *J. Mol. Biol.* **287**, 821 (1999).
15. Single-letter abbreviations for the amino acid residues are as follows: A, Ala; C, Cys; D, Asp; E, Glu; F, Phe; G, Gly; H, His; I, Ile; K, Lys; L, Leu; M, Met; N, Asn; P, Pro; Q, Gln; R, Arg; S, Ser; T, Thr; V, Val; W, Trp, and Y, Tyr.
16. P. D. Jeffrey *et al.*, *Nature* **376**, 313 (1995).
17. J. P. Kamil, D. M. Coen, *J. Virol.* **81**, 10659 (2007).
18. G. Lolli, L. N. Johnson, *Cell Cycle* **4**, 572 (2005).
19. J. P. Wolfbaum *et al.*, *J. Biol. Chem.* **282**, 3173 (2007).
20. J. W. Harper, G. R. Adami, N. Wei, K. Keyomarsi, S. J. Elledge, *Cell* **75**, 805 (1993).
21. V. Sullivan *et al.*, *Nature* **358**, 85 (1992).
22. K. K. Biron *et al.*, *Antimicrob. Agents Chemother.* **46**, 2365 (2002).

23. We thank P. Balandyk for expert technical assistance. M. Prichard and W. Bresnahan for viruses, the National Cancer Institute for flavopiridol; K. Biron and J. Drach for maribavir; D. Engel, L. Schang, P. Adams, and W. El Deiry for plasmids; and S. Reed for the *cdc28-13* yeast strain. This work was funded by NIH training grants T32 CA009135-31 and T32 GM007215 (to A.J.H.); T32 GM077078-03 (to J.S.F.), and T32 AI07245 (to J.P.K.). This work was supported by NIH grants AI26077 (to D.M.C.) and GM65172 (to M.R.C.) and grants from the American Heart Association the Wisconsin Partnership for a Healthy Future and NIH Pledge grant RS6-AI064703 (to R.F.K.). R.F.K. is a Burroughs Wellcome Fund Investigator in Pathogenesis. All experiments were conceived and designed by A.J.H. and R.F.K., and they performed all of the experiments except those in yeast (codesigned and performed by J.S.F. and R.R.C.) and in vitro (codesigned and performed by J.P.K. and D.M.C.). J.P.K. and D.M.C. generated the new recombinant HCMVs. The manuscript was written by A.J.H. and R.F.K. with comments from all authors.

Supporting Online Material

www.sciencemag.org/cgi/content/full/320/5877/797/DC1
Materials and Methods
Figs. S1 to S8
Table S1
References

23 October 2007; accepted 19 March 2008
10.1126/science.1152095

Adaptive Phenotypic Plasticity in Response to Climate Change in a Wild Bird Population

Anne Charmantier,[1,2] Robin H. McCleery,[2]† Lionel R. Cole,[3] Chris Perrins,[1] Loeske E. B. Kruuk,[3] Ben C. Sheldon[2]*

Rapid climate change has been implicated as a cause of evolution in poorly adapted populations. However, phenotypic plasticity provides the potential for organisms to respond rapidly and effectively to environmental change. Using a 47-year population study of the great tit (*Parus major*) in the United Kingdom, we show that individual adjustment of behavior in response to the environment has enabled the population to track a rapidly changing environment very closely. Individuals were markedly invariant in their response to environmental variation, suggesting that the current response may be fixed in this population. Phenotypic plasticity can thus play a central role in tracking environmental change; understanding the limits of plasticity is an important goal for future research.

It is widely acknowledged that recent global changes in climate have had notable effects on the behavior and distribution of numerous plant and animal species (*1*–*3*). Less well established is the mechanism by which these effects arise and the consequences that they have for population persistence. Two contrasting, but nonexclusive, mechanisms that can explain population responses to climate change are (i) a microevolutionary response to natural selection and (ii) phenotypic plasticity. Understanding the role that these mechanisms play, and their consequences for population mean fitness, is important for understanding the current and likely future consequences of climate change, because it illustrates the extent to which populations are subject to changing natural selection resulting from changing environments (*4*). Some recent studies present evidence that climate-driven changes in the mean behavior of populations are genetically based (*5*–*7*), but other studies have suggested that individual plasticity can largely account for population responses to climate change (*8*–*10*).

Studies of the timing of breeding of birds have been an important model for characterizing the effects of climate change, because long time series are available and because the behavior of individually marked birds can be studied across environments (*11*–*15*). In addition, timing of breeding often has a strong connection to reproductive fitness. This is especially true for insectivorous birds that rely on a short period of insect abundance to feed their young; these birds need to time their reproduction to match the timing of organisms belonging to several different trophic levels, which might easily become dissociated (*13*, *15*, *16*). We report exceptionally close tracking of a rapidly changing environment—over almost five decades—by a population of great tits (*P. major*), accomplished by phenotypic plasticity alone.

In common with some other populations for which long time series are available, the population of great tits breeding at Wytham, near Oxford, UK, shows a marked change in mean date of breeding over time. Over the past 47 years (1961–2007), the mean egg-laying date of females has advanced by about 14 days, which is equivalent to a change of more than two SDs in the mean ($F_{2,44}$ = 13.89, P < 0.0001, Fig. 1A); the advancement of mean breeding date appears to begin in the mid-1970s. Previous work in this population (*12*, *17*) and the current extended data suggest that this is due to a tight relationship between mean laying date in the population and the temperature in the period preceding egg laying (r = –0.85, n = 47 years, P < 0.0001, Fig. 1B). There has been a marked change in the pre-laying temperature over the period ($F_{2,44}$ = 12.26, P < 0.0001, Fig. 1C), with a linear increase since the mid-1970s (1975–2007 r = 0.66, n = 33 years, P < 0.0001).

Over the same period at this site, the half-fall date [a standard measure of the timing of the peak of larval biomass (*18*)] of winter moth (*Operophtera brumata*) larvae—a key food resource for the rapidly growing offspring of the great tit—has shown a similar pattern of change ($F_{2,30}$ = 14.09, P < 0.0001, Fig. 1D) to that of the great tit mean laying date. The half-fall date of the winter moth shows a similarly strong correlation with the early spring temperature (r = –0.85, n = 33 years, P < 0.0001, Fig. 1E), as was found for the mean laying date of great tits. Moreover, the rates of change in the birds' mean laying date with temperature [–0.074 ± 0.007 (± SE) days °C^{-1}] and the caterpillars' half fall date with temperature (–0.081 ± 0.009 days °C^{-1}) are similar. The result is that mean laying date and half fall date are closely matched within years (r = 0.79, n = 33 years, P < 0.0001., Fig. 1F). Most of the mismatch is explained by differences in spring temperatures after birds have laid but before the caterpillar half-fall date (*17*), for which birds are partly able to compensate by adjusting the timing of clutch incubation (*19*). Unlike some other populations of passerine birds (*13*, *15*, *20*), there is no evidence that the synchronization of birds' laying dates with the timing of caterpillar emergence has worsened over time, because the interval between the mean laying date and half fall date has not changed over the course of the study [$F_{1,31}$ = 0.03, P = 0.86; quadratic ($F_{2,30}$ = 2.01, P = 0.15) and higher-order ($F_{3,29}$ = 1.47, P = 0.24) models provide no better fit to the data].

The 47 year sequence of our study includes the two warmest early springs (mean of March and April temperatures) in the world's longest-running instrumental temperature record, the 349-year Central England Temperature data set (*21*). Hence, the great tits have closely tracked the temporal change in the emergence of a key food source over almost five decades, during which there have been marked changes (including conditions that have, in an historical context, been unusual) in the environment and in the behavior of both birds and insects.

The importance of close temporal tracking of the emergence of the main food source is illustrated by the strong relationship between the strength and form of natural selection on laying date, and the interval between mean great tit laying date and winter moth half-fall date. In years in which this interval is relatively short, natural selection on laying date is strongly directional, favoring those birds with the earliest breeding dates [i.e., with the largest intervals between laying and the half-fall date ($F_{1,30}$ = 40.27, P < 0.0001; Fig. 2A)]; most of the population breeds too late for the peak in food abundance. In years where the interval between egg laying and caterpillar half-fall is relatively large, natural selection is less strongly directional (Fig. 2A), suggesting that more of the population has bred in time for the peak. In addition, the second moment of selection changes from positive to negative as the interval increases. This indicates a switch from a convex relationship between laying date and fitness (such that when caterpillar half-fall occurs soon after mean laying, all but the very earliest birds fare poorly) to a concave one (such that, with a very long interval, fitness is reduced for the very late and very early breeders) ($F_{1,30}$ = 6.08, P = 0.020; Fig. 2B: insets contrast selection in the most extreme years). This suggests a simple evolutionary mechanism by which a close match in timing of breeding in birds and the emergence of their food supply might be achieved, because years in which birds breed too late on average will be accompanied by the strongest selection for earlier breeding, whereas selection will act

[1]Edward Grey Institute, Department of Zoology, University of Oxford, South Parks Road, Oxford OX1 3PS, UK. [2]Centre d'Ecologie Fonctionnelle et Evolutive, Unite Mixte de Recherche CNRS 5175, 1919 Route de Mende, 34293 Montpellier Cedex 5, France. [3]Institute of Evolutionary Biology, School of Biological Sciences, University of Edinburgh, Edinburgh EH9 3JT, UK.

†Deceased

*To whom correspondence should be addressed. E-mail: ben.sheldon@zoo.ox.ac.uk

most strongly against the earliest breeders when the lag between breeding date and the caterpillar timing is largest.

The mean number of offspring recruited per brood was significantly lower in years in which selection was more strongly directional ($F_{1,44}$ = 12.56, P = 0.0009; Fig. 2C) and tended to be lower in years with a shorter interval between mean laying date and half fall date ($F_{1,50}$ = 3.56, P = 0.07). As expected, because of the tracking of the timing of the food source over time, there is no evidence that the strength of selection on laying date has changed with time ($F_{1,44}$ = 0.86, P = 0.36). Various measures of population fitness suggest that this population is thriving. Population size has increased markedly over time (estimated from 1964 since when there has been a constant availability of nest sites. $F_{1,42}$ = 57.56, P < 0.0001). Further, the mean recruitment success of buds (mean offspring per breeding attempt recruited to the adult population) has increased markedly over time, when recruitment rate is corrected for the counteracting negative effect of increased population size (increase in recruitment with time = 0.019 ± 0.005 offspring per year: $F_{1,43}$ = 11.74, P = 0.0014; effect of population size on mean recruitment = −0.0077 ± 0.0009: $F_{1,42}$ = 9.52, P = 0.0035). The patterns documented for this population are in marked contrast to those from a well-studied Dutch population of great tits, where caterpillar phenology has shifted forward at three times the rate of great tit laying dates (*22*), resulting in markedly increased selection for early breeding (*13*), while mean fitness has declined (*14*).

Several lines of evidence suggest that the population-level response to spring warming over 47 years in the Wytham great tit population can be entirely explained by individual plasticity in behavior. First, when we considered the potential magnitude of individual plastic responses, which was estimated from individuals that bred in multiple years, the slope of the relationship between within-female changes in breeding date and interannual changes in warmth sum (0.071 ± 0.009 days °C^{-1}; $F_{1,42}$ = 57.81, P < 0.0001, Fig. 2D)—a direct estimate of phenotypic plasticity—is closely similar to the slope of the relationship between mean breeding date and warmth sum at the population level (0.074 ± 0.007 days °C^{-1}). Second, the strong correlation between mean laying date and spring temperature (Fig. 1B) implies a plastic response and not microevolution, because there would be mismatches in the response in a population where the phenotype in year N was a function of selection in year N−1, when the environment varies considerably from year to year (Fig. 1C). Finally, the rate of phenotypic change is too rapid to be explained by natural selection without selection being much stronger than is observed (Fig. 2A). Because breeding time is sex-limited, with a heritability of 0.16 ± 0.06 (*23*), and because mean generation time in great tits is about 2 years, a change of 2 SDs in 47 years would require a mean standardized selection differential at least four times that observed (*18*).

Our analyses show that the sustained response to changing environmental conditions in this population can be explained by adaptive individual phenotypic plasticity alone, but it remains possible that a changing environment may select for differing patterns of plasticity among individuals. Although very little is known about the basis of plasticity in free-ranging populations of animals, a few recent studies of natural populations of vertebrates have estimated individual variability in response to environmental change via a linear mixed modeling approach (*14*, *24*–*27*). This approach allows the estimation of individual "reaction norms" to environmental variables and hence the quantification of the causes and selective consequences of between individual variation in plasticity. Although there is a strong response to spring temperature variation at the population level, individual female great tits from the Wytham population show no detectable variation in their response to spring temperature (Table 1). Linear mixed models on laying date that used 2253 breeding records from 644 fe-

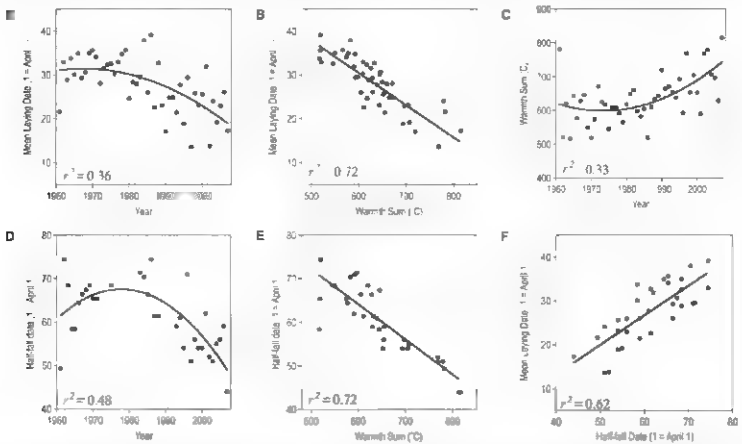

Fig. 1. Changes over time in temperature during the pre-laying period, assessed by spring warmth sum (sum of daily maximum temperatures between 1 March and 25 April) (C), mean laying date of great tits (A), and half-fall date of winter moth caterpillars (D) at Wytham, near Oxford, UK, between 1961 and 2007, as well as the interrelationships between spring warmth sum and mean laying date (B), warmth sum and half-fall date (E), and mean laying date and half-fall date (F). The numbers in the panels give the proportion of variance (r^2) explained by the regression model, lines are best-fitting linear or quadratic models.

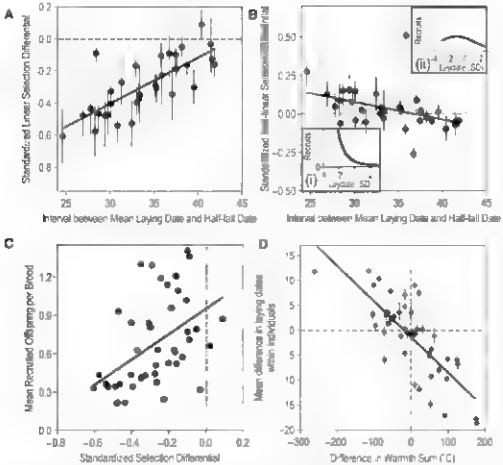

Fig. 2. Synchrony between great tit laying and caterpillar emergence: consequences for natural selection, population recruitment, and the mechanism underlying synchrony. (**A** and **B**) Relationship between synchrony of great tit egg laying and caterpillar half-fall date and the standardized selection differential on egg-laying date (**A**) or the standardized nonlinear selection differential on egg-laying date (**B**). Error bars indicate ± 1 SE. The interval between mean laying date and the half-fall date explains a large amount of the annual variation in the strength of directional selection [(**A**) $r = 0.76$, $n = 32$ years, $P < 0.0001$], but as the interval changes from small to large, selection on laying date changes in form from strongly directional [(**B**) inset (i) from 1964, the year with the smallest interval] to stabilizing [(**B**) inset (ii) from 1983, the year with the largest interval]; curves are fitted values from a general linear model with Poisson error. (**C**) Years with strong directional selection are years with reduced recruitment to the breeding population. (**D**) Relationship between the mean difference in laying date for individuals observed in successive years and the difference in spring warmth sum in the same pair of years ($r = -0.76$, $n = 44$ years, $P < 0.0001$). Error bars indicate ±1 SE.

Table 1. Linear mixed-effects models of plasticity in egg-laying date with response to spring warmth sum for 644 females that bred in three or more years, observed on a total of 2258 occasions between 1961 and 2004. All three models control for several fixed effects (*18*). Model comparison is hierarchical., from the most simple to the most complex. There is strong support for differences between years in mean egg-laying date, and for differences between females across years, but there is no evidence that individual females differ in their response to spring temperature. NA, not applicable; df, degrees of freedom.

Random terms in model	Log (likelihood)	Likelihood ratio test	
		Δdf	Likelihood ratio
Minimal model			
NA	−5382.0	NA	NA
Linear mixed-effects models			
Year	−5195.4	1	373.2***
Year, female	−5089.9	1	210.9***
Year, female, female × warmth sum	−5088.1	2	3.7

***$P < 0.0001$.

males with three or more breeding attempts between 1961 and 2004 showed significant variation between females in their average laying date but not in the slope of their response to changes in spring temperatures (Table 1). This conclusion is independent of several alternative methods of expressing individual plasticity, alternative methods of analysis, and expansion of the data to include all females ($n = 1746$) that were observed breeding in multiple years (*18*).

Our results contrast with those reported by Nussey *et al.* (*14*) for a Dutch great tit population in which there was considerable individual variation in the slope of the laying-date temperature reaction norm (Fig. 3). In the absence of evidence for significant individual variation in response to the environment, the value of further analyses of individual reaction norms is debatable at best (*27*). In any case, such analyses yield no evidence of heritability of, or selection on, variation in the response mechanism in this population of great tits, again in marked contrast to results from the Dutch population (*18*). Hence, these two populations differ markedly in the extent to which individuals vary in their response to spring temperature. In the British population, females are relatively invariant, but the mean population response is highly adaptive; in the Dutch population, there is marked variation among females, but the mean population response does not track the environment sufficiently closely,

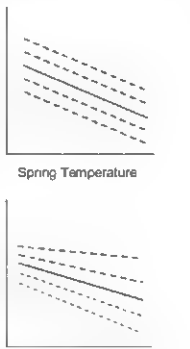

Fig. 3. Illustrative plots of the variance and covariance in average laying date (intercept) and slope (plasticity) in the laying-date response to increasing spring temperatures for UK (**A**) and Dutch (**B**) great tit populations. Dashed lines represent examples of reaction norms for four individual females, whereas solid lines represent the average population response.

with the result that the reaction norm is under increasingly strong selection for increased responsiveness, and fitness has declined correspondingly (*14*, *22*).

Relative invariance in the individual response to temperature is conceivably the result of past selection to optimize the reaction norm of the British population of great tits. As documented from the close association between the timing of their food supply and the egg laying of the birds over almost five decades—despite marked changes in the typical early spring temperatures (an increase in the mean warmth sum by 127 degree days from 1961 to 2007: a change of 1.8 SDs)—the current response mechanism appears to be adaptive. However, the relative lack of variation in plasticity in British great tits suggests that although birds are currently very well adapted to present environmental conditions and to the rate of change in those conditions over the past three decades, selection for an altered pattern of plasticity would be very inefficient. The difference between two well-studied populations of the same species in their response to similar cues, and indeed even in the presence of variation in this response, is notable and suggests that within-species variation in responses to climate change deserves further investigation (*15*, *28*). More generally, the role of phenotypic plasticity in allowing populations to track environmental changes deserves further attention. Whereas some populations are poorly adapted to changes that have occurred (*5*), with potential consequences for their range and persistence (*3*), other species may be able to cope with a wider range of environments. Studies of the phenology of different parts of trophic systems offer an important opportunity to determine whether changes occur at appropriate rates and whether the close matching demonstrated in the British population is unusual (*4*). Long-term studies of marked individuals in wild populations, for which detailed knowledge of ecological processes relevant to these populations can be combined with measures of fitness, offer many opportunities to increase our understanding of the importance of this process.

References and Notes

1. C. Parmesan, G. Yohe, *Nature* **421**, 37 (2003).
2. T. L. Root *et al.*, *Nature* **421**, 57 (2003).
3. C. D. Thomas *et al.*, *Nature* **427**, 145 (2004).
4. M. E. Visser *Proc. R. Soc. London Ser. B* **275**, 649 (2008).
5. W. E. Bradshaw, C. M. Holzapfel, *Science* **312**, 1477 (2006).
6. J. Ballanyi *et al.*, *Science* **313**, 1773 (2006).
7. M. Jonzén *et al.*, *Science* **312**, 1959 (2006).
8. R. Przybylo, B. C. Sheldon, J. Merilä, *J. Anim. Ecol.* **69**, 395 (2000).
9. D. Reale, A. G. MacAdam, S. Boutin, D. Berteaux, *Proc. R. Soc. London Ser. B* **270**, 591 (2003).
10. A. P. Møller, J. Merilä, *Adv. Ecol. Res.* **35**, 111 (2004).
11. H. Q. P. Crick, C. Dudley, D. E. Glue, D. L. Thomson, *Nature* **388**, 526 (1997).
12. R. H. McCleery, C. M. Perrins, *Nature* **391**, 30 (1998).
13. M. E. Visser, A. J. van Noordwijk, J. M. Tinbergen, C. M. Lessells, *Proc. R. Soc. London Ser. B* **265**, 1867 (1998).
14. D. H. Nussey, E. Postma, P. Gienapp, M. E. Visser, *Science* **310**, 304 (2005).
15. C. Both, S. Bouwhuis, C. M. Lessells, M. E. Visser, *Nature* **441**, 81 (2006).
16. M. E. Visser, C. Both, M. M. Lambrechts, *Adv. Ecol. Res.* **35**, 89 (2004).
17. A. J. van Noordwijk, R. H. McCleery, C. M. Perrins, *J. Anim. Ecol.* **64**, 451 (1995).
18. See the supporting online material on *Science* Online.
19. R. Cresswell, R. H. McCleery, *J. Avian. Ecol.* **72**, 356 (2003).
20. M. E. Visser, L. J. M. Holleman, *Proc. R. Soc. London Ser. B* **268**, 289 (2001).
21. Data spanning from 1659 to 2007 are available from the Met Office Hadley Centre (http://hadobs.metoffice.com/hadcet).
22. M. E. Visser *et al.*, *Oecologia* **147**, 164 (2006).
23. R. H. McCleery *et al.*, *Am. Nat.* **164**, E62 (2004).
24. D. H. Nussey, T. H. Clutton-Brock, D. A. Elston, S. D. Albon, P. S. Kruuk, *J. Anim. Ecol.* **74**, 387 (2005).
25. L. E. Brommer, J. Merilä, B. C. Sheldon, K. Gustafsson, *Evolution Int. J. Org. Evol.* **59**, 1362 (2005).
26. T. E. Reed *et al.*, *Proc. R. Soc. London Ser. B* **273**, 2713 (2006).
27. D. H. Nussey *et al.*, *J. Evol. Biol.* **20**, 831 (2007).
28. M. E. Visser *et al.*, *Proc. R. Soc. London Ser. B* **270**, 367 (2003).

29. We thank D. Garant, D. Nussey, and J. Quinn for very useful discussions; the many people that collected data during the study; and the Biotechnology and Biological Sciences Research Council, as well as the Royal Society Fellowships to J.E.B.K. and B.C.S., for funding the work.

Supporting Online Material

www.sciencemag.org/cgi/content/full/320/5877/800/DC1
Materials and Methods
Tables S1 and S2
References

29 February 2008; accepted 9 April 2008
10.1126/science.1157174

Temperature Sensing by an Olfactory Neuron in a Circuit Controlling Behavior of *C. elegans*

Atsushi Kuhara,[1]* Masatoshi Okumura,[1]* Tsubasa Kimata,[1] Yoshinori Tanizawa,[2]† Ryo Takano,[1] Koutarou D. Kimura,[3]‡ Hitoshi Inada,[3]§ Kunihiro Matsumoto,[2] Ikue Mori[1,3,4]‖

Temperature is an unavoidable environmental cue that affects the metabolism and behavior of any creature on Earth, yet how animals perceive temperature is poorly understood. The nematode *Caenorhabditis elegans* "memorizes" temperatures, and this stored information modifies its subsequent migration along a temperature gradient. We show that the olfactory neuron designated AWC senses temperature. Calcium imaging revealed that AWC responds to temperature changes and that response thresholds differ depending on the temperature to which the animal was previously exposed. In the mutant with impaired heterotrimeric guanine nucleotide–binding protein (G protein)–mediated signaling, AWC was hyperresponsive to temperature, whereas the AIY interneuron (which is postsynaptic to AWC) was hyporesponsive to temperature. Thus, temperature sensation exhibits a robust influence on a neural circuit controlling a memory-regulated behavior.

If wild-type *C. elegans* individuals are cultivated at a certain temperature, ranging from 15° to 25°C, for 3 hours with bacteria as food source and are then placed on a temperature gradient from 15° to 25°C, most of the animals migrate to the previous cultivation temperature (Fig. 1) (*1*). This behavior is called thermotaxis, and its plasticity provides an opportunity to understand molecular and neural circuit mechanisms of thermosensation, learning, and memory (*1*–*3*). By ablation of particular cells with a laser microbeam and evaluation of the consequent behavioral effects, a simple neural circuit essential for thermotaxis has been identified (Fig. 2A) (*3*).

Although wild-type animals migrate up or down the temperature gradient until reaching their cultivation temperature, *ttx8* mutants that were isolated in a genetic screen for thermotaxis-defective mutants migrated toward colder temperatures than those to which they were previously exposed (Fig. 1, B, D, and E). The *ttx8* mutation corresponded to a nearly loss-of-function mutation in the *eat-16* gene encoding a homolog of the mammalian regulator of G protein signaling (RGS) proteins, which are negative regulators for the α subunit of the G proteins (*4*).

A fusion gene encoding wild-type EAT-16 fused to green fluorescent protein (*eat-16 gfp*), which is under the control of the *eat-16* promoter, was broadly expressed in neurons (fig. S2A). To

[1]Group of Molecular Neurobiology, Graduate School of Science, Nagoya University, Nagoya 464-8602 Japan. [2]Group of Signal Transduction, Graduate School of Science, Nagoya University, Nagoya 464-8602, Japan. [3]Institute for Advanced Research, Nagoya University, Nagoya 464-8602, Japan. [4]Core Research for Evolutional Science and Technology (CREST), Japan Science and Technology Agency (JST), Japan

*These authors contributed equally to this work
†Present address: Division of Cell Biology, Medical Research Council–Laboratory of Molecular Biology, Hills Road, Cambridge CB2 0QH, UK.
‡Present address: Structural Biology Center, National Institute of Genetics, Mishima 411-8540, Japan
§Present address: Okazaki Institute for Integrative Bioscience, National Institutes of Natural Sciences, Okazaki 444-8787, Japan
‖To whom correspondence should be addressed. E-mail: m46920a@nucc.cc.nagoya-u.ac.jp

identify neurons in which EAT-16 is required for thermotaxis, we expressed *eat-16* cDNA in *eat-16(nj8)* mutants with neural promoters to drive EAT-16 expression in various sets of neurons (Fig. 1E and fig. S2B). Expressing EAT-16 in nearly all or in many neurons restored the normal migration of *eat-16* mutants toward their cultivation temperature (Fig. 1E). Although expression of EAT-16 in several subsets of neurons, including neurons essential for the neural circuit controlling thermotaxis (Fig. 2A), did not restore the normal migration of *eat-16* mutants, expression of EAT-16 from *odr-3*, *gpa-13*, and *odr-1* promoters (*5*–*7*) did (Fig. 1E). These three promoters allow the expression in a single type of sensory neuron: AWC, which is characterized as an olfactory neuron (Fig. 1E and fig. S2B) (*8*). These results suggest that *eat-16* acts cell-autonomously in AWC sensory neurons and that EAT-16 RGS is required in AWC for thermotaxis.

Using Ca^{2+} imaging, we tested whether AWC responds to temperature. We monitored temperature-evoked changes in the intracellular concentration of free Ca^{2+} in intact AWC neurons with a genetically encoded Ca^{2+} indicator cameleon (Fig. 3, A to D) (*9*). The Ca^{2+} concentration in the AWC neuron of wild-type animals increased upon warming and decreased upon cooling (Fig. 3, A and B, and fig. S3). We also tested whether two other sensory neurons respond to temperature. Although the responses of the ASE neuron were minimal, the small responses of the ASH neuron were detected (*10*, *11*) (Fig. 3B). This weak responsiveness may implicate the possibility that temperature information is conveyed by multiple sensory neurons. AWC neurons in *eat-16* mutants were hyperresponsive to temperature changes (Fig. 3C). Thus, the EAT-16 RGS protein appears to negatively regulate temperature detection in AWC neurons of wild-type animals. AWC neurons responded to increments of warming above a threshold temperature that is set by the cultivation temperature (Fig. 3D). Consequently, thermal responses of AWC are modulated by memory

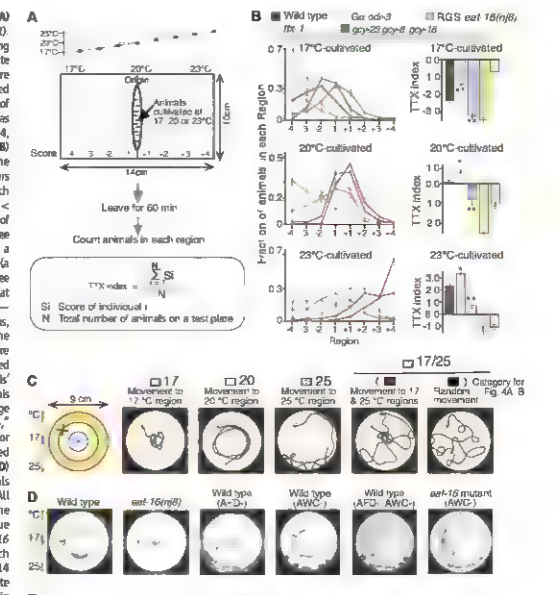

Fig. 1. Thermotaxis behavior of *C. elegans*. (**A**) Procedure for the population thermotaxis assay (*21*). A linear temperature gradient was established along the 14-cm agar surface in the thermotaxis (TTX) plate (10 cm by 14 cm). The steepness of temperature gradient was kept at 0.44°C/cm. Animals cultivated at 17°, 20°, or 23°C were placed at the surface of agar at 20°C and left for 60 min. The TTX plate was divided into eight regions with scores from −4 to +4, and the TTX index was calculated as shown. (**B**) Distributions (left) and TTX indices (right) of the animals cultivated at 17°, 20°, or 23°C. Error bars indicate SEM. n = 545 to 1063 animals for each genotype. Single and double asterisks indicate $P < 0.05$ and $P < 0.01$, respectively, in an analysis of variance (ANOVA) for multiple comparisons (see SOM). (**C**) Single-animal thermotaxis assay with a radial temperature gradient (*22*). The assay plate (a 9-cm-diameter petri dish) was divided into three areas: 0 to 1.5 cm (at about 17°C), 1.5 to 3 cm (at about 20°C), and 3 to 4.5 cm (at about 25°C—indicated as blue, yellow, and orange areas, respectively—as measured from the center of the plate (left panel). The steepness of temperature gradient was not linear. A single animal was placed on the "x" indicated on the assay plate. Animals' tracks were categorized into four groups. Animals that moved only within the blue, yellow, or orange areas were classified as "17," "20," or "25," respectively. Animals that moved randomly, or within both 17° and 25°C regions, were classified as "17/25" (further classified in detail as shown). (**D**) The tracks of wild-type or *eat-16* mutant animals in which the indicated neuron was ablated. All the animals were cultivated at 20°C before the radial gradient assay. (**E**) Cell-specific rescue experiments for defective thermotaxis of *eat-16* mutants on a radial temperature gradient. Each animal was cultivated at 20°C. n = 60 to 514 animals for each genotype. Error bars indicate SEM. Double asterisk indicates $P < 0.01$ in ANOVA for multiple comparisons.

of the past cultivation temperature, similar to those of the major thermosensory neuron AFD (*12*, *13*).

In the neural circuit model for thermotaxis, the presence of a second thermosensory neuron with a less critical role than that of the AFD neuron has been proposed (Fig. 2A) (*3*). To test whether this unidentified thermosensory neuron might be the AWC neuron, we conducted laser ablation experiments (*3*). Although ablating AFD neurons of wild-type animals resulted in aberrant migration (Figs. 1D and 4A) (*3*), ablating AWC neurons of wild-type animals did not cause detectable defects in a radial gradient assay (Figs. 1D and 4A). Ablating both AFD and AWC neurons in wild-type animals resulted in no temperature preference (Figs. 1D and 4A); a phenotype similar to that caused by mutations in the *tax-4* gene encoding a guanosine 3′,5′-monophosphate (cGMP)–gated channel that is expressed in both AFD and AWC neurons (Fig. 4B) (*14*). Moreover, ablation of AWC neurons in *eat-16* mutants restored normal migration to the mutant animals (Figs. 1D and 4A). Thus, our ablation results are consistent with the notion that AWC is a secondary thermosensing neuron.

G protein signaling (which increases the intracellular concentration of cGMP) is required for olfactory signaling in AWC neurons (Fig. 2B). ODR-1 guanylyl cyclase (GCY) and TAX-4 cGMP-gated channels are localized at the AWC sensory endings where odorants are initially received, and mutations in genes encoding either of these proteins lead to defective behavioral responses to AWC-sensed odorants (*6*, *7*, *14*). *odr-1* mutants exhibited almost normal thermotaxis after cultivation at 20°C (Fig. 4, B and C, and fig. S4, B and C), and *tax-4* mutants were not responsive to temperature (Fig. 4, B and C) (*14*). GCY-23, GCY-8, and GCY-18 all localize at sensory endings of AFD neurons and are required for thermosensory signaling in AFD (*15*). The *gcy-23 gcy-8 gcy-18* triple mutant showed abnormal migration, quite similar to that of wild-type animals in which the AFD neuron was ablated (Fig. 4, A and B) (*15*). Mutation in the *odr-1* gene enhanced the severity of the thermotaxis defect of *gcy-23 gcy-8 gcy-18* triple mutants, because *gcy-23 gcy-8 gcy-18*, *odr-1* quadruple mutants were unresponsive to temperature, similar to that observed in wild-type animals in which the AFD and AWC neurons had been ablated or in *tax-4* mutants (Fig. 4, A and B). *odr-1* mutation suppressed abnormal migration of *eat-16* mutants, and *tax-1* is epistatic to *eat-16* (mutation in *tax-4* masks the effects of mutation in *eat-16*) (Fig. 4C and fig. S4B). Thermal responses of AWC in *tax-4* mutants revealed by Ca^{2+} imaging were diminished (Fig. 3C and fig. S3, B and C). Thus, mutations in *odr-1* and *tax-4* likely interrupt AWC thermosensory function, further suggesting that temperature signaling may occur through a

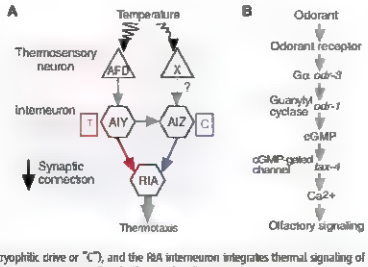

Fig. 2. A neural circuit model controlling thermotaxis and olfactory signaling. (**A**) The simplified original neural circuit model for thermotaxis (*3*). Temperature is sensed by AFD and an unidentified "X" sensory neuron. The activated AIY-RIA circuit accelerates the movement to a temperature higher than the cultivation temperature (thermophilic drive or "T"), the activated AIZ-RIA circuit accelerates the movement to a temperature lower than the cultivation temperature (cryophilic drive or "C"), and the RIA interneuron integrates thermal signaling of "T" and "C." (**B**) A model for G protein/cGMP–mediated olfactory signaling in AWC.

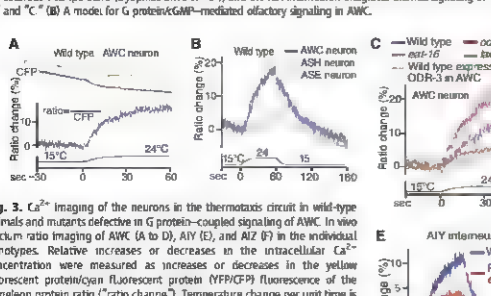

Fig. 3. Ca^{2+} imaging of the neurons in the thermotaxis circuit in wild-type animals and mutants defective in G protein–coupled signaling of AWC. In vivo calcium ratio imaging of AWC (A to D), AIY (E), and AIZ (F) in the individual genotypes. Relative increases or decreases in the intracellular Ca^{2+} concentration were measured as increases or decreases in the yellow fluorescent protein/cyan fluorescent protein (YFP/CFP) fluorescence of the cameleon protein ratio ("ratio change"). Temperature change per unit time is shown at the bottom of each graph. (B to F) Each graph represents the average response to temperature stimuli. $n = 10$ to 17 animals. (**A**) Representative FRET signal in AWC of wild-type animals cultivated at 20°C and subjected to temperature change. (**B**) Ca^{2+} imaging of AWC, ASE, and ASH sensory neurons in wild-type animals subjected to warming and cooling. The average of maximum ratio change from baseline ± SEM was 16.95 ± 2.17 for AWC, 3.18 ± 2.17 for ASE, and 5.35 ± 2.12 for ASH. $n = 14$ to 17 animals. (**C**) Changes in Ca^{2+} concentration. The average of maximum ratio change from baseline ± SEM was 17.529 ± 2.07 for wild type, 25.81 ± 2.14 for *eat-16*, 6.72 ± 1.33 for *odr-3*, 4.01 ± 2.19 for *tax-4*, and 27.74 ± 7.42 for wild type expressing excess ODR-3 in AWC. $n = 13$ to 17 animals. (**D**) Response of AWC neurons to stepwise temperature changes above a threshold temperature that nearly corresponds to the cultivation temperature. The average of maximum ratio change from baseline ± SEM was 26.61 ± 2.45 for a 15°-cultivated animal, 17.78 ± 2.69 for a 20°-cultivated animal, and 3.70 ± 2.34 for a 25°-cultivated animal. $n = 10$ to 12 animals. (**E** and **F**) Ca^{2+} imaging in AIY and AIZ neurons. The average of maximum ratio change from baseline ± SEM was 10.87 ± 1.10 for wild type (AIY), 2.67 ± 0.83 for *eat-16* (AIY), 10.41 ± 1.52 for wild type (AIZ), and 9.35 ± 1.13 for *eat-16* (AIZ). $n = 15$ to 16 animals.

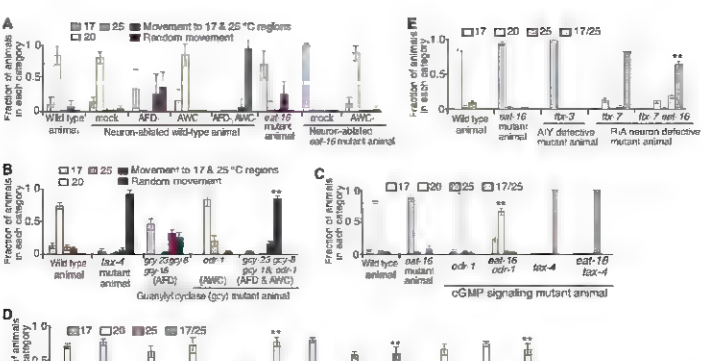

Fig. 4. Thermotaxis of animals with ablated neurons or cGMP signaling mutants. **(A)** Summary for thermotaxis of animals with ablated neurons. All the animals were cultivated at 20°C before the radial gradient assay. Error bars indicate a twofold increase in SD (see SOM). $n = 6$ to 78 assays. (**B** to **E**) Thermotaxis of animals cultivated at 20°C on a radial temperature gradient. $n = 60$ to 236 assays (**B**), $n = 48$ to 183 assays (**C**), $n = 99$ to 495 assays (**D**), and $n = 44$ to 119 assays (**E**) for each genotype. Error bars indicate SEM. Double asterisk indicates $P < 0.01$ in ANOVA for multiple comparisons.

cGMP signaling smaller to that mediating odor sensing (Fig. 2B).

We explored Gα proteins mediating AWC thermosensation by examining Gα genes—*gpa-7*, *odr-3*, *gpa-2*, and *gpa-13*—that are expressed in AWC neurons (*5*, *7*, *16*). After cultivation at 20°C, *gpa-7* and *odr-3* mutants showed nearly normal thermotaxis, whereas *gpa-2* and *gpa-13* mutants exhibited a partially abnormal phenotype in radial temperature gradients (Fig. 4D and fig. S4A). Only *odr-3* mutation suppressed abnormal migration of *eat-16* mutants (Fig. 4D and fig. S4, B and C). Expression of a dominant-negative form of ODR-3 also suppressed the defect of *eat-16* mutants (Fig. 4D). Small responses of AWC neurons in *odr-3* mutants were detected by Ca^{2+} imaging (Fig. 3C and fig. S3C). Excess expression of wild-type ODR-3 in AWC neurons of wild-type animals induced abnormal migration, which was reminiscent of that of *eat-16* mutants (Fig. 4D and fig. S4, A and B), whereas excess expression of GPA-13 and another Gα protein (EGL-30) in AWC neurons of wild-type animals did not (Fig. 4D and fig. S4B). We used Ca^{2+} imaging to reveal that AWC neurons expressing excess wild type ODR-3 in wild-type animals were hyperresponsive to temperature changes, as were the AWC neurons in *eat-16* mutants (Fig. 3C). Thus, G protein–cGMP signaling appears to mediate thermosensation in AWC neurons. Notably, in contrast to *eat-16* mutants, *odr-3* mutants previously cultivated at 17°, 20°, or 23°C migrated toward a higher temperature than their cultivation temperature in a linear temperature gradient (Fig. 1B), which implicates RGS-mediated Gα thermosensory signaling of AWC neurons.

We evaluated AWC temperature signaling in a neural circuit for thermotaxis by Ca^{2+} imaging. The AIY neuron receives synaptic inputs from both AFD and AWC neurons, AIZ receives synaptic inputs from AIY, and RIA receives synaptic inputs from both AIY and AIZ (*17*). The AIY neuron is thought to mediate movement toward warmer temperatures, AIZ is thought to mediate movement toward colder temperatures, and the regulation between AIY and AIZ activities through RIA is thought to be important for proper migration to a memorized temperature on a temperature gradient (Fig. 2A) (*3*). Upon warming, fluorescence resonance energy transfer (FRET) ratios in AIY neurons changed less in *eat-16* mutants than in wild type animals (Fig. 3E), whereas thermal responses of AIZ were nearly normal (Fig. 3F). Given that wild-type animals in which AIY is ablated and AIY-defective mutants migrate toward temperatures colder than the cultivation temperature (Fig. 4E) (*3*, *18*), the decrease of AIY activity in *eat-16* mutants revealed by Ca^{2+} imaging (Fig. 3E) may cause abnormal migration to colder temperatures (fig. S5). Thus, regulation of AWC-AIY connectivity may be critical for the circuit controlling thermotaxis. The importance of AWC AIY wiring was also reported recently for olfactory behavioral responses (*19*). A thermotactic defect in *myo-inositol monophosphatase*-defective *ttx-7* mutants is caused by aberrant synapse localization on the RIA neuron (Figs. 2A and 4E) (*20*). Abnormal migration of *eat-16* mutants was suppressed by *ttx-7* mutation (Fig. 4E), which is consistent with the model that the transmission of neural signals from AWC and AIY neurons to RIA is also indispensable for thermotaxis (fig. S5). Our current work helps explain a complex mechanism for control of behavior from stimulus sensing through the neuronal circuit that produces behavioral output.

References and Notes

1. E. M. Hedgecock, R. L. Russell, *Proc. Natl. Acad. Sci. U.S.A.* **72**, 4061 (1975).
2. D. Biron *et al.*, *Nat. Neurosci.* **9**, 1499 (2006).
3. I. Mori, Y. Ohshima, *Nature* **376**, 344 (1995).
4. Y. M. Hajdu-Cronin, W. J. Chen, G. Patikoglou, M. R. Koelle, P. W. Sternberg, *Genes Dev.* **13**, 1780 (1999).
5. G. Jansen *et al.*, *Nat. Genet.* **21**, 414 (1999).
6. M. D. L'Etoile, C. I. Bargmann, *Neuron* **25**, 575 (2000).
7. K. Roayaie, J. G. Crump, A. Sagasti, C. I. Bargmann, *Neuron* **20**, 55 (1998).
8. C. I. Bargmann, E. Hartwieg, H. R. Horvitz, *Cell* **74**, 515 (1993).
9. A. Akhayanki *et al.*, *Nature* **388**, 882 (1997).
10. M. Tomioka *et al.*, *Neuron* **51**, 613 (2006).
11. H. S. Fukuto *et al.*, *Neuron* **42**, 581 (2004).
12. D. A. Clark, D. Biron, P. Sengupta, A. D. Samuel, *J. Neurosci.* **26**, 7444 (2006).
13. K. D. Kimura, A. Miyawaki, K. Matsumoto, I. Mori, *Curr. Biol.* **14**, 1291 (2004).

14. H. Komatsu, ... Mori, J. S. Rhee, N. Akaike, Y. Ohshima, *Neuron* **17**, 707 (1996).
15. H. Inada *et al.*, *Genetics* **172**, 2239 (2006).
16. R. R. Zeitzel, J. E. Mendel, P. W. Sternberg, R. H. Plasterk, *Genetics* **145**, 715 (1997).
17. J. G. White, E. Southgate, J. N. Thomson, S. Brenner, *Philos. Trans. R. Soc. London Ser. B* **314**, 1 (1986).
18. O. Hobert *et al.*, *Neuron* **19**, 345 (1997).
19. S. H. Chalasani *et al.*, *Nature* **450**, 63 (2007).
20. Y. Tamirana *et al.*, *Genes Dev.* **20**, 3296 (2006).
21. H. Ito, H. Inada, *Mori, J. Neurosci. Methods* **154**, 45 (2006).
22. A. Mahn *et al.*, *Genetics* **169**, 1437 (2005).
23. We thank C. Bargmann, N. L'Etoile, D. Garbers, B. Wedel, P. Swoboda, J. Sze, J. McGhee, G. Jansen, and W. Schafer for sharing constructs and strains; A. Fire for pPD plasmids; Y. Kohara for yk clones; T. Stiernagle and the *Caenorhabditis* Genetic Center for strains; Y. Oliuchi for isolating novel mutants; H. Ito and S. Tachibana for unpublished results; C. Bargmann, L. Avery, H. Sayaltura, E. Kodama, T. Singh, and members of Mori laboratory for comments on this manuscript and stimulating discussion, and anonymous reviewers for invaluable comments on the manuscript. A.K. was supported by the Brain Science Foundation, the Mochida Memorial Foundation for Medical and Pharmaceutical Research, and the Ministry of Education, Culture, Sports, Science and Technology of Japan (MEXT) (grant no. 18770003). A.M. is a Scholar of the Institute for Advanced Research in Nagoya University. This work was supported by CREST (JST) and (in part) by a Grant-in-Aid for Scientific Research on Priority Areas (Molecular Brain Science) from MEXT (grant no. 17024023) to I.M.

Supporting Online Material

www.sciencemag.org/cgi/content/full/1148922/DC1
Materials and Methods
Figs. S1 to S7
References
Movie S1

8 August 2007; accepted 5 March 2008
Published online 10 April 2008.
10.1126/science.1148922
Include this information when citing this paper

Discovery of a Cytokine and Its Receptor by Functional Screening of the Extracellular Proteome

Haishan Lin,[1] Ernestine Lee,[2] Kevin Hestir,[1] Cindy Leo,[2] Minmei Huang,[1] Elizabeth Bosch,[1] Robert Halenbeck,[1] Ge Wu,[1] Aileen Zhou,[1] Dirk Behrens,[1] Diane Hollenbaugh,[1]* Thomas Linnemann,[1] Minmin Qin,[1] Justin Wong,[1] Keting Chu,[1]† Stephen K. Doberstein,[1] Lewis T. Williams[1,2]‡

To understand the system of secreted proteins and receptors involved in cell-cell signaling, we produced a comprehensive set of recombinant secreted proteins and the extracellular domains of transmembrane proteins, which constitute most of the protein components of the extracellular space. Each protein was tested in a suite of assays that measured metabolic, growth, or transcriptional responses in diverse cell types. The pattern of responses across assays was analyzed for the degree of functional selectivity of each protein. One of the highly selective proteins was a previously undescribed ligand, designated interleukin-34 (IL-34), which stimulates monocyte viability but does not affect responses in a wide spectrum of other assays. In a separate functional screen, we used a collection of extracellular domains of transmembrane proteins to discover the receptor for IL-34, which was a known cytokine receptor, colony-stimulating factor 1 (also called macrophage colony-stimulating factor) receptor. This systematic approach is thus useful for discovering new ligands and receptors and assessing the functional selectivity of extracellular regulatory proteins.

Complex organisms rely on an extensive system of secreted and cell-surface molecules for communication between cells, tissues, and organs. Many secreted proteins function as ligands for membrane-spanning receptors, which serve as the transducers by which extracellular signals influence intracellular physiology. Some ligands have highly specific functions because their receptors are expressed in a limited number of tissues, whereas other ligands act on a broad spectrum of tissues. There are ~2200 human genes encoding secreted proteins, of which only a minority have functions that are well understood. We classified proteins as being secreted on the basis of one or more of the following algorithms: (i) the presence of a signal sequence; (ii) the presence of conserved domains of secreted proteins and extracellular regions of transmembrane proteins; (iii) presence of non-canonical secreted proteins and nonsecreted proteins found in human plasma (*1*), and (iv) a "secreted" classification by a supervised learning algorithm based on random decision trees (*2*–*4*).

We produced recombinant secreted proteins from ~3400 cDNAs that encode secreted proteins and extracellular domains of transmembrane proteins (table S2). Each cDNA was individually transfected into 293T cells in a high-throughput format, and samples of conditioned medium containing each protein were collected for testing in cell-based assays within 12 hours. A parallel set of cDNAs that encode the proteins in tagged forms was similarly transfected into 293T cells and the amount of protein released into the medium was estimated by Western blot analysis (fig. S1A) and enzyme-linked immunosorbent assay (fig. S1B). More than 90% of the proteins were detected in the culture supernatant with a mean concentration of 75 ng/ml and a median of 20 ng/ml (fig. S1B).

To identify the functions and potential therapeutic utility of all human secreted proteins and their receptors, we chose a wide range of cells that represent different tissue types and various assay readouts (table S4) that measured cellular responses to secreted factors. The complete recombinant protein collection was screened in an automated high-throughput format across a wide spectrum of assays (table S4).

We focused on the subset of secreted proteins with high functional selectivity by comparing the activities of a given protein across multiple assays (table S4) and searched for those that were active in only a small number of assays. More than 201,000 data points generated from this set of assays were used for functional selectivity analysis of the secreted proteins (Fig. 1B). To identify the proteins with the highest functional selectivity, we defined a measure of activity that can be compared across multiple assays and readouts and devised a quantitative assessment of selectivity.

The activity of each protein in eliciting a cellular response in a given assay was measured. Within an assay, the measurements of responses to n proteins were assigned ranks 1 to n from the lowest through highest numerical values of the assay measurements. Ranks for the responses to a protein from assays performed in replicate were summed, giving a Wilcoxon rank sum statistic. This statistic was used to test the null hypothesis that the ranks are random, versus the alternative hypothesis that the protein has some effect on the cells. The P value is the probability that the rank sum (as an activator or an inhibitor) is as strong as or stronger than observed, assuming there was only assay noise and that there was no effect of the protein. The quantity $\log P$, called activity in Fig. 1A, is then a positive number (a small value of P gives a large value of $-\log P$) whose magnitude reflects the response of cells to a protein in a given assay.

For each protein, the assays were then sorted from the assay with the highest activity for that protein to the assay with the lowest activity. These relative activities across sorted assays were plotted for four examples, covering a range of selectivity (Fig. 1A). The order of the assays in Fig. 1A is different for each protein. For example, the values for interleukin-34 (IL-34) and IL-15

[1]Five Prime Therapeutics, Inc., 1650 Owens Street, Suite 200, San Francisco, CA 94158, USA. [2]School of Medicine, University of California, San Francisco, CA 94143, USA.
*Present address: Schering-Plough Biopharma, Palo Alto, CA 94304, USA.
†Present address: DigiTAB, Inc., Burlingame, CA 94010, USA.
‡To whom correspondence should be addressed. E-mail: rusty.williams@fiveprime.com

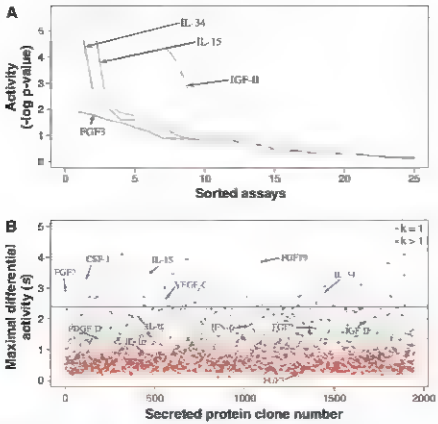

Fig. 1. Identification of IL-34 using a functional screening approach. **(A)** Comparison of functional selectivity of IL-15, GF-II, FGF3 and IL-34. Using *P* values for a Wilcoxon rank sum test, activities ($-\log P$) for several proteins against their respective sorted assays are shown. The assays were sorted from the lowest to the highest *P* value, producing a protein-dependent list of sorted assays. Assay descriptions are shown in table S4. **(B)** Analysis of functional selectivity of secreted proteins. Functional selectivity of 1910 secreted proteins in the screening set was analyzed using the maximal differential activity *s* and selectivity index *k*.

decrease sharply across assays compared with those for insulin-like growth factor II (IGF-II), indicating that they were active in one or two assays, whereas IGF-II was active in many fibroblast growth factor 3 (FGF3) gave a low signal in many assays but did not maximally activate any assay (Fig. 1A).

The notion of selectivity of a protein in eliciting responses across many assays was quantified with a pair of numbers (s, k), where s is the maximal differential activity and k is the selectivity index. Suppose there are n assays, and $P_1 < P_2 < \ldots < P_n$ are the corresponding sorted P values. The difference between adjacent activities $(-\log P_1)$ and $(-\log P_2)$ is equal to the log ratio

$$(-\log P_1) - (-\log P_2) = \log \frac{P_2}{P_1}$$

Let $r_1, r_2, \ldots r_{n-1}$ denote the activity differences

$$r_1 \quad \log \frac{P_2}{P_1}, r_2 \quad \log \frac{P_3}{P_2}, \ldots, r_n \quad \log \frac{P_n}{P_{n-1}}$$

and define $s \quad \max\{r_1, r_2, \ldots r_{k-1}\}$ and k $\max\{i \;\; 1 \le i \le n \;\; 1 \text{ and } r_i \;\; s\}$. Briefly, s is the maximum difference and k is the index where the maximum occurs. Clones with high values of s and low values of k will be highly active in just a few assays. Figure 1B plots s for 19,0 clones in n 25 assays, showing some proteins—such as interferon α (IFN-α), FGF2, FGF3, platelet-derived growth factor D (PDGF-D), IGF-II, IL-1α, and IL-6—with low selectivity and

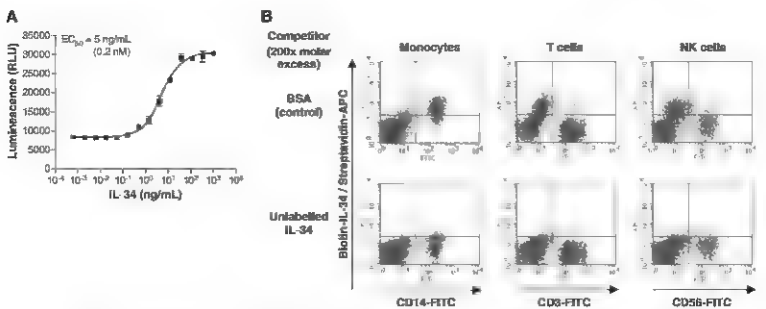

Fig. 2. Activities and cell-binding selectivity of purified IL-34 protein. **(A)** Dose-response curve of purified IL-34 protein in a monocyte viability assay. Recombinant IL-34 protein was purified from conditioned medium of 293T cells stably transfected with IL-34 cDNA. Relative viability (survival and/or proliferation) of primary human monocytes induced by the purified IL-34 protein was determined by the cell viability (CellTiter-Glo) assay (Promega). In this assay, the amount of ATP released from lysed cells was determined based on the luminescence signal [relative light unit (RLU)] generated from reaction with luciferin in the presence of luciferase. **(B)** Specific binding of IL-34 to human monocytes in PBMC. PBMC incubated with unlabeled IL-34 or bovine serum albumin (BSA) as competitors at 200-fold molar excess were incubated with biotinylated IL-34 protein and stained with streptavidin-allophycocyanin (APC). The cells also were labeled with fluorescein isothiocyanate (FITC)–conjugated antibodies against lineage markers, CD14 (monocytes), CD3 (T cells), and CD56 (NK cells) and analyzed by flow cytometry.

others with high functional selectivity. Among the 100 clones with the highest selectivity (Fig. 1B), all but nine of these have $k = 1$ and thus are selective for one of the assays. Although this analysis is limited by the small number (25) of assays relative to all possible biological activities and by the fact that the assays were not representative of all tissues, the data provided a starting point for selecting proteins that might have a high degree of selectivity.

Because the secreted proteins used in the screening assays were expressed at various levels, we questioned whether the functional selectivity of proteins might correlate with protein concentration. Analysis of more than 700 proteins for their activity or maximal differential activity and expression levels demonstrated no correlation between activity or maximal differential activity of a protein and its expression level (fig. S2, A and B, and tables S7 and S8).

We focused on the proteins with a high selectivity score (Fig. 1B) for further analysis. The proteins that were highly selective included a number of known cytokines or growth factors, such as colony-stimulating factor 1 (CSF 1), selective for the monocyte viability assay; vascular endothelial growth factor C (VEGF-C), selective for the cardiomyocyte phosphoprotein assay; FGF19, selective for the H4-II E PCK1 expression assay; IL-15, selective for the T lymphocyte and natural killer (NK) cell viability assays; and FGF21, selective for the adipocyte assay (Fig. 1B and table S4). These proteins are known to be selective in their actions (*5*–*10*).

In the pool of highly selective proteins, we were especially interested in uncharacterized proteins. For further study, we chose a protein that had a high selectivity score and stimulated monocyte viability. This 241–amino acid protein was encoded by a cDNA clone, which differs by one amino acid residue from a hypothetical protein in the public database (GenBank accession number NP 689669). This protein increased monocyte viability (fig. S3 and table S5) and has been designated as IL-34, isoform 1 (GenBank accession number EU599219, referred to as IL-34 in this paper).

The amino acid sequence of human IL-34 shares a sequence identity of 99.6%, 72%, and 71% with that of the chimpanzee, rat, and mouse IL-34 orthologs, respectively (fig. S4), and the *IL-34* gene is syntenic in the human, chimpanzee, rat, and mouse genomes. We detected no similarity of the IL-34 protein sequence to that of any other human protein, and IL-34 has no apparent consensus structural domain or motif. IL 34 mRNA is expressed in various tissues, including heart, brain, lung, liver, kidney, spleen, thymus, testes, ovary, small intestine, prostate, and colon, and it is most abundant in the spleen (fig. S5A). Consistent with its role in regulating myeloid cell growth and differentiation, IL-34 protein was also detected by immunohistochemistry in the sinusoidal endothelium in the red pulp of the spleen (fig. S5B).

We purified the human IL-34 protein (99% purity) as a homodimer consisting of 39 kD monomers. The purified protein increased the number of monocytes in an assay that uses adenosine 5′-triphosphate (ATP) content as a measure of cell number (Fig. 2A). This measurement, which we termed "viability," does not distinguish between change in survival or proliferation. IL-34 activity also was detected in an assay measuring DNA replication (fig. S6), suggesting that an increase in cell proliferation indeed contributes to the increase in viable cells. In flow cytometry analysis, biotinylated IL-34 protein specifically bound to $CD14^+$ monocytes in peripheral blood mononuclear cells (PBMCs), and this binding was decreased in the presence of unlabeled IL 34 (Fig. 2B). In contrast, IL-34 did not bind to $CD3^+$ T cells or $CD56^+$ NK cells (Fig. 2B).

We searched for an IL 34 receptor in our collection of extracellular domains (ECDs) of membrane-spanning proteins. There are ~1100 type I transmembrane proteins and ~500 type II transmembrane proteins encoded by the human genome (table S2), as determined by literature sources and our prediction algorithms (*4*).

We screened our collection of ECDs for the ability to block the functional activity of IL-34 on monocytes through binding and sequestration of IL 34. Purified IL 34 was incubated with each ECD and then assayed for the effect on human monocyte viability (Fig. 3). Ten of the 858 ECDs screened inhibited IL-34 activity in the primary screen (Fig. 3 and table S6), but only one of these proteins gave reproducible inhibition in repeated testing (table S6). This protein was encoded by a cDNA for the CSF-1 receptor (CSF 1R) ECD, suggesting that CSF 1R is a receptor for IL 34. The inhibitory activity of CSF 1R ECD appeared to be specific because inhibition was not seen with other ECDs in the screening set or with granulocyte-macrophage CSF receptor (GM-CSFR) ECD or interferon-γ receptor (IFNγR) ECD (fig. S7). CSF 1R ECD blocked binding of biotinylated IL-34 to the human monocytic cell line THP 1, whereas GM-CSFR ECD or IFNγR ECD had no effect on IL-34 binding (Fig. 4A). Furthermore, unlabeled IL-34, CSF-1, or antibody to CSF-1R blocked binding of biotinylated IL-34 to THP 1 cells (Fig. 4A). The binding affinity of IL-34 to the immobilized CSF 1R ECD was determined by Biacore analysis with a dissociation constant (K_d) of about 1 pM (fig. S8A). CSF 1 bound to the CSF-1R ECD with a K_d of 34 pM (fig. S8B).

In functional studies, the activity of IL-34 on monocyte viability was blocked by antibodies to IL-34 but not by an antibody to CSF 1, whereas the activity of CSF 1 was blocked only by its own antibody and not by antibodies to IL 34 (Fig. 4B), suggesting that the IL-34 activity in monocyte viability was independent of CSF-1. The activity of IL-34 could be abolished when the IL 34 protein was heat-inactivated (Fig. 4B). IL-34, like CSF-1, stimulated phosphorylation of extracellular signal-regulated kinase-1 and 2 (ERK1/2) in human monocytes (Fig. 4C). Furthermore, the IL-34–induced phosphorylation of ERK1/2 was inhibited by a CSF 1R–specific inhibitor, GW2580 (*11*) (Fig. 4C). In addition, IL 34 promoted the formation of the colony-forming unit–macrophage (CFU M), a macrophage progenitor, in human bone marrow cultures (Fig. 4D). The IL 34–promoted CFU-M colonies (fig. S9, A to C) had a size and morphology

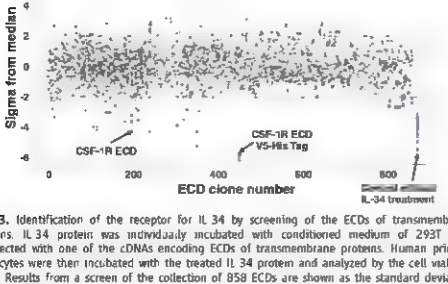

Fig. 3. Identification of the receptor for IL 34 by screening of the ECDs of transmembrane proteins. IL 34 protein was individually incubated with conditioned medium of 293T cells transfected with one of the cDNAs encoding ECDs of transmembrane proteins. Human primary monocytes were then incubated with the treated IL 34 protein and analyzed by the cell viability assay. Results from a screen of the collection of 858 ECDs are shown as the standard deviation from the median (sigma from median). Purple circles (inhibitors) indicate clones for which activity was detected with greater than twofold standard deviation of the assay plate for more than one test. Cells without IL-34 treatment were used as controls (blue circles) on each assay plate. The activities of the ECD clones that inhibited IL 34 activity on monocytes in primary and secondary screens are shown in table S6. CSF-1R ECD V5-His Tag, CSF1R ECD with a V5-His epitope tag.

similar to those of colonies promoted by CSF-1 (fig. S9, D to F). Upon staining with the May Grünwald-Giemsa stain, cells derived from these colonies showed vacuole-containing cytoplasm (fig. S9, G to J), confirming that they are cells of CFU-M (*12*).

The selectivity pattern of IL-34 across many assays was predictive of the biology of this protein. IL-34 is a new ligand for a highly selective and relatively well-studied receptor, the CSF-1 receptor. Our discovery of IL-34 illustrates that even in well-understood systems, there are functional protein regulators yet to be discovered using a systematic screening approach. CSF-1 and CSF-1R are important for monocyte formation and subsequent differentiation into the various functional phagocytes (*6*). Mice defective in CSF-1R have a more severe osteopetrosis in

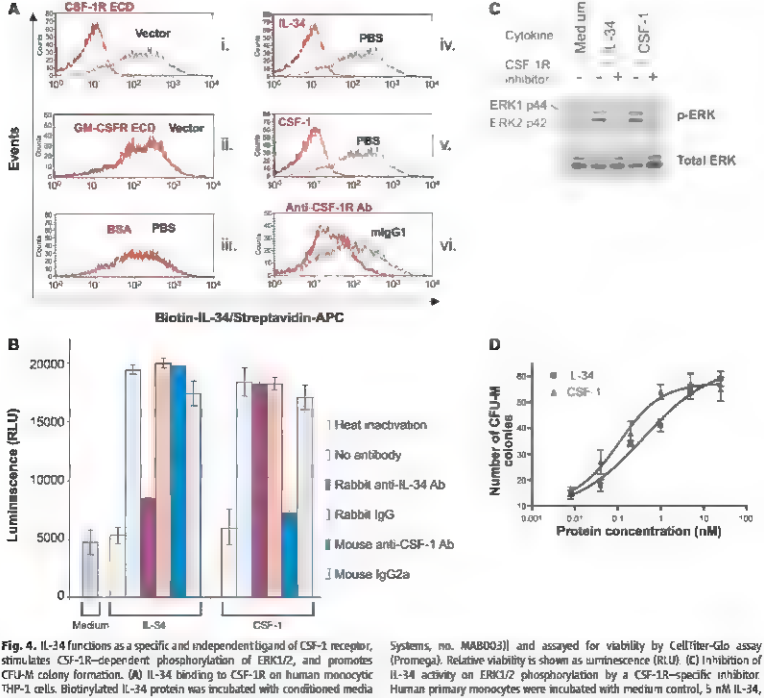

Fig. 4. IL-34 functions as a specific and independent ligand of CSF-1 receptor, stimulates CSF-1R–dependent phosphorylation of ERK1/2, and promotes CFU-M colony formation. (**A**) IL-34 binding to CSF-1R on human monocytic THP-1 cells. Biotinylated IL-34 protein was incubated with conditioned media of 293T cells transfected with cDNA encoding CSF-1R ECD (i), GM-CSFR ECD (ii), or vector. THP-1 cells were then incubated with the treated IL-34 protein, labeled with streptavidin-APC, and analyzed by flow cytometry. THP-1 cells preincubated with BSA (iii), unlabeled IL-34 (iv), CSF-1 (v), neutralizing antibody to CSF-1R (Anti-CSF-1R Ab) and control mouse immunoglobulin G1 (mIgG1) (vi), or buffer control [phosphate-buffered saline (PBS)] were labeled with biotinylated IL-34, stained with streptavidin-APC, and analyzed by flow cytometry. (**B**) IL-34 function on monocytes is independent of CSF-1. Human monocytes were incubated with IL-34 or CSF-1 that was heat-inactivated (100°C for 5 min) or treated with rabbit polyclonal antibodies to IL-34 (rabbit anti-IL-34 Ab), a mouse antibody to CSF-1 [mouse anti-CSF-1 Ab (R&D Systems, no. MAB216], or control IgG [rabbit IgG (Millipore) and mouse IgG2a (R&D Systems, no. MAB003)] and assayed for viability by CellTiter-Glo assay (Promega). Relative viability is shown as luminescence (RLU). (**C**) Inhibition of IL-34 activity on ERK1/2 phosphorylation by a CSF-1R–specific inhibitor. Human primary monocytes were incubated with medium control, 5 nM IL-34, or 5 nM CSF-1 at 37°C for 3 min in the presence or absence of 60 nM CSF-1R–specific inhibitor, GW2580 (*11*). The monocyte cell lysate was analyzed by Western blotting using an antibody to phospho-ERK1/2 (p-ERK) (Santa Cruz Biotechnology, Inc., no. sc-7383). The Western blot was then stripped and probed with antibodies to ERK (Santa Cruz Biotechnology, Inc., no. sc-94) for detection of the total ERK. The results were reproducible in three experiments. (**D**) IL-34 promotes CFU-M colony formation from human bone marrow. Colony formation assays were performed by StemCell Technologies, Inc. as described (*14*, *15*), using CSF-1 (R&D Systems, Inc.) or IL-34, at indicated concentrations. Representative data ($n = 3$ replicates for each concentration and treatment) from one of three experiments are shown. Images of the CFU-M colonies and of the May-Grunwald-Giemsa–stained cells are shown in fig. S9.

the femur and a more severe depletion of F4/80^{+} macrophages in the kidney than the CSF-1 deficient mice (*13*). Thus, the existence of a second ligand, in addition to CSF-1, for CSF-1R has been proposed (*13*). Here we report the identification of such a factor, IL-34.

References and Notes

1. N. L. Anderson *et al.*, *Mol. Cell. Proteomics* **3**, 311 (2004).
2. E. A. Lee, L. Hansen, K. Hestir, L. T. Williams, D. Farrelly, *Protein Pept. Lett.*, in press.
3. L. Breiman, *Mach. Learn.* **45**, 5 (2001).
4. Materials and methods are available as supporting material on *Science* Online.
5. T. A. Waldmann, *Nat. Rev. Immunol.* **6**, 595 (2006).
6. V. Chitu, E. R. Stanley, *Curr. Opin. Immunol.* **18**, 39 (2006).
7. E. Tomlinson *et al.*, *Endocrinology* **143**, 1741 (2002).
8. A. M. Byrne, D. J. Bouchier-Hayes, J. H. Harmey, *J. Cell. Mol. Med.* **9**, 777 (2005).
9. M. H. Xie *et al.*, *Cytokine* **11**, 729 (1999).
10. A. Kharitonenkov *et al.*, *J. Clin. Invest.* **115**, 1627 (2005).
11. J. G. Conway *et al.*, *Proc. Natl. Acad. Sci. U.S.A.* **102**, 16078 (2005).
12. C. Missen-Druey, A. Tichelli, S. Meyer-Monard, *Acta Haematol.* **113**, 5 (2005).
13. X. M. Dai *et al.*, *Blood* **99**, ... (2002).
14. C. Pereira, J. Damen, A. Eaves, E. Clarke, *BioProcess International* **2**, 70 (2004).
15. M. G. Testa, G. Molineux, Eds., *Haemopoiesis: A practical approach* (Oxford University Press, Inc., New York, 1993).

16. We thank T. Chang, A. Farsad, S. Giese, S. Gomes, M. Ji, K. Justin, D. McDonough, A. Pham, S. Ramirez, A. Sadra, S. Shi, T. Wang, and R. Zhang for technical support and discussions, and other colleagues at Five Prime Therapeutics, Inc. for providing screening assay data in the functional selectivity analysis. We thank J. Damen and C. Pereira of StemCell Technologies, Inc. for performing the colony-formation assays. H.L., E.L., K.H., C.L., M.H., E.B., R.H., G.W., A.Z., D.B., T.L., J.W., S.K.D., and L.T.W. of Five Prime Therapeutics, Inc. have filed a U.S. patent application (#20070264277) based on the work in this paper.

Supporting Online Material
www.sciencemag.org/cgi/content/full/320/5877/807/DC1
Materials and Methods
Figs. S1 to S9
Tables S1 to S8
References

19 December 2007; accepted 10 April 2008
10.1126/science.1154370

Regulation of the Cellular Heat Shock Response in *Caenorhabditis elegans* by Thermosensory Neurons

Veena Prahlad, Tyler Cornelius, Richard I. Morimoto*

Temperature pervasively affects all cellular processes. In response to a rapid increase in temperature, all cells undergo a heat shock response, an ancient and highly conserved program of stress-inducible gene expression, to reestablish cellular homeostasis. In isolated cells, the heat shock response is initiated by the presence of misfolded proteins and therefore thought to be cell-autonomous. In contrast, we show that within the metazoan *Caenorhabditis elegans*, the heat shock response of somatic cells is not cell-autonomous but rather depends on the thermosensory neuron, AFD, which senses ambient temperature and regulates temperature-dependent behavior. We propose a model whereby this loss of cell autonomy serves to integrate behavioral, metabolic, and stress-related responses to establish an organismal response to environmental change.

The heat shock response counteracts the detrimental effects of protein misfolding and aggregation that result from biochemical and environmental stresses, including increases in temperature (*1*, *2*). This response, orchestrated by the ubiquitously expressed heat shock factor-1 (HSF-1), involves the rapid transcription of a specific set of genes encoding the cytoprotective heat shock proteins (HSPs) (*1*, *2*). The stress-induced appearance of non-native proteins imbalances cellular homeostasis, and the resulting shift in chaperone requirements is thought to trigger the heat shock response (*1*, *2*). Because all these events occur at the cellular level, the heat shock response is thought to be cell-autonomous. Indeed, isolated cells in tissue culture, unicellular organisms (*1*, *2*), and individual cells within a multicellular organism (*3*) can all produce a heat shock response when exposed directly to heat.

Although the heat shock response is essential for the survival of cells exposed to stress, the accumulation of large amounts of HSPs can be detrimental for cell growth and division (*2*, *4*). Therefore, although cellular autonomy in initiating this response may be beneficial for unicellular organisms and isolated cells, the uncoordinated triggering of the heat shock response in individual cells within a multicellular organism could interfere with the complex interactions between differentiated cells and tissues.

In *Caenorhabditis elegans*, a pair of thermosensory neurons, the AFDs, detect and respond to ambient temperature (*5*, *6*). The AFDs, and their postsynaptic partner cells, the AIYs, regulate the temperature-dependent behavior of the organism and are required for finding the optimal temperature for growth and reproduction (*6*). We tested whether this thermosensory neuronal circuitry also regulates the heat shock response of somatic cells. For this, we exposed wild-type *C. elegans* or animals carrying loss-of-function mutations affecting the AFD or AIY neurons (Fig. 1A) to a transient increase in temperature and assayed their heat shock response. The mutations chosen [*gcy-23*, *gcy-8* (*7*), *tax-4*, *ttx-1*, and *ttx-3* [for details of these mutations see (*8*)]] exclusively affect neuronal function because the wild-type gene products are not expressed in other tissues, with *gcy-8* and *gcy-23* expressed solely in the AFDs (*7*). Wild type and mutant adult animals, grown at low population densities at 20°C in the presence of abundant bacteria (*8*), were exposed to a transient increase in temperature (30°C or 34°C for 15 min), and their heat shock response was measured as the total amount of mRNA encoding the major heat-inducible cytoplasmic *hsp70*, C12C8.1 (*9*), 2 hours after heat shock. Mutations affecting the AFD or AIY neurons reduced heat shock–dependent accumulation of *hsp70* (C12C8.1) mRNA at both temperatures (*8*) (table S1 and Fig. 1, B and C), whereas a mutation, *ocr-2* (*10*), affecting four other sensory neurons of the animal had no effect (*8*) (table S1).

The decrease in *hsp70* (C12C8.1) abundance was not merely due to a delay in the onset of heat shock response (Fig. 1D). The *gcy-8* and *ttx-3* mutants had consistently lower amounts of *hsp70* (C12C8.1) mRNA compared with wild-type over a 6-hour period after heat shock, with some mRNA accumulation seen 4 hours after heat shock. Mutants with defective AFD or AIY neurons also had reduced heat shock-dependent accumulation of another cytoplasmic *hsp70*, F44E5.4 (*9*), and the small heat shock protein, *hsp16.2*, mRNAs (*11*) (Fig. 1, E and F).

The diminished expression of HSP genes in the *gcy-8* and *ttx-3* mutants might make them less viable than wild-type animals under conditions of heat stress. This was the case (Fig. 1G): The decrease in thermotolerance of the thermosensory mutants was similar to that of animals carrying a *hsf-1* loss-of-function allele (*12*) (Fig. 1G), although *hsf-1* mRNA levels were not diminished in *gcy-8* and *ttx-3* mutants (*8*) (fig. S3A) relative to that of wild type.

We examined whether the decreased accumulation of inducible *hsp70* mRNA in the thermosensory mutants reflected selective reduction in neuronal tissue or corresponded to diminished expression in all cells throughout the animal. Heat shock promotes *hsp* mRNA expression in numerous somatic cells of wild-type *C. elegans* as monitored with a *hsp70* (C12C8.1) promoter green fluorescent protein (GFP) reporter construct (*13*) (Fig. 1H). The expression of this *hsp70*

Department of Biochemistry, Molecular Biology, and Cell Biology, Rice Institute for Biomedical Research, Northwestern University, Evanston, IL 60208, USA.

*To whom correspondence should be addressed. E-mail: r-morimoto@northwestern.edu

reporter in strains with mutant *gcy-8* and *ttx-3* genes was reduced in all somatic cells 2 hours after heat shock (Fig. 1, I and J) and continued to be impaired after 24 hours, although these somatic cells of the thermosensory mutants should have experienced the same heat shock temperature as the equivalent wild-type cells (*8*) (figs. S1 and S2). These results indicate that the heat shock response in *C. elegans* is not cell-autonomous. Instead, the AFD and AIY neurons appear to regulate both the magnitude and the time course of heat shock gene expression in nonneuronal cells, influencing organismal thermotolerance. Subsequent experiments were done at 34°C with use of the AFD-specific mutant *gcy-8* that is the most upstream component known in the thermosensory neuronal circuitry.

To control the heat shock response of nonneuronal cells, the AFD neurons must regulate the activities of cellular transcription factors. In eukaryotes, HSP expression after heat shock is HSF-1–dependent (*2*). Organismal thermotolerance also requires the FOXO transcription factor, DAF-16 (*14*). To test which transcription factor is required for AFD-dependent *hsp70* (C12C8.1) mRNA expression after heat shock, we used RNA interference (RNAi). Depletion of *hsf-1* mRNA but not *daf-16* mRNA in wild-type *C. elegans* decreased *hsp70* (C12C8.1) expression throughout the organism (Fig. 2A). Depletion of *hsf-1* mRNA, however, had no effect on the already diminished amounts of *hsp70* (C12C8.1) mRNA in the *gcy-8* mutants (Fig.

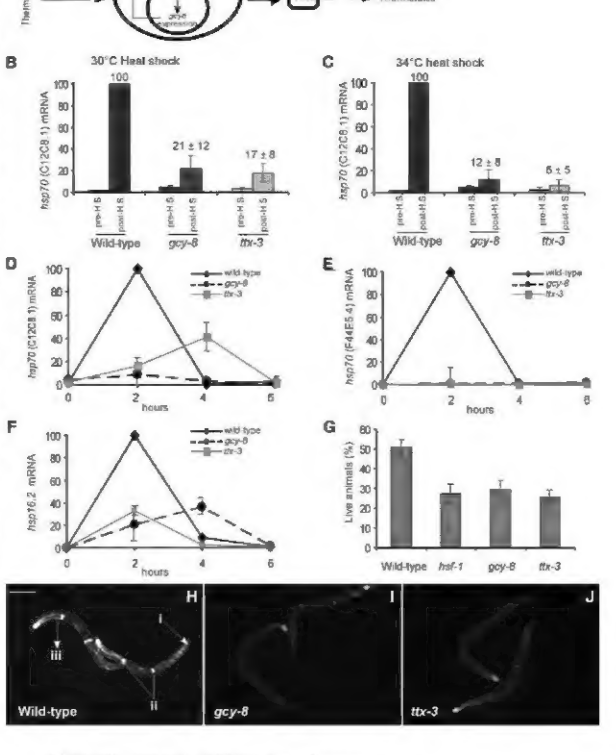

Fig. 1. Role of AFD and AIY neurons in the organismal heat shock response. (**A**) Schematic depiction of genes affecting AFD and AIY function. AFD detects temperature by using the cyclic guanosine 5′-monophosphate (cGMP)–dependent TAX-4/TAX-2 cyclic-nucleotide–gated (CNG) channel. Guanylyl cyclases, *gcy-8*, *gcy-18*, and *gcy-23*, function upstream of *tax-4*. ODX transcription factor, TTX-1, regulates *gcy-8* expression, and AIY function is specified by the LIM homeobox gene, *ttx-3*. Total *hsp70* (C12C8.1) mRNA levels in *gcy-8* and *ttx-3* mutants relative to wild-type animals before heat shock (pre–H.S.) and 2 hours after heat shock (post-H.S.) at (**B**) 30°C and (**C**) 34°C for 15 min. Time course of total (**D**) *hsp70* (C12C8.1), (**E**) *hsp70* (F44E5.4), and (**F**) *hsp16.2* mRNA accumulation after heat shock (34°C, 15 min) in *gcy-8* and *ttx-3* mutants relative to wild-type animals. mRNA amounts were measured by quantitative reverse transcription polymerase chain reaction (RT-PCR) and normalized to maximal wild-type values. (**G**) Survival of wild-type, *gcy-8*, *ttx-3*, and *hsf-1* mutant animals. Error bars indicate ±SE [(B) and (C) and ±SD [(D) and (E)]. *hsp70* (C12C8.1) promoter-GFP reporter expression in (**H**) wild-type, (**I**) *gcy-8*, and (**J**) *ttx-3* mutant animals 2 hours after heat shock (34°C; 15 min). (i) pharynx, (ii) spermatheca, and (iii) intestinal cell. Scale bar = 100 μm.

2A). Thus, AFD appears to regulate HSP expression through HSF-1, although we cannot rule out the existence of a parallel transcriptional mechanism.

We tested whether the deficiency in HSF-1–dependent heat shock induction of HSPs in the *gcy-8* mutants resulted from high constitutive expression of chaperones that negatively autoregulate HSF-1 activity or other inhibitors of HSF-1 (*2*, *14*). This appeared not to be the case: Both wild-type and mutant animals expressed similar amounts of constitutive *hsp70* (*hsp-1*) (fig. S3B), the stress-inducible *hsp70s* [(C12C8.1 and F44E5.4 (*8*) (table S1)], *hsp90* (daf-*21*), and *daf-16* (fig. S3B). To test whether the *gcy-8* mutant animals were deficient in their ability to mount any stress-inducible transcriptional response, we exposed animals to another stress, the transition metal cadmium (*15*), and assayed their ability to activate transcription of two cadmium-responsive genes: *hsp70* (C12C8.1) and *cdr-1* (*15*). In contrast to what was observed upon heat shock, both *hsp70* and *cdr-1* mRNA were similarly increased in wild-type and *gcy-8* mutant animals (Fig. 2B) after 3 hours of exposure. Moreover, as for wild-type animals, the cadmium-dependent induction of *hsp70* (C12C8.1) was HSF-1–dependent in *gcy-8* mutants (Fig. 2C). Thus, a deficiency in the AFD neuron does not compromise the molecular machinery required for the stress-dependent HSF-1 transcriptional response. The *gcy-8* mutant animals are not preadapted to stress but instead are selectively impaired in their ability to induce HSF-1–dependent heat shock gene expression. Given the role of the AFD in sensing ambient temperature, this suggests that AFD signaling is required for heat shock–dependent gene expression. This was further confirmed by transiently and reversibly inhibiting neuronal activity in wild-type animals with the volatile anesthetics (VAs) halothane and isoflurane and observing a concomitant inhibition of *hsp70* (C12C8.1) expression in somatic cells (*8*) (fig. S4).

The AFD neurons and associated thermosensory circuitry in *C. elegans* also regulate thermotaxis behavior, integrating temperature information with environmental signals that modulate growth and metabolism (*6*). One such potent environmental signal is dauer pheromone: Low concentrations of dauer pheromone, when animals are at low population densities in the presence of food, promote continuous growth; high concentrations signal starvation and alter metabolism (*16*). AFD mutants show altered sensitivity to dauer pheromone (*16*, *17*). Thus, dauer pheromone might also modulate the heat

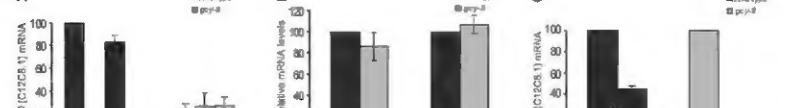

Fig. 2. Impairment of HSF-1–dependent gene expression in *gcy-8* mutants after temperature stress. **(A)** Total *hsp70* (C12C8.1) mRNA, 2 hours after heat shock (34°C, 15 min), in wild-type and *gcy-8* mutant animals subjected to RNAi-mediated knockdown of *hsf-1* or *daf-16*. Relative mRNA levels were measured by quantitative RT-PCR and normalized to wild-type values on control RNAi. **(B)** Total *hsp70* (C12C8.1) and *cdr-1* mRNA levels in wild-type and *gcy-8* mutants after cadmium stress (*8*). Relative mRNA levels were determined by quantitative RT-PCR and normalization to wild-type values. **(C)** Relative *hsp70* (C12C8.1) mRNA levels in cadmium-treated wild-type animals and *gcy-8* mutants subjected to RNAi-mediated knockdown of *hsf-1*. Relative mRNA levels were determined by quantitative RT-PCR and normalization to wild-type and *gcy-8* values on control RNAi. Error bars indicate ±SE.

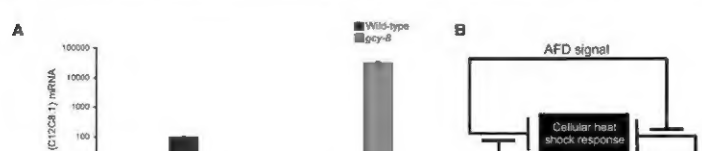

Fig. 3. AFD-dependent regulation of the cellular heat shock response is modulated by metabolic signals. **(A)** Relative *hsp70* (C12C8.1) mRNA levels before and 2 hours after heat shock (34°C, 15 min) in wild-type and *gcy-8* mutant animals grown at low population densities or exposed to dauer pheromone 10 min before and during the 2 hours of recovery after heat shock. Note semi-logarithmic scale. Relative mRNA levels were determined by quantitative RT-PCR and normalized to maximal wild-type values. Error bars indicate ±SE. **(B)** Model depicting the regulation of the cellular heat shock response by AFD-dependent signaling of temperature and dauer pheromone–dependent signaling of growth conditions.

shock response in an AFD-dependent manner, integrating the organismal stress response with metabolism. *C. elegans* animals raised at low population density initiate transcription of *hsp* mRNA after heat shock (Figs. 1 and 3A). However, exposure of wild-type animals to high concentrations of dauer pheromone before or during heat shock decreased the amounts of *hsp70* (C12C8.1) mRNA induced (Fig. 3A). Thus, the heat shock response in *C. elegans* is affected by the metabolic state and is dampened under conditions that do not support continuous growth and reproduction. In contrast, exposure of *gcy-8* mutant animals to dauer pheromone had the opposite effect and induced even higher amounts of *hsp70* (C12C8.1) mRNA after heat shock than is normally seen upon heat shock of wild-type animals raised under optimal growth conditions (Fig. 3A).

The opposing effects of dauer pheromone on wild-type and *gcy-8* mutant animals can be explained by a model in which the heat shock response is regulated at the organismal level by two inputs: the AFD-dependent temperature input and a metabolic signal that responds to growth conditions (Fig. 3B). Each of these inputs negatively regulates the other and inhibits HSP expression. In wild-type animals under conditions that support growth, the growth-dependent inhibitory signal is active, and an increase in temperature activates the AFDs, which suppresses the inhibitory signal, thus allowing induction of the heat shock response. In the presence of positive growth signals but absence of AFD signaling during heat shock (as in *gcy-8* mutants), the growth input is not inhibited, and the heat shock response is suppressed. The addition of dauer pheromone to wild-type animals suppresses the signal from the growth input, resulting in the inhibition of the cellular heat shock response by AFD signaling. In the absence of both AFD and growth signals, as occurs in the *gcy-8* mutant exposed to dauer pheromone, the heat shock response is not inhibited.

The model we propose for the regulation of the heat shock response in *C. elegans* suggests that cells induce this response in the presence of AFD and growth signals, as in wild-type animals, but also in the complete absence of these regulatory signals, as observed for isolated cells in culture. Thus, neuronal control may allow *C. elegans* to coordinate the stress response of individual cells with the varying metabolic requirements of its different tissues and developmental stages. Indeed, neuronal signaling has been shown to modulate cellular homeostasis in *C. elegans* (*18*). Because the AFD neurons do not directly innervate any of the downstream tissues in which heat shock gene induction is affected, it is likely that this regulation is mediated through neuroendocrine signaling. The override of the cell-autonomous heat shock response by neuronal circuitry seen for *C. elegans* may be a common mechanism of regulation in other metazoans. Indeed, HSF-1 in rats can be activated by neuroendocrine signaling from the hypothalamic-pituitary-adrenal axis in the absence of external stress (*19*). Thus, the hierarchical organization of regulatory networks may allow organized tissues comprised of heterogeneous cell types to establish a highly orchestrated stress response in the metazoan organism.

References and Notes

1. S. Lindquist, E. A. Craig, *Annu. Rev. Genet.* **22**, 631 (1988).
2. R. I. Morimoto, *Genes Dev.* **12**, 3788 (1998).
3. E. G. Stringham, E. P. Candido, *J. Exp. Zool.* **266**, 277 (1993).
4. J. H. Fecker, J. M. Rossi, J. Solomon, N. Solomon, S. Lindquist, *Genes Dev.* **6**, 1402 (1992).
5. D. A. Clark, C. V. Gabel, H. Gabel, A. D. Samuel, *J. Neurosci.* **27**, 6083 (2007).
6. I. Mori, *Annu. Rev. Genet.* **33**, 399 (1999).
7. H. Inada *et al.*, *Genetics* **172**, 2239 (2006).
8. Materials and methods are available on *Science* Online.
9. T. P. Sautch, M. F. Heschl, D. L. Baillie, *Gene* **64**, 241 (1988).
10. I. Sakaidchik, T. Tanabe, P. F. Baldi, J. Y. Sze, *J. Neurosci.* **25**, 1015 (2005).
11. C. D. Link, J. R. Cypser, C. J. Johnson, T. E. Johnson, *Cell Stress Chaperones* **4**, 235 (1999).
12. Y. M. Hajdu-Cronin, W. J. Chen, P. W. Sternberg, *Genetics* **168**, 1937 (2004).
13. J. F. Morley, R. I. Morimoto, *Mol. Biol. Cell* **15**, 657 (2004).
14. A. L. Hsu, C. T. Murphy, C. Kenyon, *Science* **300**, 1142 (2003).
15. Y. Cai, S. J. McBride, W. A. Boyd, S. Alper, J. H. Freedman, *Genome Biol.* **8**, R122 (2007).
16. P. J. Hu, Ed., *The C. elegans Research Community, WormBook*, 10.1895/wormbook.1.144.1, http://www.wormbook.org., 3 (2007).
17. J. W. Golden, D. L. Riddle, *Proc. Natl. Acad. Sci. U.S.A.* **81**, 819 (1984).
18. S. M. Garcia, M. O. Casanueva, M. C. Silva, M. D. Amaral, R. I. Morimoto, *Genes Dev.* **21**, 3006 (2007).
19. T. W. Fawcett, S. L. Sylvester, K. D. Sarge, R. I. Morimoto, N. J. Holbrook, *J. Biol. Chem.* **269**, 32272 (1994).

20. We thank the Morimoto lab members for discussions and comments; T. Shimaoka and the *Caenorhabditis elegans* Genetics Center, supported by a grant from National Institute of General Medical Sciences (NIGMS) and the International Consortium, for providing strains; and I. Mori at Nagoya University, Nagoya, Japan for the *gcy-8(oy44)* strain. These studies were supported by grants to R.I.M. from NIH (NIGMS and National Institute on Aging), the Huntington's Disease Society of America Coalition for the Cure, and the Daniel F. and Ada L. Rice Foundation.

Supporting Online Material

www.sciencemag.org/cgi/content/full/320/5877/813/DC1
Materials and Methods
Figs. S1 to S4
Table S1
References

5 February 2008; accepted 1 April 2008
10.1126/science.1156093

New Products Focus: RNAi

High Throughput Transfection System

CellaxessHT is an automated, high throughput transfection system that enables reagent-free delivery of small interfering RNA and complementary DNA to a wide range of biologically relevant cell types with excellent transfection efficiencies and viabilities. The system features a patented capillary electrode array technology for transfection of cells cultured in 384 well plates and offers a capacity of up to 50,000 wells per day.

Cellectricon
For information +46 (0) 31 760 35 15
www.cellectricon.com

RNA Stabilizer

RNAstable is for preserving RNA at room temperature, which eliminates the need for cold storage and refrigerated shipping. RNA samples are difficult to work with given their labile nature and tendency to degrade even in cold storage. Exposure to slightly elevated temperatures for even a short time can compromise RNA integrity. RNAstable makes use of technology that forms a thermostable barrier, securely "shrink wrapping" RNA samples to protect them from degradation. To store RNA, researchers simply pipette samples directly into a tube or well of RNAstable and let them dry. Sample recovery requires only adding water, with no further purification required. RNAstable preserves RNA at room temperature for up to five months and is better at preventing degradation than freezer storage. The preserved samples can be used in applications such as bioanalyzer and microarray analysis, end-point polymerase chain reaction, gel analysis, reverse transcription, and more without inhibition or interference.

Biomatrica
For information 858-550-0308
www.biomatrica.com

Profiling Array

The T7-oligonucleotide ligation assay-based microRNA (miRNA) profiling array allows the user to access miRNA expression cost effectively. Expression of multiple miRNAs can be determined simultaneously in a single, simple assay that does not require preisolation of small RNA. The analysis has the power to differentiate miRNA isoforms with a single nucleotide difference and to differentiate all miRNA isoforms. Captured miRNAs are subjected to T7 amplification without introduction of bias in polymerase chain reaction. Total RNA can be used in the assay directly, without preisolation of miRNA.

Signosis
For information 877-266-8388
www.signosisinc.com

Capillary-Mimicking Platform

The VenaFlux Platform is a semiautomated, high throughput, microfluidic cell-based assay system. It measures cell adhesion to antibody-coated or endothelial-cell cultured microchannels, producing curves under shear stress conditions that mimic physiological flows. The VenaFlux is simple to use, reduces costly layers of animal model studies, and delivers specific, accurate, and reproducible results. Scientists can use the VenaFlux to rapidly obtain quantitative analyses and results for potential drug candidates in cardiovascular, respiratory, immunological, autoimmune, and oncological diseases. These analyses can reduce drug development costs by accelerating false-lead elimination. The VenaFlux replicates cell behavior in human capillaries, which is an expanding area of research. The technology provides researchers with a single platform for executing dynamic studies to analyze the effects of drugs on cell adhesion, proliferation, and transmigration under well-defined shear stress protocols that replicate physiological conditions.

Cellix
For information 917-623-4456
www.cellixltd.com

RNAi Duplexes

PlateSelect RNA interference (RNAi) duplexes offer the ability to customize 96-well plates with Invitrogen's chemically modified Stealth or standard BLOCK-iT RNAi duplexes. Users develop their customized plates through an intuitive web interface, and they can order from one to 96 different duplexes in a single plate. The RNAi duplexes are synthesized on demand to take advantage of the most up-to-date bioinformatics and are provided at 1 nmol/well in the well orientation that the customer chooses. The duplexes arrive in ready-to-transfect format and are synthesized based on algorithms designed to reduce the chances of off-target effects.

Invitrogen
For information 800-955-6288
www.invitrogen.com/plateselect

RNA Purification Kit

The MasterPure RNA Purification Kit offers increased yields of total RNA, compared with methods such as spin-column kits. Starting with tissue, eukaryotic cells, or bacterial culture, the gentle salt precipitation preserves microRNAs and other small RNAs that would be lost with a spin-column kit. Up to 25 µg of RNA can be obtained from 5 mg of mouse liver.

Epicentre Biotechnologies
For information 800-284-8474
www.EpiBio.com

Electronically submit your new product description or product literature information! Go to **www.sciencemag.org/products/newproducts.dtl** for more information.

Newly offered instrumentation, apparatus, and laboratory materials of interest to researchers in all disciplines in academic, industrial, and governmental organizations are featured in this space. Emphasis is given to purpose, chief characteristics, and availability of products and materials. Endorsement by *Science* or AAAS of any products or materials mentioned is not implied. Additional information may be obtained from the manufacturer or supplier.